NASA Contractor Report 3996

Development of Pressure Containment and Damage Tolerance Technology for Composite Fuselage Structures in Large Transport Aircraft

P. J. Smith, L. W. Thomson,
and R. D. Wilson

CONTRACT NAS1-17740
AUGUST 1986

NASA

NASA Contractor Report 3996

Development of Pressure Containment and Damage Tolerance Technology for Composite Fuselage Structures in Large Transport Aircraft

P. J. Smith, L. W. Thomson,
and R. D. Wilson

Boeing Commercial Airplane Company
Seattle, Washington

Prepared for
Langley Research Center
under Contract NAS1-17740

National Aeronautics
and Space Administration

**Scientific and Technical
Information Branch**

1986

FOREWORD

This final report was prepared by The Boeing Commercial Airplane Company, Renton, Washington, under NASA contract NAS1-17740. It covers work performed between May 7, 1984, and December 20, 1985. The program was sponsored by the National Aeronautics and Space Administration, Langley Research Center (NASA-LRC). Herman L. Bohon and John G. Davis were the NASA-LRC ACEE project managers and Jon S. Pyle was the NASA-LRC technical manager.

Use of commercial products or names of manufacturers in this report does not constitute official endorsement of such products or manufacturers, either expressed or implied, by the National Aeronautics and Space Administration.

This report was prepared by P. J. Smith, L. W. Thomson, and R. D. Wilson. The following Boeing personnel were principal contributors to the program:

ACDP Program Director
S. T. Harvey
R. T. Ostlund

ACDP Technology Advisor
J. T. Quinlivan

Program and Technology Manager
R. D. Wilson

Engineering Design Manager
M. J. Thould

Structural Analysis and
Test Coordination
P. J. Smith, Lead Engineer
M. A. Ocasio
J. M. Schinke
L. W. Thomson

Business Management
V. L. Dostert
R. E. Sever

Systems
D. G. Moss

Design
M. Ely
J. Simmons

Weight and Balance Analysis
J. T. Parsons
T. S. Whitehurst

Materials
R. G. Maguire
W. C. Potter

Structural Test
W. C. Larson, Manager
J. Moroney, Manager
H. W. Buse
J. E. Chavey
J. A. Gertis
M. A. Litzkow
M. A. Parsons
W. O. Swift
L. Wendt

Manufacturing Technology
H. R. Fenbert
L. R. Hause
R. M. Mullen
R. B. Snyder

TABLE OF CONTENTS

TABLE OF CONTENTS (Concluded)

SUMMARY

This program was conducted to identify and resolve technological issues involved in the application of advanced composites to fuselage structure for commercial and military transport aircraft for 1990 production. The principal issues addressed by this program were damage tolerance and pressure containment. These issues were separated into areas relating to materials, structure, and manufacturing, and were addressed simultaneously by this program.

Several material systems were evaluated for use in two designs, a stiffened laminate shell structure and a honeycomb sandwich shell structure. Material selection considerations for these applications included operating environments, design configurations, structural loading requirements, manufacturing producibility, reliability, cost, and system integrations. Both qualitative and quantitative procedures were used to compare material performance and requirements.

The material system selected for the fabrication of laminate test panels for phase 1 was Hercules 2220-3/AS6. The factors considered in making this selection included basic property data, manufacturing and inspection experience, and panel test data from the LCPAS wing program (NAS1-16863) and the Air Force Damage Tolerance program (contract F33615-82-C-3213). Hercules 2220-3 is classified as a toughened resin, and the AS6 high-strain fiber was chosen for its improved tensile elongation.

An additional consideration for a material system for honeycomb sandwich panel fabrication is the pressure applied during autoclave cure. This pressure is limited by the strength of the honeycomb core. This sandwich part pressure is 45 lb/in^2. The sandwich face sheets must process into a void-free laminate at that pressure.

Hexcel F584/AS6 was selected for fabrication of the sandwich test panels after an evaluation of candidate materials. Honeycomb sandwich long beam flexure tests were the basis of the evaluation.

Because little data had been developed on composite material systems optimized for sandwich designs of primary structure, a comprehensive material characterization program was performed on the Hexcel F584/AS6 system. Tests for establishing the mechanical, physical, and chemical properties were included in the characterization program.

The subject of design strain levels for composite fuselage structure is a basic issue. Ultimate design strains are influenced by damage tolerance criteria in both tension and compression designed structure. Tension designed structure is controlled primarily by large-area damage. Compression designed structure is controlled by either large-area damage or residual strength after impact. The ultimate design strains of 0.006 in/in in tension and 0.005 in/in in compression were selected for this program, based on the available test data. The 1.5% elongation capability of the AS6 fiber allowed the critical strain for a fiber-dominated laminate with severe damage to be raised to 0.0015 in/in from the previous 0.0010 in/in critical strain established in NASA TM-84116, Volume II, "Tear Strap Design in Graphite/Epoxy Structure," by Porter and Pierre.

The stiffened laminate shell design used I-section stringers co-bonded to low modulus skins with skin pads beneath the stringers. This configuration was designed to contain

the large-area damage in the tension/pressure designed areas of the fuselage and to provide damage tolerance for the postbuckled skins in the shear and compression designed areas.

The sandwich shell configuration used glass honeycomb core to stabilize graphite face sheets with integral longitudinal skin pads and circumferential tear straps to address the damage tolerance/pressure containment requirements. The sandwich design did not need to address damage tolerance in the postbuckled range, but had to provide residual strength for the same damage/load conditions as the laminate design.

Subcomponent panels and elements were designed, fabricated, and tested to investigate the relative structural characteristics of the selected designs and verify analysis methods for damage tolerance. These developmental tests evaluated tension fracture characteristics, compression and shear postbuckling behavior, compression damage tolerance, and pressure pillowing pulloff effects for skin-stringer-frame interfaces. Testing was performed primarily at room temperature. Selected tension fracture testing was conducted at -65°F.

Analyses of the tension fracture panels were performed by constructing finite element models. The NASTRAN code was used for these analyses. The curved pressure panel analysis included nonlinear elements and out-of-plane effects.

Finite element analyses, using the STAGSC-1 code, were performed to model the initial buckling and postbuckling response of the flat shear and curved compression panels. The effect of initial panel out-of-plane warpage due to curing strains was included in the analyses.

A weight reduction analysis compared the stiffened skin design with the baseline aluminum fuselage. The comparison was made on participating aluminum structure only. A weight reduction of 4510 lb or 22.7% was calculated for the composite structure from the aluminum baseline design.

The fabrication sequence used for the I-section stiffened skin panels was the standard method at The Boeing Company. This process uses a flat tape laminator, a numerically controlled ply cutting machine, and graphite layup mandrels.

The fabrication sequence used for the honeycomb sandwich panels was to hand lay up and trim the skins, drape skins and core into the layup mandrel, assemble frame-tees to the inside skin, and cure the complete assembly in one autoclave cycle. No precured strips were used, and good compaction and the elimination of voids in the tear strap areas were achieved by the use of modified frame tooling using local shimming.

The results of the development tests have, in most cases, shown good correlation with buckling and failure predictions from the finite element analyses. The stiffened laminate shell designs have shown adequate damage tolerance and pressure containment characteristics. The honeycomb sandwich configuration did not produce the required residual compression strength after either impact damage or large-area damage. The 4.0 lb/ft^3 glass core proved to be too brittle, and the conclusion of this program is that a heavier metal or Nomex core will be needed to qualify sandwich designs for fuselage structure.

SYMBOLS AND ABBREVIATIONS

A	section area, in^2
a_o	characteristic dimension, in
B	panel width, in
b_c	half width of stringer cap, in
BL	buttock line
C	core thickness, in
C_L	centerline
DMA	dynamic mechanical analysis
DSC	differential scanning calorimetry
DUL	design ultimate load
E	modulus of elasticity, lb/in^2
EI	bending stiffness, $lb\text{-}in^2$
Ep	epoxy
E_{11}	lamina modulus of elasticity in fiber direction, lb/in^2
E_{22}	lamina modulus of elasticity in transverse direction, lb/in^2
F	Fahrenheit
F_{CR}	critical buckling stress
FEM	finite element model
ft	foot
G	shear modulus, lb/in^2
gal	gallon
Gr	graphite
G_{12}	lamina shear modulus, lb/in^2
Hg	mercury
HPLC	high pressure liquid chromatography
in	inch
IML	inner mold line
IR&D	independent research and development
K	empirical correction factor for temperature, moisture, pressure, and curvature
kip	10^3 lb
kn	knot
ksi	10^3 lb/in^2
lb	pound
lb/in^2	pounds per square inch
LEFM	linear elastic fracture mechanics
min	minute
MHz	megahertz

msi	$1x10^6$ pounds per square inch
n	number of plies
N	running end load, lb/in
NDI	nondestructive inspection
N_{xy}	shear load, lb/in
OML	outer mold line
P	load, lb
PE	pulse echo
R	radius, in
RT	room temperature
S	percent stiffening; in laminate code, designates symmetry
sta	station identification along longitudinal direction of fuselage
sym	symmetric
t	laminate thickness, in
$\bar{t}$	smeared thickness, in
t_c	stringer cap flange thickness, in
Tg	glass transition temperature
t_p	skin padup thickness, in
t_{sk}	skin thickness, in
TTU	through-transmission ultrasonic
t_w	stringer web thickness, in
V	shear load, lb/in
WBS	proposal work breakdown structure number
x	coordinate reference axis
y	coordinate reference axis
γ	shear strain
ε	strain
ε_C	compression strain allowable
ε_{CR}	critical buckling strain
ε_T	tension strain allowable
θ	laminate angle, deg
μ	10^{-6}
ν_{12}	lamina Poisson's ratio
ϱ	density, lb/in^3
σ	stress, lb/in^2

1.0 INTRODUCTION

Advanced composite materials promise significant cost and weight savings when applied to aircraft structure. For example, an internal Boeing study has shown a 25% cost reduction compared to aluminum when an advanced composite wing is manufactured using the automated methods currently under development. A similar study has shown a 30% cost reduction for a fuselage shell manufactured of advanced composites rather than aluminum. Both the wing and the fuselage shell advanced composite concepts reduce the structural weight by 25% to 30%. Even greater weight and cost reductions are believed possible with resized aircraft, emerging material improvements, and innovative designs that exact more performance from the advanced composite material.

NASA-sponsored research and development programs were set in place to develop the critical engineering technologies necessary to achieve these cost and weight reductions in large transport aircraft structures. This NASA-Boeing program focused on several critical issues generic to the fuselage structure of large pressurized aircraft.

The wing and fuselage account for approximately equal fractions of aircraft structural weight, as shown in Figure 1. Also, as shown in Figure 1, the fuselage accounts for the greatest cost per pound of structure. Therefore, to maximize the benefits of composites application to large commercial and military transport primary structure, the fuselage also must be considered and investigated. In the recently completed Fuselage Study program, NASA contract NAS1-17417 (ref. 1), Boeing identified damage tolerance/pressure containment as a critical technology required for composite fuselage development. As shown in Figure 2, a majority of the fuselage is designed by pressure. Damage tolerance design features for pressure containment will influence a major portion of the shell structure.

A basic design criterion for damage tolerance is that the fuselage shell must survive a significant damage of the structure during normal flight conditions. The energy of the damaging object may be sufficient to completely sever a frame and/or a stringer. In addition, the structure must be designed for impact damage that may be barely visible. The shell designs developed in this program were evaluated for these varying damages to appropriate load conditions. Analyses that modeled the structural response to the severe damage conditions were developed.

The issue of panel postbuckled strength is another critical technology necessary for composite fuselage structure development. Boeing pursued two shell design concepts in this program. These concepts are a honeycomb sandwich construction and a laminate skin design with discrete stringers. The honeycomb shell design effectively carried design loads without buckling, and therefore did not raise postbuckling concerns. The stiffened laminate skin design was designed in the postbuckled range to achieve the necessary weight efficiency when compared to conventional aluminum designs.

Skin-stringer designs were developed that can maintain structural integrity in the postbuckling range with damage. The skin-stringer design has low modulus skins and skin pads beneath the stringer. The low modulus, padded skin design concept has proven successful for damage tolerant wing panel development in NASA-Boeing large composite primary aircraft structure (LCPAS) study (contract NAS1-16863). This configuration, as applied to the fuselage, can be made damage tolerant and capable of achieving design ultimate loads in the postbuckling range.

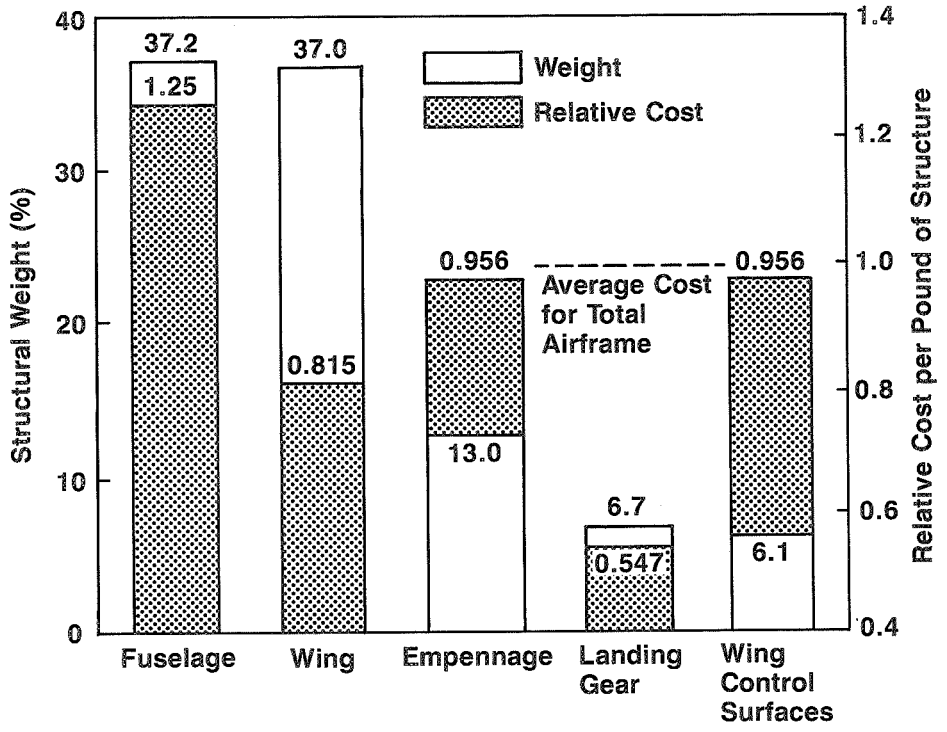

Figure 1. Typical Commercial Transport Component Weight Distribution and Relative Cost Breakdown

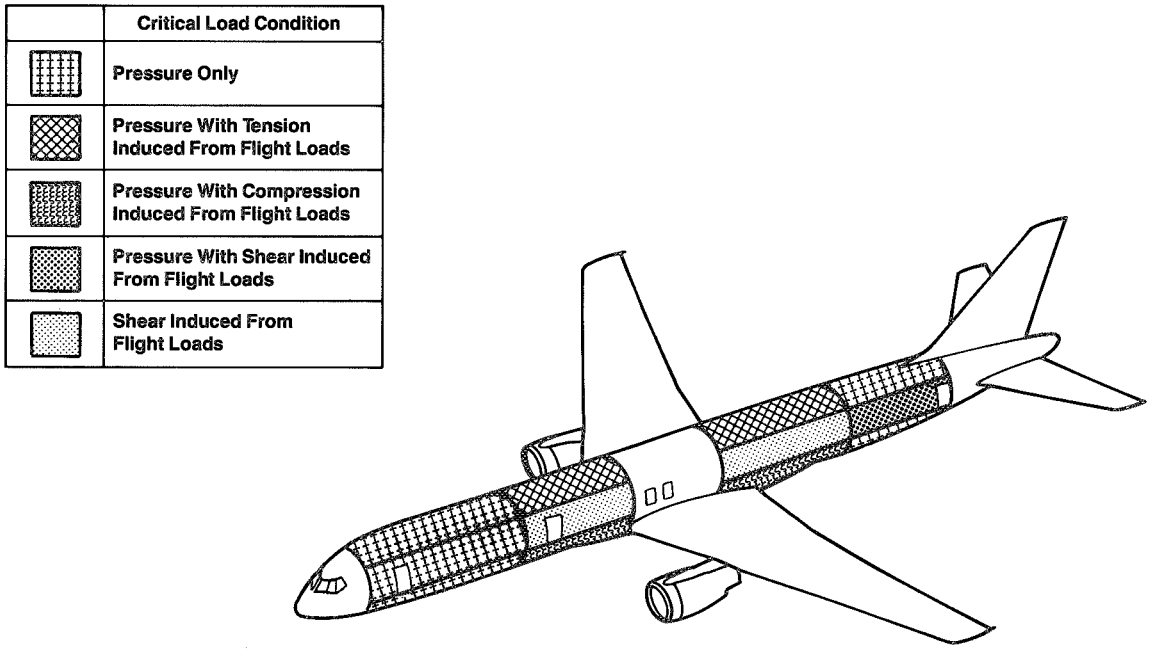

Figure 2. Critical Load Conditions for Pressure-Damage-Tolerant Design

The fuselage development program originally consisted of two phases. Phase I work emphasized the basic issue of (1) pressure damage containment, (2) stability and postbuckling, and (3) compression damage tolerance. The program master schedule is shown in Figure 3. These basic design issues were evaluated in a series of development tests, outlined in Figure 4. Each development test was designed to provide specific solutions to the three basic technology issues.

Previous works have examined the advantages of tear straps for damage containment (ref. 2). However, none of these works considered large enough initial damage and panel sizes to represent fuselage geometry. Tests and analyses of flat laminate and honeycomb fracture panels (tests 1A and 1B) and curved pressurized panels (test 2) provided data for designing damage tolerant composite fuselage structure for pressure containment.

Postbuckling of composite structures has been investigated in several works (refs. 3 and 4). These works have indicated the need for test validation of analysis procedures to determine ultimate strength of postbuckled structure. Skin-stringer compression and shear tests (tests 3, 4, and 5) were performed to provide data for validating design procedures used to size buckled skin-stringer fuselage structure.

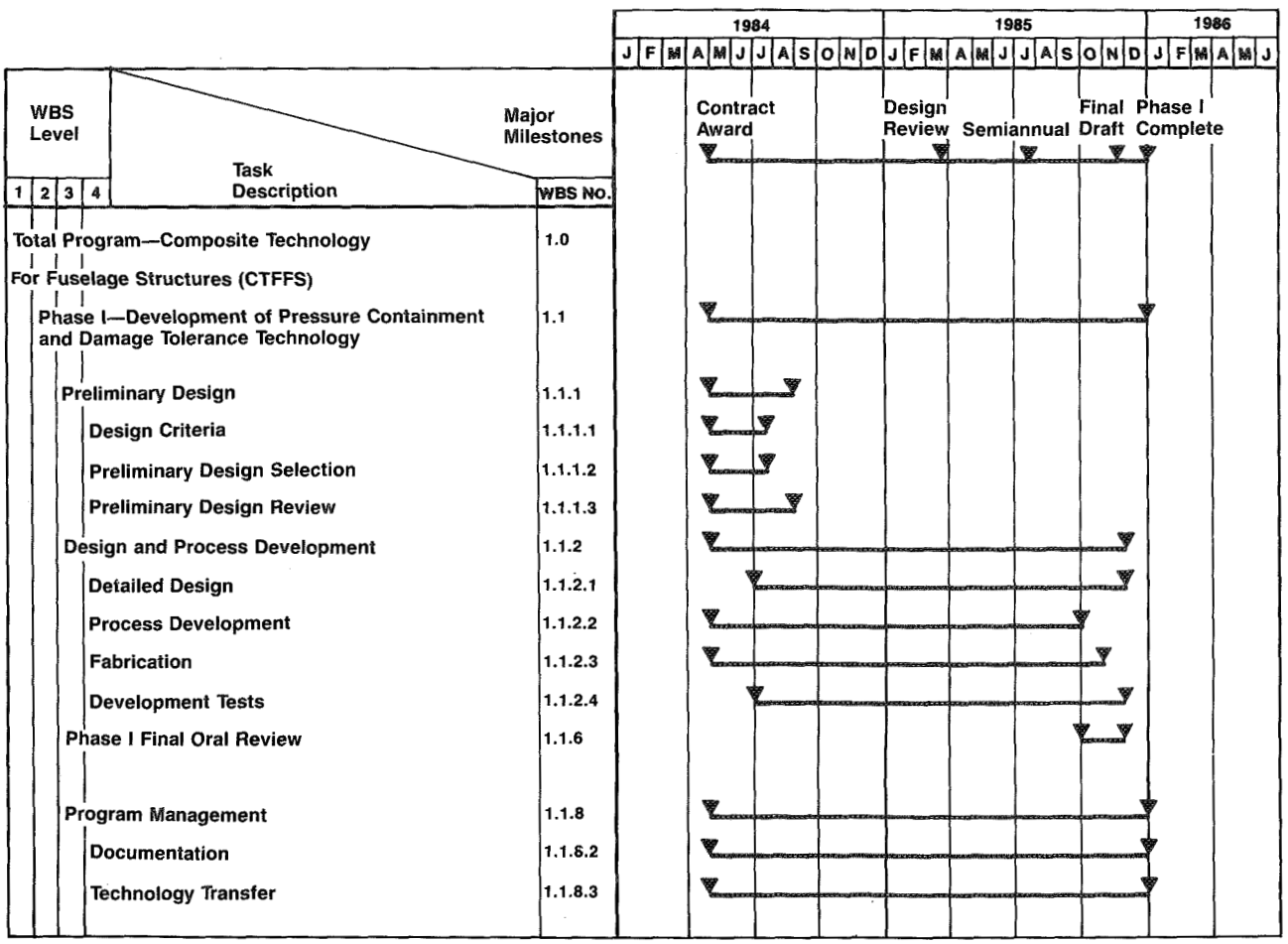

Figure 3. Program Master Schedule

Technology Issue	Tests ( ) — Number of Specimens
Pressure Damage Containment	Test 1A and 1B Flat Fracture Laminate (10) Honeycomb (2) 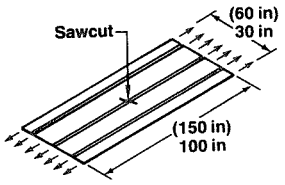 Test 2 Curved Laminate Fracture (6) 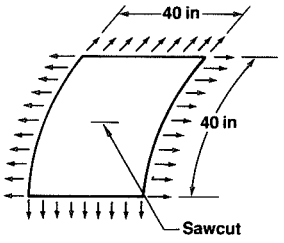
Postbuckling Skin-Stringer Design	Test 3 Single Stiffener Crippling (5) 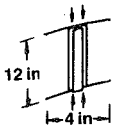 Test 4 Curved Compression Panels (4) 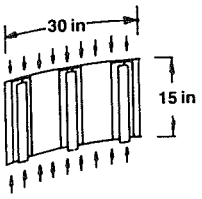 Test 5 Shear Panels (2) 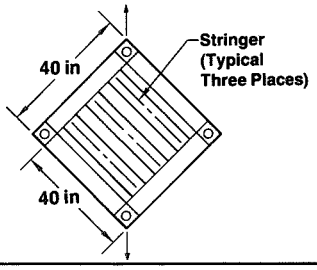
Compression Damage Containment	Test 6A Skin-Stringer Compression Panel (3) 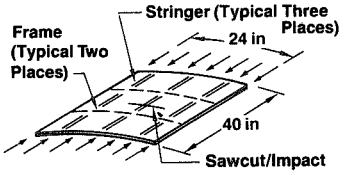 Test 6B Honeycomb Compression (2) 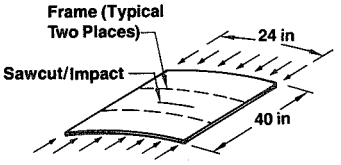
Pressure Pillowing: Shell-Frame Attachment	Test 7A Skin-Stringer (4) 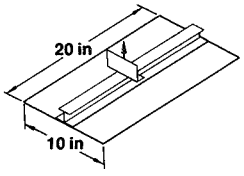 Test 7B Honeycomb (2) 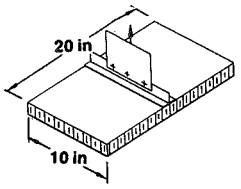

Figure 4. Phase I Test Plan Related to Technology Issues

Compression tests of skin-stringer and honeycomb shell configurations (tests 6A and 6B) provided test data to determine the adequacy of procedures for sizing shell structure for compression damage tolerance. Panels were tested with damages ranging from impacts to large discrete skin and stringer cuts.

Test 7 validated the strength of the frame-to-skin attachment to ensure the adequacy of this detail for the planned large panel demonstration tests. This detail is designed to tension loads from pressure pillowing of the skin panel between frames.

The technology development and design requirements established in these tests were intended to be verified in large panel demonstration tests and then extended in phase II for large component testing. Due to limited NASA funding, planned phase I demonstration tests and the phase II program were canceled. Additional fuselage technology was being developed by Lockheed and McDonnell Douglas aircraft companies in parallel NASA technology programs. These technologies include impact dynamics, noise attenuation, bolted joints, and cutouts.

2.0 PRELIMINARY DESIGN

2.1 Design Criteria

The Boeing 757 was chosen as a reference airplane for design development. The airplane dimensions and principal characteristics are shown in Figure 5. The reference airplane is a current technology, standard body, single aisle, medium range transport. The design study focused on the aft section of the airplane, shown in Figure 6.

The primary emphasis of the design effort focused on the shell structure, since the shell typically accounts for 43% of the total fuselage weight of a metal aircraft, as shown in Figure 7. For design development purposes, the composite designs retained the same internal and external configuration as the 757 airplane, including frame spacing, inner mold lines (IML), and outer mold lines (OML). The following items are included in the aftbody section:

- Shell structure, including skin, stringers, and frames
- 45 windows
- Two passenger doors (one per side)
- One cargo door (right side only)
- Keel beam and surrounding redistribution material
- Panel splices

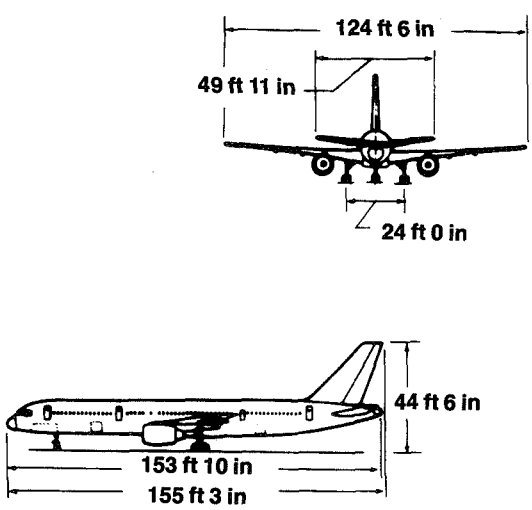

Principal Characteristics	
Maximum Taxi Weight (Basic)	221 000 lb
Maximum Takeoff Weight	220 000 lb
Maximum Landing Weight	198 000 lb
Maximum Zero-Fuel Weight	184 000 lb
Engine Thrust	37 000 lb
Passenger Capacity	175 to 200
Fuel Capacity	10 880 gal
Cargo Capacity	
All Bulk	1 770 ft^3
Cruise Air Speed	350 kn
Mach Number	0.86

Figure 5. Commercial Transport Baseline Model

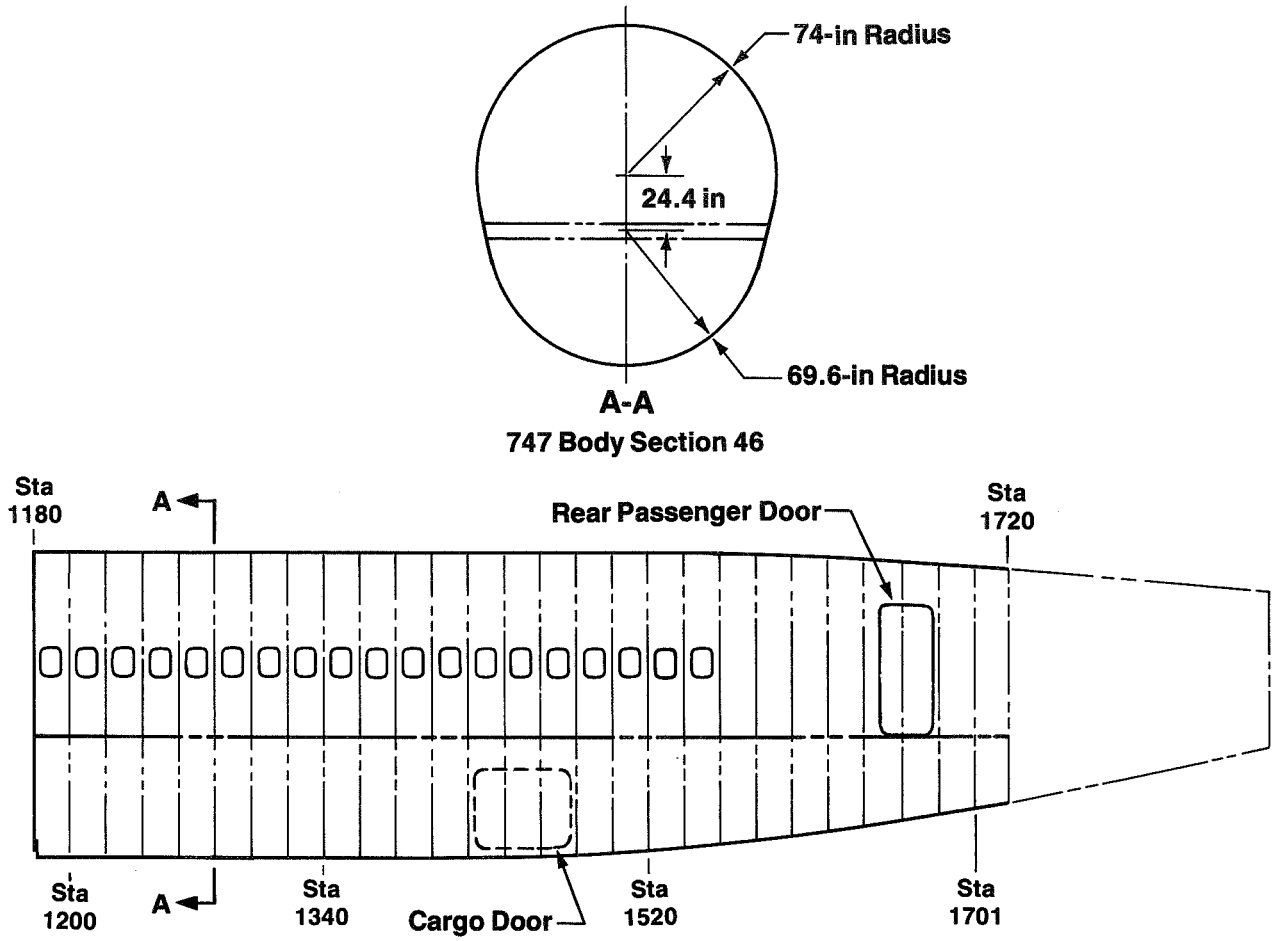

Figure 6. Fuselage Study Section

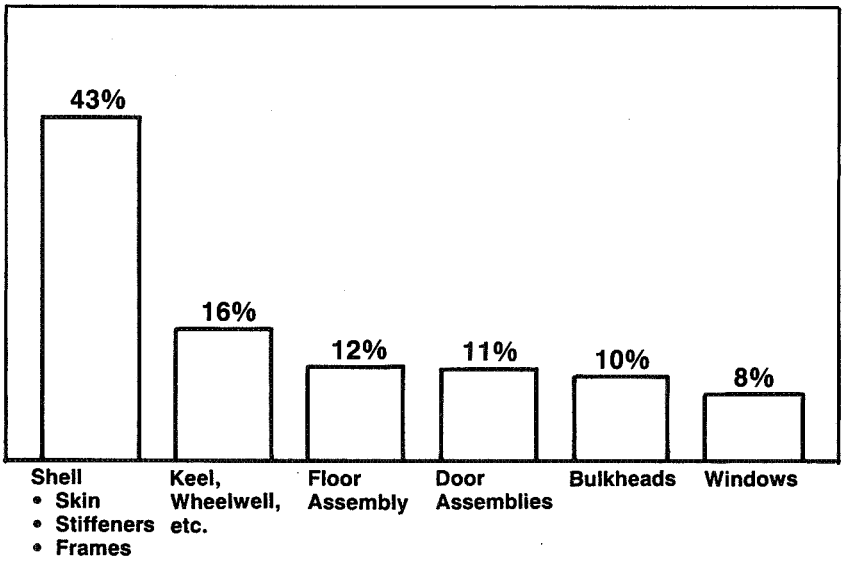

Figure 7. Commercial Transport Fuselage Typical Weight Distribution

Existing internal design loads for the 757 were used to size all parts. Design loads in the aft fuselage study section are shown in Figure 8. In the crown, the maximum tensile loads result from down-tail loads and internal pressure. In the keel, the maximum compression loads result from down-tail loads with no internal pressure. Compression loads in the crown, due to an up-tail load, define the buckling requirements for the crown skins. The tension loads in the keel, due to an up-tail load, have no significant influence on the keel design.

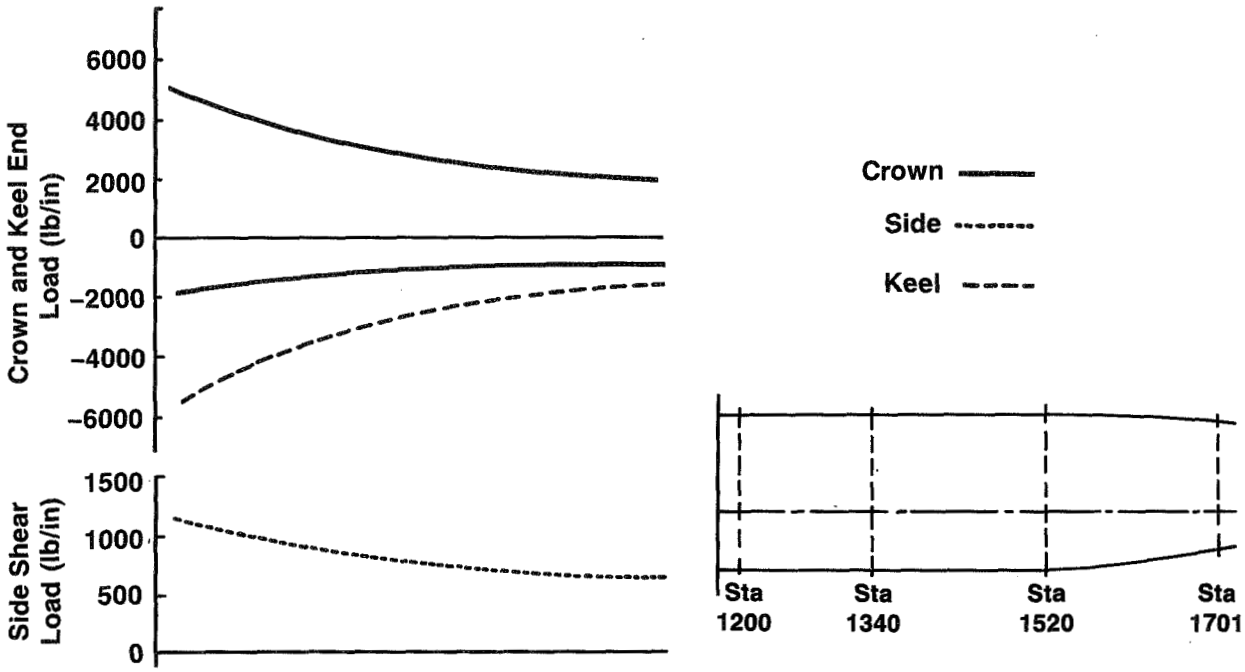

Figure 8. Design Loads

The design criteria for the composite fuselage development program are listed as follows:

1. Basic material ultimate design strains
   - Tension $\varepsilon_T = 0.006$ in/in
   - Compression $\varepsilon_C = 0.005$ in/in
   - Shear $\gamma = 0.010$

2. Pressure design load cases
   - Normal operating pressure: 8.6 lb/in^2
   - Maximum pressure relief: 9.1 lb/in^2
   - Ultimate pressure with flight loads: 1.5 x 9.1 = 13.65 lb/in^2
   - Ultimate pressure only: 2.0 x 9.1 = 18.2 lb/in^2
   - Maximum damage tolerance pressure: 9.6 lb/in^2

3. The fuselage skin panels shall be damage tolerant to a 12-in cut in any direction.

4. Laminate skin elements shall be buckling resistant to 30% design ultimate load (DUL) in stringer stiffened designs. Honeycomb sandwich skin configurations shall be buckling resistant to 100% DUL.

5. The frame stiffnesses shall be sufficient to produce an equivalent margin of safety against general shell buckling at the baseline aluminum configuration.

6. The body frames shall be shear tied to the skin over a region similar to that of the baseline aluminum configuration.

7. The composite fuselage shall be designed using balanced, symmetric cross-ply laminates with moduli in the range of 6 to 12 msi.

The ultimate material design strain values are based on the results of Boeing IR&D test programs and the NASA-funded LCPAS studies conducted by Boeing (ref. 5). The 30% DUL buckling criteria was selected to provide buckle-resistant fuselage panels at normal cruise condition. This minimizes fatigue cycling of the buckled structure and provides minimum aerodynamic drag.

Boeing uses a 12-in damage criterion to demonstrate damage tolerance. This criterion allows damage to occur at any location in the skin and to completely sever a frame and/or a stringer. The damage is arrested at the next frame or stringer. Integrally co-cured tear straps are incorporated into the shell design to provide the arrest mechanism. Tear strap design curves, shown in Figure 9, were developed in NASA contract NAS1-17417 (ref. 1).

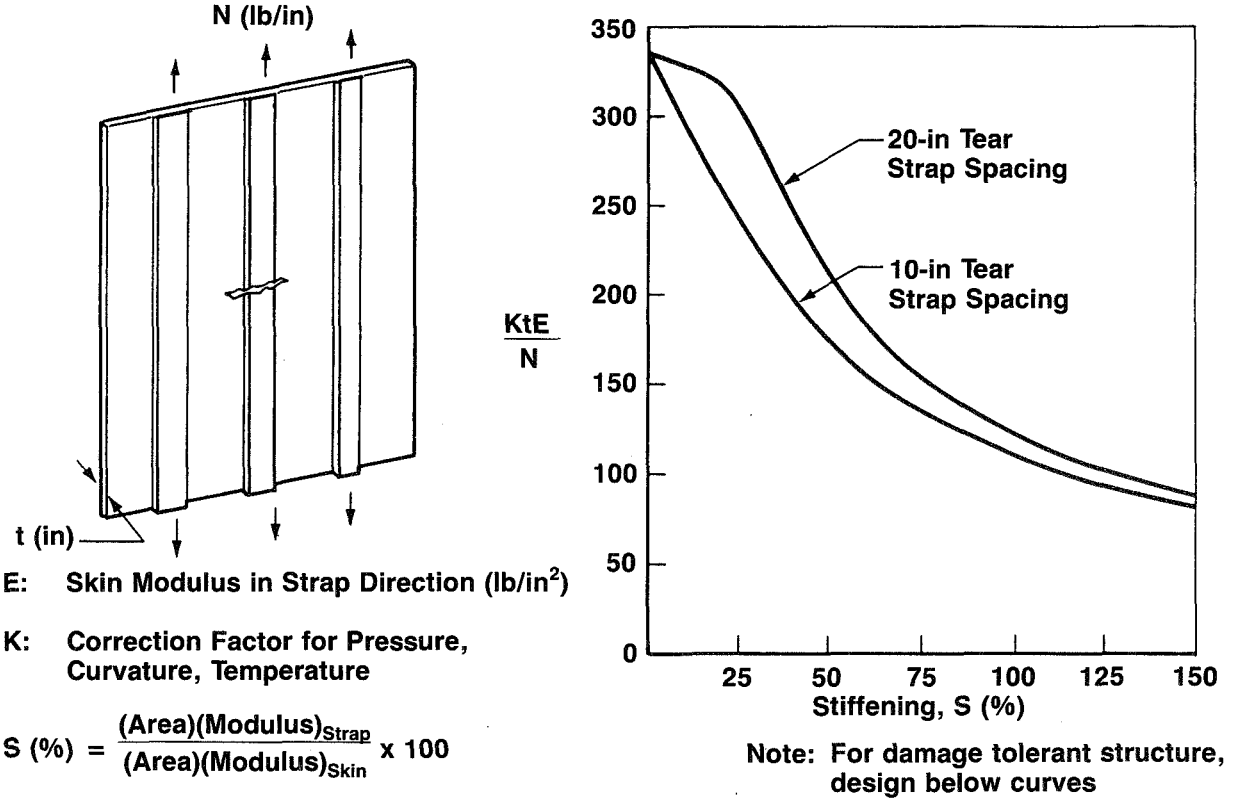

Figure 9. Tear Strap Design Curves

Stability requirements for the fuselage design include local stringer buckling, column stability, local panel buckling, and general cylinder stability. The stringer elements were designed to be stable to DUL. The column stability of stringer-skin elements between adjacent frames was analyzed using the conventional Euler column relationship. An effective width of unbuckled skin was included in the stiffness of the element. The laminate skin panels were designed to remain stable until 30% DUL, and honeycomb skins were designed to be stable until 100% DUL. The skin panel thickness requirements were calculated based on Boeing analysis code LEOTHA. The procedure, originally developed by Davenport (refs. 6 and 7), was expanded to address the orthotropic characteristics of composite laminates. Example laminate and honeycomb design curves are shown in Figures 10 and 11.

The crown frame stiffness was designed to resist general shell instability for the up-tail body-bending load case. The end load capability of the skin-stringer-frame configuration at the crown was determined using a Boeing version of the computer code GIOS, described in Reference 8. This code computes the general shell buckling load of a longitudinally and circumferentially stiffened cylinder. The composite frame sections were sized at each body station by comparing the critical load with that of the baseline aluminum configuration at the same location.

In addition to the basic criteria, several design ground rules were established. The designs were based on using grade 145 graphite-epoxy tape with a 0.0056-in thickness per ply. This grade of tape allows more flexibility in laminate tailoring than thicker grade tapes. The tape material is normally supplied in 3-in widths and was compatible with automated layup facilities. The laminate stacking sequences were built up by orienting plies at 0 deg, 45 deg, -45

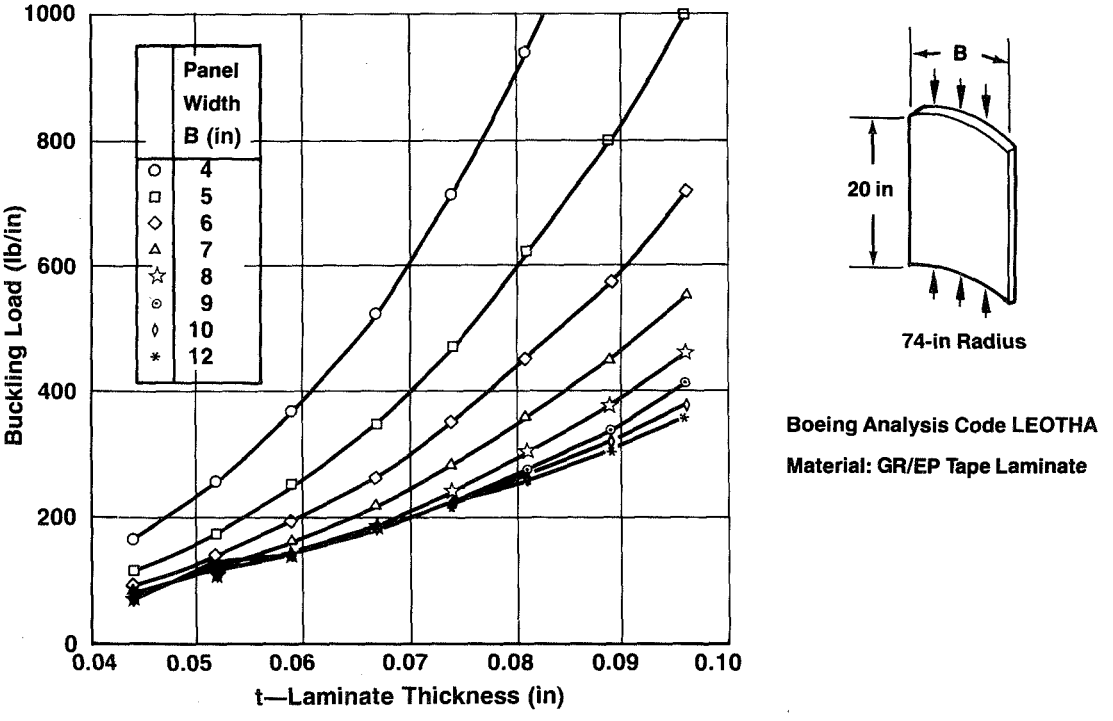

Figure 10. Buckling of Curved Laminate Fuselage Skin Panels

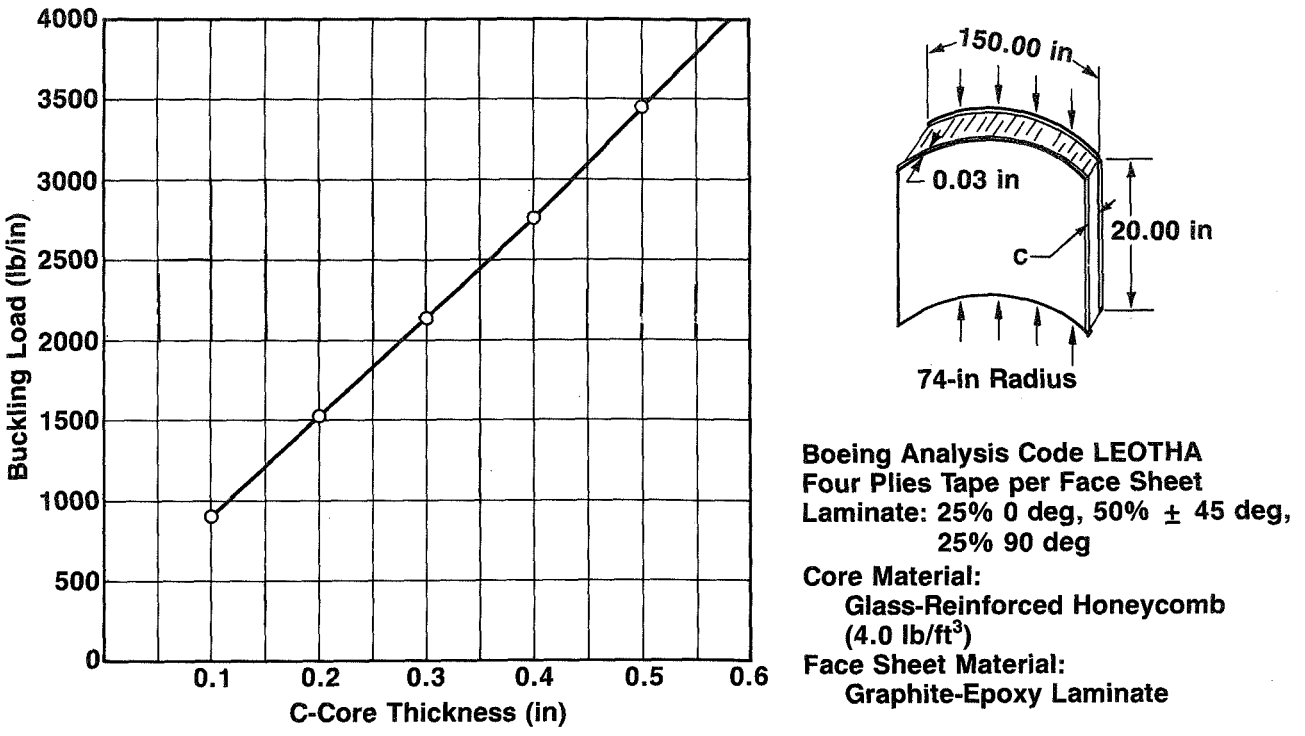

Figure 11. Buckling of Curved Honeycomb Fuselage Skin Panels

deg, or 90 deg, with respect to the longitudinal direction of the fuselage. Laminate warping during curing was minimized by using balanced and symmetric stacking sequences whenever possible. In addition, stackups of more than five plies of a single orientation and 90-deg interfaces between plies were discouraged to minimize interlaminar stresses. Underneath the stringer, the skin was padded up with 0-deg-oriented plies. In addition to the damage containment capability of the section, the added bending stiffness of the padup helps to reduce the tendency of the skin buckles to propagate into the stringer. A precured strip was placed between the skin and stringer. This prevented the stringer from sinking into the skin during cure.

2.2 Preliminary Design Selection

Six fuselage shell concepts were developed under NASA contract NAS1-17417 (ref. 1). All design concepts were developed to a level sufficient for comparing structural efficiency, weight, and ease of manufacturing. These six design concepts are:

- Concept 1, frame stiffened honeycomb skin (fig. 12)
- Concept 2, I-section stringer stiffened laminate skin (fig. 13)
- Concept 3, hat-section stringer stiffened laminate skin with frames co-cured to skin (fig. 14)

- Concept 4, hat-section stringer stiffened laminate skin with frames mechanically attached to skin (fig. 14)
- Concept 5, I-section stringer stiffened honeycomb sandwich skin (fig. 15)
- Concept 6, hat-section stringer stiffened honeycomb sandwich skin (fig. 15)

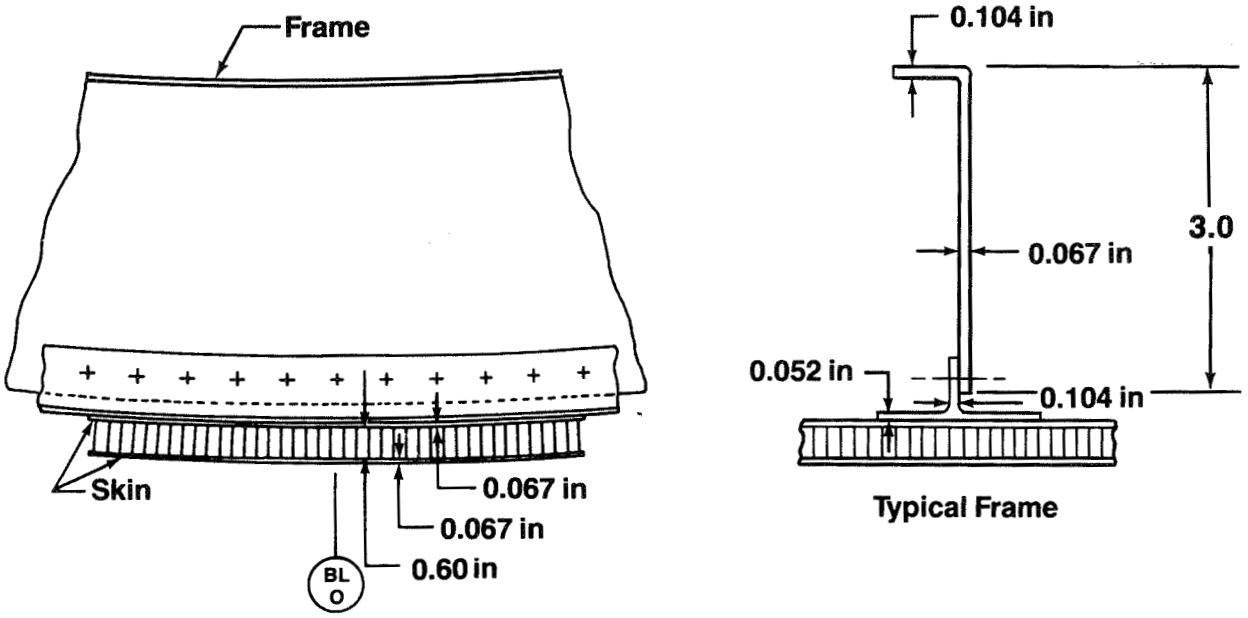

Figure 12. Concept 1—Honeycomb Sandwich Skin

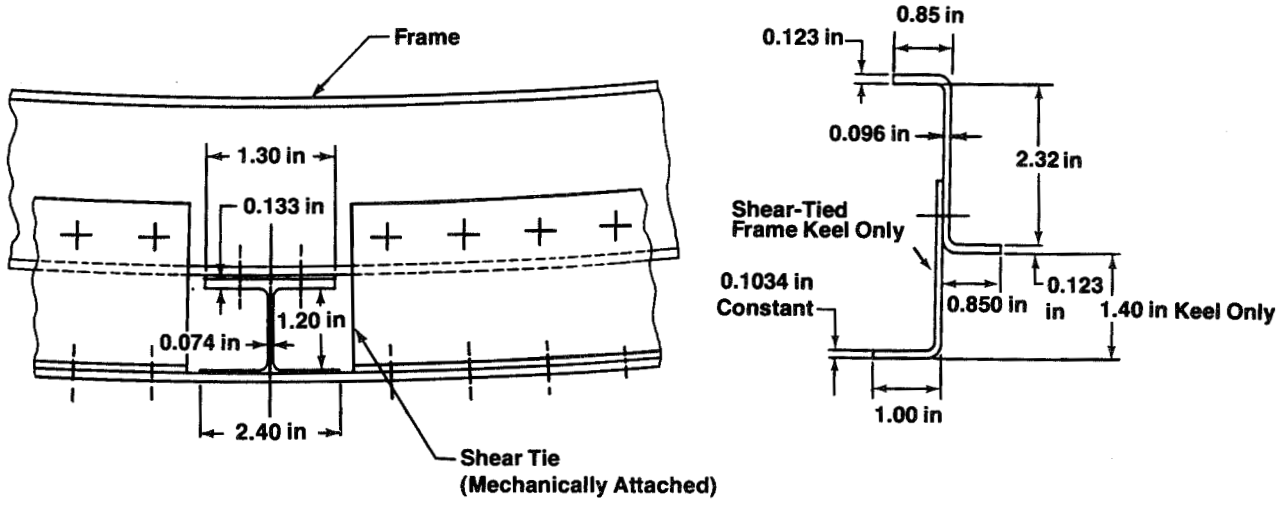

Figure 13. Concept 2—Laminate Skin With I-Section Stringers

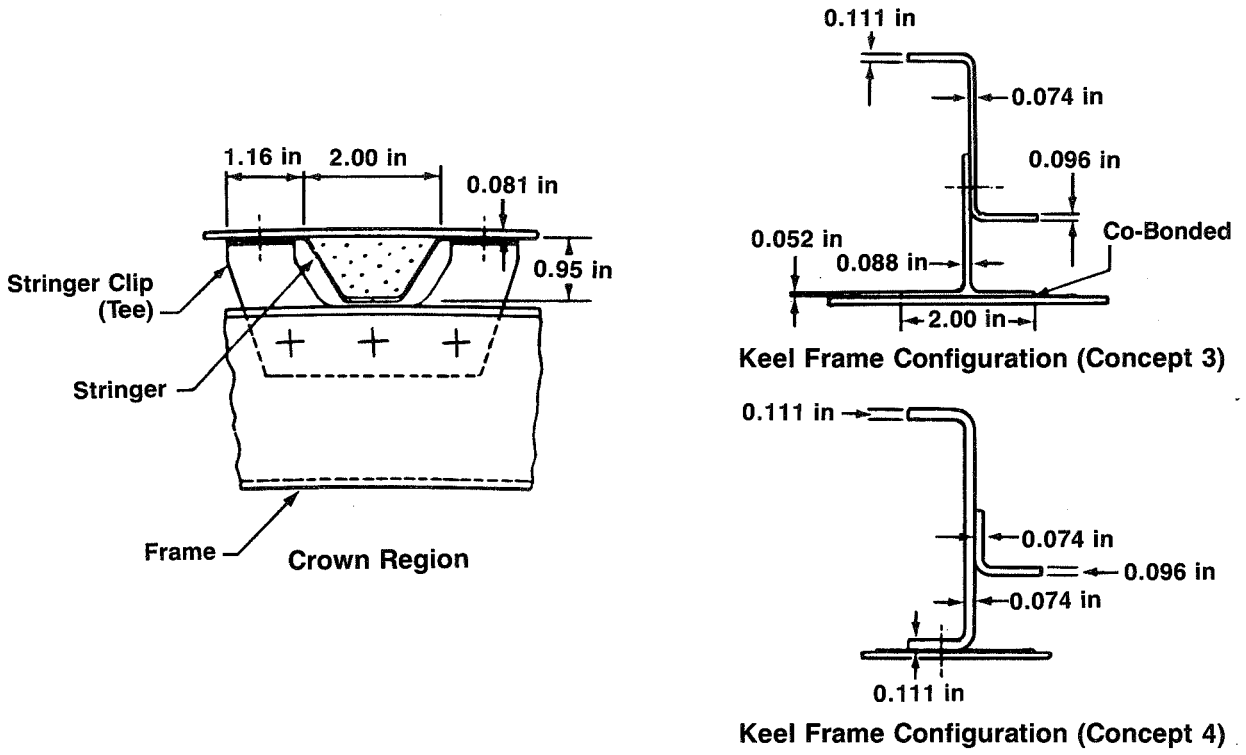

Figure 14. Concepts 3 and 4—Laminate Skin With Hat-Section Stringers

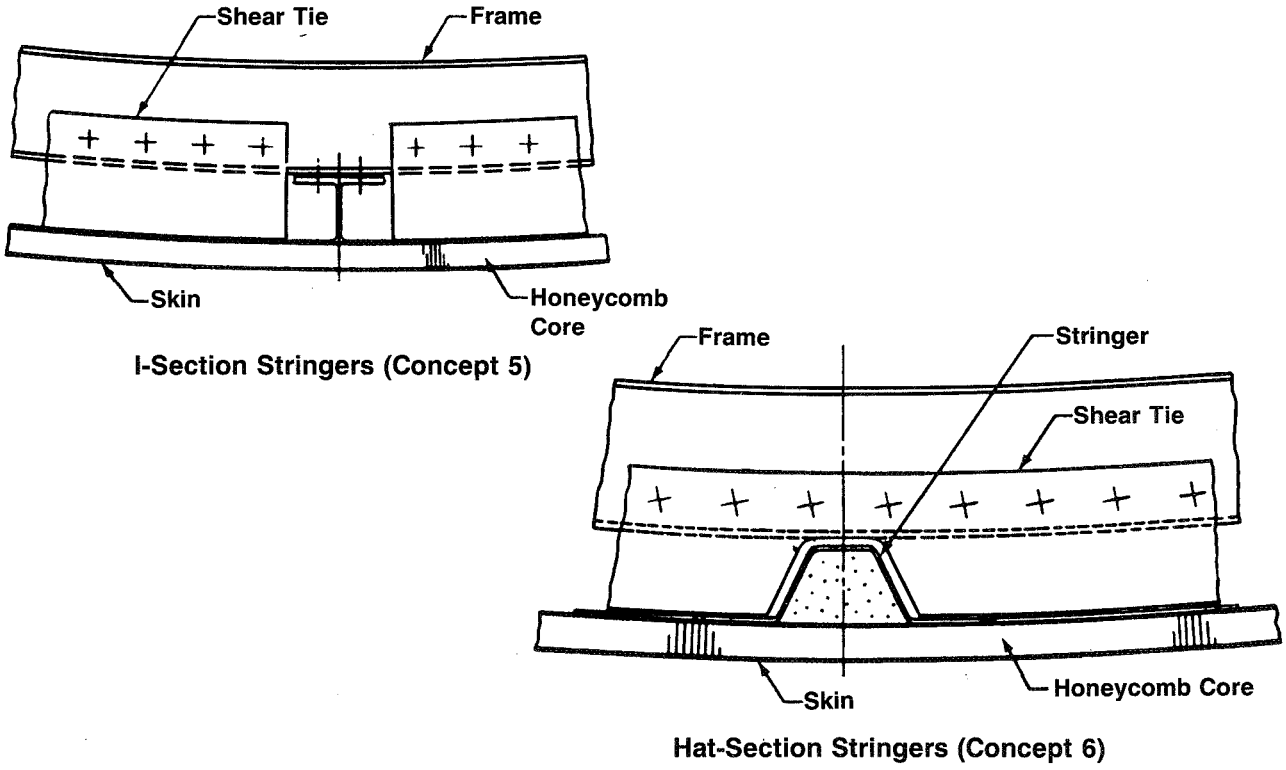

Figure 15. Concepts 5 and 6—Honeycomb Sandwich Skin With Discrete Stringers

Weight comparisons of the six graphite-epoxy design concepts to a baseline aluminum design for a 540-in fuselage study section were determined, and producibility of the concepts was evaluated in terms of recurring factory labor requirements. The results of the weight and producibility studies are summarized in Figure 16. A more complete discussion of the cost and weight analysis is presented in Reference 1.

Fuselage Study Program Shell Concept (Reference NAS1-17417)		Shell Weight Reduction (%) [1]	Basic Factory Labor (hr) [2]
1	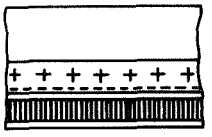 Honeycomb Sandwich No Stringers	28	1000
2	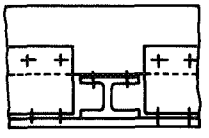 Laminate Skin I-Section Stringers	28	1050
3	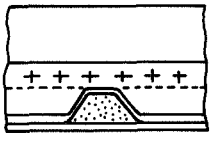 Laminate Skin Hat-Section Stringers Frame Bonded to Skin	32	1040
4	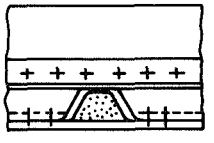 Laminate Skin Hat-Section Stringers Frame Mechanically Attached to Skin	29	1040
5	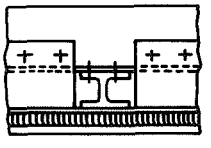 Honeycomb Sandwich Skin I-Section Stringer	29	1280
6	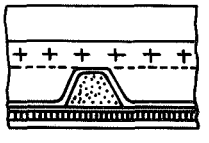 Honeycomb Sandwich Skin Hat-Section Stringer	30	1400

[1] For study section 540 in long

[2] Normalized labor hours based on fabrication of constant section with body frames at 20-in spacing. Studies have shown a 30% cost reduction for a shell manufactured of advanced composites rather than aluminum

Figure 16. Weight and Cost Study Results of Candidate Fuselage Shell Concepts

Concepts 1 and 2 were selected for the current program and represent two fundamentally different approaches to fuselage design in that the honeycomb design is buckling resistant up to DUL, while the skin in the laminate stiffened design is permitted to buckle at 30% DUL. The foam filled hat-section designs, concepts 3 and 4, were not selected even though the relative weights and costs were better than the I-section stringer. An extensive inspection evaluation was performed on the hat-section stringer, and the results showed that the foam filled hat-stringer panels are not fully inspectable by current technology. Ultrasonic through-transmission sound waves that are used during inspection are attenuated through the foam material, thus obscuring any detection signals. Other inspection methods, such as ultrasonic pulse echo, radiography, thermal imaging, and optical laser holography, do not provide adequate inspection quality for the foam filled stringers at this time. Concepts 5 and 6 were not considered due to high labor costs even though they are weight competitive.

The frame stiffened honeycomb design (concept 1) and the I-section stringer stiffened design (concept 2) were incorporated into the design of developmental test hardware. The updated designs are discussed in Section 3.1, Detailed Design.

2.3 Material Selection

The considerations in selecting the materials for aircraft structure include operating environments, design configurations, structural loading requirements, manufacturing producibility, reliability, costs, and systems integration. Figure 17 lists these considerations. Both qualitative and quantitative procedures are used in comparing material performance and requirements. In addition to development program data, the knowledge gained on production aircraft programs is used. This knowledge includes that obtained during design, production, and service.

Selection procedures and criteria used for secondary materials such as adhesives, honeycomb core, core splice materials, coatings, and potting compounds are similar to those used for the primary structural materials.

The material selected for the laminate test panels, fabricated during phase I, is Hercules 2220-3/AS6, grade 145 tape (0.0056-in thickness/ply). The factors considered in making this selection include basic property data, manufacturing and inspection experience, and large panel tests performed on the LCPAS wing program (NAS1-16863, ref. 5), as well as the Air Force Damage Tolerance program (contract F33615-82-C-3213, ref. 9).

Hercules 2220-3 is classified as a toughened resin system and improved properties have been verified on coupon and stiffened panel tests. The AS6 high strain fiber was chosen for its improved tensile elongation, which is required for the pressurized fuselage shell damage tolerance requirements. Grade 145 tape was selected because it allows better tailoring of skin and stiffener laminates than higher grade materials. The 2220-3/AS6 mechanical property data used for the design of the test panels is presented in Figure 18. The specimen configurations used to obtain the data are shown in Figures 19 and 20.

A. Environmental effects
   - Operational temperatures
   - Moisture temperatures
   - Weather environments
   - Aircraft fluids
   - Emergency conditions and fire resistance

B. Design/Structures
   - Strength and weight
   - Fatigue
   - Damage tolerance
   - Bearing strength
   - Fiber forms

C. Manufacturing/Cost
   - Productibility
   - Compatibility with automation
   - Inspectability
   - Cost—labor and materials efficiency
   - Product consistency
   - Processing criticality
   - Repairability

D. Systems integration
   - Direct lightning effects
   - Indirect lightning effects on systems
   - System attachments and interfaces—corrosion
   - Electrical bonding and grounding
   - Electrical returns—primary and fault currents

Figure 17. Material Selection Criteria

Test	Average Test Value
0-deg Tension Strength, ksi, Room Temp.	314
0-deg Tension Modulus, msi, Room Temp.	20.0
0-deg Tension Strain,* %, Room Temp.	1.57
Open-Hole Tension, ksi, Room Temp.	64
0-deg Compression, ksi, Room Temp.	192
0-deg Compression, ksi, 200°F Dry	158
0-deg Compression, ksi, 180°F Wet	160
Open-Hole Compression, ksi, Room Temp.	49
Open-Hole Compression, ksi, 180°F Wet	38
Compression After Impact, ksi, 1500 in-lb	23.6

*Calculated from measured modulus and tension ultimate

Figure 18. Hercules 2220-3/AS6 Mechanical Property Data

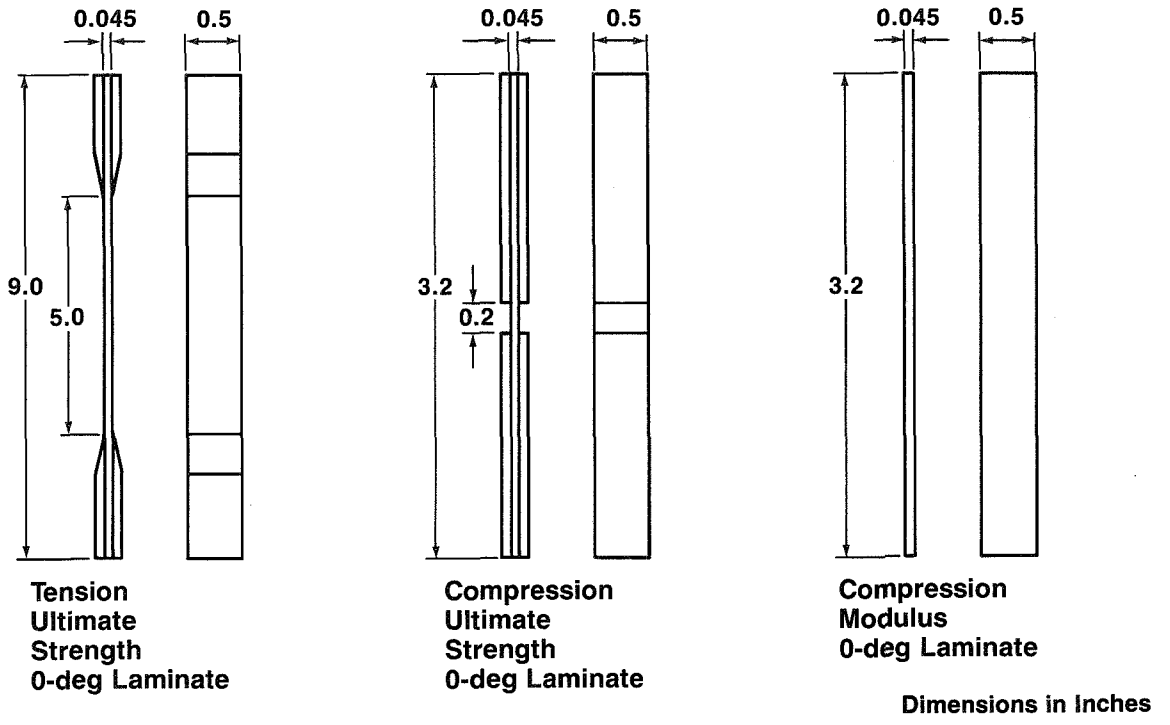

Figure 19. Tension and Compression Coupons

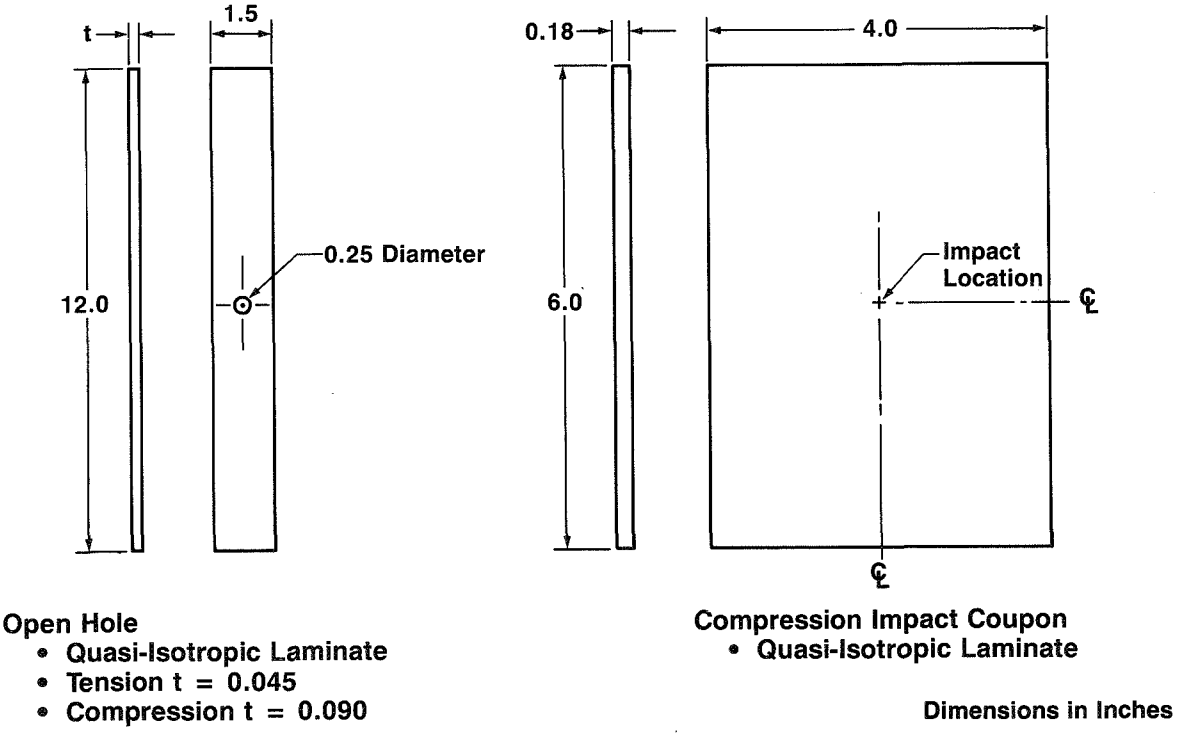

Figure 20. Open-Hole and Compression Impact Coupons

The considerations for selecting a composite material system for honeycomb sandwich skins include all of the criteria identified in Figure 17 and additionally:

1. The pressure applied to sandwich parts during autoclave curing is limited by the strength of the honeycomb core. The pressure is normally 45 lb/in^2; therefore, the skin material must process into a void-free laminate at that pressure.

2. Compatibility among core material, adhesive, and uncured face skin material must be considered.

Four graphite-epoxy material systems were evaluated for use in honeycomb sandwich structures. The resin systems were (1) Hercules 2220-3, (2) Ciba-Geigy 2566, (3) Hexcel F584, and (4) Narmco 5245. In each case, the resin system was combined with AS6 fibers to make a composite prepreg.

The candidate materials were tested as the face sheets in honeycomb sandwich long beam flexure tests. The specimens were co-cured with FM300 adhesive between the graphite-epoxy face sheets and the honeycomb core using standard fabrication procedures. The Narmco resin system was unsuitable for co-curing at 45 lb/in^2 and was eliminated from further consideration. Layups and test panels representative of fuselage structure were designed to achieve design ultimate compression strains in the face sheets. The specimen configurations and the test results are presented in Figure 21. The four-point loading configuration provides a span in the center of the specimen that is free of shear and has a constant bending moment. The test setup, shown in Figure 22, is based on MIL-STD-401.

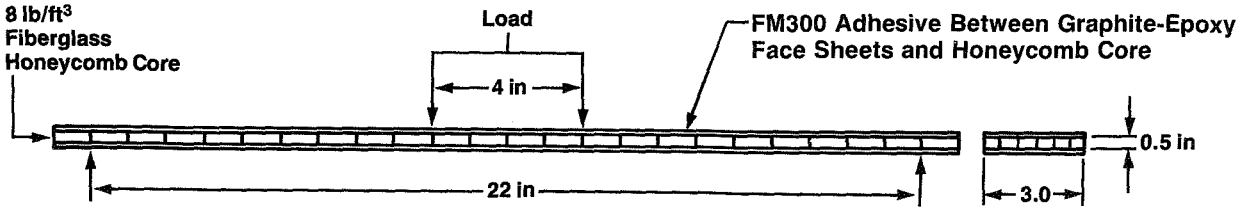

Long Beam Flexure Test Setup

Material	Fiber Grade	Face Sheet Thickness (in)	Face Sheet Layup	Failure Strain (in/in)
Hercules 2220-3/AS6	190	0.051	$(45/0/-45/90)_s$	0.0080
Ciba-Geigy 2566/AS6	190	0.050	$(45/0/-45/90)_s$	0.0087
Hexcel F584/AS6	145	0.051	$(45/90/-45/0_3)_s$	0.0090

Figure 21. Honeycomb Configuration and Test Results

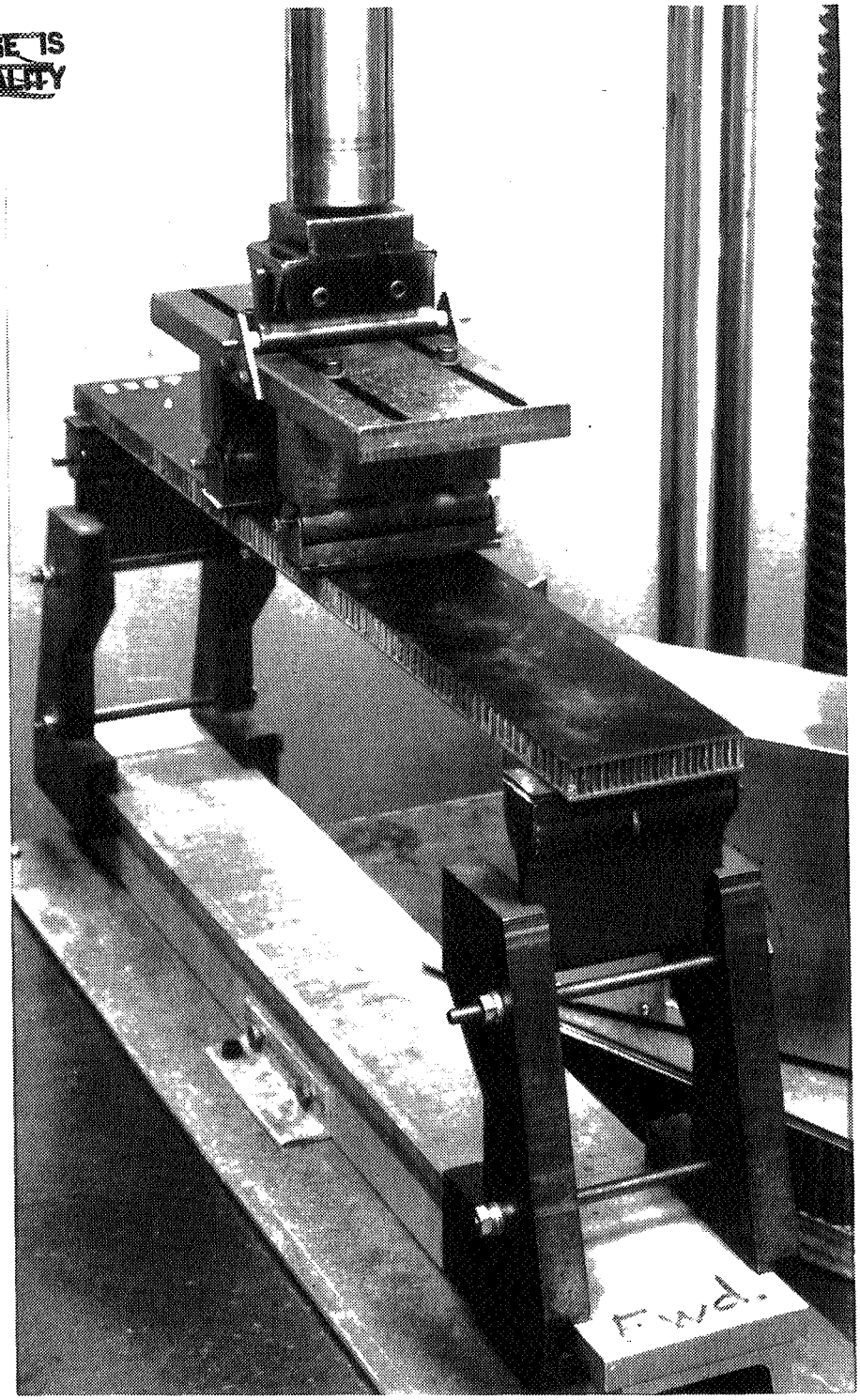

Figure 22. Long Beam Flexure Test

The Hexcel material strain to failure (fig. 21) was highest, and the photomicrographs show a more uniform laminate with less porosity for the Hexcel material than for the other materials (figs. 23 through 25). For these reasons, the Hexcel material was selected for use in honeycomb sandwich structure.

The core material selected for the sandwich panels is Hexcel HFT honeycomb. HFT is a biased weave glass fabric impregnated with a heat resistant resin. This core was selected because the biased weave fabric gives the best structural efficiency.

Tests used for characterizing the mechanical, physical, chemical, and processibility of the Hexcel material were performed and are discussed in Section 4.0, Process Development.

ORIGINAL PAGE IS
OF POOR QUALITY

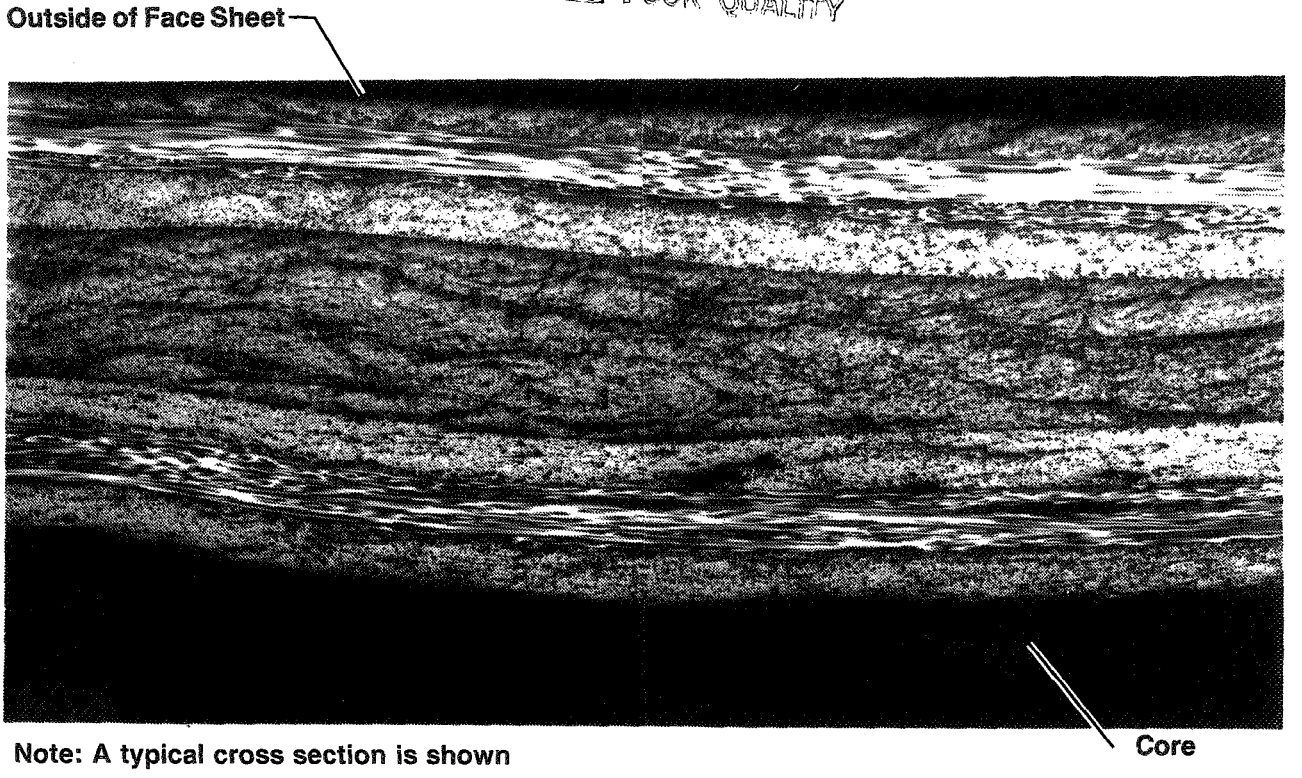

Figure 23. Photomicrograph of the Hexcel F584/AS6 Material System

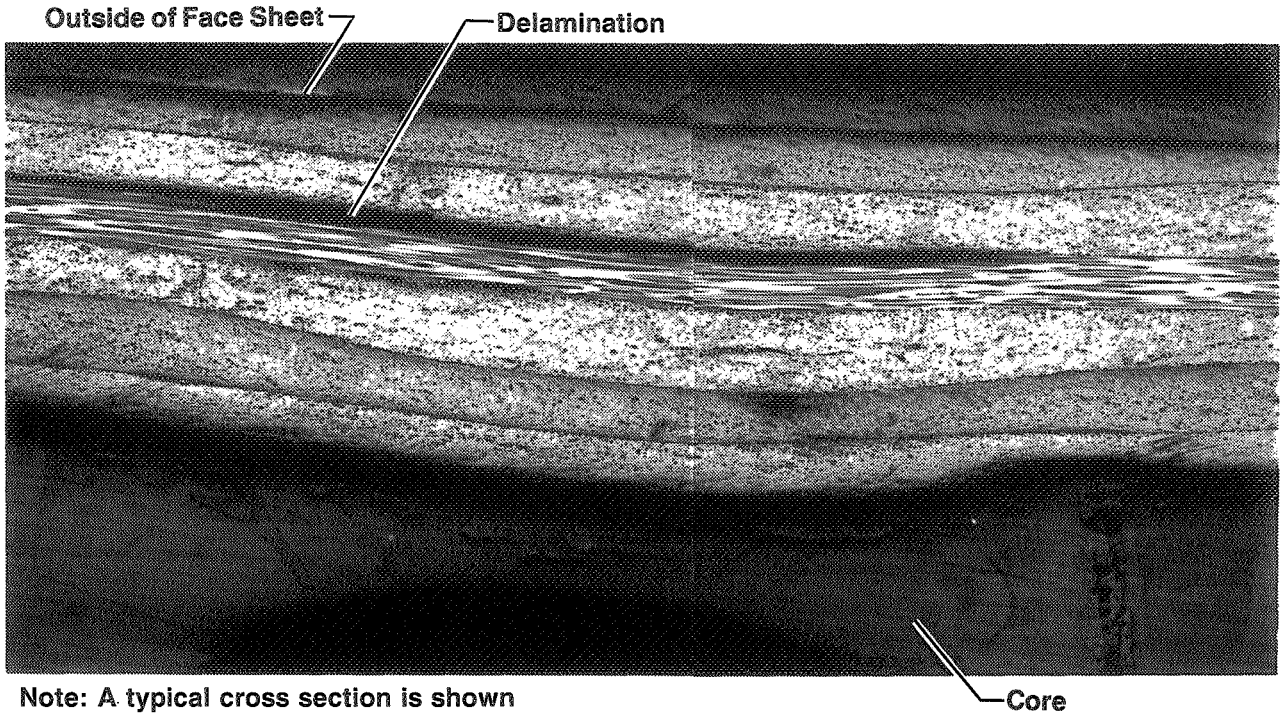

Figure 24. Photomicrograph of the Hercules 2220-3/AS6 Material System

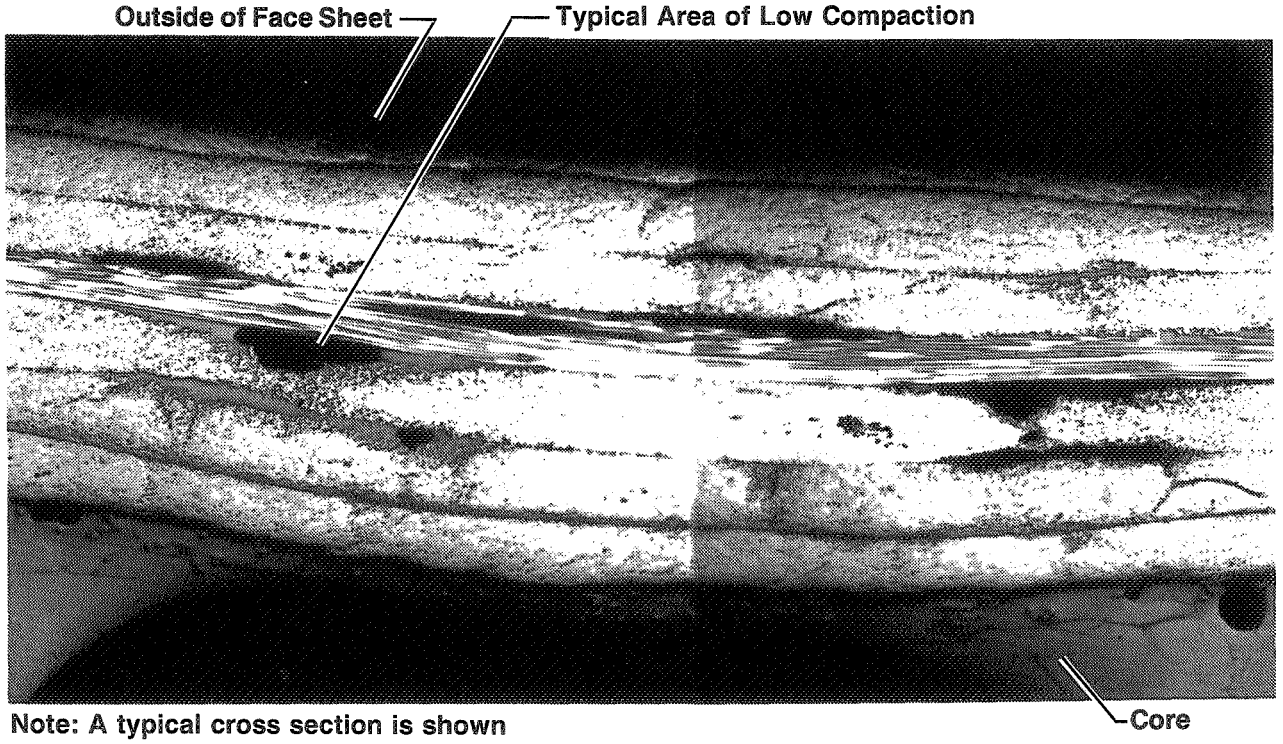

Figure 25. Photomicrograph of the Ciba-Geigy 2566/AS6 Material System

3.0 DETAILED DESIGN

Detailed designs were initially performed to define the test panels. The concepts developed were (1) a laminate skin design with I-section stringers and (2) full depth honeycomb sandwich skin. The basic configuration of these designs is discussed in Section 3.1.

A detailed design for the total study section (fig. 6) was performed to provide a base for calculating a total fuselage weight reduction. The laminate skin design with I-section stringers was selected for this task. The details of the fuselage study section design are discussed in Section 3.2. The weight reduction results are presented in Section 3.3.

3.1 Concept Development

The detailed designs used for defining the development test sections are discussed in following sections.

3.1.1 Laminate Skin With I-Section Stringers

The general configuration of the I-section stiffened skin shell concept is shown in Figure 26. The major subassemblies of this concept are:

1. Co-cured skin I-section stringer panels

2. Zee-section body frames

3. Shear-tied angles (keel and side regions)

In the crown region, the stringers are spaced 10 in apart. This spacing was selected to provide adequate stiffening for buckling requirements due to compression loads that result from up-tail fuselage bending loads. In the keel region, where compression load requirements are more severe, a narrower stringer spacing is better for stiffness and stability requirements. The 8-in stringer spacing in the keel was selected to provide sufficient space for frame shear ties.

Typical skin-stringer dimensions for a crown and keel section are shown in Figure 27. Laminate stacking details for a typical crown and keel section are shown in Figure 28. All of the I-section stringers were designed with a web height of 1.2 in. This allows common tooling to be used throughout the fuselage. A precured strip (fig. 28) is placed between the stringer and skin laminate to reduce localized pressures developed during cure and to prevent the stringer from sinking into the skin laminate.

The stringers were designed with a high number of 0-deg plies in the cap to carry a majority of the axial loading and to create an efficient stringer section for column stability. The skins were sized to be stable up to 30% of the DUL using cross-ply laminates containing a high percentage of layers oriented at ± 45 deg. The stringer web and free flange dimensions were selected to eliminate localized buckling or crippling.

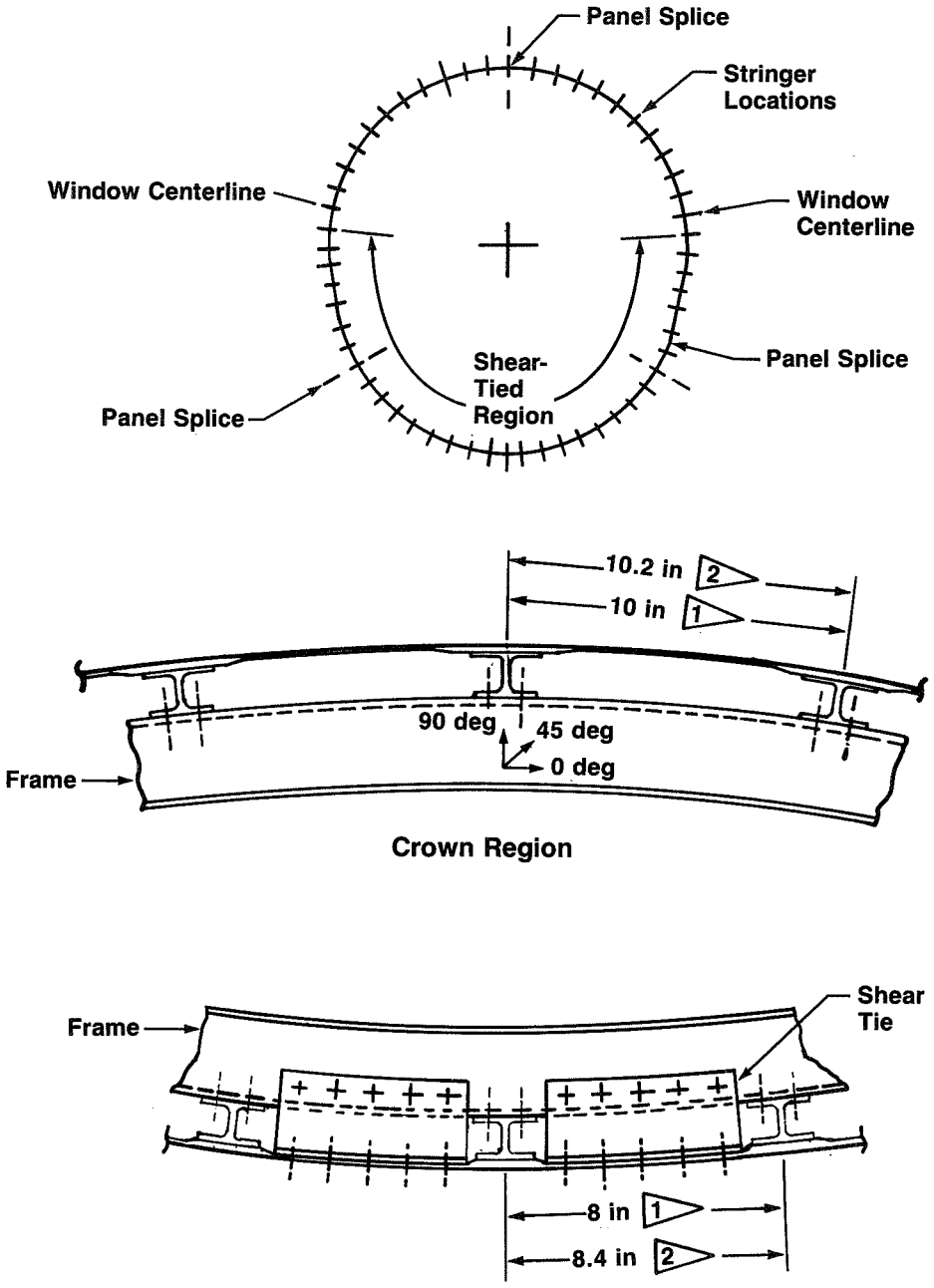

Figure 26. Skin-Stringer Shell Concept

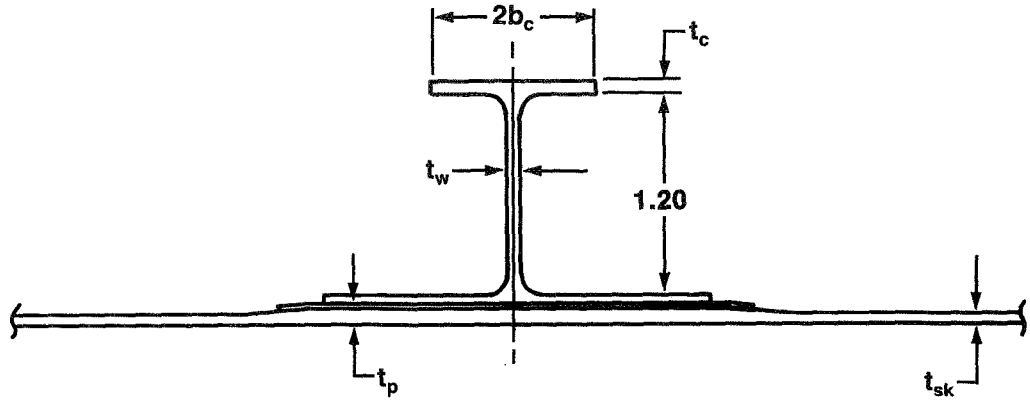

	Crown Station 1460	Keel Station 1200
Stringer Spacing	10	8
Skin Padup (t_p)	0.095	0.118
Skin Thickness (t_{sk})	0.056	0.067
Skin Laminate	0/8/2	2/8/2
Web Thickness (t_w)	0.067	0.112
Web Laminate	2/8/2	10/8/2
Cap Thickness (t_c)	0.062	0.112
Cap Laminate	4/6/1	11/8/1
Cap Width ($2b_c$)	1.00	1.25

- Laminate Definition (0 deg/ ± 45 deg/90 deg)
- Ply Thickness: 0.0056, All Dimensions Inches

Figure 27. Typical Skin-Stringer Details

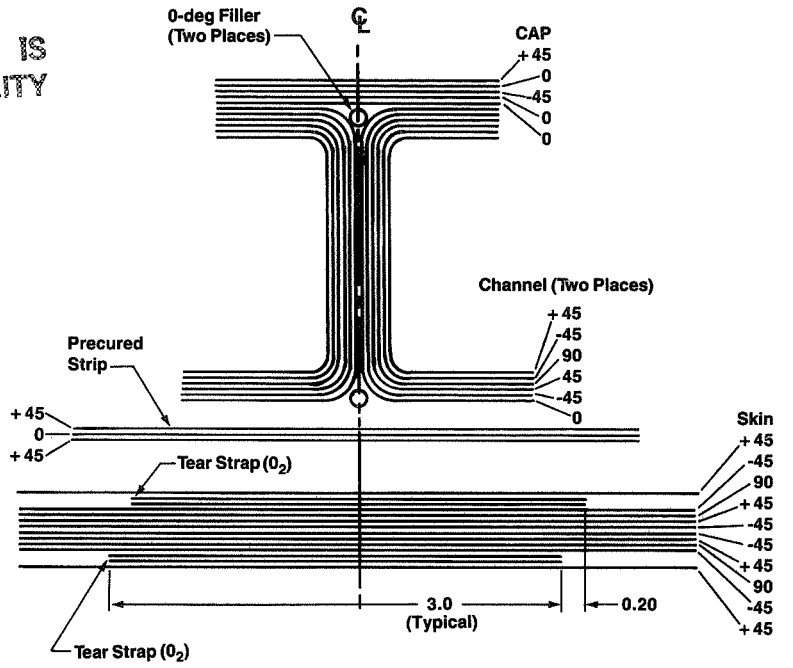

a. Crown Station 1460

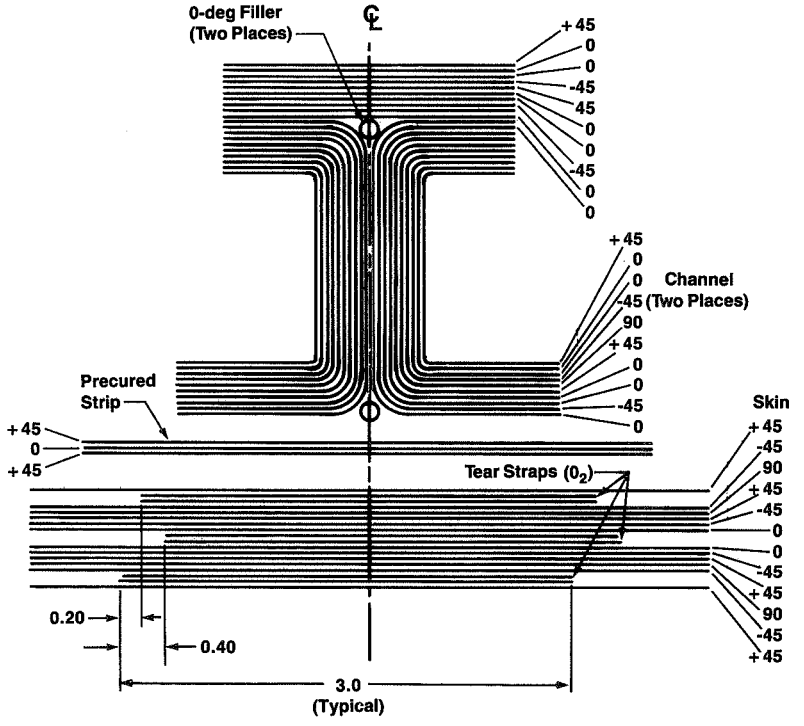

b. Keel Station 1200

- Dimensions in Inches
- Ply Orientation in Degrees

Figure 28. Typical Crown Panel and Keel I-Stringer and Skin Layups

Longitudinal 0-deg tear straps were located in the skins under the stringers to provide axial load capability, allow the basic skin to be softened, and provide damage tolerance. The longitudinal tear straps (0-deg orientation) consist of 3-in-wide tape interleaved into the skin directly under the stringers, shown in Figure 28. The circumferential tear straps (90-deg orientation) are located at the body frame locations, perpendicular to the fuselage longitudinal direction to provide damage containment (fig. 29).

The skin, stringer, and tear strap details were tailored to the load requirements (fig. 8) of the fuselage section. Laminate stacking sequences were selected at the high load forward end of the fuselage section, and plies were dropped out as the load level decreased in the aft direction. The ply drop-off sequence was arranged to maintain well balanced and symmetric laminates at all cross sections. Tailoring of the design to the loads did not always permit true balance and symmetry in the stringers along the entire length of the section. The laminate in the cap-flange section at crown station 1460 (fig. 28) is not symmetric. This amount of laminate asymmetry in the I-stringer flange did not cause unacceptable warping during fabrication of the developmental test articles.

The body frames are zee-sections as shown in Figure 30. The frame depth was selected to maintain an IML consistent with the 757 aircraft. The basic web section is fabricated with 10 plies of fabric. The shear capability of the web is obtained by orienting a high percentage of the fabric at 45 deg to the frame length. The bending stiffness of the frame is enhanced by interleaving 0-deg-oriented tape into the zee-section flanges.

When pressurized, the fuselage shell is restrained by the body frames. In the upper quadrant area, the frames are mechanically attached to the cap flanges of the I-section stringer, as shown in Figure 31. The frame-to-stringer attachment must resist the pull-off loads that result from the pressure pillowing. In the frame-to-stringer attachment area, the width of the cap flange is selected to provide an adequate fastener edge margin. Since this width requirement exceeds that for structural strength and stability, the stringer cap width is tapered to a narrower width between frames, as shown in Figure 31. Requirements for radius filler reinforcement under the cap flanges were evaluated in a series of pressure pillowing tests in the development test program (sec. 6.4).

The body frames are shear tied to the skin in the keel and side panel region similar to that of the baseline aluminum configuration, as shown in Figure 26. The number of shear ties at a particular location depends on localized load requirements. In regions adjoining doors and other cutout structures, the number of shear ties is increased to improve load distribution.

3.1.2 Full Depth Honeycomb Sandwich Skin

The skin configuration for the honeycomb concept was designed to meet all requirements of extensional strain and stability without need for stringers. Body frames are mechanically attached to a tee-section that is co-cured to the honeycomb skin panel (fig. 32). Typical sections and laminate definitions are shown in Figures 33 and 34.

Circumferential and longitudinal tear straps are contained in the skin panel to provide damage containment. The circumferential tear straps are located in the inner skin under the frame-tee, as shown in Figure 33. The longitudinal tear straps are located in the outer skin,

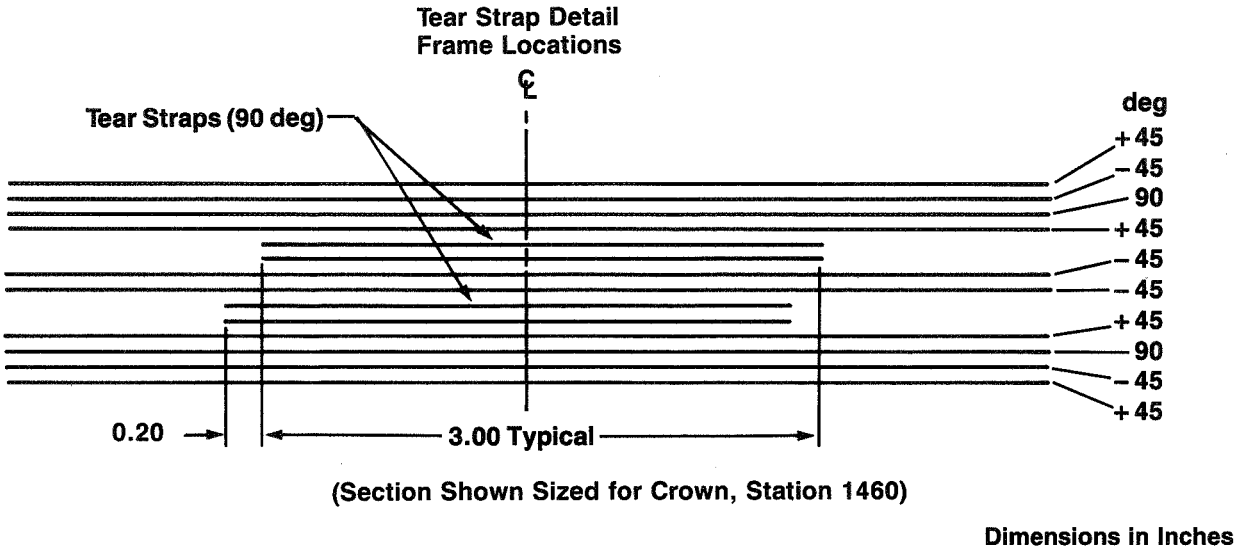

Figure 29. Typical Circumferential Tear Strap Detail

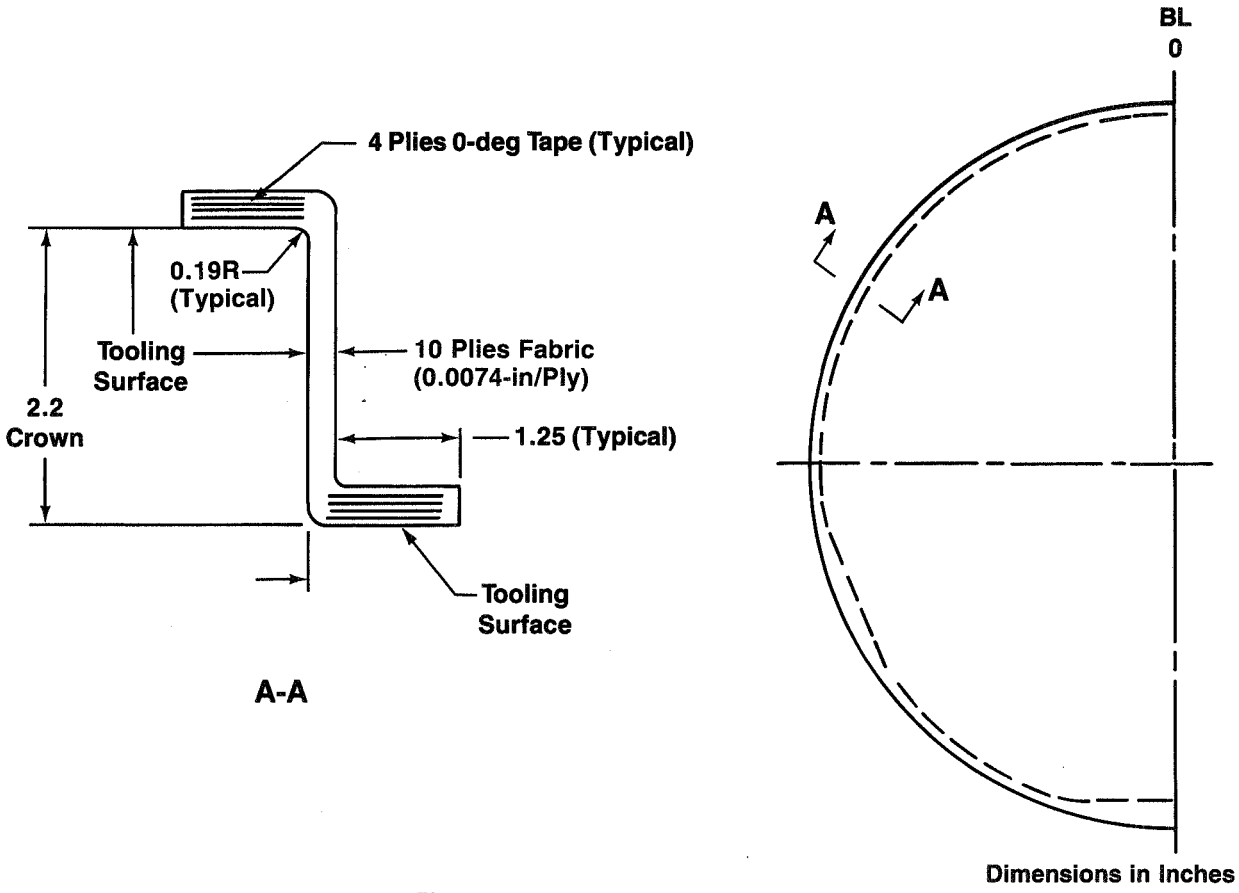

Figure 30. Typical Frame Section

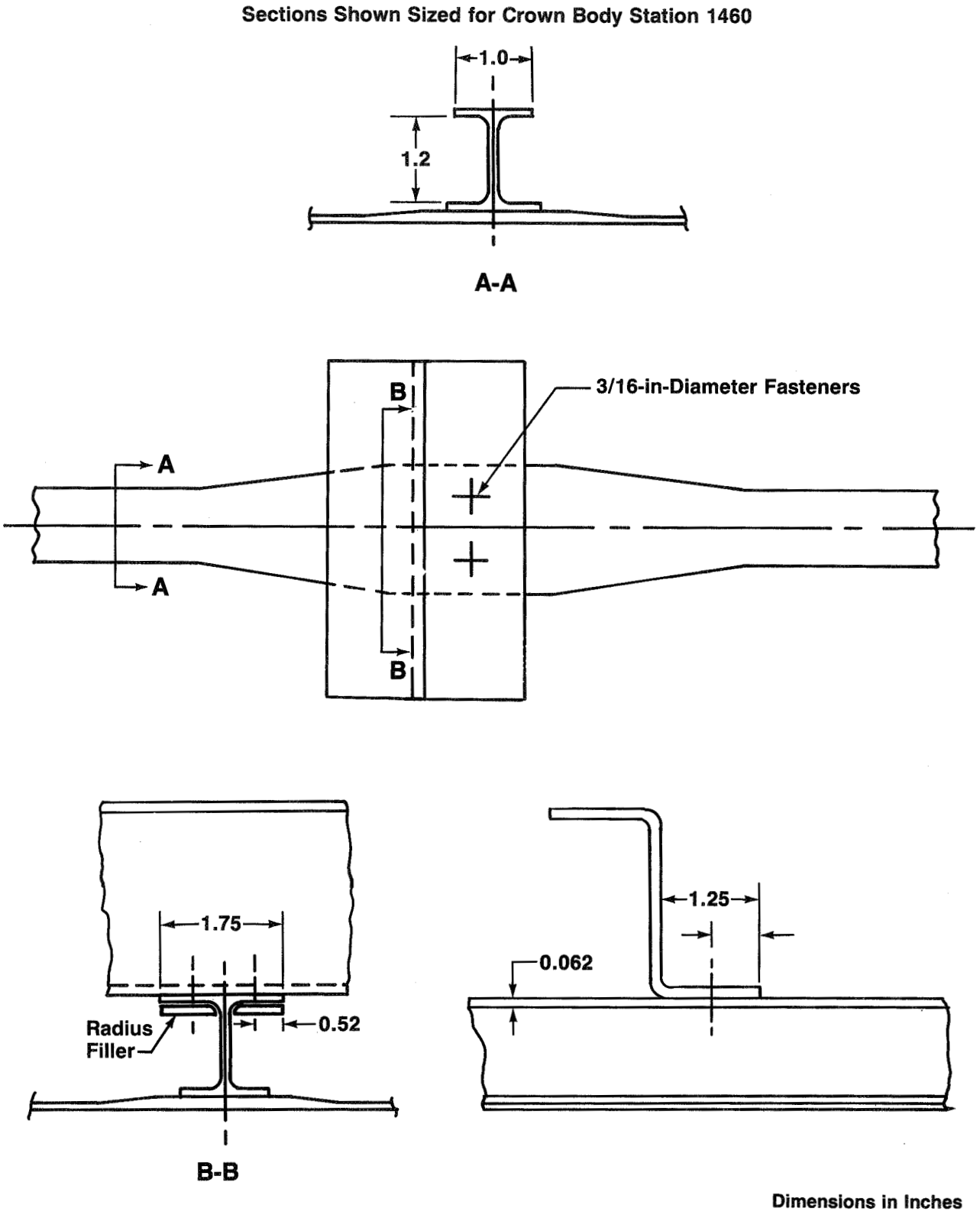

Figure 31. Typical Body Frame-to-Stringer Attachment

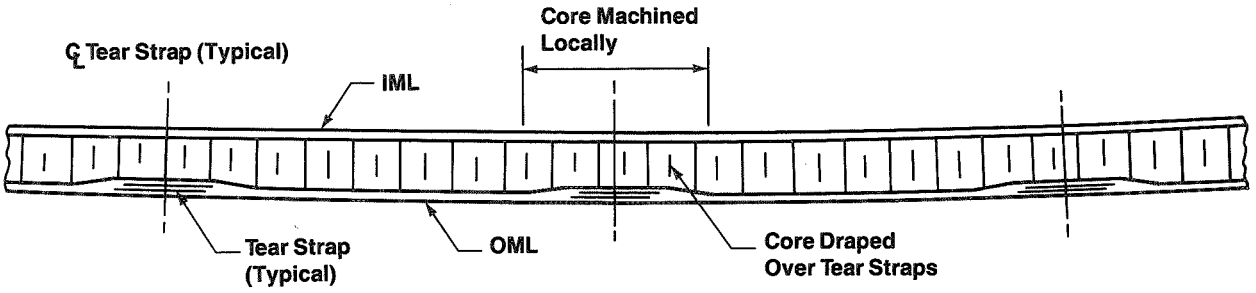

a. Circumferential Section Cut

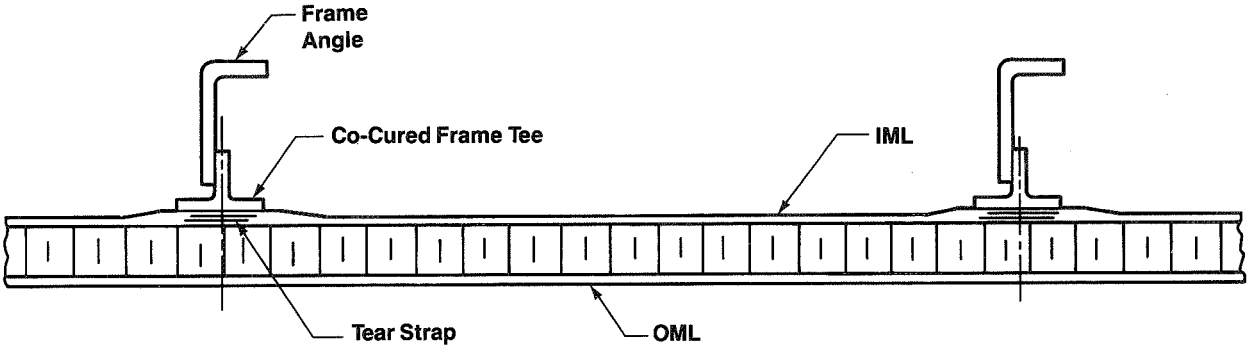

b. Longitudinal Section Cut

Figure 32. Honeycomb Shell Design

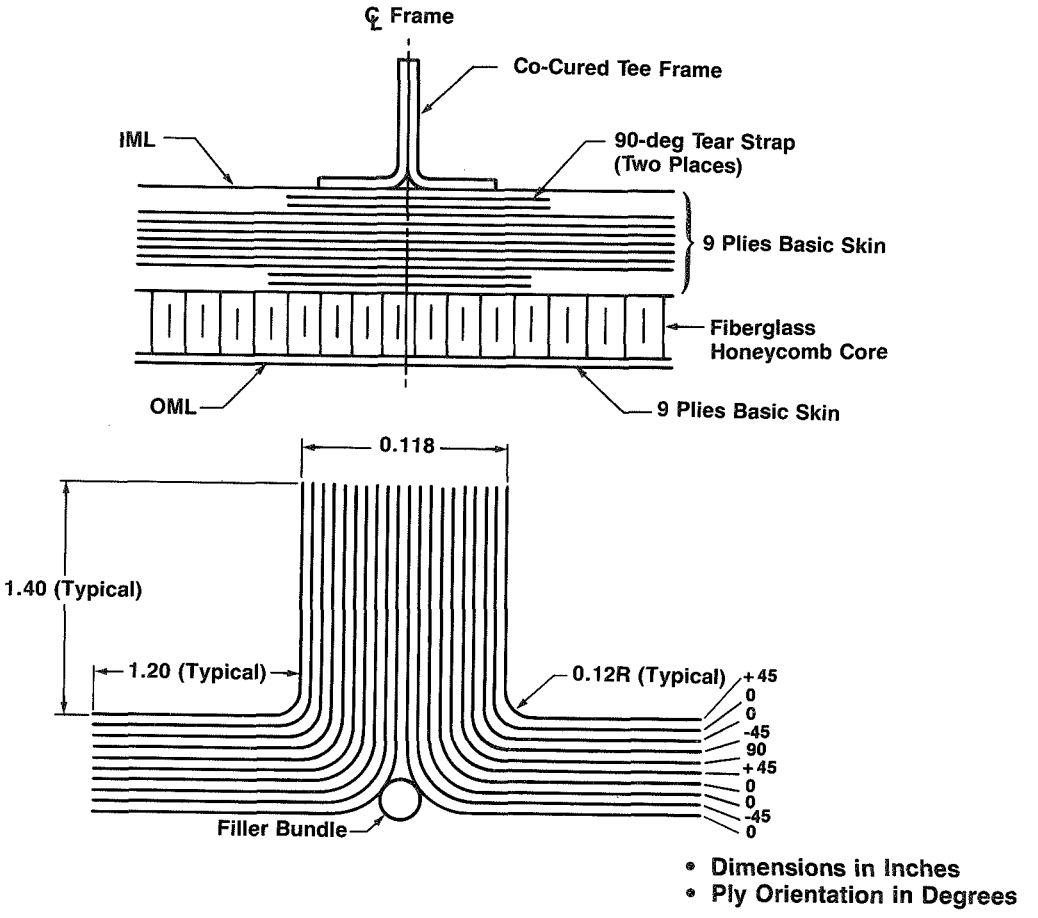

Figure 33. Detail View of Honeycomb Concept Frame and Circumferential Tear Strap

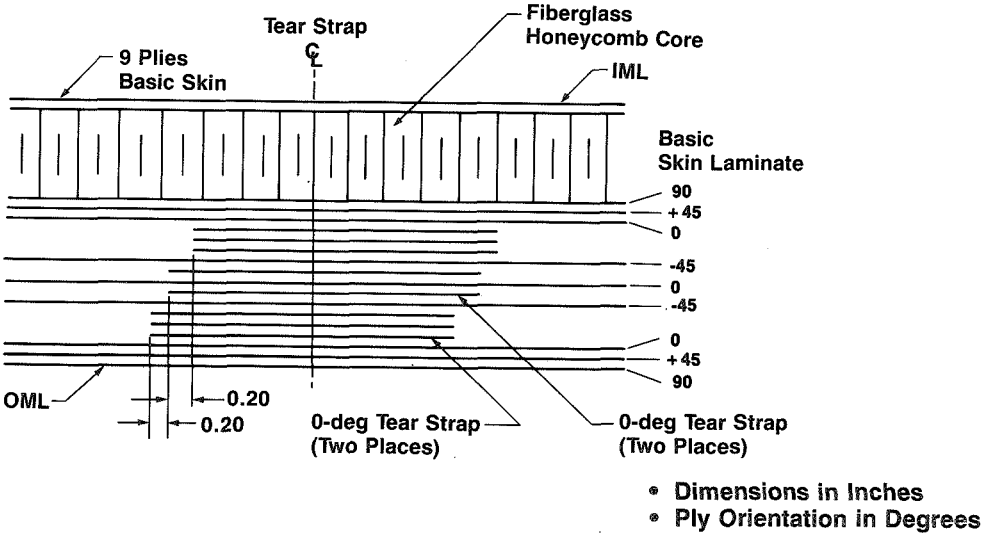

Figure 34. Detail View of Honeycomb Concept Longitudinal Tear Strap

as shown in Figure 34. The two sets of tear straps have been separated to minimize core machining and to provide a smooth surface for the frame-tee.

3.2 Fuselage Shell Design Development

A design of the fuselage study section based on an I-section stiffened skin concept was initially developed during the NASA-Boeing study on Utilization of Advanced Composites (ref. 1). The fuselage study section has been updated for consistency with the designs described in Section 3.1.1 for the development test hardware.

In the current fuselage design, the principal changes compared to the design developed during the previous study (ref. 1) are (1) use of grade 145 tape (0.0056 in/ply) instead of grade 190 tape (0.0074 in/ply); (2) a skin layup with higher shear modulus, lower extensional modulus, and with co-cured longitudinal 0-deg and circumferential 90-deg tear straps; (3) an optimized zee-section frame design; and (4) a revised window frame and window belt design. The configuration of the skin and stringers is shown at several locations along the aft fuselage shell study section in Figure 35.

The fuselage shell design has been evaluated to ensure that the requirements for strength and stability have been met without exceeding strain allowables. The strains at the DULs for each body station have been analyzed and are summarized in Figure 36. These strain values are obtained from the design axial load and the extensional stiffness of the updated section. The skin was considered to be fully effective under tension loading. Only the effective portion of unbuckled skin was considered with the skin under compression loading. In both compression and shear, the buckling loads of the skins were calculated based on the Boeing analysis code LEOTHA. The stringer elements were designed to be stable to the DUL. The design criteria for local stringer buckling or crippling and for compression and shear skin buckling have been evaluated in the developmental test program (tests 3, 4, and 5).

The body frames, shown in Figure 37, are mechanically attached to the stringer flange and to the skin using shear ties in the side and keel region. In the crown region, the frame is connected to the outer shell mechanically, attaching the frame to the stringer cap only. The zee-section frame configuration was developed during a study on Manufacturing Technology for Large Aircraft Composite Primary Structure Fuselage (ref. 10).

The window frame and surrounding skin structure are shown in Figure 38. The frame is made of aluminum and is typical of designs currently used in transport aircraft. The thickness of the surrounding graphite-epoxy skin padup was selected to reduce local stress levels to below static and fatigue requirements for aluminum window frame design.

3.3 Total Fuselage Weight Reduction

To predict a realistic weight reduction for the use of graphite-epoxy in fuselage structure design, it is necessary to identify the structure in the baseline aluminum fuselage suitable for designs in graphite-epoxy. Structure considered candidate for material substitution is referred to as participating structure.

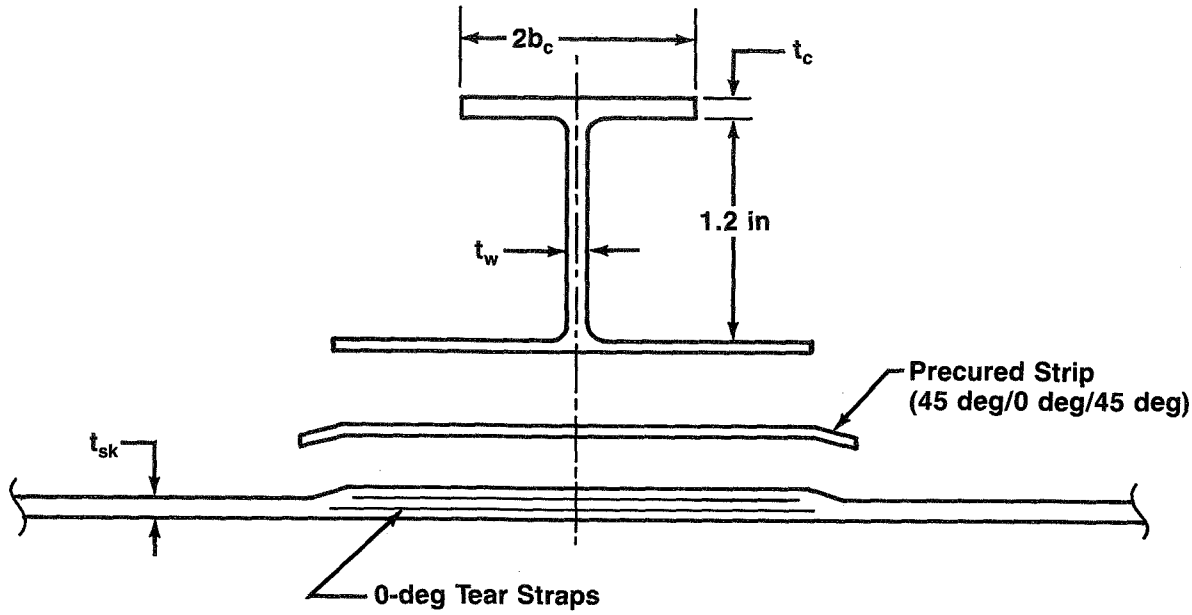

Body Station	Laminate*			Number of 0-deg Tear Straps	t_{sk} (in)	t_w (in)	t_c (in)	$2b_c$ (in)
	Skin	Stringer Web	Stringer Cap					
Crown								
1200	(2/8/2)	(10/8/2)	(8/6/1)	5	0.067	0.112	0.084	1.00
1270	(2/8/2)	(8/8/2)	(7/6/1)	5	0.067	0.101	0.078	1.00
1340	(1/8/2)	(6/8/2)	(6/6/1)	4	0.062	0.090	0.073	1.00
1460	(1/8/2)	(4/8/2)	(5/6/1)	4	0.062	0.078	0.067	1.00
1520	(0/8/2)	(2/8/2)	(4/6/1)	4	0.056	0.067	0.062	1.00
1610	(0/8/2)	(2/8/2)	(4/6/1)	4	0.056	0.067	0.062	0.75
1701	(0/8/2)	(2/8/2)	(4/6/1)	4	0.056	0.067	0.062	0.75
Keel								
1200	(2/10/2)	(12/8/2)	(6/4/1)	6	0.078	0.123	0.118	1.25
1270	(2/10/2)	(8/8/2)	(4/4/1)	6	0.078	0.101	0.095	1.25
1340	(2/8/2)	(8/8/2)	(4/4/1)	5	0.067	0.101	0.095	1.25
1460	(1/8/2)	(4/8/2)	(2/4/1)	4	0.062	0.078	0.062	1.25
1520	(0/8/2)	(4/8/2)	(2/4/1)	4	0.056	0.078	0.073	1.00
1610	(0/8/2)	(4/4/2)	(2/4/1)	4	0.056	0.056	0.062	1.00
1701	(0/8/2)	(4/4/2)	(2/4/1)	4	0.056	0.056	0.062	1.00

*Laminate definition (0 deg/$\pm$45 deg/90 deg)

Figure 35. Configuration of Laminate Skin With I-Section Stringer for Fuselage Shell Detail Design

Station	Stringer Spacing (in)	Smeared Thickness, $\bar{t}$ (in)	Tension 1		Compression 2				
			Design Load, N (lb/in)	Strain at Design Load (in/in)	Design Load, N (lb/in)	Strain at Design Load (in/in)	Euler Buckling Load (lb/in)	Load in Skin at 30% DUL (lb/in)	Skin Buckling Allowable (lb/in)
Keel									
1200	8.4	0.149	—	—	−5500	−0.0048	−8630	−560	−620
1270	8.4	0.139	—	—	−4550	−0.0047	−6460	−540	−620
1340	8.4	0.126	—	—	−3560	−0.0040	−6180	−410	−410
1460	8.4	0.109	3	3	−2500	−0.0040	−3760	−310	−330
1520	8.4	0.101	—	—	−2000	−0.0037	−3150	−200	−260
1610	8.4	0.093	—	—	−1800	−0.0035	−2860	−190	−260
1701	8.4	0.093	—	—	−1500	−0.0029	−2860	−160	−260
Crown									
1200	10.2	0.115	5000	0.0051	−1800	−0.0024	−4570	−230	−300
1270	10.2	0.112	4350	0.0047	−1600	−0.0023	−4060	−220	−300
1340	10.2	0.101	3670	0.0050	−1330	−0.0024	−3350	−170	−250
1460	10.2	0.098	2900	0.0043	−1050	−0.0021	−2860	−150	−250
1520	10.2	0.089	2500	0.0048	− 900	−0.0023	−2270	−110	−200
1610	10.2	0.089	2200	0.0042	− 900	−0.0023	−2270	−110	−200
1701	10.2	0.088	1950	0.0039	− 900	−0.0023	−1900	−110	−200

1 Allowable tension strain ε_T = 0.006 in/in
2 Allowable compression strain ε_C = −0.005 in/in
3 Tension loading in keel does not influence design

Figure 36. Analysis of I-Section Stiffened Skin Fuselage Section Design

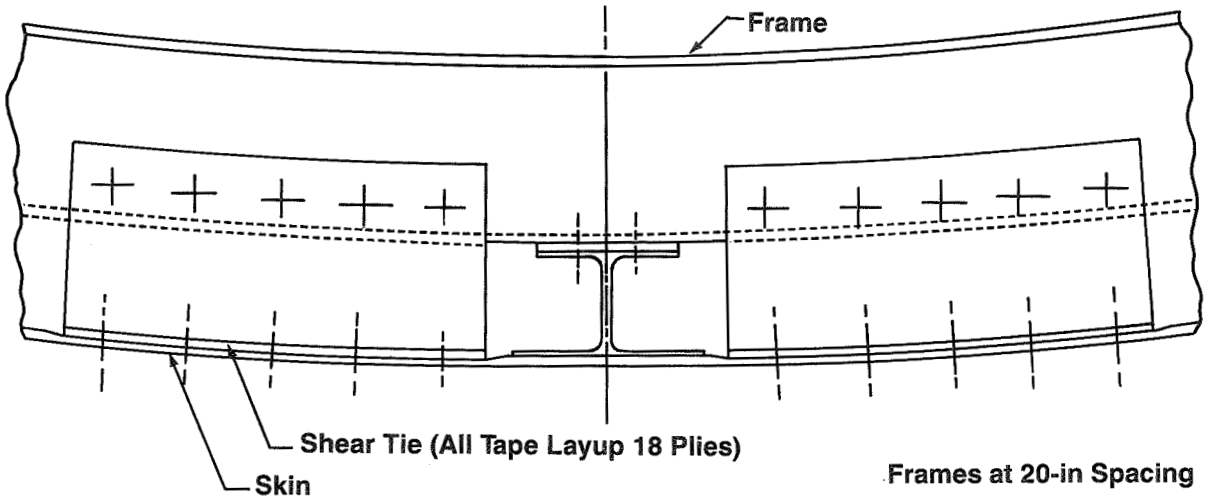

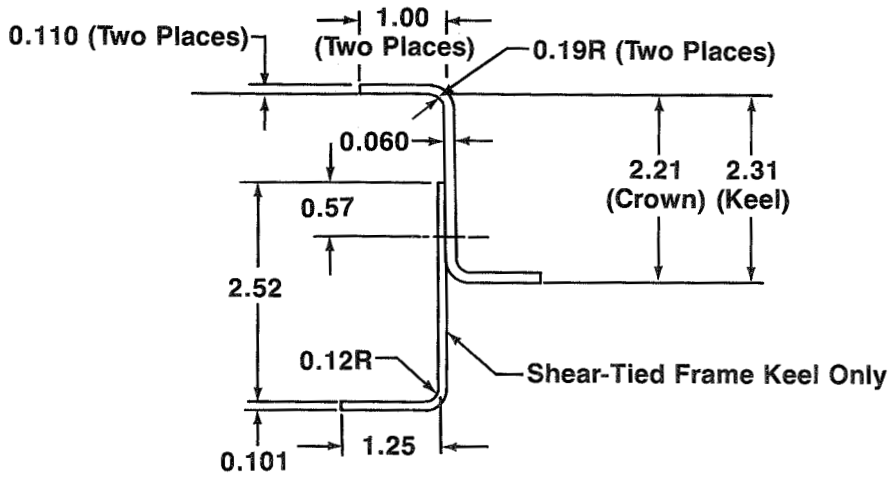

Figure 37. Frame Configuration for Fuselage Section Design

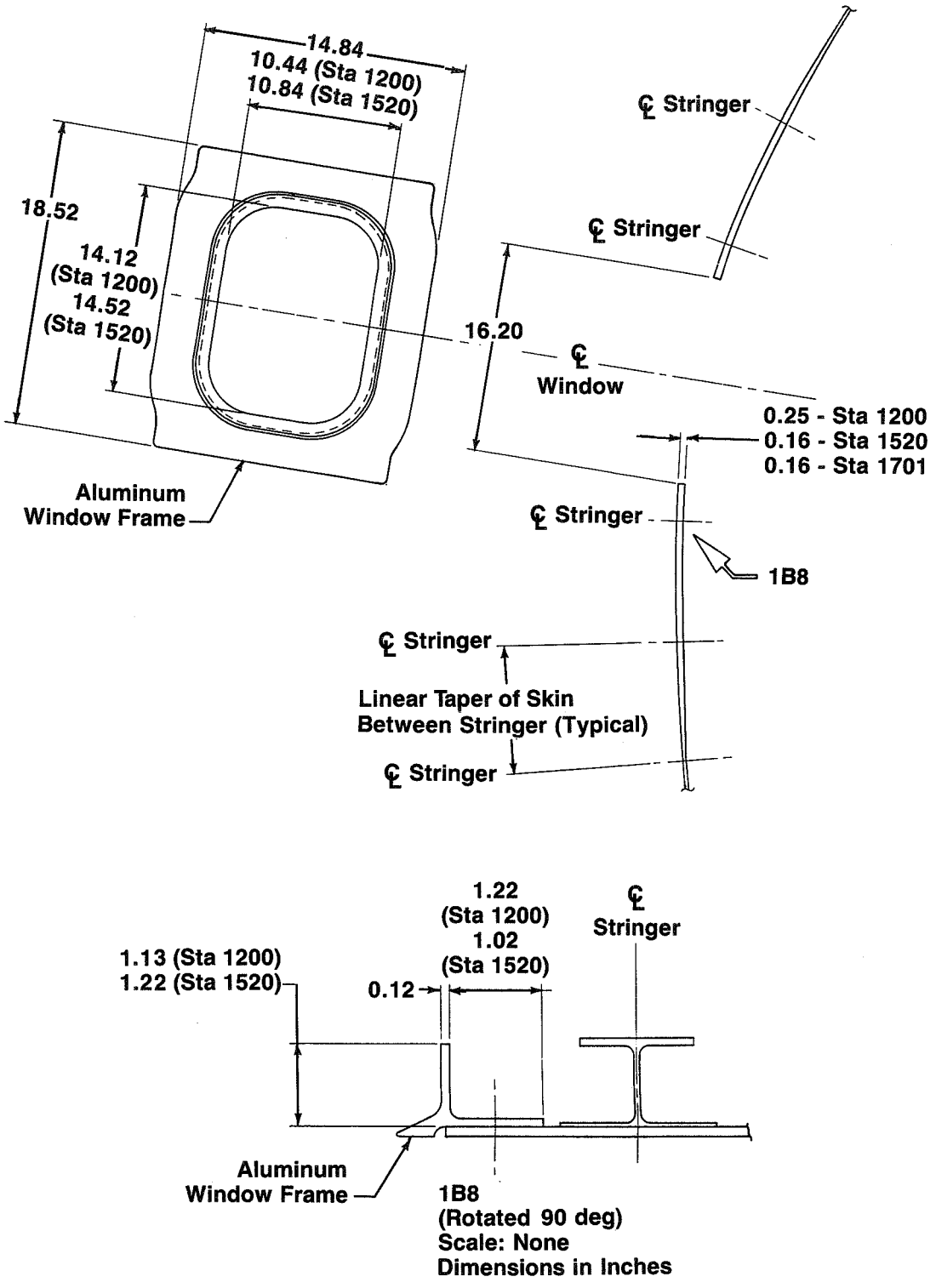

Figure 38. Window Belt and Window Frame Details for Fuselage Section Design

The participating structure of the reference airplane has been identified and includes skin panels, stiffeners, longerons, frames, bulkheads, door structure, door surround structure, floor beams, floor support structure, nose and main landing gear wheelwell structure, keel beam, and major fittings.

The current definition of the nonparticipating structure and the location on the airplane are shown in Figures 39 and 40, respectively. The aluminum baseline participating structure was revised to reflect the removal of window frames from participating structure and including them as nonparticipating structure. In addition, the padup reinforcement material around the door has been included as part of the aluminum baseline skin structure. This change makes the aluminum skin weight consistent with the composite skin weight where the door strap material is integral with the basic skin.

Item	Reason
Passenger Window Frame	Graphite-Epoxy Frames Not Yet Competitive Using Current Technology
Passenger Window Installation	Transparent Material
Windshield Installation	Transparent Material
Windshield Support Structure	One Piece Titanium Forging—Bird Strike Consideration
Cockpit Floor Panels	Inservice Abuse—Bare Floor—No Carpet
Cargo Hold Floor Panels	Inservice Abuse—No Covering
Seat Tracks	Machined Aluminum Extrusions—Inservice Abuse
Galley and Lavatory Supports	Small Fittings and Seat Track Extrusions
Miscellaneous Valves and Fittings	Vacuum Relief Valves, Drain Fittings, etc.
Door Mechanisms	Stops, Latches, Handles, Hinges, Snubbers, etc.
Door Seals	Rubber Seals
Scuff Plates	Titanium Entry Scuff Plates
APU Firewall	High-Temperature Titanium Structure*
Tailcone Structure	Subjected to APU Exhaust Temperatures*
Miscellaneous Sealants and Paint	Required for Nonparticipating Structures
Passenger Floor Panels	Fiberglass-Honeycomb Panels
Wing-Body Fairing	Currently Lightweight Composite Structure Design
Nose and Main Landing Gear Doors	Currently Lightweight Composite Structure Design
Fairings, Aft Fuselage	Currently Lightweight Composite Structure Design
Fairings, Body-Empennage	Currently Lightweight Composite Structure Design

*Also not currently considered to be cost effective

Figure 39. Nonparticipating Fuselage Structure (7440-lb Total Weight)

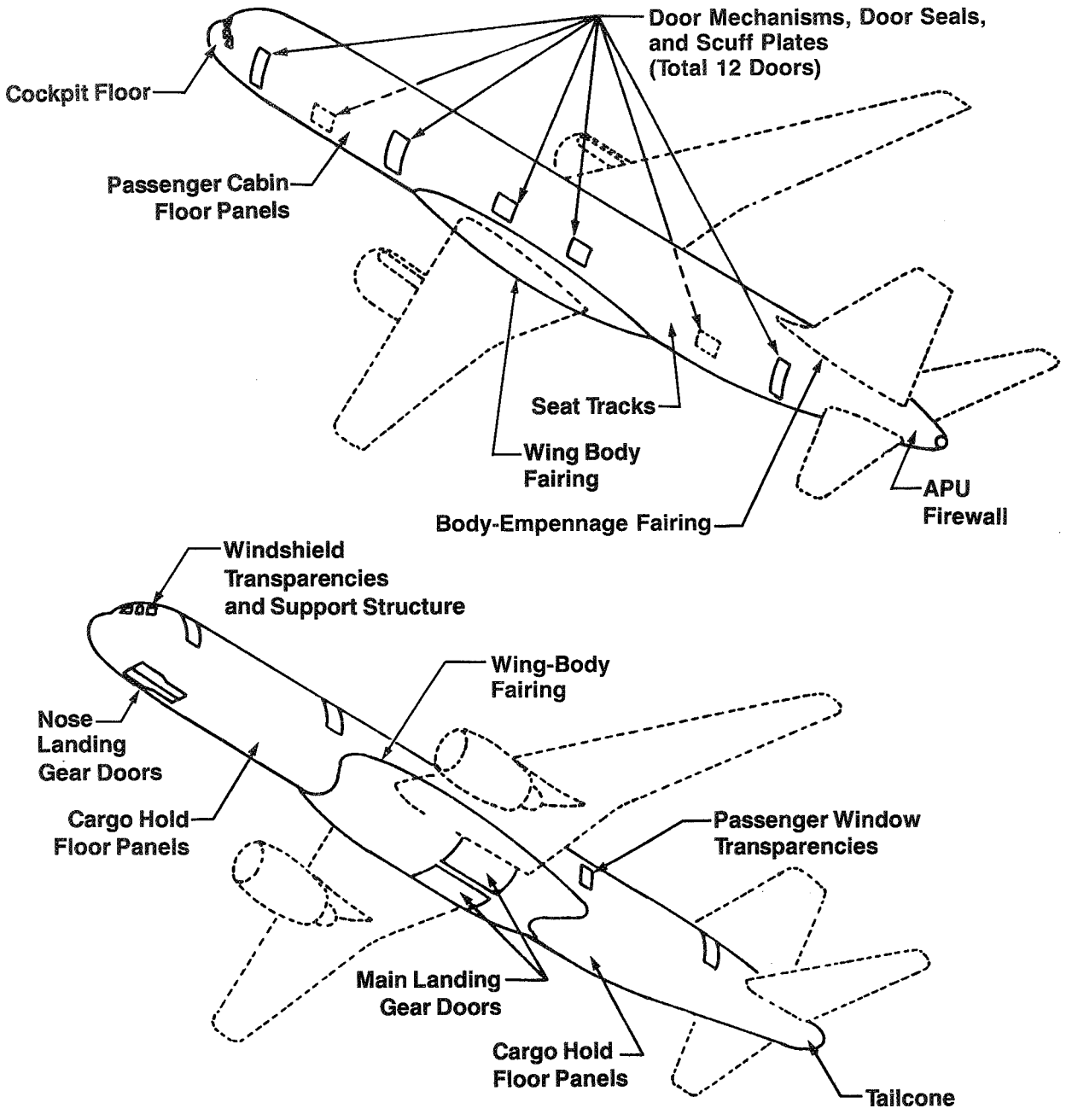

Figure 40. Location of Nonparticipating Fuselage Structure

To more accurately assess the composite skin weight reduction over the baseline aluminum skin, the co-cured longitudinal 0-deg tape tear strap weight was extracted from the composite skin panel weight and added as an increment to the I-stringer weight, since this material is analytically considered to be stringer material. The co-cured circumferential 90-deg tape tear strap weight was also extracted from the skin panel weight and compared directly to the aluminum baseline tear strap weight.

A weight reduction analysis has been performed, based on the I-section skin stiffened design discussed in Section 2.1 and the baseline aluminum section discussed in preceding sections. The result of this weight reduction analysis on the total fuselage participating structure is shown on the bar chart in Figure 41. A weight reduction of 22.7% is shown.

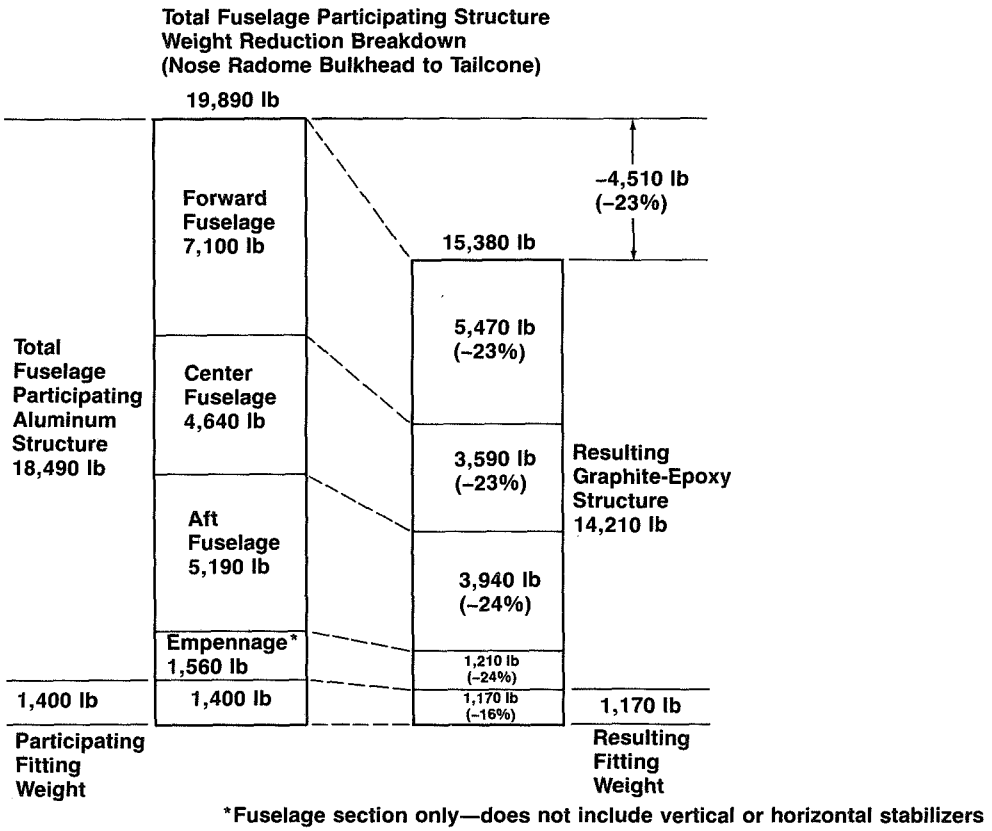

Figure 41. Weight Reduction of Fuselage Study Section

A weight reduction time history, starting with results obtained during the fuselage study program (ref. 1), is shown in Figure 42. Five weight reduction values are shown. The first value of -4000 lb was developed during the study program. It was based on the hat stiffened laminate concept. The aluminum baseline differed from the current baseline fuselage. Subsequently, the I-section stringer stiffened laminate concept was selected as the laminate concept instead of the hat stiffened concept.

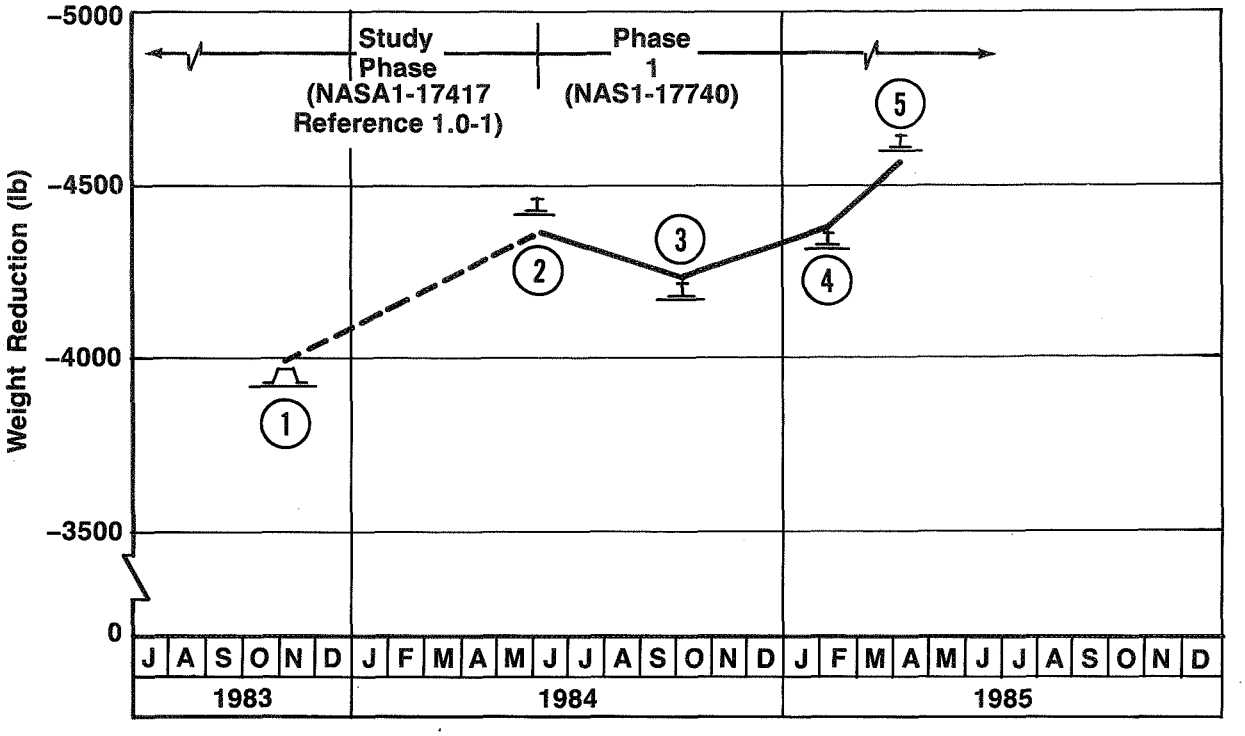

Figure 42. Weight Reduction Time History

The second weight reduction value (4310 lb) was developed during the preliminary design phase of this contract. This was based on the I-section stringer concept.

The aluminum baseline participating structure was refined to provide a more accurate basis for the weight reduction analysis. This refinement resulted in a reduction of the aluminum participating fitting weight from 2500 lb to 1400 lb and an increase in the aluminum participating structure weight by 280 lb. Using this revised aluminum fuselage baseline weight resulted in the third weight reduction of 4200 lb, shown in Figure 42.

The initial update layout drawing for the phase I fuselage study section was analyzed and the resultant weights compared to the phase I aluminum study section weights. Applying the percentage reductions obtained in this analysis to the fuselage participating structure showed a weight reduction of 4340 lb. The principal changes made to the layout drawing update were (1) the use of grade 145 tape (0.0056 in/ply) in lieu of grade 190 tape (0.0074 in/ply); (2) skin layup; (3) longitudinal planks beneath the stiffeners; and (4) circumferential tear straps at the fuselage frame locations.

Analysis of the stress approved layout drawing resulted in the fifth and latest weight reduction of 4520 lb. The most significant change from the unreleased layout drawing was the inclusion of an optimized frame design. The current weight represents the 22.7% weight reduction from the aluminum baseline.

4.0 PROCESS DEVELOPMENT

This section presents the results of manufacturing efforts in the development of processing procedures for fabricating developmental test parts. Details of test hardware fabrication are discussed in Section 5.0.

Standard cure cycles and fabrication techniques were used for fabrication of the test panels. The cure cycle used for the laminate and honeycomb panels is shown in Figure 43. The layup and bagging techniques used for the laminate and honeycomb panels are shown in Figures 44 and 45, respectively.

4.1 Skin-Stringer Shell Fabrication

The process flow for fabricating I-section stiffened skin panels is shown in Figure 46. The primary steps to this process are (1) laminate and trim skin and stringer plies, (2) drape form skin and stringer channels, (3) assemble and locate stringers on skin, and (4) cure panel.

The plies for the skin and stringers are laid up flat on a computerized tape laminating machine using 3-in-wide tape. The skin and stringer preplies are then trimmed to size using a

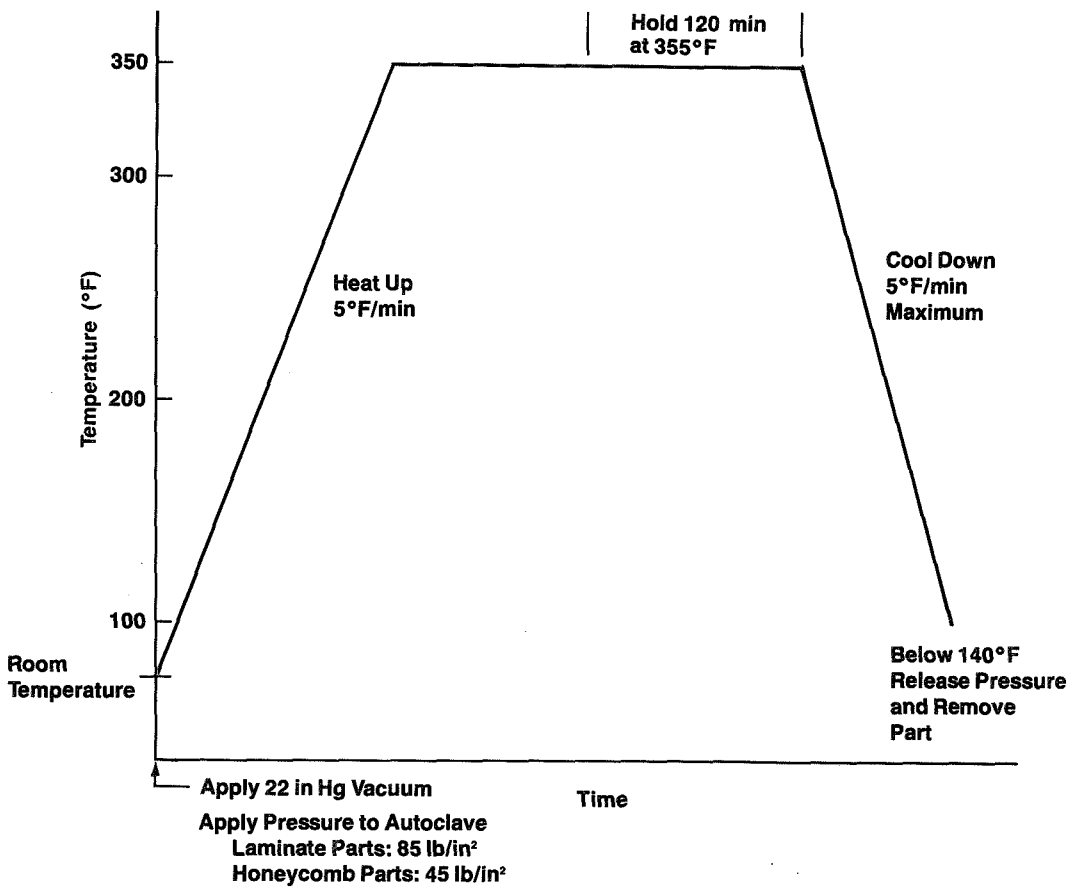

Figure 43. Cure Cycles for Laminate and Honeycomb Panels

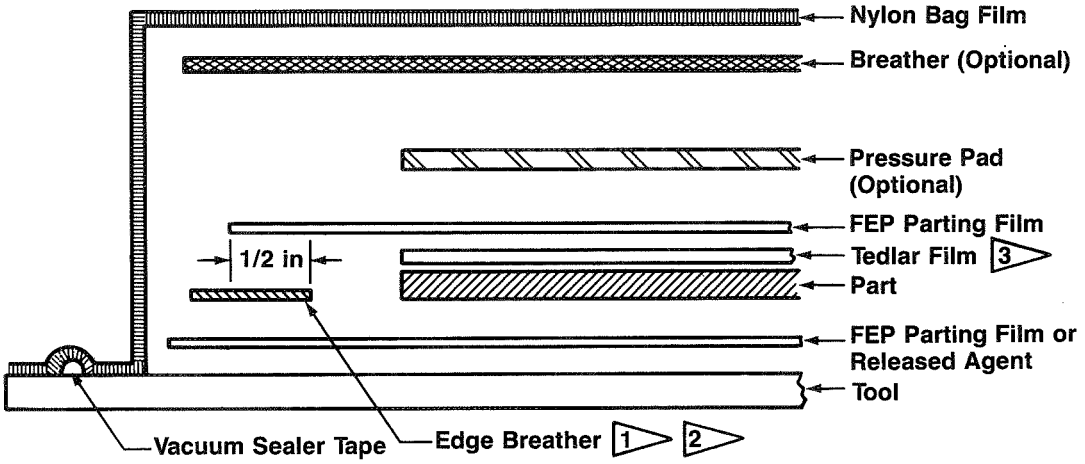

1 1-in minimum width edge breather with direct connection to vacuum source—at one corner of the layup, place a single fiberglass yarn between the edge of the layup and the edge breather to allow evacuation of air from the layup. Additional yarns may be used to provide adequate removal of trapped air

2 Allow 3/4-in minimum between part edge and inside edge of edge breather. Do not allow breather to contact layup

3 Use Tedlar if called out on drawing. For process control panels, do not use Tedlar. Solid FEP film required

Figure 44. Typical Bagging Procedure for Laminate Panels

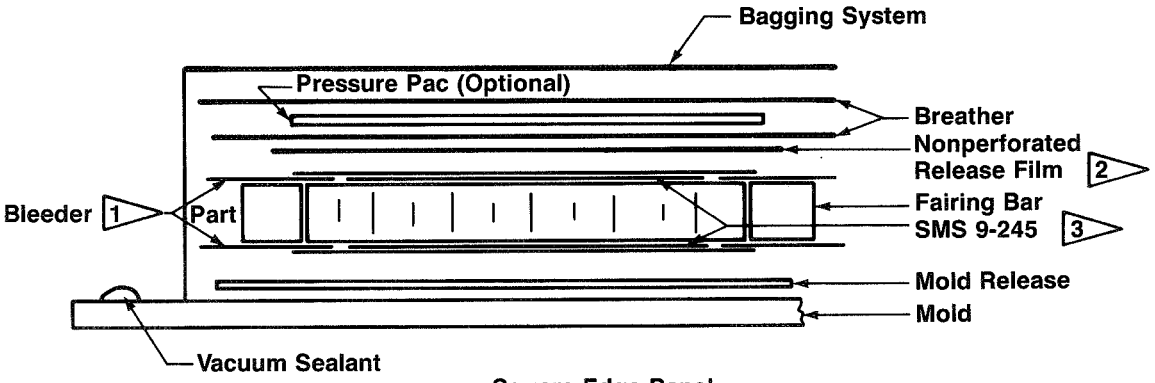

Square Edge Panel

1 Use a 3-in wide minimum fiberglass bleeder plies. Bleeders typically overlap 1/4 in of skin plies and doublers. Bleeders must be at least 1/2 in from part net trimline. Bleeders must provide vacuum path to breathers

2 Extend 1 in past prepreg

3 FM 300 adhesive is required next to core

Figure 45. Typical Bagging Procedure for Sandwich Panels

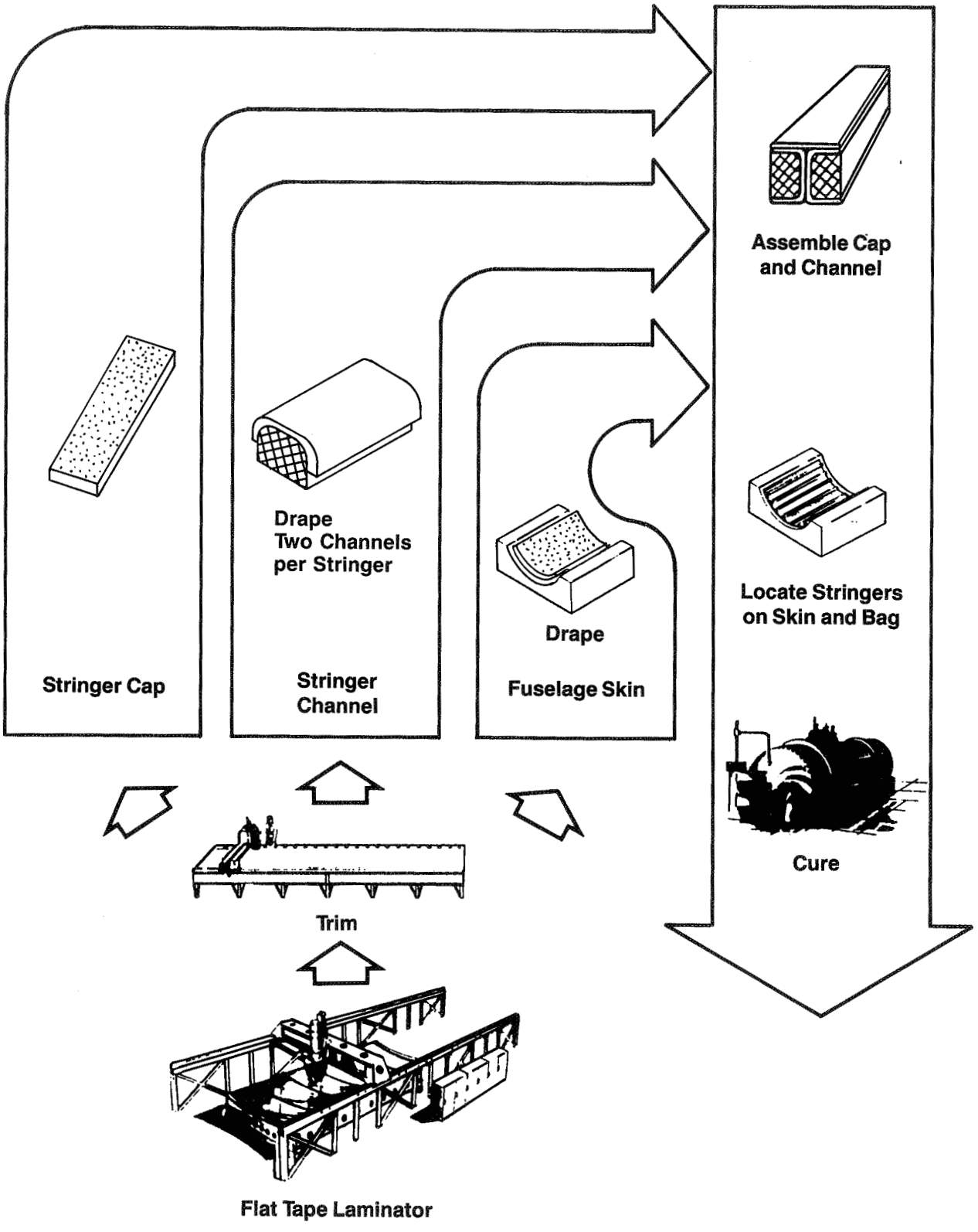

Figure 46. I-Stringer Panel Fabrication Flow

numerically controlled cutter. The stringer preplies are drape formed onto the layup mandrels, and the stringer halves and cap plies are assembled as shown in Figure 46. The skin panel is drape formed to the layup mandrel, and the stringer assemblies are located on the skin panel. A strip of precured graphite laminate is placed between the stringer and the skin laminate to provide a foundation for the stringer tool. This reduces localized pressures developed during cure and prevents the stringer from sinking into the skin laminate. The skin-stringer panel is then bagged and cured in an autoclave to produce an integrally co-cured stiffened panel. Graphite-epoxy material is used for the skin layup mandrel and the stringer mandrels to minimize thermal expansion differences. This procedure for fabricating I-section stringer stiffened panels has been validated on the LCPAS wing program (NAS1-16863) and the Air Force Damage Tolerance program (ref. 9) and has been successful for fabricating parts in this program.

4.2 Honeycomb Shell Fabrication

Two processing approaches have been considered for fabricating honeycomb sandwich shell panels. The two processes, shown in Figures 47 and 48, have different tooling and curing procedures. In production, the laminate face sheets would be laid up on an automated tape laminator. The approach that was used for fabricating the panels in this program was to manually lay up the material for the skin laminates using 12-in-wide tape.

The first approach for fabricating honeycomb panels, shown in Figure 47, is to lay up the outer skin, drape the outer skin and core into the layup mandrel, and co-cure the skin and core. The inner surface of the core is then locally machined to remove the bump caused by the tear strap and provide a smooth surface for the inner skin. The inner skin is then preplied and draped over the inner core surface. The precured strip and the frame-tee are then added, and the assembly is bagged and cured.

The second approach for fabricating honeycomb panels uses a single-stage cure, as shown in Figure 48. The face skins are laid up on a computerized tape laminating machine and cut out with a numerically controlled cutter. The outer skin is draped into the layup mandrel. The core is located on the outer skin, the inner skin is draped onto the core, and frame-tee subassemblies are positioned on the inner skin. The entire assembly is then bagged and co-cured.

Since the core is not machined, the bump caused by the longitudinal tear strap extends through the core into the inner skin. The tee-section frame must then bridge across this bump as shown in Figure 49. A 34-in by 36-in honeycomb panel was fabricated to evaluate this process. Unacceptable areas of low compaction under the tee-sections and next to the tear strap bump were identified using ultrasonic methods and micrographs (fig. 49).

Two methods for eliminating the areas of low compaction were considered. The first method uses either graphite-epoxy or adhesive filler material located under the tee-frames between the tear strap bumps. The second method uses a frame tool contoured to fit over the tear strap.

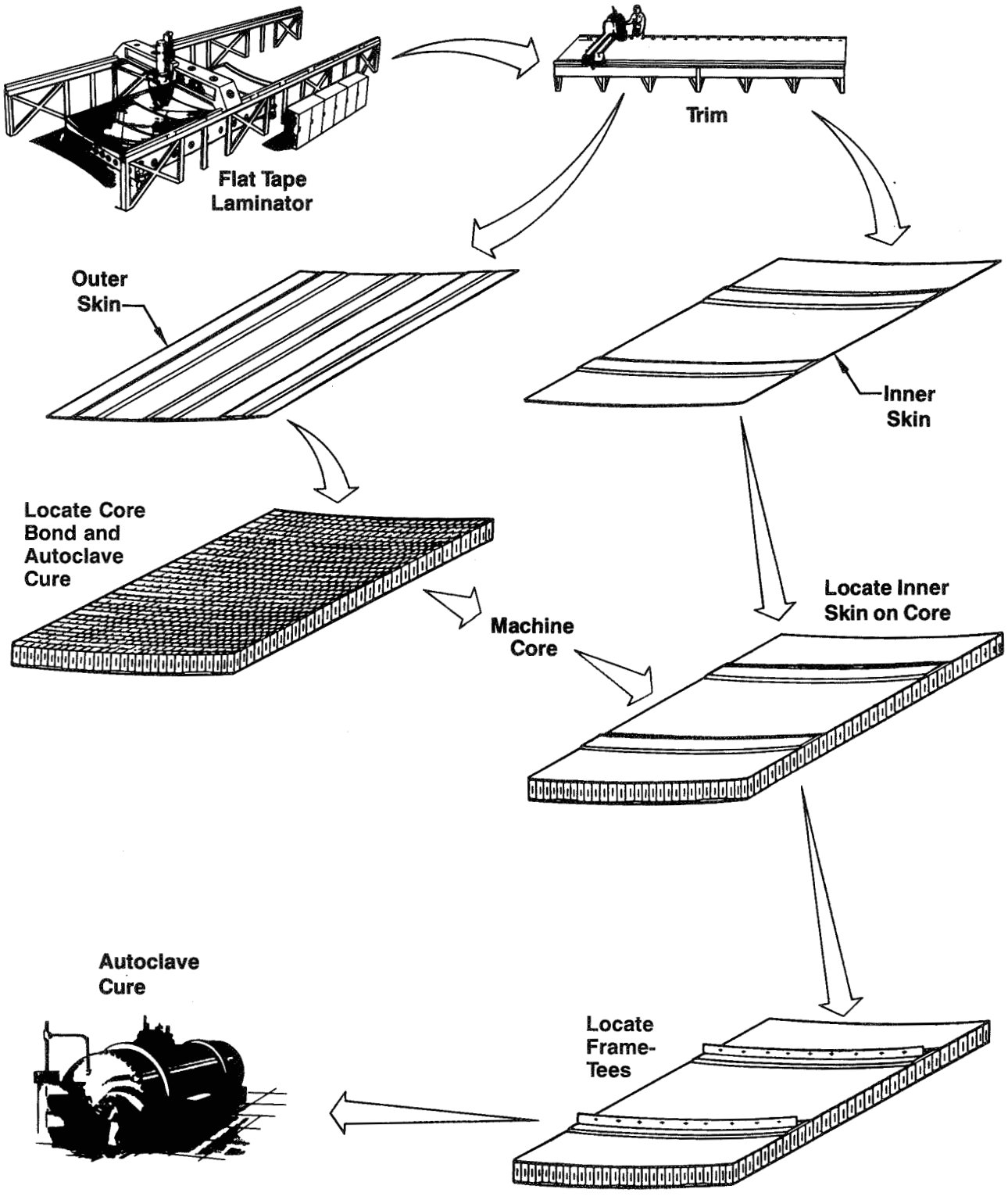

Figure 47. Two-Stage Core Honeycomb Sandwich Panel Fabrication Flow

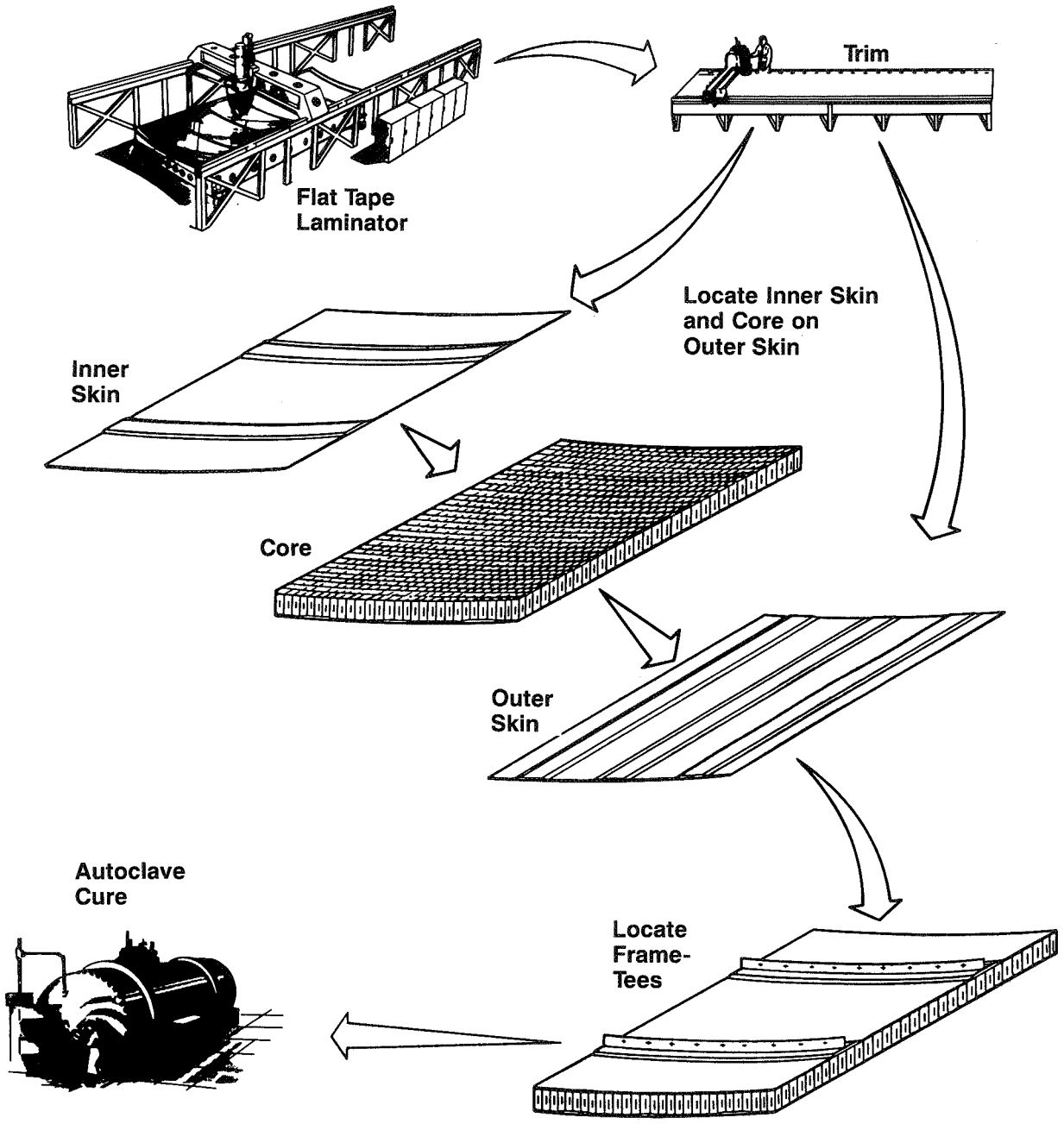

Figure 48. Single-Stage Cure Honeycomb Sandwich Panel Fabrication Flow

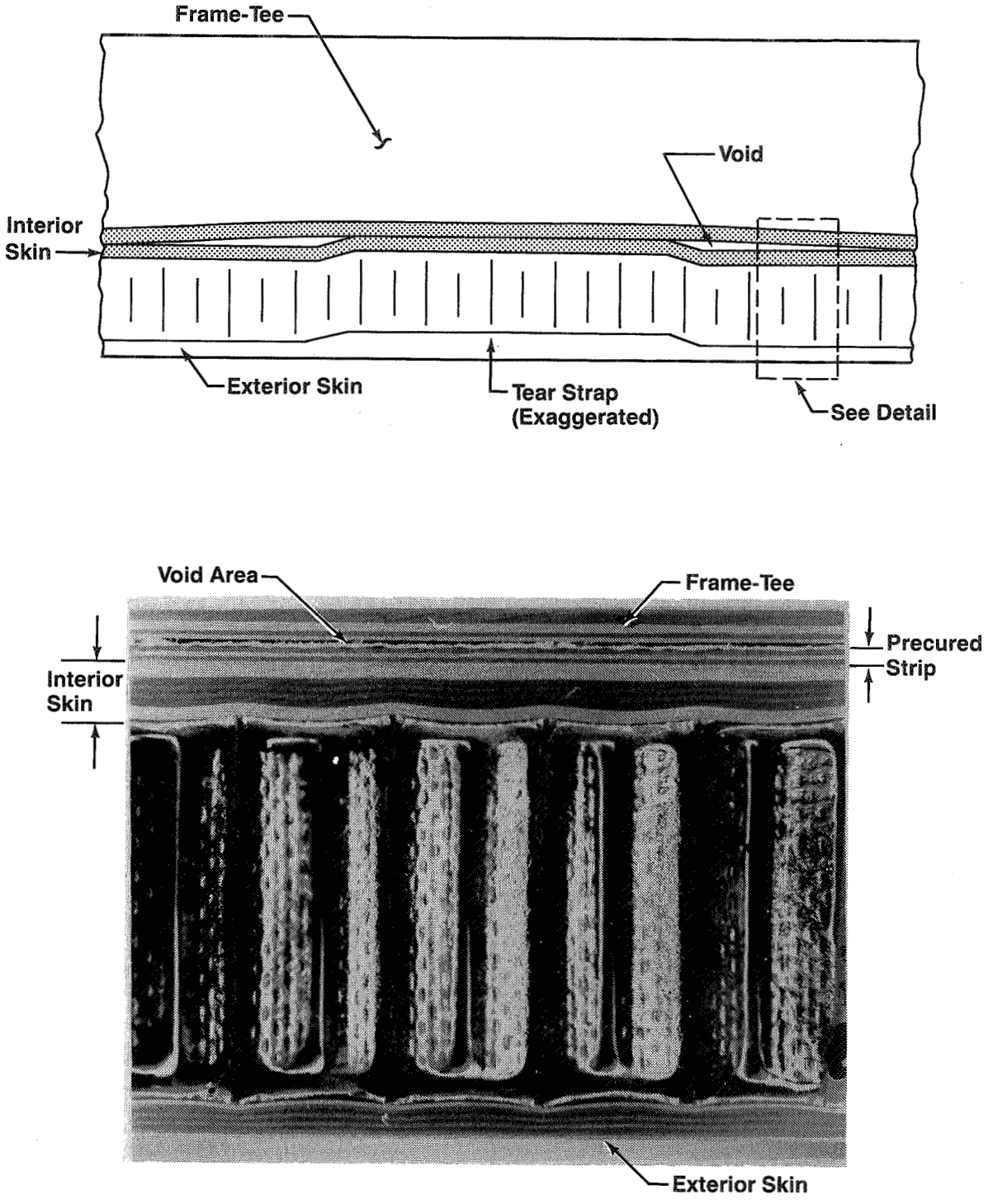

Figure 49. Photomicrograph of Void Between Frame-Tee and Skin on Interior Surface Adjacent to Tear Strap

A 34-in by 36-in honeycomb panel was fabricated to evaluate the use of filler plies. Four variations of filler plies were added under the frame-tees, resulting in a smooth transition over the tear strap (fig. 50). The location of filler plies is visible in a photograph of the panels, shown in Figure 51. The four filler ply concepts were as follows:

A. 1 ply graphite-epoxy tape

B. 2 plies graphite-epoxy tape

C. 2 plies adhesive

D. 3 plies adhesive

Visual, ultrasonic inspection, and photomicrographs (fig. 52) of the test panel showed that all fillers provided acceptable results. The honeycomb fracture panels (test 6B) were fabricated using the smallest and lightest filler ply, concept A. Some areas of low compaction were noted in these panels, indicating that the use of only filler plies yields inconsistent results.

A contoured frame tool was used in addition to a single ply of filler for fabricating the pressure pillowing panels of test 7. The frame mandrels were shimmed with Teflon tape (up to 0.02 in thick) at all locations that correspond to spaces between the bulges of the outer face sheet tear straps (fig. 53). Inspection of these panels indicated that a tool contoured to fit around the tear strap bulges provides for even compaction all along the frame.

The single-stage cure fabrication process shown in Figure 48 was selected over the two-stage cure process. The single-stage cure process has fewer machining operations and is less labor intensive.

Originally, the use of precured strips between frame flanges and the inner skins of honeycomb panels was planned to prevent the frame-tee from sinking into the skin. Photomicrographs taken of honeycomb evaluation panels without precured strips indicated that at the 45-lb/in^2 autoclave pressures used in honeycomb panel fabrication, the frame-tee sections did not sink into the skin. Precured strips were therefore eliminated from the fabrication processes.

4.3 Material Characterization

The effort to develop composites for primary structure has been directed toward solid laminates for wing design. Because of this, very little data has been developed on composites optimized for sandwich designs. The material selected for fabricating laminate panels was Hercules 2220-3/AS6, grade 145 tape. The characteristics of this system have been established and are discussed in Reference 5. The material selected for fabricating honeycomb sandwich panels was Hexcel F584/AS6, grade 145 tape. Tests for characterizing the mechanical, physical, and chemical properties, and the processibility of this material have been performed and are discussed in following sections.

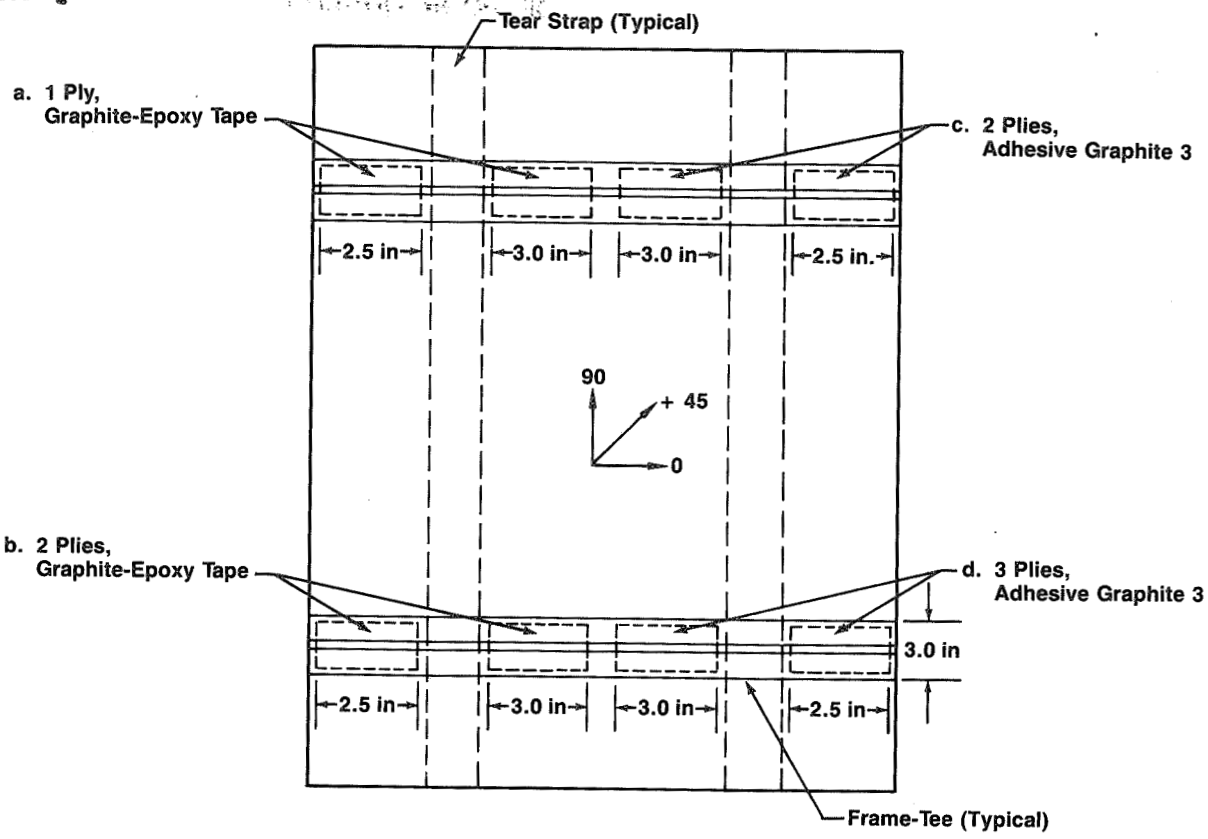

Figure 50. Location of Filler Plies in a Flat Honeycomb Process Test Panel

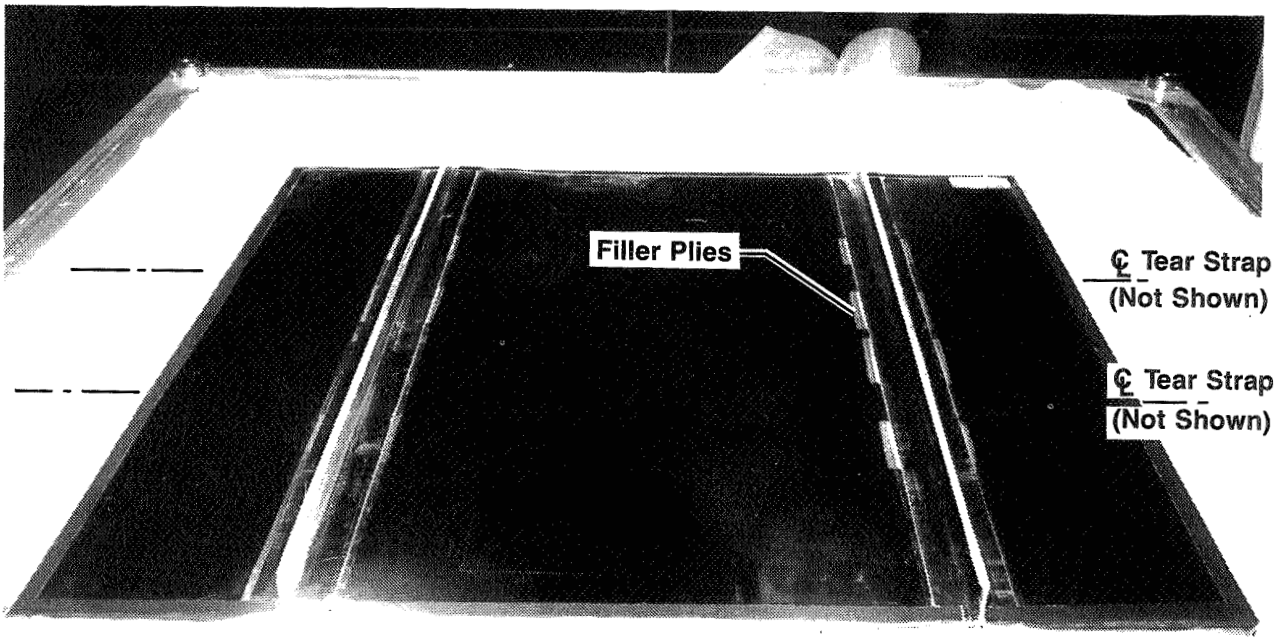

Figure 51. Single-Cure Fabrication Honeycomb Process Test Panel

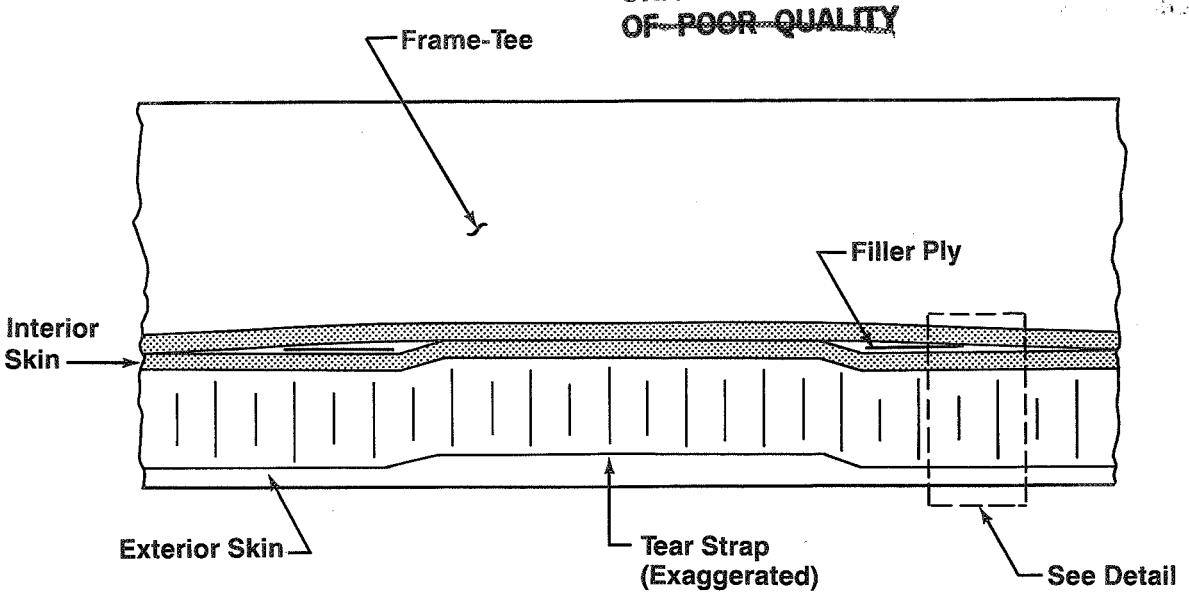

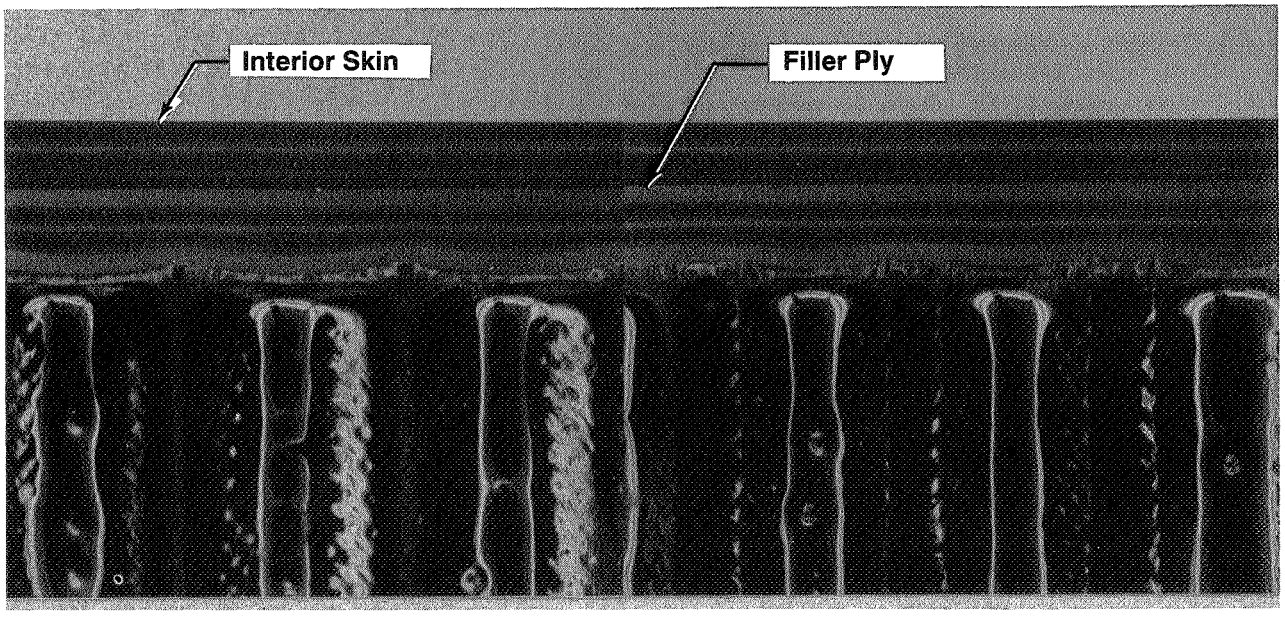

Figure 52. Photomicrograph of Filler Region Between Frame-Tee and Skin on Interior Surface

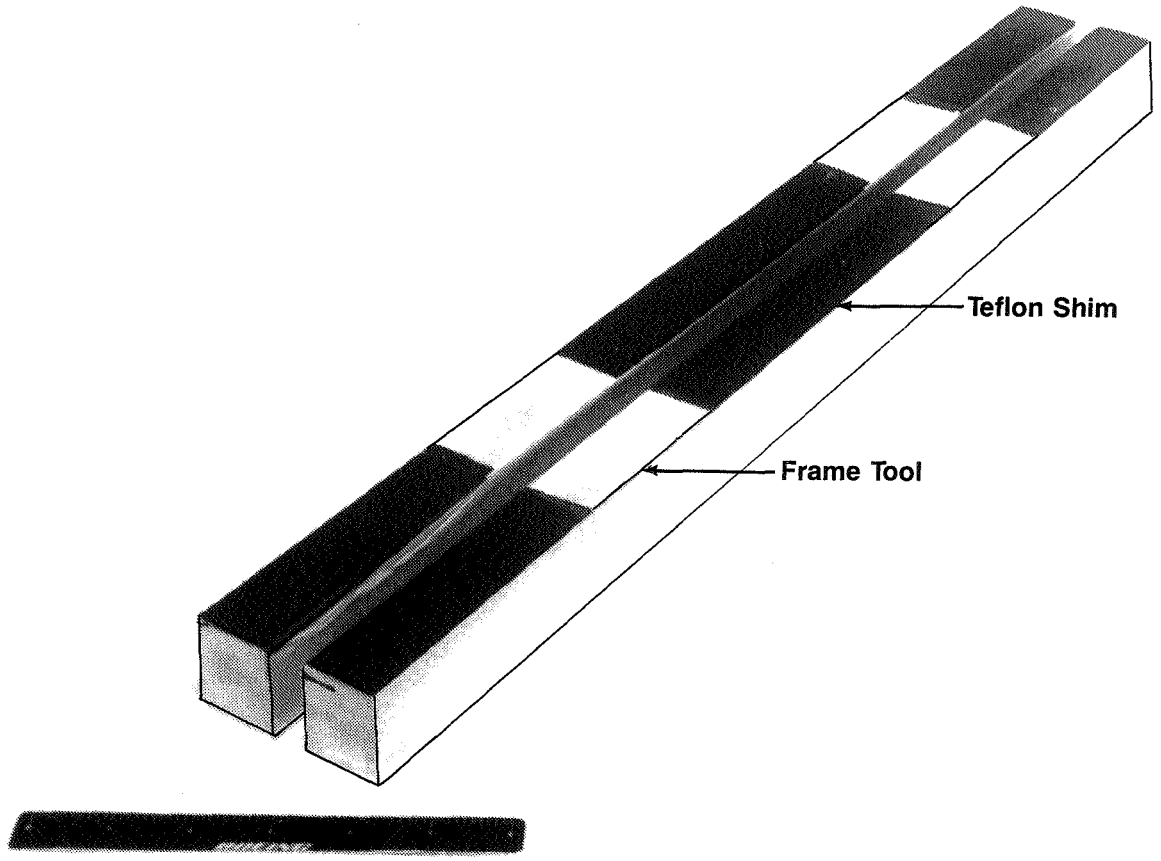

Figure 53. Test 7B Honeycomb Panel Frame Tools With Teflon Tape Shims Applied to Lower Flange Surfaces

4.3.1 Mechanical Tests

Tests for establishing the mechanical properties of the Hexcel F584/AS6 tape material were performed on both laminate and honeycomb coupons. The laminate tests, summarized in Figure 54, included tension and compression tests of 0-deg coupons, compression interlaminar shear, compression after impact, and open-hole tension and compression. The results of the compression-after-impact tests, including nondestructive inspection, are shown in Figure 55.

The initial results obtained for the F584/AS6 material tension tests were not consistent with Hexcel quality assurance tests. As shown in Figure 56, the strain to failure achieved by Boeing was 18% higher than that achieved by Hexcel, and the extensional modulus was 15% lower. For this reason, Boeing performed some additional tests using the same roll of material used by Hexcel. The results from this second test and results of tests from a third roll of material are shown in Figure 56. The values reported in the summary chart (fig. 54) are the average of the three Boeing tests.

The honeycomb tests included flatwise tension, inplane shear, and long beam flexure. The results of these tests are summarized in Figure 57.

Material Characterization Task	Condition	Results	Boeing Material Specification Requirements [1]
0-deg Tension			
Strength	Room Temp.	366 ksi	320 ksi
	−75°F	350 ksi	300 ksi
Modulus	Room Temp.	19.5 msi	20 msi
	−75°F	18.7 msi	19 msi
0-deg Compression Strength	Room Temp.	199.7 ksi	200 ksi
0-deg Compression Strength	180°F, Wet [2]	164.6 ksi	150 ksi
Compression Interlaminar Shear	Room Temp.	11.1 ksi	10 ksi
	200°F, Dry	9.7 ksi	9 ksi
	180°F, Wet [2]	8.8 ksi	9 ksi
Compression After Impact [3]	Room Temp.		
	750 in-lb/in	31.3 ksi	—
	1000 in-lb/in	28.9 ksi	—
	1500 in-lb/in	24.9 ksi	22
	2000 in-lb/in	21.1 ksi	—
	Through Thickness	14.7 ksi	—
Open-Hole Tension [4]	Room Temp.	82.3 ksi	55
	−75°F	81.1 ksi	45
Open-Hole Compression [4]	180°F, Wet [2]	37.7 ksi	40
	200°F, Dry	38.6 ksi	40

[1] Boeing material specification requirements for a laminate material system
[2] Wet specimens immersed in 160°F water for two weeks
[3] Layup: $(45/90/-45/0)_{4s}$
[4] Layup for tension: $(45/90/-45/0)_{s}$; compression: $(45/90/-45/0)_{2s}$

Figure 54. F584/AS6 Laminate Material Mechanical Property Characterization Tests

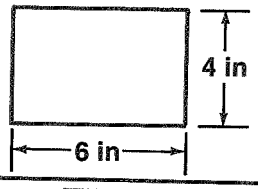 Delamination Pattern Derived From Through-Transmission Ultrasonic Scan Layup: $(45/90/-45/0)_{4S}$	Impact Energy (in-lb/in)	Delamination Area (in^2)	Compression Stress (ksi)
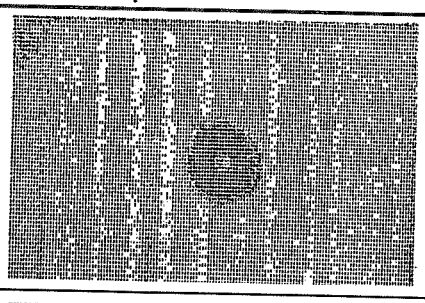	750	1.0	31.3
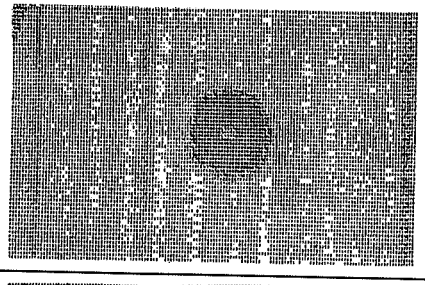	1000	1.3	28.9
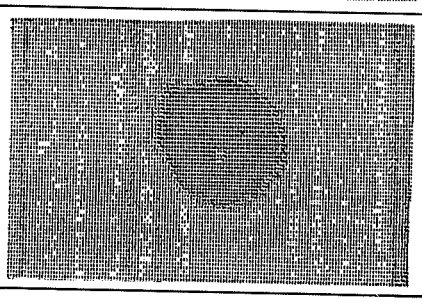	1500	2.9	24.9
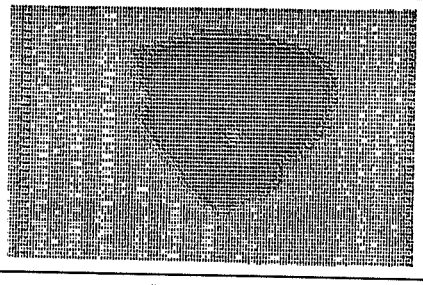	2000	5.6	21.1
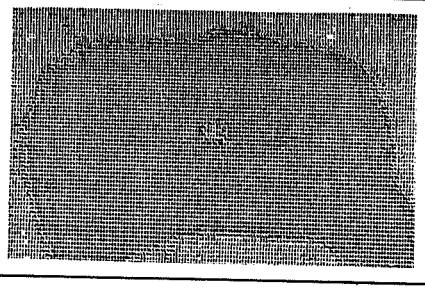	Through Penetration	15.2	14.7

Figure 55. Compression-After-Impact Test Results for F584/AS6 Material Characterization

Properties	Hexcel Results	Boeing Test No. 1	Boeing Test No. 2	Boeing Test No. 3
Batch Roll	12091 1A	12091 2A	12091 1A	12091 3A
Ultimate Tension Strength	373 ksi (3.7)	373 ksi (5.5)	350 ksi (3.3)	374 msi (5.2)
Modulus	21.8 msi (4.2)	18.5 msi (2.0)	19.1 msi (0.8)	20.8 msi (8.3)
Ultimate Tension Strain	0.017 in/in (3.2)	0.020 in/in (3.7)	0.018 in/in (3.2)	0.0181 in/in (6.1)

(X.X) = Coefficient of variance

Figure 56. 0-deg Laminate Tension Tests for Characterization of Hexcel F584/AS6 Material

Material Characterization Task	Condition	Results	Boeing Material Specification Requirements [1]
Flatwise Tension	Room Temp. 200°F, Dry	774.8 lb/in^2 674.5 lb/in^2	450 lb/in^2 400 lb/in^2
Inplane Shear	Room Temp.	712.2 lb/in	—
Long-Beam Flexure Ultimate Load	Room Temp. 180°F, Wet [2] 200°F, Dry	390.5 lb 255.4 289.3	200 lb — 180 lb
Load/Deflection	Room Temp. 180°F, Wet [2] 200°F, Dry	377.0 lb/in 340.4 lb/in 347.5 lb/in	235 lb/in — 235 lb/in

[1] Boeing material specification requirements for a sandwich structure

[2] Wet specimens immersed in 160°F water for two weeks

Figure 57. F584/AS6 Laminate-Honeycomb Sandwich Material Mechanical Property Characterization Tests

Mechanical tests were performed on neat resin samples to determine resin toughness (G_{IC}) and shear modulus. The results of these studies are shown in Figure 58.

4.3.2 Physical Tests

As manufacturing makes the transition to automated layup procedures, part quality and production efficiency depend to a larger degree on the quality assurance of the material's physical parameters. The results of the physical tests are summarized in Figure 59. The resin content and fiber areal weight were determined using the nitric acid digestion method. From this, the fiber volume fraction is available for analysis. Specimens were sectioned, polished, and photomicrographs taken to ensure laminate integrity. Some porosity was evident in the face sheet of the 3-ply long beam flexure specimen. No voids, though, were found in the face sheets of the 9-ply long beam flexure specimens or in the laminate specimens. Photographs of sandwich and laminate sections are shown in Figures 60 and 61. Laminate density and ply thickness were determined from samples taken from the mechanical test specimens. Thermal properties, viscosity, and glass transition temperature were obtained as important processing parameters indicating flow of resin during cure and extent of cure, respectively.

Material Characterization Task	Condition	Results
Toughness	Room Temp.	0.35 in-lb/in^2
Shear Modulus Using Dynamic Mechanical Analysis	Room Temp. 200°F, Dry 180°F, Wet	15.5x10^{10} dyn/cm^2 12.5x10^{10} dyn/cm^2 11.0x10^{10} dyn/cm^2

Figure 58. Neat Resin Mechanical Tests for F584/AS6 Material Characterization

Material Characterization Task	Results	Specification Requirements
Microsection	Complete	
Ply Thickness	0.00575 in	
Resin Content	36.9%	35% ± 2%
Fiber Areal Weight	145 g/m^2	145 g/m^2 ± 5 g/m^2
Laminate Density	0.0564 lb/in^3	
Viscosity - Minimum Jell Point	6.3 Poise 166°C	3-10 Poise
Tg per TMA Laminate Sandwich	162°C 112°C	180°C 180°C

Figure 59. Physical and Chemical Test Results for F584/AS6 Material Characterization

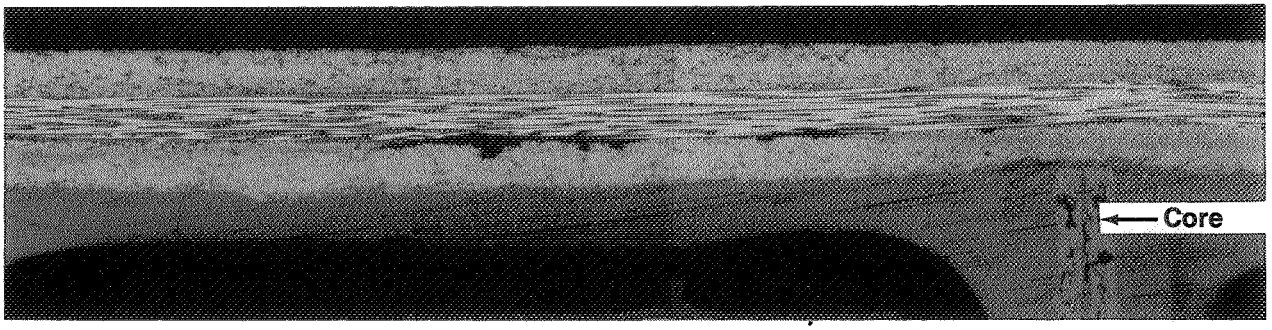

a. Tool Side Face Sheet

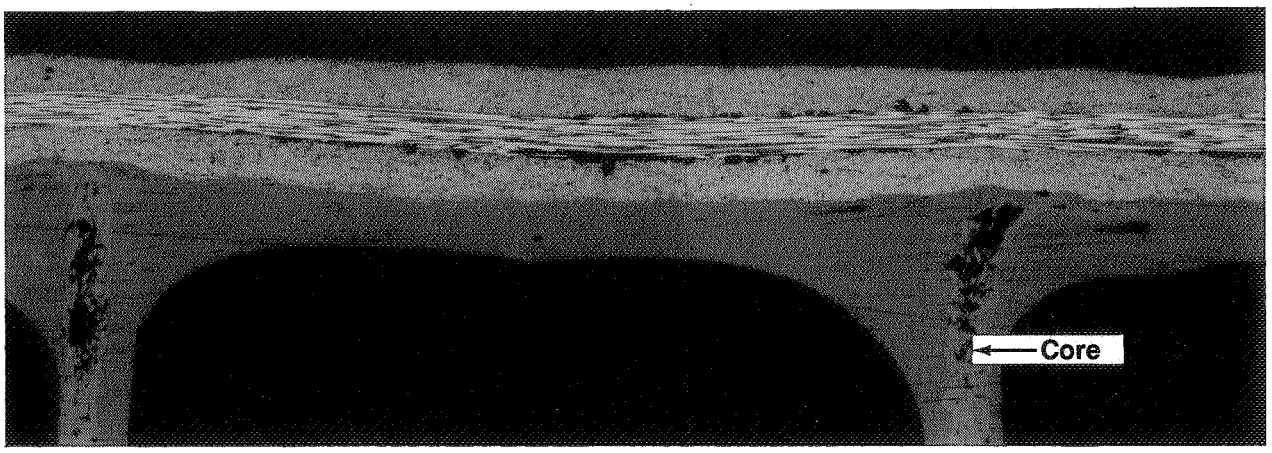

b. Bag Side Face Sheet

Figure 60. Photomicrograph of the Hexcel F584/AS6 Material

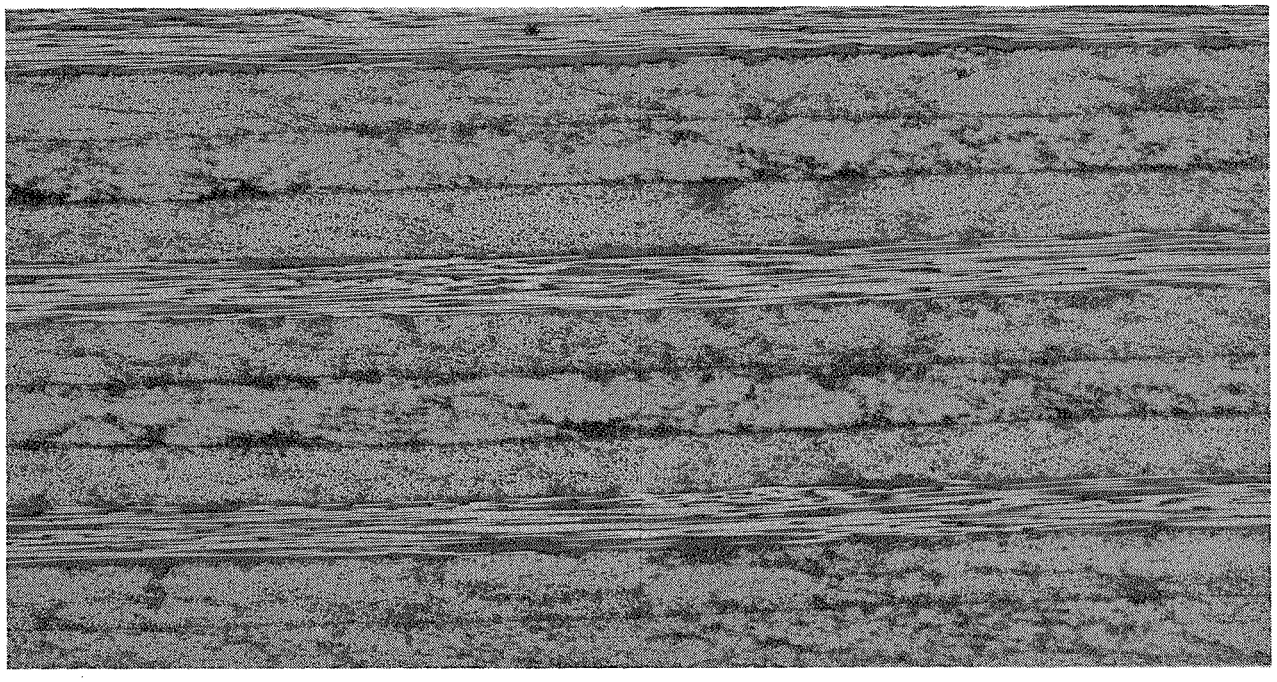

Figure 61. Photomicrograph of F584/AS6 Thick Laminate Specimen

4.3.3 Chemical Tests

Improved quality control methods such as differential scanning colorimetry (DSC), high pressure liquid chromatography (HPLC), and infrared analysis can be used to help ensure consistent, high-quality structure. These methods can differentiate variations in resin chemical formulation to a greater degree than mechanical or dynamic thermal methods, and are necessary indicators of proper storage and adherence to out-time limits. The HPLC sample was done in duplicate and each was run twice. The retention times were:

Catalyst P_1 = 1.93 min

First Curing Agent P_2 = 4.08 min

Second Curing Agent P_3 = 5.01 min

First Epoxy Resin P_4 = 5.66 min

Second Epoxy Resin P_5 = 6.76 min

The peak ratios obtained were:

	P_1/P_4	P_2/P_4	P_5/P_4	P_2/P_3
First	0.20	3.48	0.03	0.89
	0.20	3.41	0.04	0.89
Second	0.21	3.47	0.03	0.89
	0.21	3.42	0.04	0.90

4.3.4 Processibility

Processing variables need to be established and controlled for part consistency. Neat resin tests, which are relatively easy and inexpensive, provide an efficient means to establish limits and determine sensitivity to process parameter variations. These were used in conjunction with hot/wet 0-deg compression tests to determine the effects of (1) heat-up rate during cure, (2) out-time prior to cure, and (3) temperature and humidity during layup.

The standard process cure cycle proposed for primary structure permits a heat-up rate of between 1°F/min and 5°F/min. Tests were performed to ensure that no loss of properties would result from this range of heat-up rates. Neat resin dynamic mechanical analysis (DMA) tests were performed for both dry and hot/wet exposed specimens at rates ranging between 1°F/min and 5°F/min. Because the effects, if any, of heat-up rates could be obliterated in the standard tabbed compression specimens by the secondary curing of the bonded tabs, a tabless specimen was used in this study. The specimen configuration is presented in Figure 62. The results, summarized in Figure 63, indicate no significant differences in the matrix shear storage modulus (G′), or the ratio of viscous to elastic modulus values (tan δ). The former is an indicator of laminate compression strength, and the latter is used to obtain relative glass transition temperatures (Tg) of the laminate, defined here as the peak value of tan δ, and for evaluating validity of the cure.

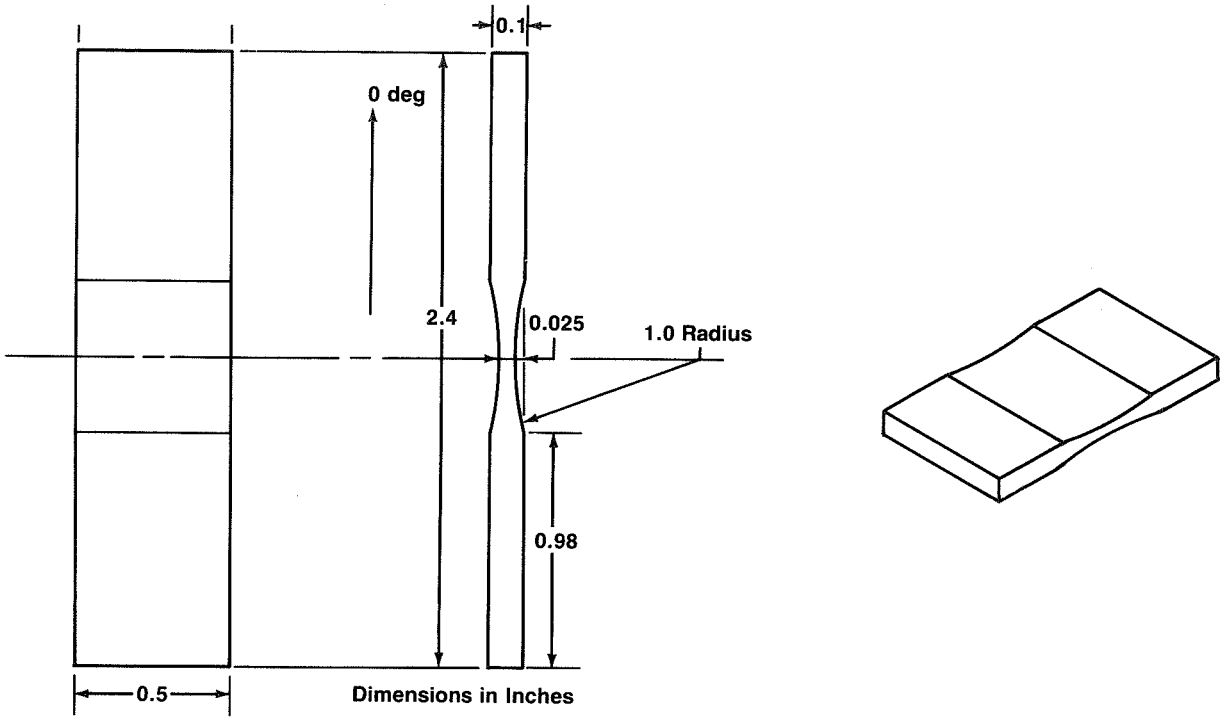

Figure 62. Tabless Compression Specimen

	Compression Strength (ksi)	
	1°F/min	5°F/min
Room Temp.	197.9 (3.8)	201.6 (3.2)
200°F Dry	164.8 (3.1)	166.0 (5.5)
180°F Wet [1]	148.0 ([2])	152.0 (2.3)

[1] Soaked two weeks in 160°F water

[2] Only one out of five specimens failed properly

(X.X) Coefficient of Variance (%)

Figure 63. Tabless Compression Test Results

4.3.5 Flammability

Since existing safety levels must be maintained, the methods used to determine the adequacy of fire protection on both exterior and interior sides of the fuselage shell are kept compatible with current methods. Composite specimens were tested for flammability, smoke, and toxicity. A standard burn requirement is that a vertical surface must self-extinguish in 60 sec. The honeycomb sandwich specimens self-extinguished within the 60-sec required time. The smoke and toxicity data are shown in Figure 64.

Mode — Flaming **Number of Specimens - 3**
Heat Flux — 2.5 W/cm^2

Average Specific Optical Density at 1.5 min — 7.63
Standard Deviation at 1.5 min — 3.0
Average Specific Optical Density at 4.0 min — 254.4
Standard Deviation at 4.0 min — 57.51
Average of Maximum Specific Optical Densities — 395.53
Standard Deviation of Maximum Specific Optical Densities — 77.95
Average Time of Maxima — 6.94
Average Specific Optical Densities at End — 382.47
Maximum of Average Specific Optical Density Curve — 395.03
Time of Maximum of Average Specific Optical Density Curve — 6.83

Toxicity Data				
Toxicant	PPM	Time	Samples per Flame Group	*Method
502	0	4.0	1	D
HCN	8	4.0	1	D
NO_x	130	4.0	1	D
CO	187	4.0	3	NDIR
CO_2	3567	4.0	3	NDIR
HCl	2	4.0	1	D

*NDIR = Specific Gas Monitors
D = Drag Colorimetric Tube

Figure 64. Smoke and Toxicity Results

5.0 FABRICATION

Forty developmental test components were produced, using fabrication methods developed and outlined in Section 4.0, Process Development. The fabrication of test hardware is discussed in this section.

5.1 Tool Fabrication

Tooling was fabricated for the layup and cure of curved skin panels, I-section stringers, and body frames. All of the curved test panels have a 74-in OML radius. This is the same radius as the reference aluminum fuselage body. The curved skin tools were made from graphite-epoxy material in a two-step process. In the first step, a convex aluminum part is made that represents the required final shape of the test hardware. The part model is then used as a mandrel for laying up the graphite-epoxy tool. The part model for the 74-in-radius panels is based on the dimensions shown in Figure 65. This part model was used to fabricate two graphite-epoxy mandrels. The final layup mandrels have peripheral dimensions of 84 in by 124 in. These dimensions were large enough to fabricate all of the curved test articles.

The fabrication of I-section stringers required two graphite-epoxy layup mandrels and one cap caul plate for each stringer. The mandrels are 140 in long with a fixed web height of 1.20 in. These mandrels, made to the dimensions shown in Figure 66, were used to fabricate all of the stringer stiffened panels. A set of stringer layup mandrels and cap caul plates (also graphite-epoxy) for four I-section subassemblies is shown in Figure 67.

The contoured mandrels on which zee-section frames for skin-stringer shells and the tee-frames for honeycomb sandwich skins were machined from aluminum. Figure 68 shows one set of the mandrels in place around a tee-section frame on a honeycomb panel.

5.2 Test Hardware Fabrication

5.2.1 Flat and Curved Laminate Fracture Panels

All of the flat and curved laminate fracture panels (tests 1A and 2) were laid up on a computerized tape laminating machine using Hercules AS6/2220-3 tape, as shown in Figure 69. Initially, it was determined that the AS6/2220-3 material supplied by Hercules had an excessive amount of tack. The level was unacceptably high for use on the automated tape laying machine and created several problems. These problems were:

1. The composite prepreg would not release from the backing paper.

2. In the event of a lamination error, the prepreg was difficult to remove when laid onto itself.

3. The tape created cutting problems on the automated tape laying machine.

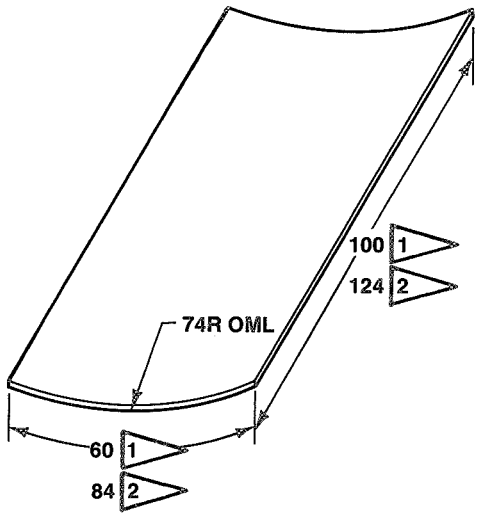

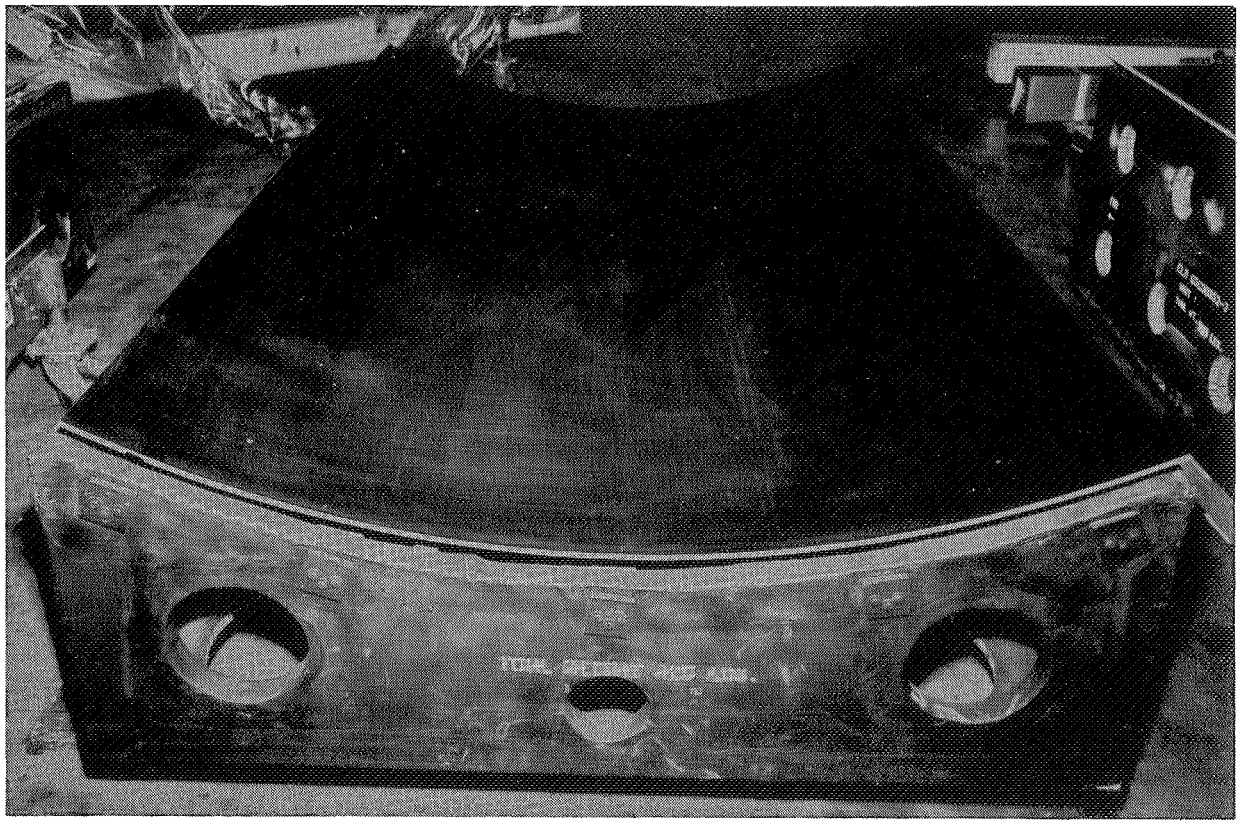

Figure 65. Graphite-Epoxy Layup Mandrel Used for Fabricating Curved Panels

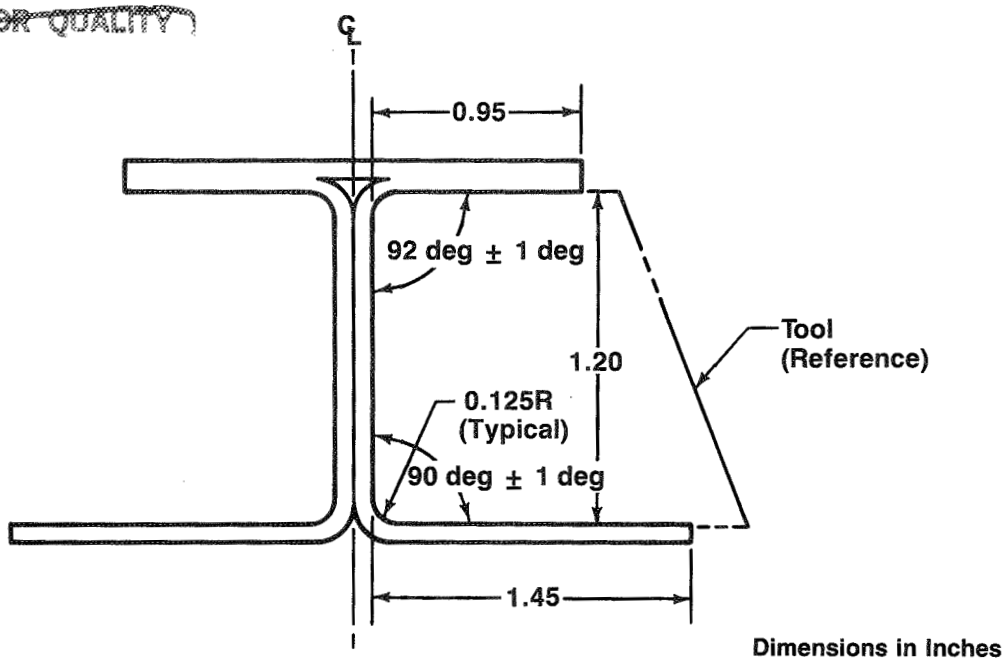

Figure 66. Stringer Dimensions for Tool Design

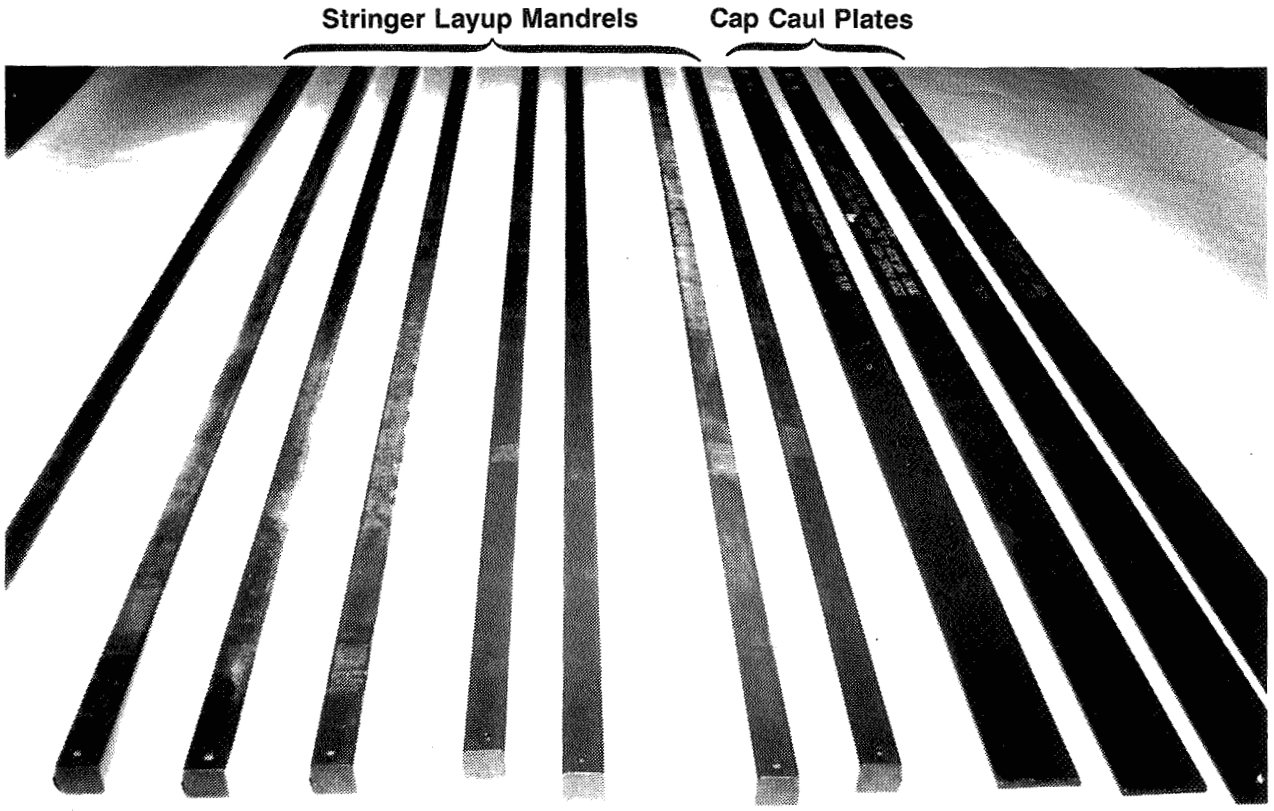

Figure 67. Graphite-Epoxy Stringer Layup Mandrels and Cap Caul Plates

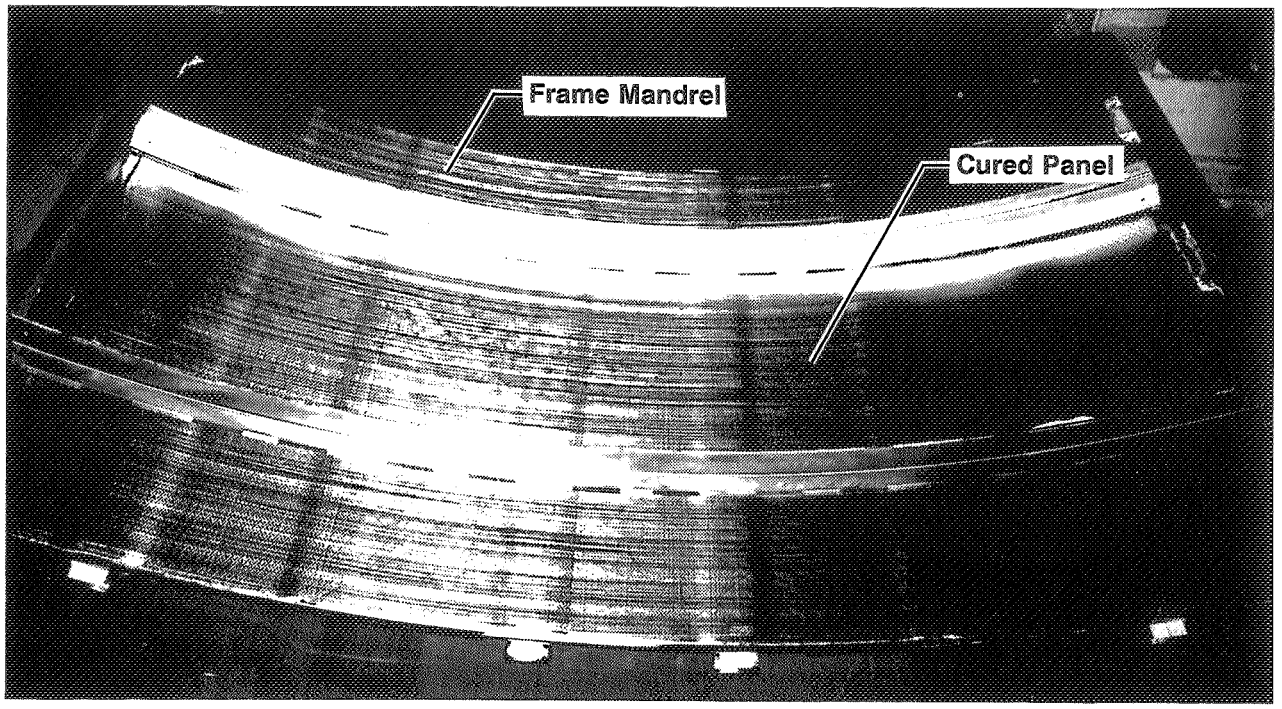

Figure 68. One Set of Aluminum Tee-Frame Mandrels in Place on a Cured Panel

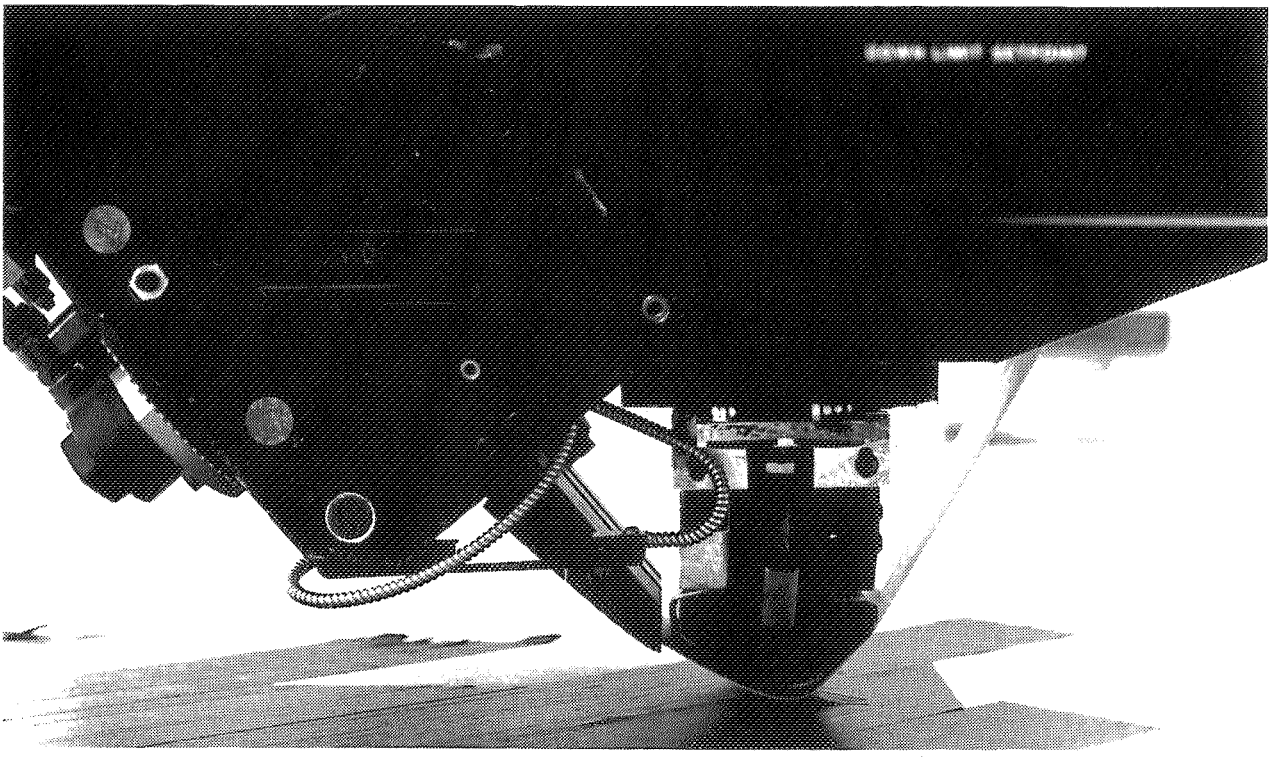

Figure 69. Computerized Tape Laminating Machine Beginning Layup

Hercules provided new material on a less sticky backing paper. Three of the test 1A panels were fabricated using this material. Although the material on the less sticky backing paper was usable, it did not satisfy all of the requirements. The graphite tape tended to slip during the manufacturing process causing misalignment, and the cutting operation was difficult and inconsistent. Careful monitoring of this process caused an increase in labor hours and a reduction in the rate of tape laydown.

The initial problems with the tape laminating machine caused by the excessively tacky AS6/2220-3 tape were solved by allowing the material to age slightly, being careful not to exceed the out-time requirements of the material specification. In addition, Hercules supplied material with improved tack characteristics for use with the remaining fabrication effort.

After lamination, the preplied panels were trimmed using a numerically controlled Gerber cutter, as shown in Figure 70. The panels were transferred to layup mandrels, vacuum bagged, and autoclave cured. The curved panels were drape formed into the 74-in-radius layup mandrels at room temperature. A typical panel with preimpregnated grip doublers located is shown in Figure 71. After curing, grip doublers were installed and co-bonded to the panels. The grip doublers were then drilled for mounting in the test fixtures.

5.2.2 Skin-Stringer Panels

The skin-stringer panels for tests 3, 4, 5, 6A, and 7A were fabricated using the process described in Section 4.1 and diagramed in Figure 46.

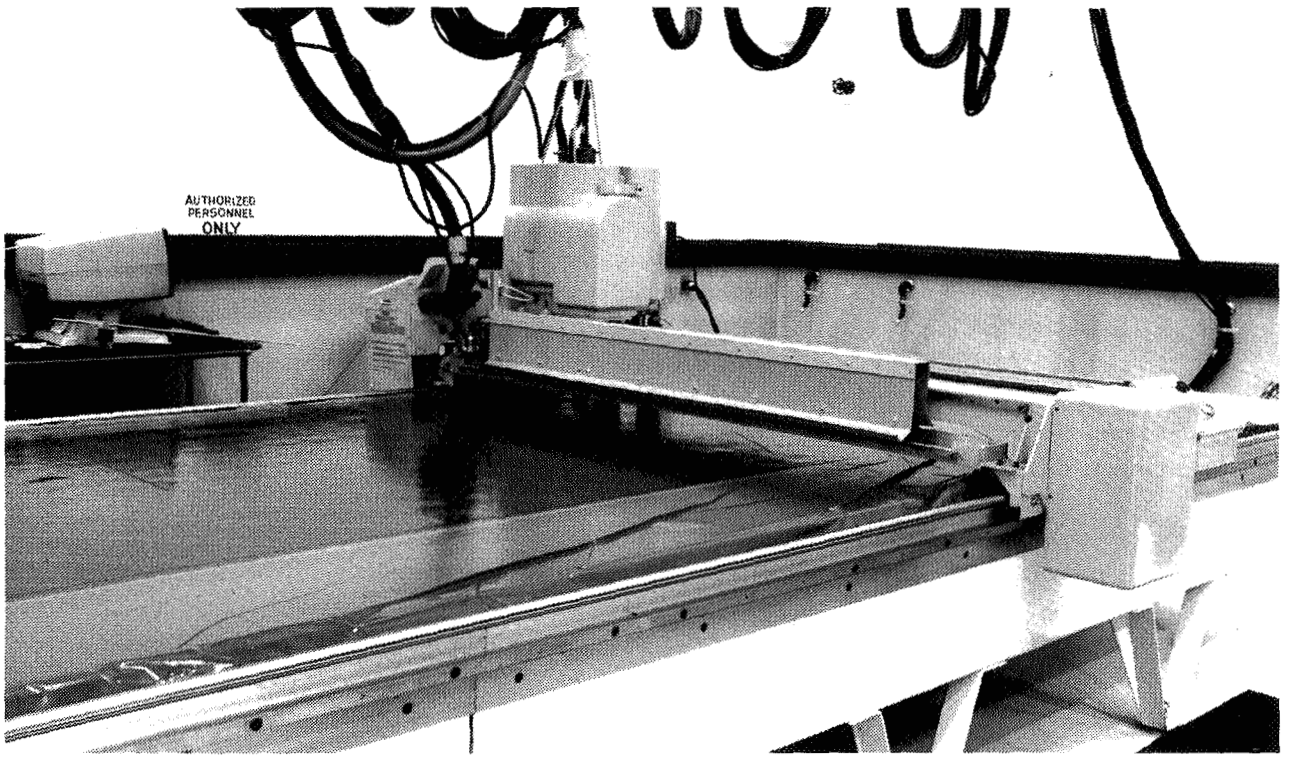

Figure 70. Numerically Controlled Cutter in Operation

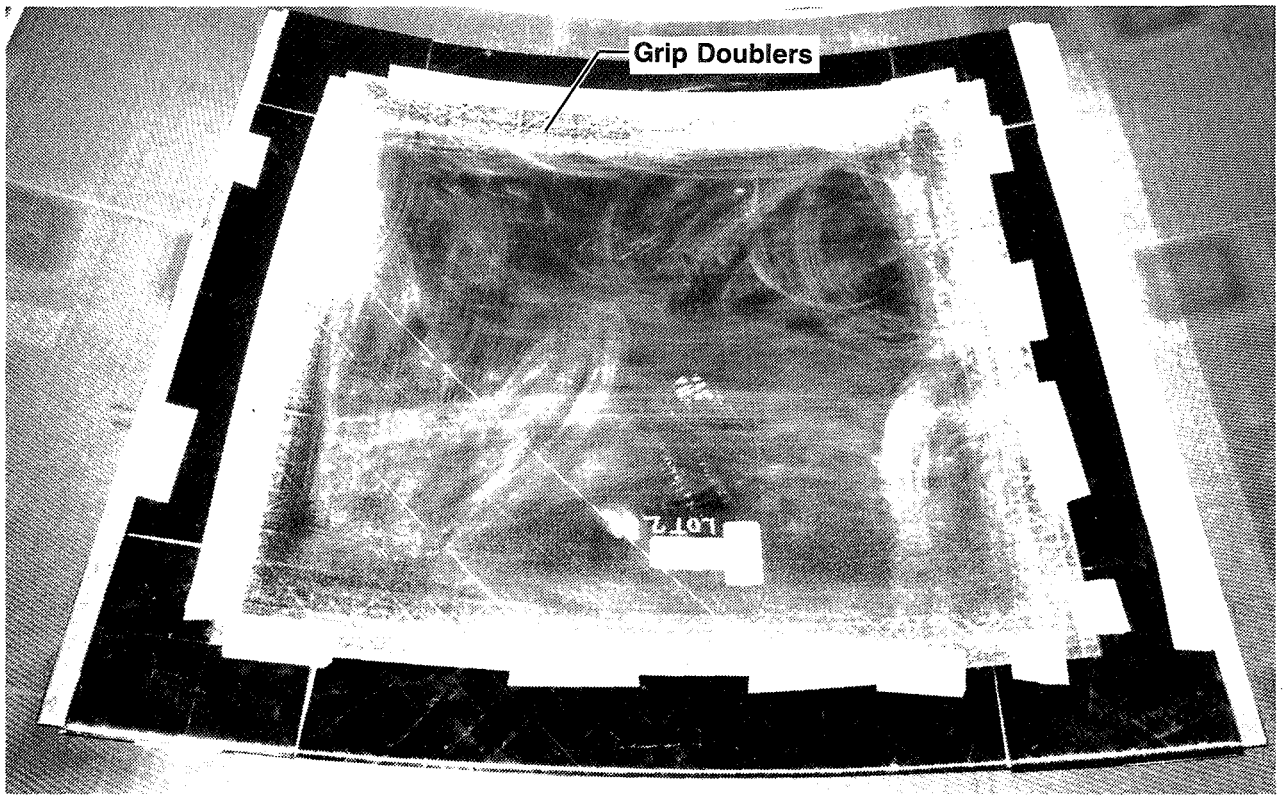

Figure 71. Cured Panel With Prepreg Grip Doublers Located, Ready for Final Autoclave Cure (Test 2)

Both crown and keel panel assemblies consisted of preplied skin and stringer material prepared by the tape laminating machine and a numerically controlled cutter. The skins were draped into the layup mandrels at room temperature. Except for the flat skin-stringer panels of test 5 and the pressure pillowing panels of test 7A, the curved layup mandrels were used for all of the skin-stringer fabrication.

The stringer channels were formed by draping laminate material over mandrels, shown in Figure 72. Prior to forming, the laminate material was softened by heating the laminate to 150°F. A vacuum bag was used to provide the pressure to conform the warm layups to the stringer mandrels. After cooling down, the formed channels were trimmed and then compacted together at the web area using a vacuum bag. Filler strips were placed in the radii between the assembled channel sections, and cap plies were added to complete the I-section stringer. The entire subassembly was compacted by a vacuum bag.

Precured strips placed between the stringers and the skin were located by using a template. Following this, the template was again used to locate the stringer subassemblies. The stringer subassemblies were then positioned on the skin layup. The entire panel assemblies were then vacuum bagged and autoclave cured. Following cure, the panels were debagged, removed from the tools, and trimmed.

The single-stringer crippling elements for test 3 and the three-stringer compression panels for test 4 were cut from representative keel and crown panels. The keel panel crippling elements

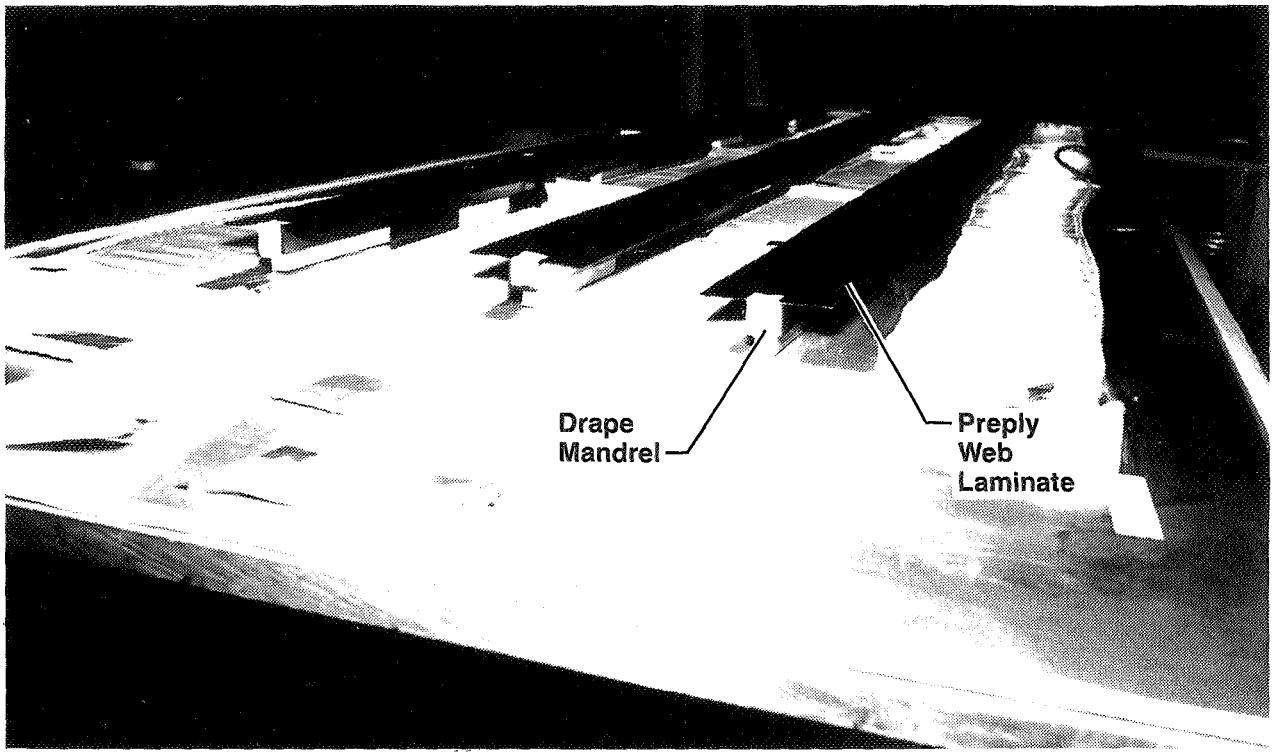

Figure 72. Stringer Web Preplies Prior to Heat-Assisted Drape Forming (Tests 3 and 4)

(test 3) and compression panels (test 4) with grip doublers bonded on are shown in Figure 73. The ends of each compression panel and crippling element were later potted and machined flat and parallel to ensure even load distribution during test.

The two skin-stringer shear panels for test 5 were laid up and cured in a single 102-in-long assembly. After cure and cooling, the panel was found to be warped approximately 0.25 in out of plane. A thermal analysis of the section indicated that this warpage developed from a mismatch in thermal expansion coefficients between the skin and stringers and the aluminum caul plates. Figure 74 shows the cured test 5 skin-stringer panels with grip doublers located prior to co-bonding. The doublers were cured onto the first panel unrestrained and came out of cure considerably warped (approximately 1.0-in out-of-plane warpage, corner to corner). The second panel was bagged and then restrained with weights. This panel was considerably flatter after curing.

During testing, the panels were clamped flat around the edges. When the panels were clamped to a planar perimeter frame, the maximum out-of-plane deformation of either panel was 0.060 in.

The skin-stringer panels of test 6A were laid up and cured on a curved 74-in-radius skin tool. Figure 75 shows a view of the inner surface of one of the test 6A compression panels following co-bonding of the end doublers.

The ends of the panels were then potted and machined. Curved aluminum zee-frames were fabricated and mechanically fastened to the stringers of both of the two test panels.

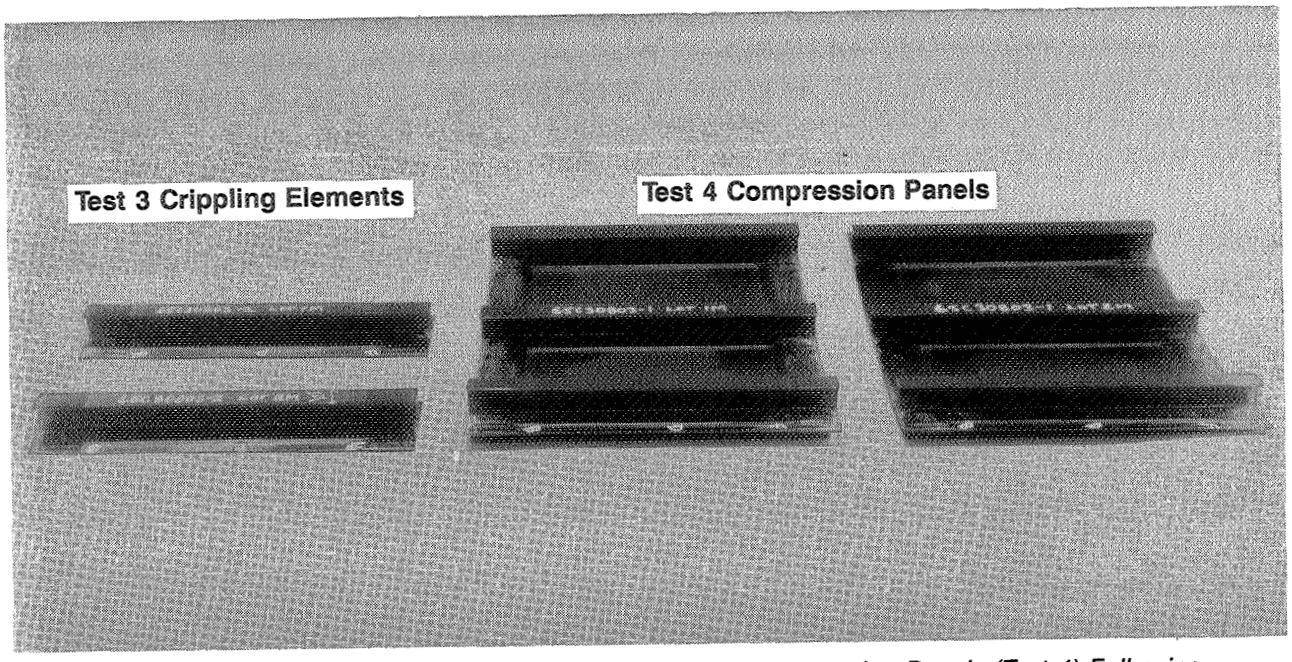

Figure 73. Keel Panel Crippling Elements (Test 3) and Compression Panels (Test 4) Following Curing of Grip Doublers

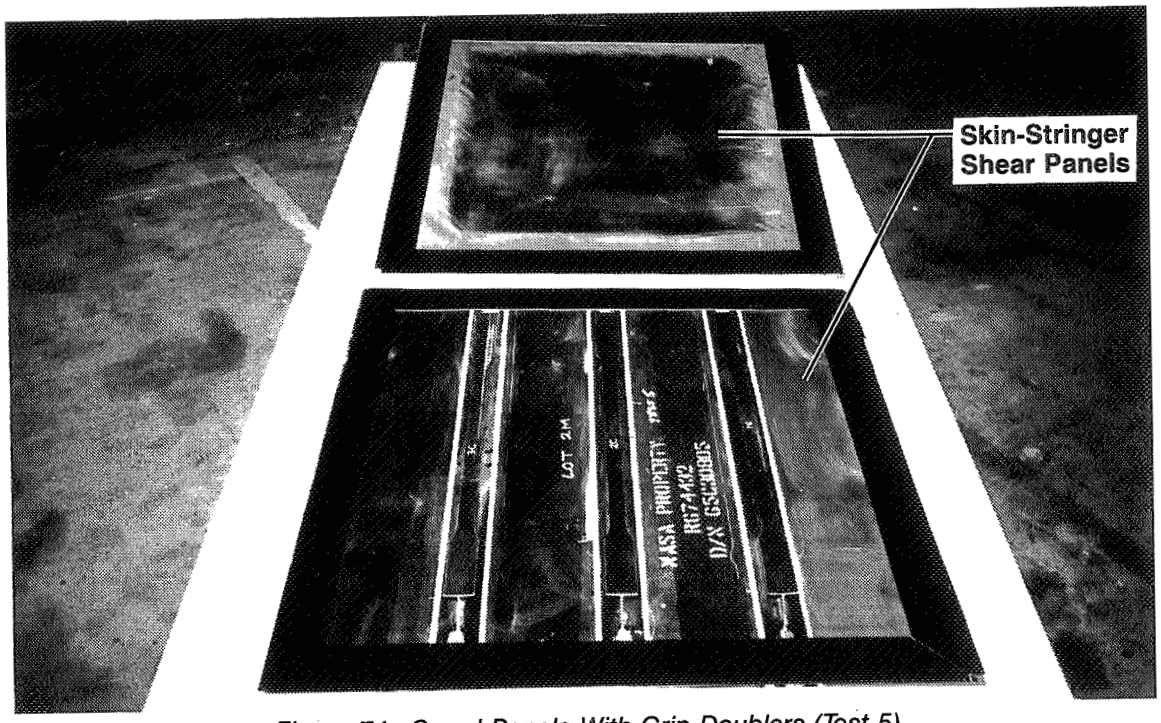

Figure 74. Cured Panels With Grip Doublers (Test 5)

Figure 75. Panel With Doublers Bonded on Both Ends (Test 6A)

The test 7A panels have a single co-cured I-stringer cured to laminate skin using a flat caul plate. After cure, the panel was trimmed into four specimens. Graphite-epoxy angle frames were fabricated and mechanically fastened to the stringer cap of each specimen at its center. Figure 76 shows one of the panels, together with the angle frame, and radius fillers prior to assembly. Two of the panels used radius fillers mounted underneath the stringer cap flanges to help distribute the load transmitted through the bolts during testing. The other two panels did not use radius fillers.

5.2.3 Honeycomb Panels

The test articles for the sandwich panels of tests 1B, 6B, and 7B were fabricated with 4.0-lb/ft^3 fiberglass reinforced bias weave honeycomb core and Hexcel AS6/F584 graphite-epoxy face sheets in a single-stage cure. The face sheets of all of the honeycomb panels were laid up by hand with 12-in-wide tape. In production, the panel face sheets would be laminated by automated methods.

The cells at the ends of the honeycomb core were filled with a thermoset potting compound to prevent the panels from being crushed during test. After the potting was cured, the core was machined and assembled between the prepreg skin layups. After the panels were cured, doublers were installed and co-bonded to the panels. A 30-in by 100-in honeycomb flat fracture panel is shown in Figure 77. After the flat fracture panels were cured and edge trimmed, holes were drilled in the grip areas for mounting the test fixtures.

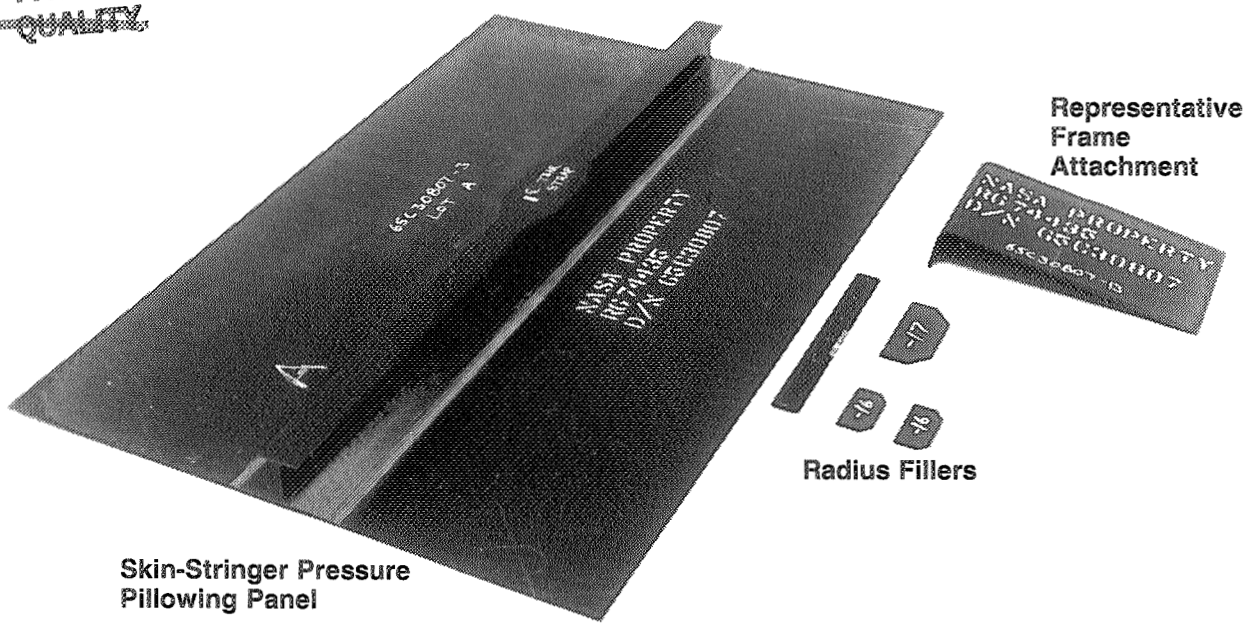

Figure 76. Pressure Pillowing Panel, Angle Frame Test Fixture and Radius Fillers (Test 7A)

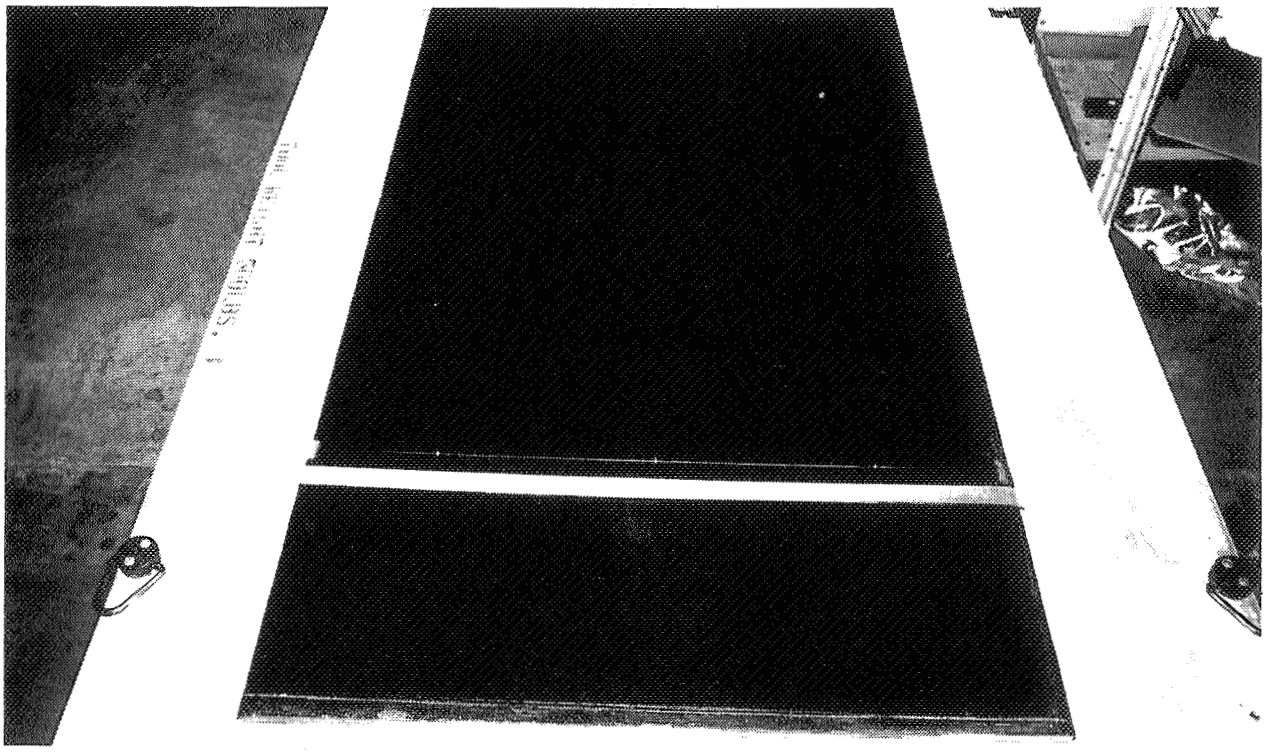

Figure 77. Cured 30-in by 100-in Panel Prior to Application of Grip Doublers (Test 1B)

Some problems developed during the layup and co-cure of the tee-section frames on the curved compression damage tolerance panels for test 6B. Maintaining the 0-deg orientation along the curvature of the tee-frames with prepreg tape proved difficult without introducing wrinkles into the web of the tee. To overcome this problem, the individual 0-deg plies were applied in two sections: (1) The curved pattern of the web was cut from 0-deg tape using the tee-frame tool as a cutting template, as shown in Figure 78, and (2) the 0-deg ply on the flange (base) of the tee was applied as a separate piece butted to the 0-deg web ply, as shown in Figure 78. The 0-deg orientation in the web is not parallel to the curvature of the skin. The 90-deg ply was laid up with the edges of adjacent pieces of tape touching around the smaller radius of the layup mandrel. The tape was then heated and spread near the larger radius to eliminate gaps between individual segments. Laying of the $\pm$45-deg plies was started at the center of the mandrel. The tape edges were butted together. As the ply layup approached the ends of the mandrels, the orientation varied from a true $\pm$45 deg with respect to the flange surface. The results of the compression damage tolerance test were not affected by the modified layup in the tee-section frames.

In production, the curved tee-section frames would be laid up using fabric. This procedure has been verified in an Air Force manufacturing program (ref. 10). After layup, the tee-frame halves were fitted together and vacuum compacted to form the frame subassemblies. Single-ply tape filler strips were located on the sandwich panel inner skin between tear strap protrusions. Following this, the frames were located on the inner skin. The entire assembly was then vacuum bagged. After autoclave cure, the panel was cut into halves and the halves trimmed. One of the completed panels is shown in Figure 79. As discussed in Section 3.2, some areas of low compaction were found below the frames. Since this detail is not critical in the compression damage tolerance tests, the panels were acceptable for test. The curved ends were then potted and machined. Curved aluminum angle frames were roll formed, heat treated, and mechanically fastened to the tee-frames to form zee-frames.

Fabrication of the 7B panel was similar to that of the 6B panel except that it was laid up and cured on a flat caul plate rather than on a curved layup mandrel.

As in the case of the test 6B panel, the problem of low compaction under the frame flanges, discussed in Section 3.2, was a concern during the fabrication of the test 7B panels. However, it was determined that contoured lower stringer flange mandrels to offset the tear strap protrusions would ensure consistent compaction along the flanges. Teflon tape shims were applied to the mandrel lower flange areas between tear strap protrusions, shown in Figure 53. This approach was successful. Through-transmission ultrasonic (TTU) inspection of the cured parts revealed no areas of low compaction.

The panel was then halved and the halves trimmed. Aluminum test fixtures were mechanically fastened to the tee-frames of both panels. One such assembly is shown in Figure 80. The potting at the ends of the panel (where it is restrained in the test machine) is evident in the photo.

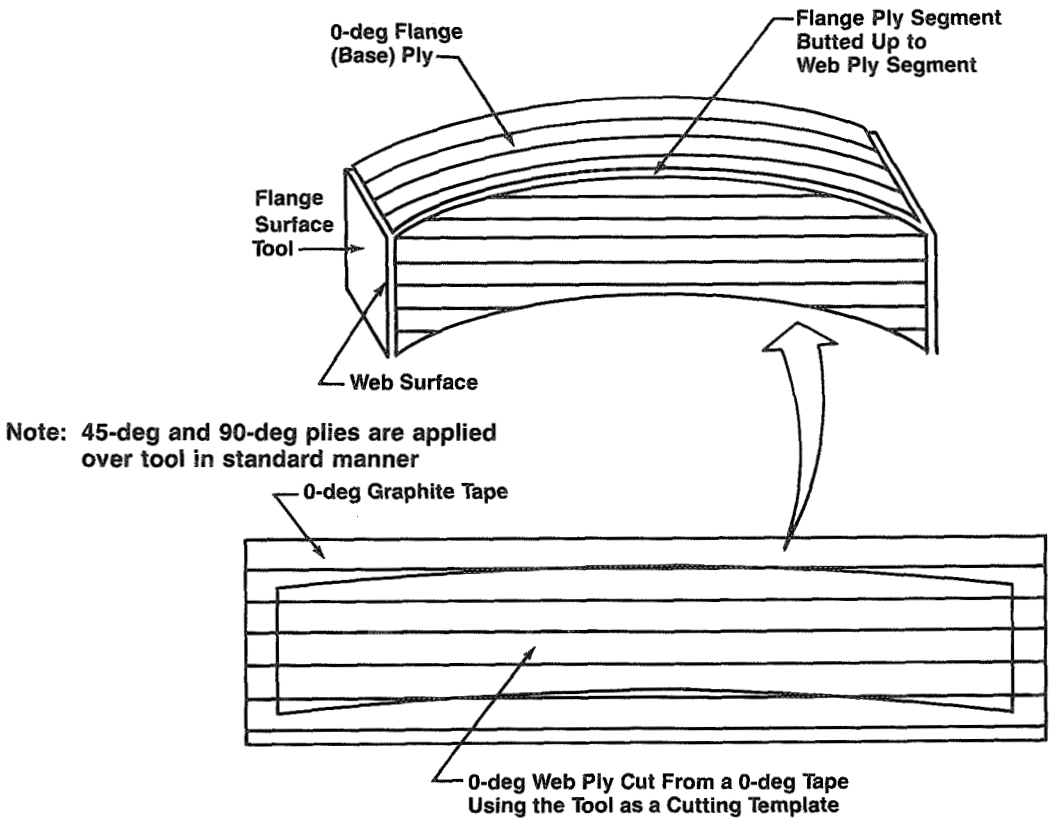

Figure 78. Application of 0-deg Ply to Tee-Frame Tool

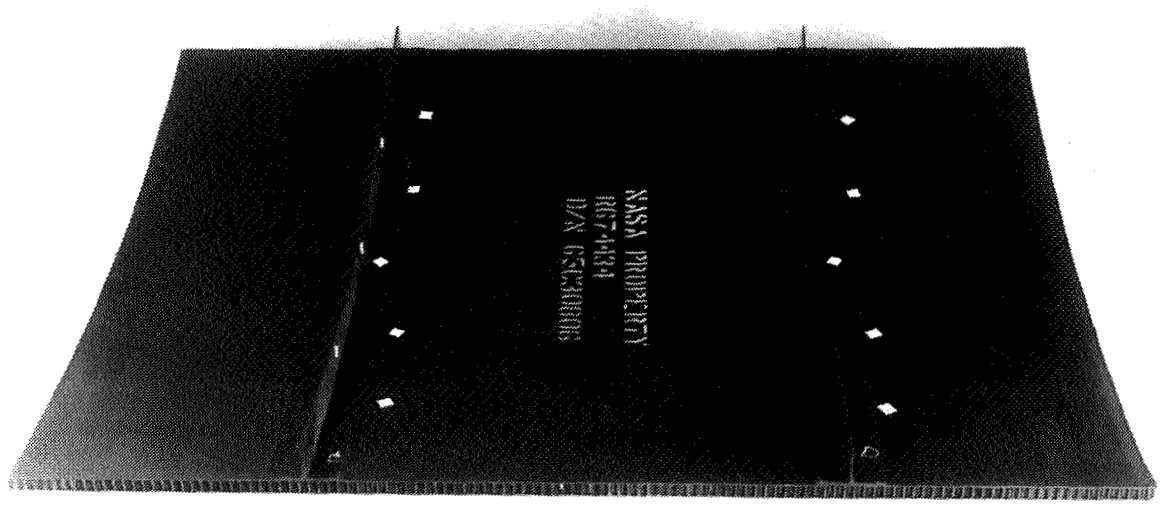

Figure 79. Cured Panel (Test 6B)

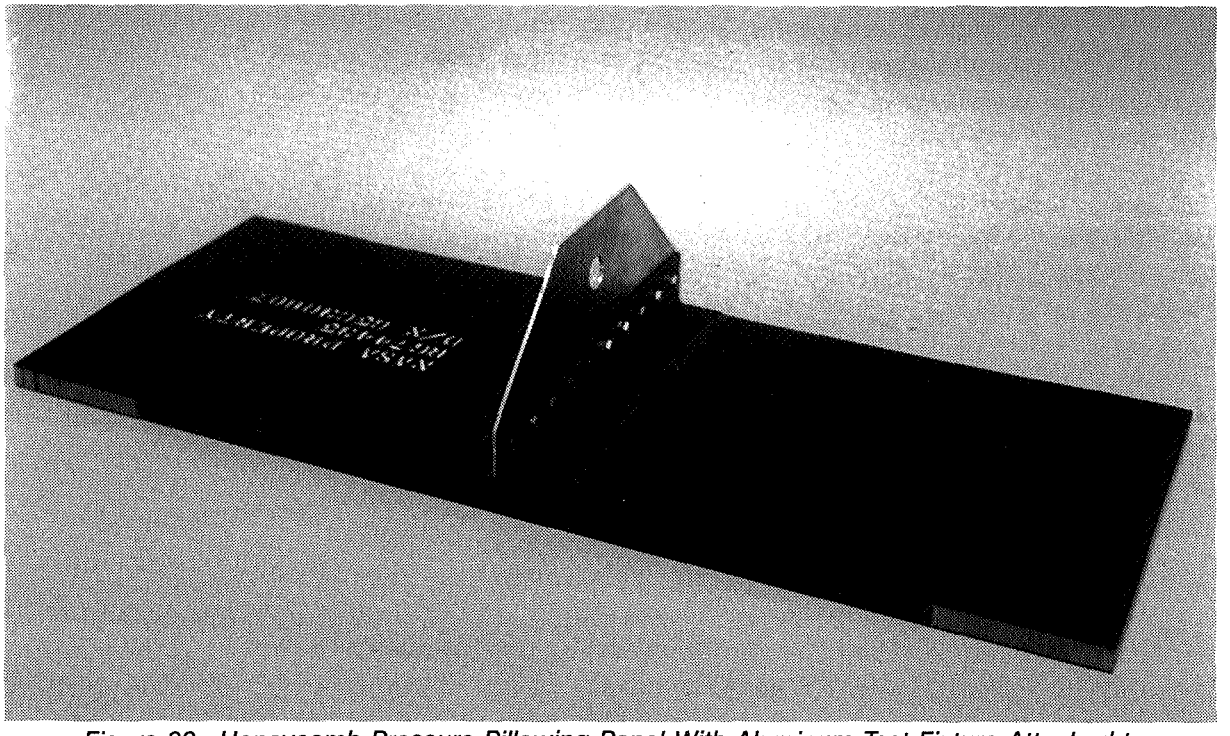

Figure 80. Honeycomb Pressure Pillowing Panel With Aluminum Test Fixture Attached to Tee-Frame (Test 7B)

5.3 Quality Assurance

Part quality was monitored and documented throughout all phases of fabrication and assembly. Inspection data requirements included the following:

- Material verification and traceability
- Cure process verification
- Process control tests
- Nondestructive inspection (NDI)

The data developed for ensuring that part quality is documented and traceable, starting from the receipt of raw materials until final part assembly is complete. Prior to part layup and fabrication, all materials were inspected to ensure that basic chemical, physical, and mechanical properties were acceptable. During cure, autoclave pressures and temperatures were monitored and controlled within required tolerances. The completeness of cure was evaluated by performing glass transition temperature (Tg) tests on material trimmed from the fabricated panel.

Finished part dimensions and critical thicknesses, as specified on the engineering drawings, were measured and recorded.

All areas of cured panels were checked by NDI to determine the quality of the laminate and/or bond area. Laminate and bond area anomalies greater than that allowed by the process specification and/or drawing were recorded by the rejection tag process, and Engineering was notified of the discrepancy.

Ultrasonic inspection of stringer panel assemblies was accomplished using multiple ultrasonic techniques. Skin areas and accessible areas of the stringer web were inspected using conventional TTU methods. A modified TTU technique, pulse echo loss of back, was used for inspecting the skin flange, flange-to-skin bondline, and skin region. In this technique, ultrasonic waves reflected off the back surface of the part were used to detect the size and depth of anomalies within the laminate. Free flange sections were inspected by immersing the part in water and reflecting ultrasonic waves off a reflector plate placed behind the flange. Free flange and skin flange radius areas were inspected with a line scan TTU at a 30-deg angle to the skin surface.

Foam tape markers, 0.5-in square, were applied to the part surfaces for position identification on the resulting scan recordings and for verification of the inspection process.

Areas of low compaction were identified in the crown configuration skin-stringer panels for tests 3 and 4. Typical anomalies from this panel are shown in Figure 81. The effect that these areas have on compression strength was evaluated by test and is discussed in Section 6.2.1. No other areas of low compaction were noted in any of the other skin-stringer panel assemblies.

Honeycomb composite structures were subjected to two types of ultrasonic inspection. The first was TTU, and it was used to identify the outer boundary of all anomalies. The second, pulse echo, was used on the skin face sheets to identify anomalies or damages within the skin.

The TTU scanning was performed using test frequencies in the 0.5- to 1-MHz range and narrow jets of water couplant for obtaining maximum resolution. TTU has no time domain sensitivity and cannot be used to define the type of damage or depth of damage within the cross section.

Pulse echo scanning of the skin configuration was performed using high frequency focused transducers to obtain high spatial and depth resolution, with the resultant echo signal levels recorded in proportionate gray scales. Skin damage is indicated by either the loss of the background adhesive-honeycomb pattern or the presence of the highly reflecting ply delamination signal.

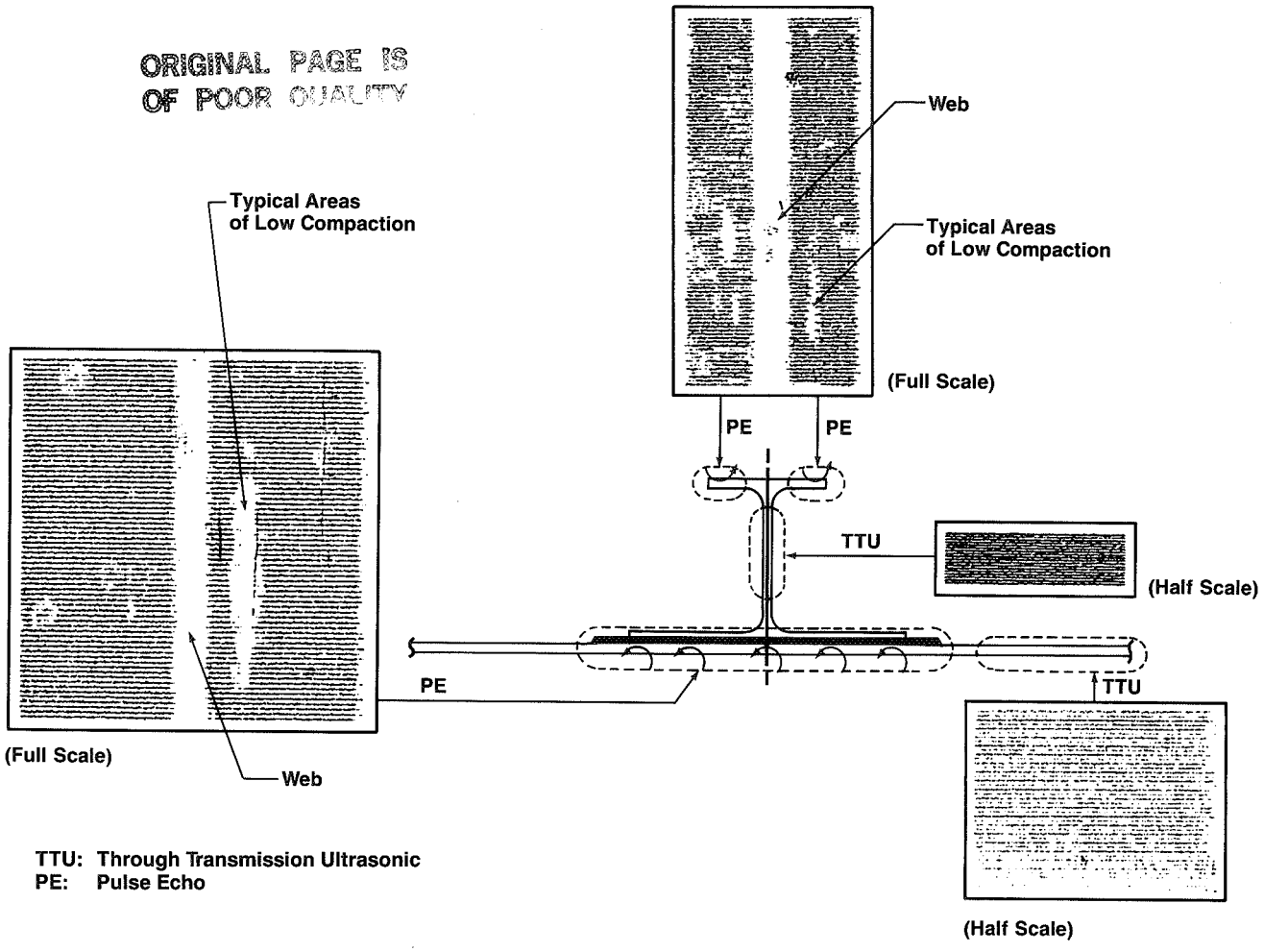

Figure 81. Nondestructive Inspection Results for Skin-Stringer Crown Section

6.0 DEVELOPMENT TESTS

Subcomponent panels and elements have been designed, fabricated, and tested to investigate the relative structural characteristics of the selected designs and verify analysis methods for damage tolerance. The development tests, summarized in Figure 82, evaluated (1) tension fracture characteristics, (2) compression and shear postbuckling behavior, (3) damage tolerance for compression panels, and (4) pressure pillowing pulloff effects for skin-stringer and frame. Typical testing was done at room temperature. Selected fracture testing was conducted at -65°F.

Inplane tension fracture strength and laminate and honeycomb configurations at ambient and low temperatures were assessed in tests 1A and 1B. The effects of curvature and local pressure loading at the edge of the damage on the laminate fracture strength were evaluated in test 2. The dynamic effect of imposing damage on a panel under load was also considered.

Test 3 provided compression crippling strength data for the selected stringer sections. Test 4 assessed the stability and postbuckled compression strength of the selected skin-stringer panels. Postbuckling integrity and strength of a stiffened shear panel were evaluated in test 5.

Test 6 provided information on impact resistance and the severity of a large cut on curved skin-stringer and honeycomb panels loaded in compression.

Test 7 established the capability of the frame-to-skin connection to resist pressure pillowing loads.

The details of the analyses and tests of the development program are discussed in the following sections.

6.1 Tension Fracture

Tests and analyses were performed to characterize the fracture response of fuselage laminate and honeycomb shell structure due to tension and pressure loading. Ten axially loaded flat laminate panels were tested in test 1A to determine fracture strength with large discrete damage. Two skin layups, representative of fuselage shell structure, were evaluated. To provide damage tolerance, 3-in-wide 0-deg-oriented tear strap plies were interleaved into the skin laminate panels. Various combinations of tear strap spacing and stiffening were evaluated. In addition, two honeycomb panels were tested (test 1B) to evaluate the adequacy of interleaving tear straps in the face sheets of a honeycomb shell structure.

The influence that curvature and pressure have on fracture strength was analyzed by test and analysis of six biaxially and pressure loaded constant thickness laminate panels (test 2). Additional analyses were performed to evaluate varying values of stiffening and shell radius.

The analyses for both flat and curved fracture panel studies were performed by constructing finite element models (FEM) to represent a quarter panel section containing basic laminate material and tear strap areas. The analysis code NASTRAN (ref. 11) was used for these tasks. The results of the tests and analyses are discussed in the following sections.

Test No.	Description	Number of Configurations	Number of Specimens	Test Environment	Purpose

1A	Flat Laminate Fracture Panel 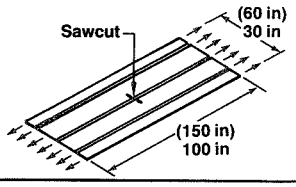	7	10	Room Temp. Dry
				-65°F Dry
					• Determine In-Plane Fracture Strains at Which:
					  ◦ Flaw Growth Is Initiated
					  ◦ Flaw Growth Is Arrested
					• Establish Analytical Data Base for Determining Pressure Containment Capability of Composite Fuselage Structure

1B	Flat Honeycomb Fracture Panel 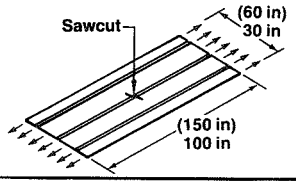	2	2	Room Temp. Dry	

2	Curved Laminate Fracture Panel 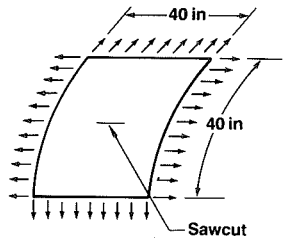	2	6	Room Temp. Dry
				-65°F Dry
					• Determine Out-of-Plane Effects on Fracture Strains at Which Flaw Growth Is Initiated:
					  ◦ Curvature
					  ◦ Pressure
					  ◦ Applying Damage While Panel Is Loaded
					• Evaluate Effects of Varying Panel Edge Supports (Axial or Biaxial)
					• Establish Analytical Data Base for Determining Pressure Containment Capability of Composite Fuselage Structure

3	Single Stiffener Crippling Element 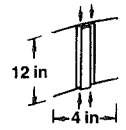	2	5	Room Temp. Dry	• Determine Local Stability and Crippling Capability of Stiffener Element • Verify Analysis Methods
4	Curved Skin/Stringer Compression Panel 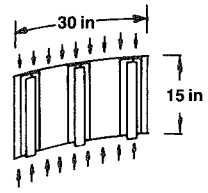	2	4	Room Temp. Dry	• Evaluate Postbuckled Stability and Compression Capability of Skin-Stringer Panel • Verify Analysis Methods
5	Skin/Stringer Shear Panel 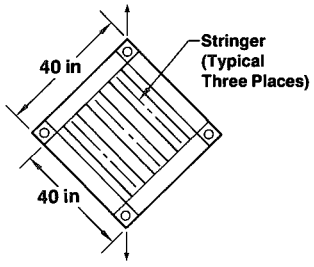	1	2	Room Temp. Dry	• Evaluate Postbuckled Shear Strength of Skin-Stringer Shear Panel • Determine Shear Buckling Allowable of Skin-Stringer Shear Panel • Verify Analysis Methods

Figure 82. Development Tests

Test No.	Description	Number of Configurations	Number of Specimens	Test Environment	Purpose
6A	Skin/Stringer Compression Panel 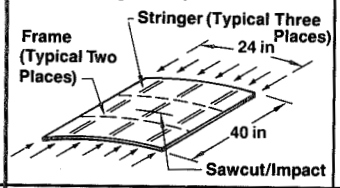	1	3	Room Temp. Dry	• Determine Compressive Fracture Strains • Determine Tolerance to Impact Damage • Correlate Analytical Analysis Model With Test Results
6B	Honeycomb Compression Panel 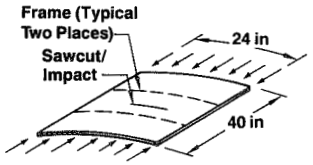	1	2	Room Temp. Dry	
7A	Pressure Pillowing Panel (Skin Panel/ Frame Attachment) 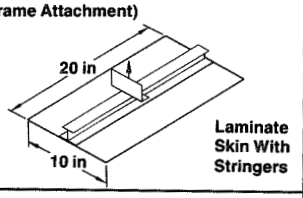	2	4	Room Temp. Dry	• Develop and Verify Design Details of Skin Panel to Frame Attachment
7B	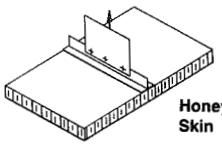	1	2		

Figure 82. Development Tests (concluded)

6.1.1 Flat Fracture Panels

The primary objective of these tests was to verify the damage containment capability of the tear strap design. The design procedure is shown in Figure 9. The development of this procedure was initiated in the Composite Fuselage Study program, contract NAS1-17417 (ref. 1). The tear strap design curves were based on the same type of FEMs used to analyze the test panels discussed in following sections.

The configurations of the 10 solid laminate panels of test 1A and the two honeycomb fracture panels of test 1B are summarized in Figures 83 and 84, respectively. Typical interleaved tear strap details are shown in Figure 85. The tear straps were spaced at 10 in to represent stringer spacing, and at 20 in to represent circumferentially oriented tear straps located under body frames. Seven of the laminate panels and one honeycomb sandwich panel were fabricated with a 2/8/2 laminate, that is, 16.7% 0-deg, 66.6% ±45-deg, 16.7% 90-deg oriented plies. The remaining panels were fabricated with a quasi-isotropic laminate, that is, 25% 0-deg, 50% ±45-deg, 25% 90-deg oriented plies. The relative amount of tear strap stiffening varied from 0% (no tear straps) to 37% stiffening.

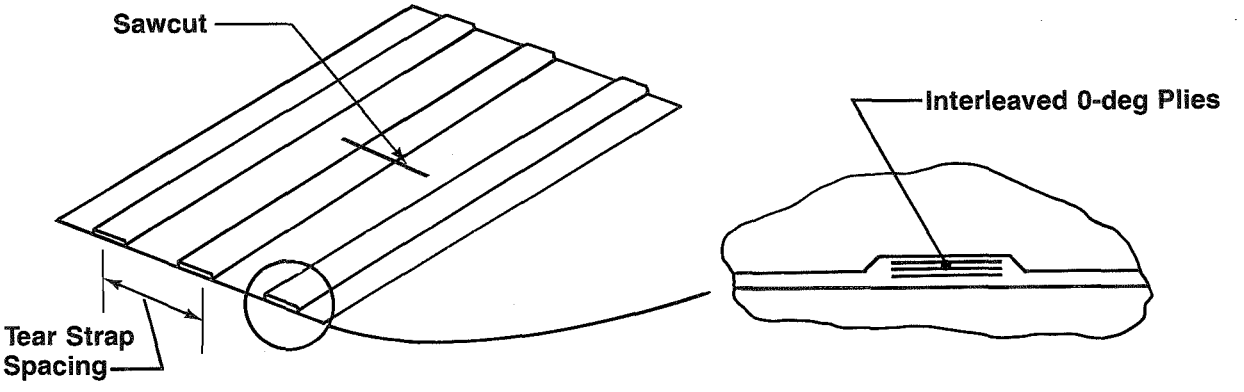

Panel Number	Skin Layup	Tear Strap Plies	Tear Strap Spacing (in)	Stiffening (%)	Panel Spacing (in)	Test Temperature
-1	2/8/2	0	—	0	30x100	Room Temp.
-2	4/8/4	0	—	0	30x100	Room Temp.
-3	2/8/2	5	20	18	60x150	Room Temp.
-4	2/8/2	10	20	36	60x150	Room Temp.
-5R	2/8/2	3	10	22	30x100	Room Temp.
-5C	2/8/2	3	10	22	30x100	-65°F
-6R	2/8/2	5	10	36	30x100	Room Temp.
-6C	2/8/2	5	10	36	30x100	-65°F
-7R	4/8/4	8	10	37	30x100	Room Temp.
-7C	4/8/4	8	10	37	30x100	-65°F

Figure 83. Flat Laminate Fracture Panels (Test 1A)

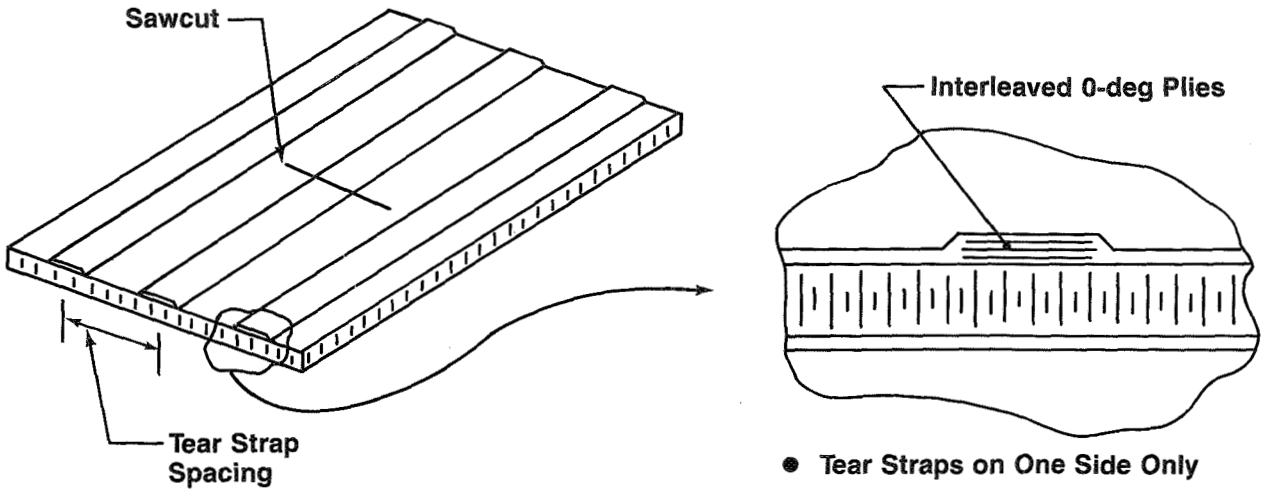

Panel Number	Layup of Each Face Sheet	Tear Strap Plies	Tear Strap Spacing (in)	Stiffening (%)	Panel Size (in)	Test Temperature
-1	2/8/2	10	20	18	60x150	Room Temp.
-2	4/8/4	8	10	18	30x100	Room Temp.

Figure 84. Flat Honeycomb Fracture Panels (Test 1B)

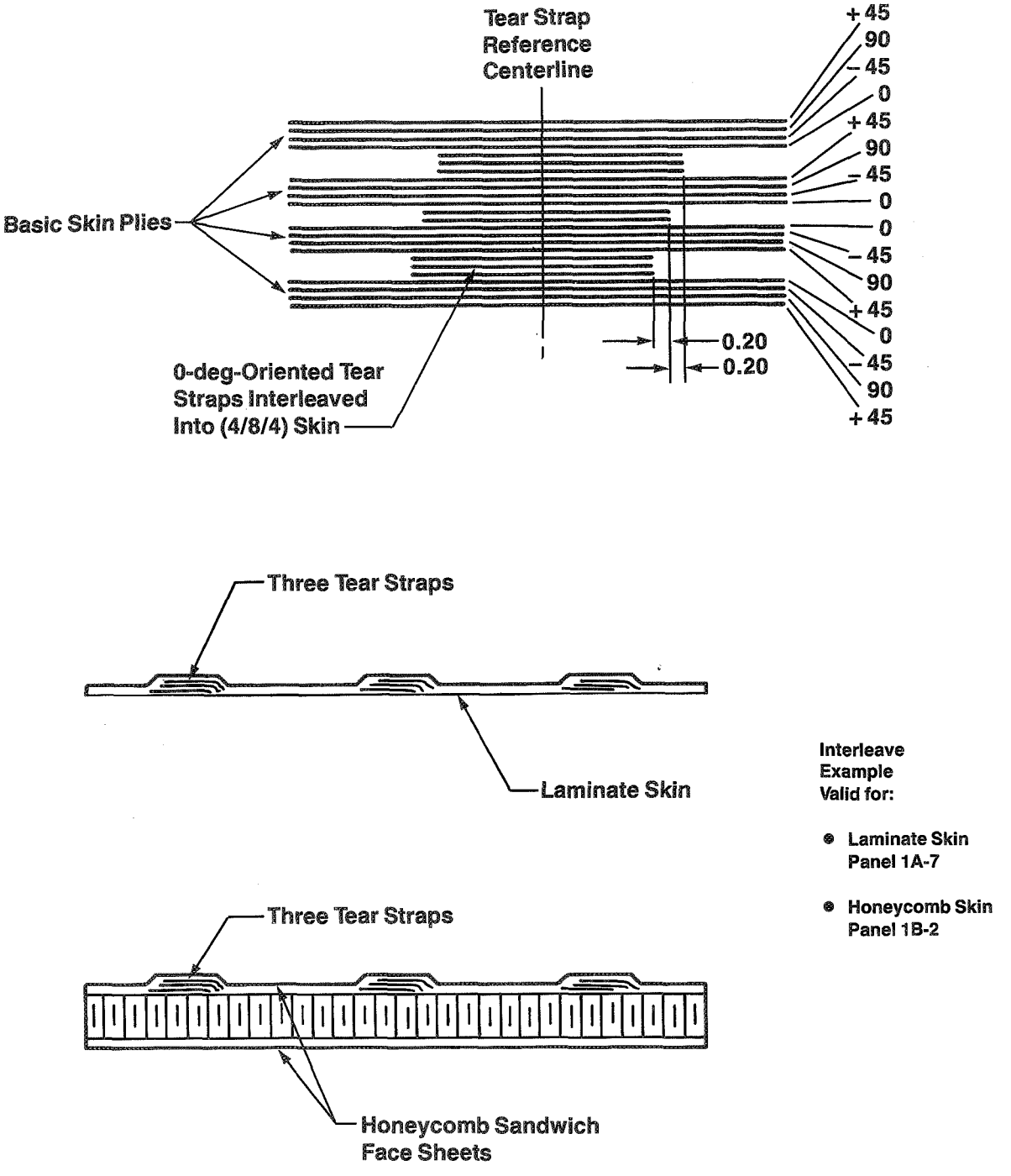

Figure 85. Typical Tear Strap Details for Flat Fracture Panel (Tests 1A and 1B)

The failure criteria used to predict strength, as analyzed by a finite element fracture model, is defined as the load that produces a critical strain at the boundary of an intense energy region at a characteristic dimension a_0 from the crack tip. The intense energy region approach was initially proposed by Whitney and Nuismer (ref. 12). The intense energy region characteristic dimension approach is also used by Garbo and Ogonowski in their analysis of bolted joints (ref. 13). The value of the characteristic dimension a_0 was initially selected as 0.10 in, based on test results reported in References 2 and 14. The critical strain is the fiber ultimate strain capability normal to the crack. In these analyses, the ultimate fiber strain was assumed to be 0.015 in/in, based on material test values. Coupon tests were performed to quantify the values for critical strain and characteristic dimension.

The analysis was performed by uniformly displacing the edge of the analysis panel. The nodal reactions along the panel boundary were then summed up and divided by the width of the panel to calculate the average end load per inch. The strain in the critical analysis element was determined from the finite element solution. The critical end load per inch was determined by multiplying the end load per inch, calculated from the finite element analysis, by the ratio of the critical fiber strain to the strain in the critical finite element.

The quarter panel NASTRAN model for the 30-in by 100-in panels with 10-in tear strap spacing has 861 elements, and the quarter panel model for the 60-in by 150-in panels with 20-in tear strap spacing has 1458 elements. These models are shown in Figure 86. For panels without tear straps, the tear strap analysis elements in the FEM are given the same properties as the basic skin.

The analysis models contain complete stress plates that have biaxial and shear stiffness properties. The boundary constraints imposed on the analysis models are shown in Figure 86. The models are constrained in the X-Y plane, and no out-of-plane loads or deformations are considered. In the region of the crack tip, the models contain plate elements that are 0.04 in by 0.04 in, as shown in Figure 87a. A similar FEM was used by Porter and Pierre (ref. 2) in their studies of damage containment in graphite-epoxy panels.

To evaluate the influence that element size has on the strain distribution near the crack tip, the crack tip element size in the 30-in by 100-in model was cut in half from 0.04 in by 0.04 in to 0.02 in by 0.02 in (fig. 87b). As shown in Figure 88, the change to 0.02-in by 0.02-in elements predicted strains very nearly the same as those predicted by the 0.04-in by 0.04-in elements. For reasons of simplicity and cost, the original 0.04-in by 0.04-in element grid was used in subsequent analyses.

The suitability of the fine-grid portion of the FEM was further evaluated by comparing the strain distribution generated in front of the crack tip by the FEM to that analytically predicted by linear elastic fracture mechanics (LEFM). The analytical strain distribution shown in Figure 88 was calculated from the biaxial stress state predicted by LEFM (ref. 15). These results indicate that LEFM and the FEM used to analyze the test panels predict similar crack tip strain distributions in isotropic materials.

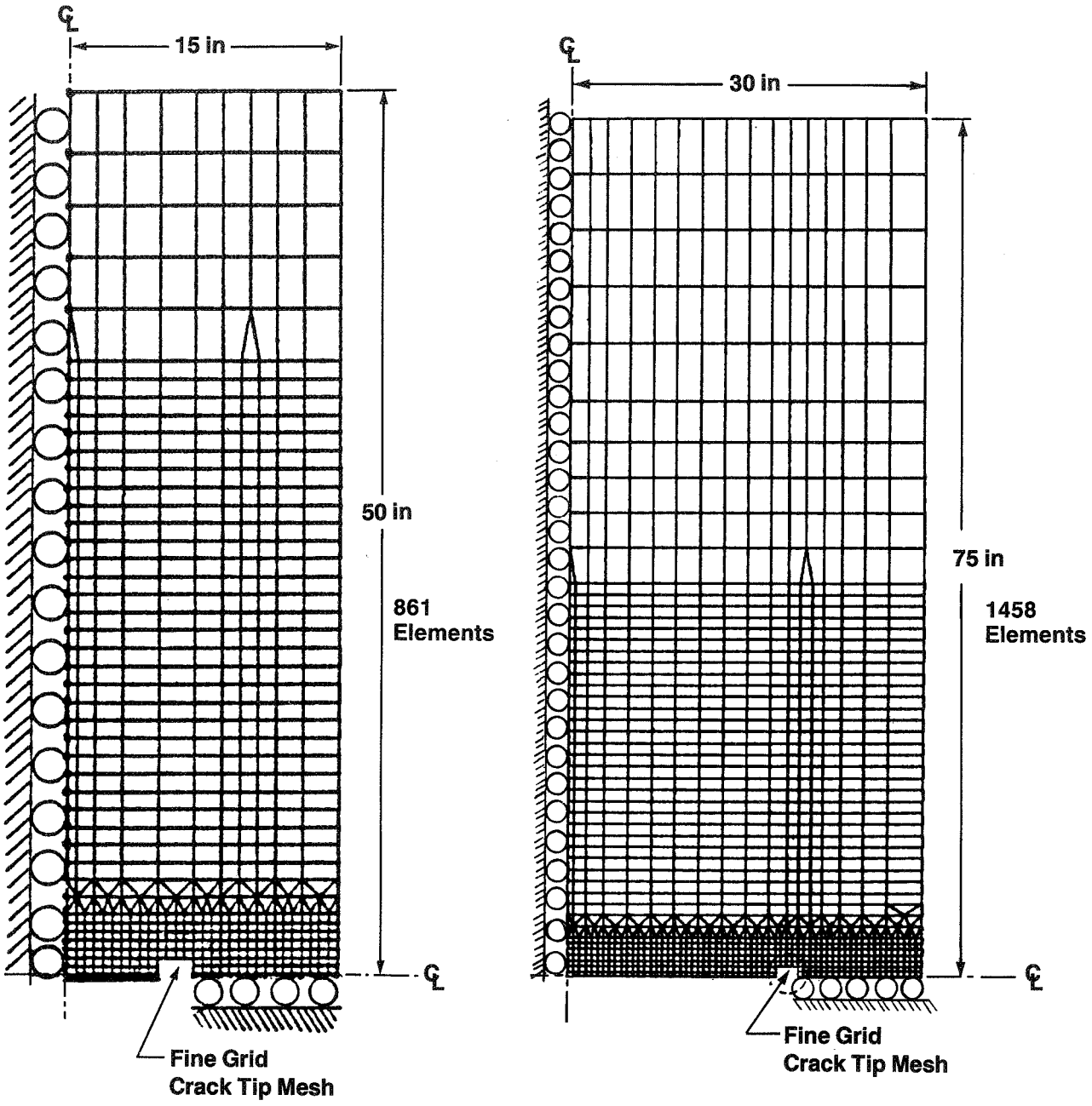

Figure 86. Finite Element Models for Flat Fracture Panel Tests

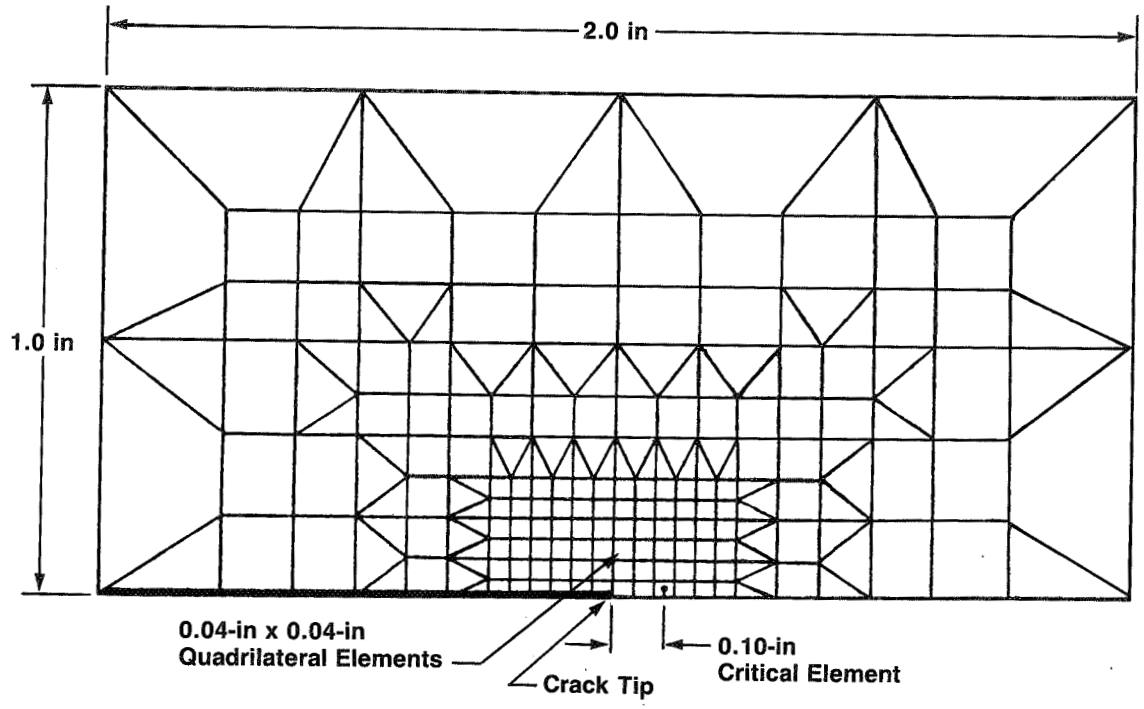

a. Standard Crack Tip Mesh

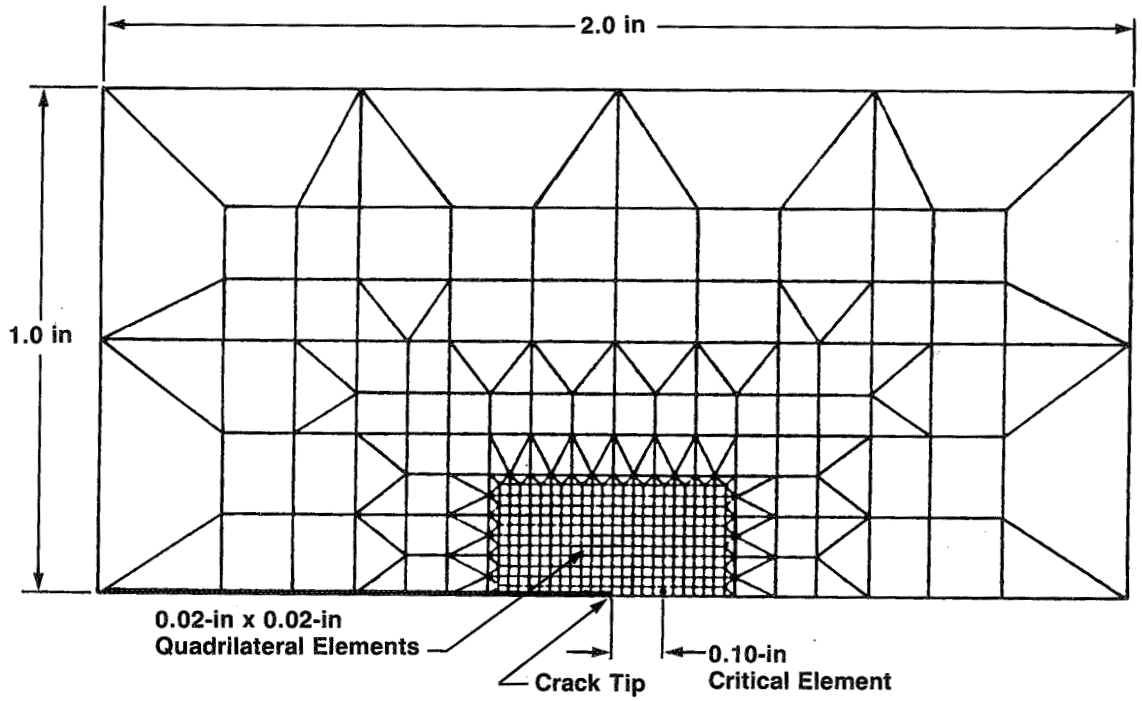

b. Refined Crack Tip Mesh for Model Verification

Figure 87. Fine Grid Crack Tip Meshes for Finite Element Fracture Models

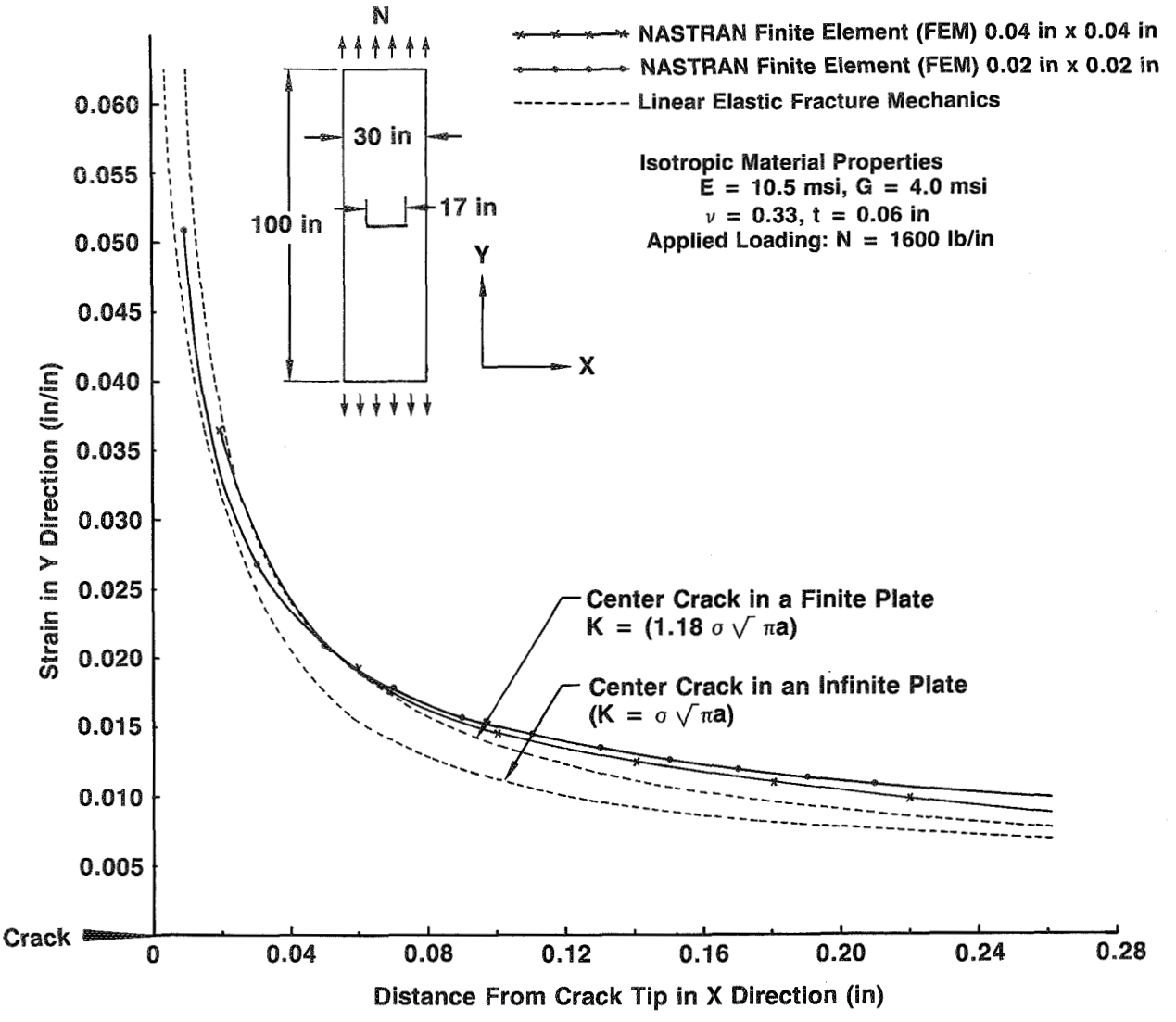

Figure 88. Comparison of FEM and LEFM Analysis of Strain Distribution in Front of Crack Tip in an Isotropic Material

6.1.1.1 Flat Laminate Fracture Panel Tests—The panel configurations, failure load predictions, and test results are summarized in Figure 89. The test data is compared with the design curve analysis results for 10- and 20-in stiffening tear strap spacing in Figure 90.

The predicted failure load for the unstiffened panels -1 and -2 was based on a 12-in centered sawcut. This damage size was chosen to represent possible damage caused by an engine blade or similar projectile penetration. The predicted failure loads of the stiffened panels, -3 through -7, were based on an initial damage that had been arrested at the edges of the adjacent tear straps.

The predicted failure loads of the tear strap panels with various initial damage sizes were calculated from the finite element analysis models. Typical results for panels with tear straps spaced at 10 and 20 in are shown in Figure 91. This analysis, which demonstrates the influence of sawcut width on residual strength, was used to select damage widths for the test panels.

For the 60-in by 150-in panels, -3 and -4, a 33-in initial cut length was chosen. The panel predicted failure loads for cuts longer or shorter than 33 in are greater, so this length produces a minimum failure load for the cut panels and the best chance to evaluate crack arrestment. For the 30-in by 100-in panels, -5 through -7, a 15-in initial cut was chosen. A longer damage length would have been too close to the tear strap to allow enough crack progression to evaluate crack arresting capabilities.

The initial sawcut lengths chosen for each panel were incorporated into the test preparation plan, and axial and rosette strain gages were installed at the locations shown in Figure 92. Each panel was then loaded in 5000-lb increments to 60% of the predicted failure load. Strain gage and acoustic emission data were monitored during each load increment. For the room temperature panels, pulse echo inspections were performed in the vicinity of the crack tip if acoustic emission data indicated damage growth. Upon review of the data, the panel was then loaded and instrumentation monitored continuously to failure. A typical test setup is shown in Figure 93.

Upon completion of each test, coupons were cut from the skin and/or tear strap regions of each of the failed panels. Test coupon configurations are shown in Figure 94. The center notch coupon results were used to determine the characteristic dimension of each panel layup. The tension and V-notch specimen results were used to determine longitudinal and shear moduli, respectively.

Panel Number [1]	Panel Size (in)	Tear Strap Spacing (in)	Skin Layup [2]	Tear Strap Plies	Tear Strap Stiffening (%)	Damage Width (in)	Test Temperature (Laboratory Dry Environment)	Predicted [3] Failure Load (kips)		Tested Failure Load (kips)	$\frac{P}{AE}$ Gross Area Failure Strain (in/in)	Continued Safe Flight Strain (in/in) [6]
								$a_0 = 0.010$ [4]	Adjusted a_0 [5]			
Solid Laminate												
1A-1	30 x 100	[5]	2/8/2	0	0	12	Room Temp.	44.5	32.2 [7]	36.1	0.0029	0.002
1A-2	30 x 100	[5]	4/8/4	0	0	12	Room Temp.	62.7	58.1 [7]	50.4	0.0026	0.002
1A-3	60 x 150	20	2/8/2	5	18	33	Room Temp.	72.8	74.3	66.4	0.0023	0.002
1A-4	60 x 150	20	2/8/2	10	36	33	Room Temp.	103.1	117.0	105.0	0.0031	0.002
1A-5R	30 x 100	10	2/8/2	3	22	15	Room Temp.	49.4	44.9	44.3	0.0029	0.002
1A-5C	30 x 100	10	2/8/2	3	22	15	–65°F	49.4	44.9	45.1	0.0030	0.002
1A-6R	30 x 100	10	2/8/2	5	36	15	Room Temp.	60.5	62.8	70.4 [8]	0.0042 [8]	0.002
1A-6C	30 x 100	10	2/8/2	5	36	15	–65°F	60.5	62.8	61.6	0.0037	0.002
1A-7R	30 x 100	10	4/8/4	8	37	15	Room Temp.	88.2	104.6	104.8	0.0039	0.002
1A-7C	30 x 100	10	4/8/4	8	37	15	–65°F	88.2	104.6	91.6	0.0034	0.002
Laminate Honeycomb Sandwich												
1B-1	60 x 150	20	2/8/2	10	18	33	Room Temp.	184.5	[7] 201.2	205.0	0.00353	0.002
1B-2	30 x 100	10	4/8/4	8	18	15	Room Temp.	175.0	[7] 207.5	190.2	0.00414	0.002

[1] Solid laminate panel materials: AS6/2220-3 grade 145 tape; laminate honeycomb face sheet material: AS6/F584 grade 145 tape

[2] Layup: 0-deg plies/ ± 45-deg plies/90-deg plies

[3] Failure load based on a center tear strap sawcut with damage extending to the adjacent tear straps. All analysis performed on a NASTRAN finite element model. Critical fiber strains: laminate—0.015 in/in; honeycomb—0.0175 in/in

[4] Initial assumption for characteristic dimension a_0 = 0.010 in

[5] Characteristic dimension adjusted by coupon tests

[6] Contained safe flight is 33% of design ultimate load

[7] No tear straps. Failure load based on a 12-in sawcut

[8] Panel inadvertently subjected to a large load during installation into the test machine. This pretest load is estimated to be in excess of 50 kips by comparing the damage sustained in this panel to previously tested panels

Figure 89. Summary of the Fracture Panel Tests

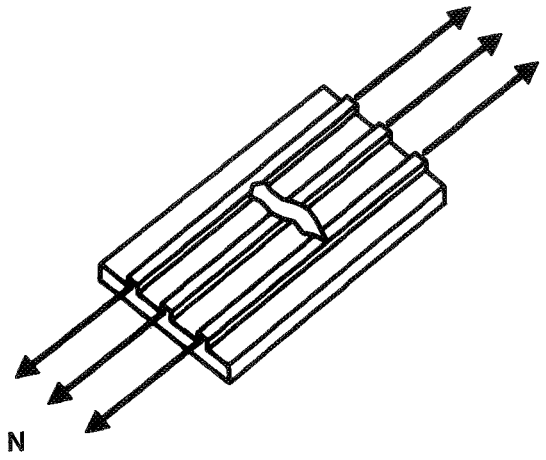

Laminate	Honeycomb	Tear Strap Spacing (in)	Initial Damage Width (in)	Temperature
■		No Straps	12	Room Temp.
○	●	10	15	Room Temp.
□		10	15	-65°F
△	▲	20	33	Room Temp.

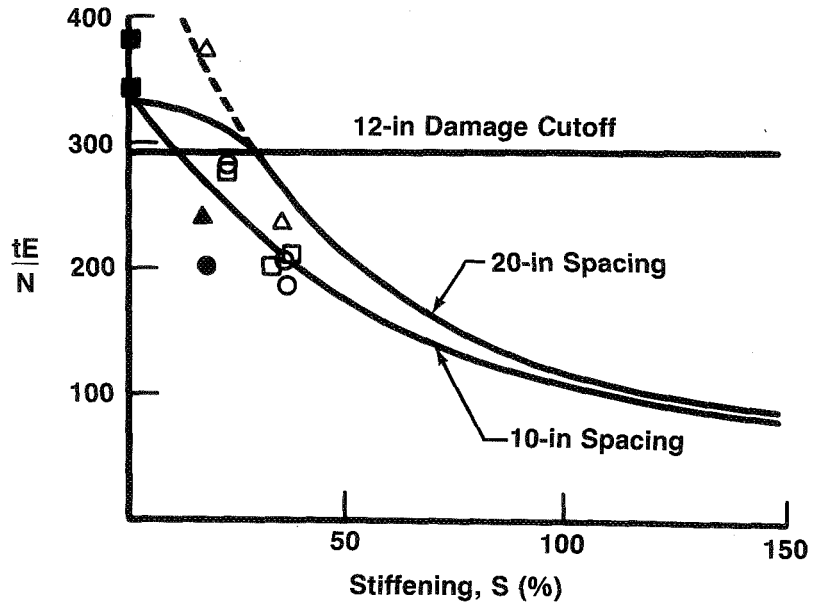

Figure 90. Comparison of Flat Fracture Panel Test Results With Analysis

Panel	Size (in)	Tear Strap Spacing (in)	Skin Layup [1]	Tear Strap Stiffening (%)	31-in Cut [2] Critical Load (lb)	33-in Cut [2] [3] Critical Load (lb)	35-in Cut [2] Critical Load (lb)	Maximum Damage 37-in Cut [2] [4] Critical Load (lb)
–3	60 x 150	20	2/8/2	18	63 000	60 000	60 400	72 700
–4	60 x 150	20	2/8/2	36	73 200	71 100	74 000	102 700

Panel	Size (in)	Tear Strap Spacing (in)	Skin Layup [1]	Tear Strap Stiffening (%)	15-in Cut [2] [3] Critical Load (lb)	16-in Cut [2] Critical Load (lb)	Maximum Damage 17-in Cut [2] [4] Critical Load (lb)
–5	30 x 100	10	2/8/2	22	46 200	44 800	49 300
–6	30 x 100	10	2/8/2	36	52 000	51 200	60 600
–7	30 x 100	10	4/8/4	37	73 200	72 600	90 500

[1] Layup: 0-deg plies/ ± 45-deg plies/90-deg plies
[2] Cuts: Sever center tear strap and extend into adjacent skin bay
[3] Length selected for test article
[4] Maximum damage extends from tear strap to tear strap

Figure 91. Residual Strengths of Panels With Various Cut Lengths (Test 1A)

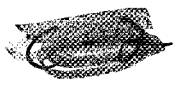

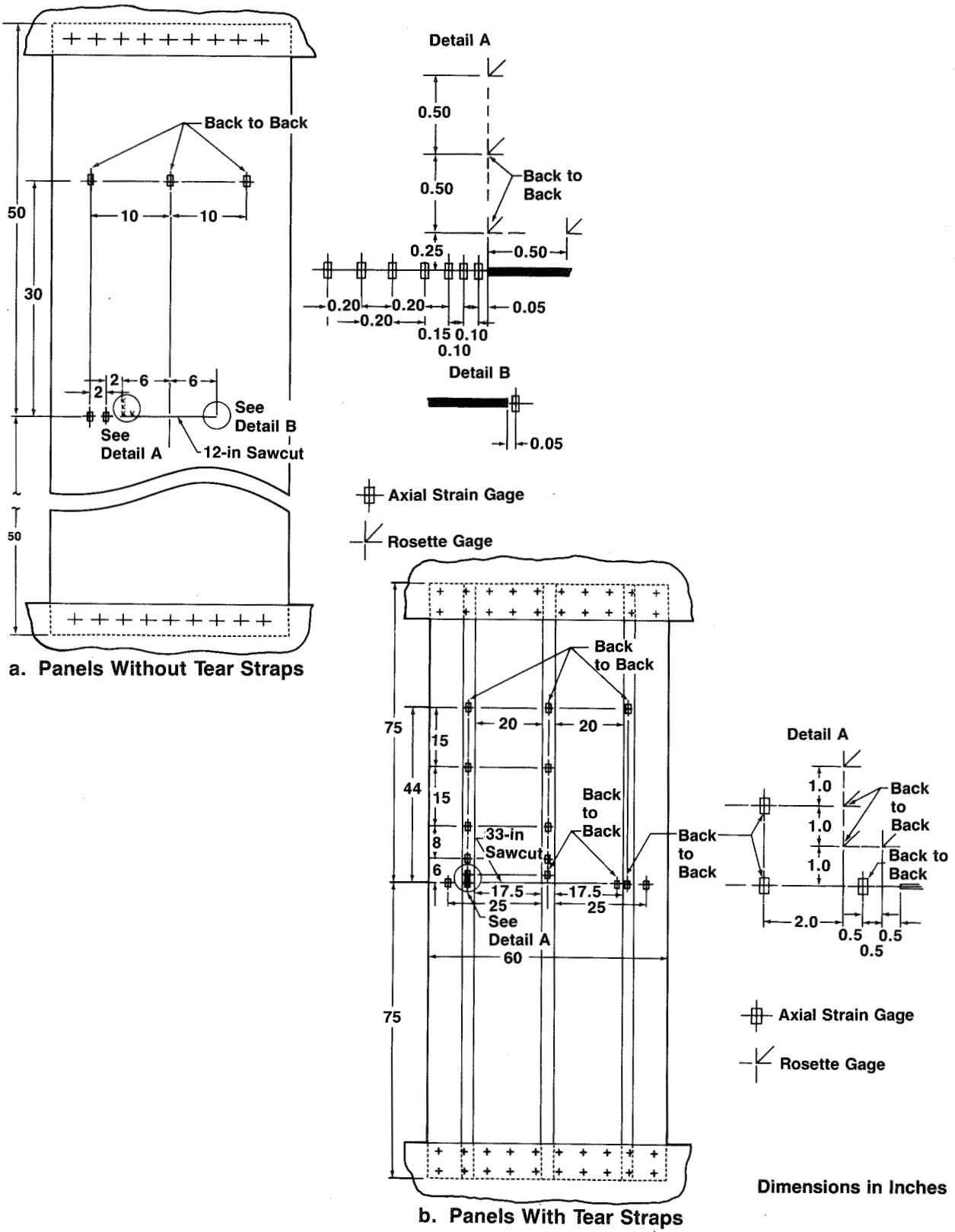

Figure 92. Typical Strain Gage Locations for Fracture Panels (Test 1A)

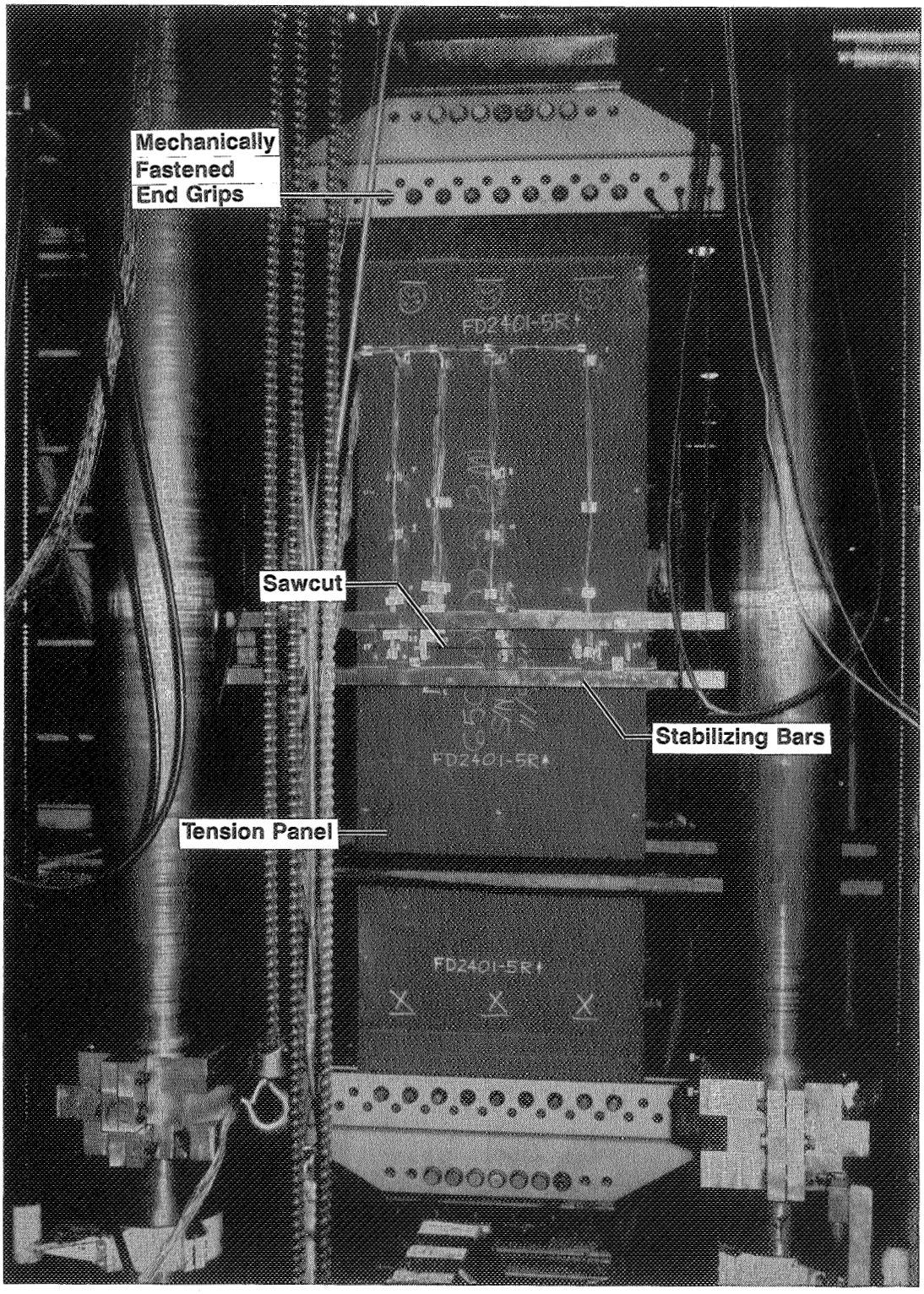

Figure 93. Typical Test Setup for a Flat Laminate Fracture Panel

C-2

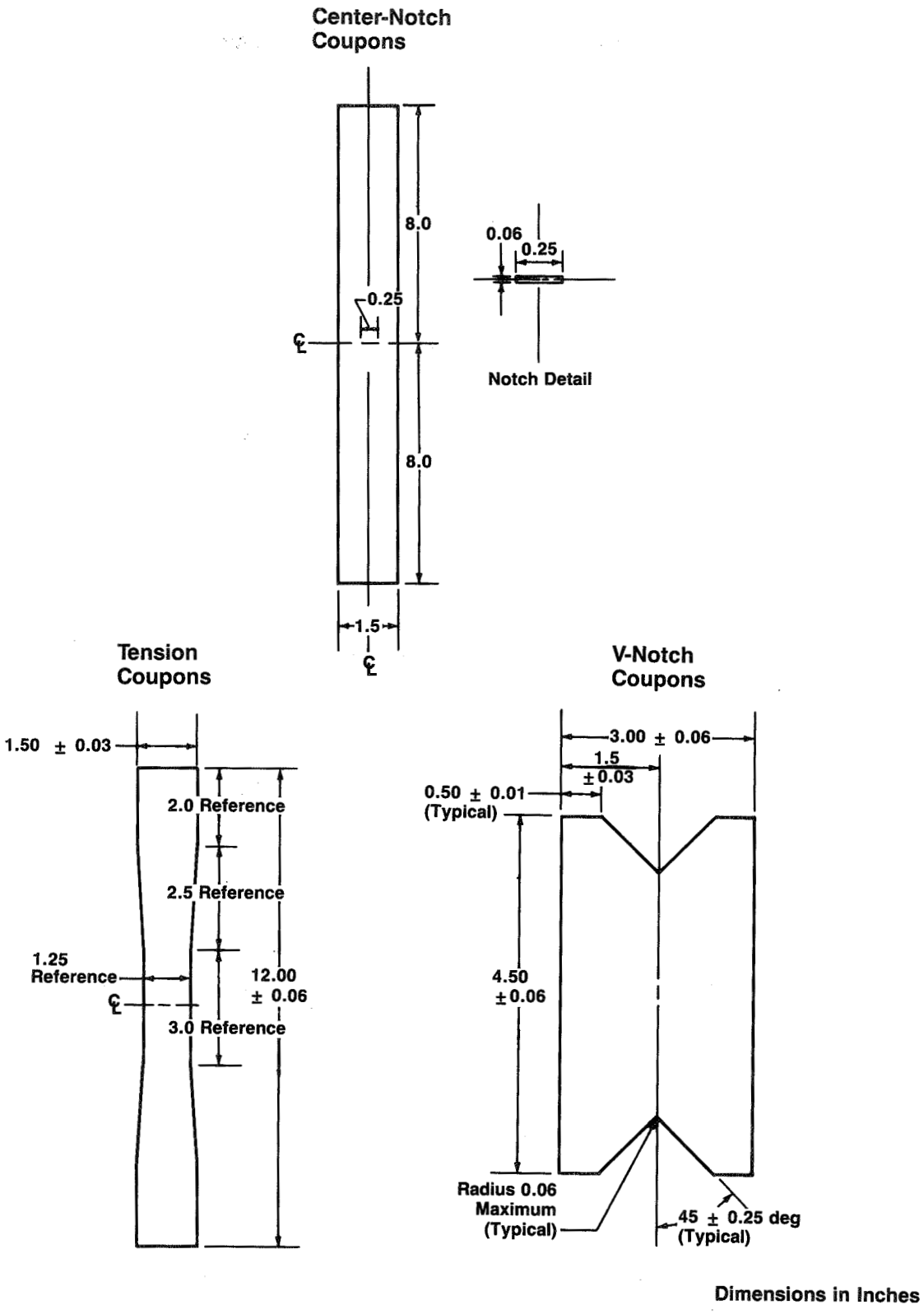

Figure 94. Coupon Specimens To Determine Panel Properties for Use in Model Analysis

Initially, the lamina values

$E_{11} = 18.0 \times 10^6$ lb/in^2

$E_{22} = 1.4 \times 10^6$ lb/in^2

$G_{12} = 1.0 \times 10^6$ lb/in^2

$\nu_{12} = 0.40$

were used to calculate laminate properties for each individual element layup. Upon completion of coupon testing, the values used were revised to

$E_{11} = 20.0 \times 10^6$ lb/in^2

$E_{22} = 1.4 \times 10^6$ lb/in^2

$G_{12} = 0.60 \times 10^6$ lb/in^2

$\nu_{12} = 0.325$

to better represent the laminate properties obtained from the tension and shear coupon tests. This resulted in up to a 10% increase in laminate moduli. Incorporating the new laminate properties into the FEMs produced a somewhat different distribution of strains at the modeled sawcut tip and therefore a different panel failure prediction.

Two failure predictions were made for each fracture panel, shown in Figure 89. The first set of predictions was based on an assumed characteristic dimension value of $a_0 = 0.010$ in. In the second set of analyses, the characteristic dimension was based on coupon test results, shown in Figure 95. It should be noted that the characteristic dimension values presented here are dependent on the specific material, layup, stacking sequence, and coupon results from this program, and are not intended to represent a general characteristic dimension curve for use in analysis.

The inclusion of the updated material properties and characteristic dimension values into the finite element analysis method used in this program improved the accuracy of the failure load predictions. Original panel failure predictions varied -15% to +25% from the actual panel test failure loads. With the new data incorporated, predictions vary -11% to +15% from the actual panel test failure loads. Strain distribution predictions also compared well to recorded test data, both near the sawcut (figs. 96 and 97) and far field (fig. 98).

Pulse echo inspections made during testing showed that damage tended to propagate from the sawcut tips as delamination rather than through-thickness crack propagation. It appeared, in most cases, that delamination growth was slowed by the presence of the tear straps, as shown in Figure 99. This data demonstrates the effectiveness of the tear straps as a damage arrestment feature. By comparing strain gage data, pulse echo information, and acoustic emission recordings, it appears that acoustic emissions can indicate delamination onset and growth. The prediction of damage arrestment by acoustic emission techniques is not a mature technology.

The -65°F environment had little effect on the residual strength of the damaged panels tested in this program. Each panel failed within 12% of its corresponding room temperature panel (fig. 100). Pulse echo inspection was not performed on the cold panels due to the cold box test setup.

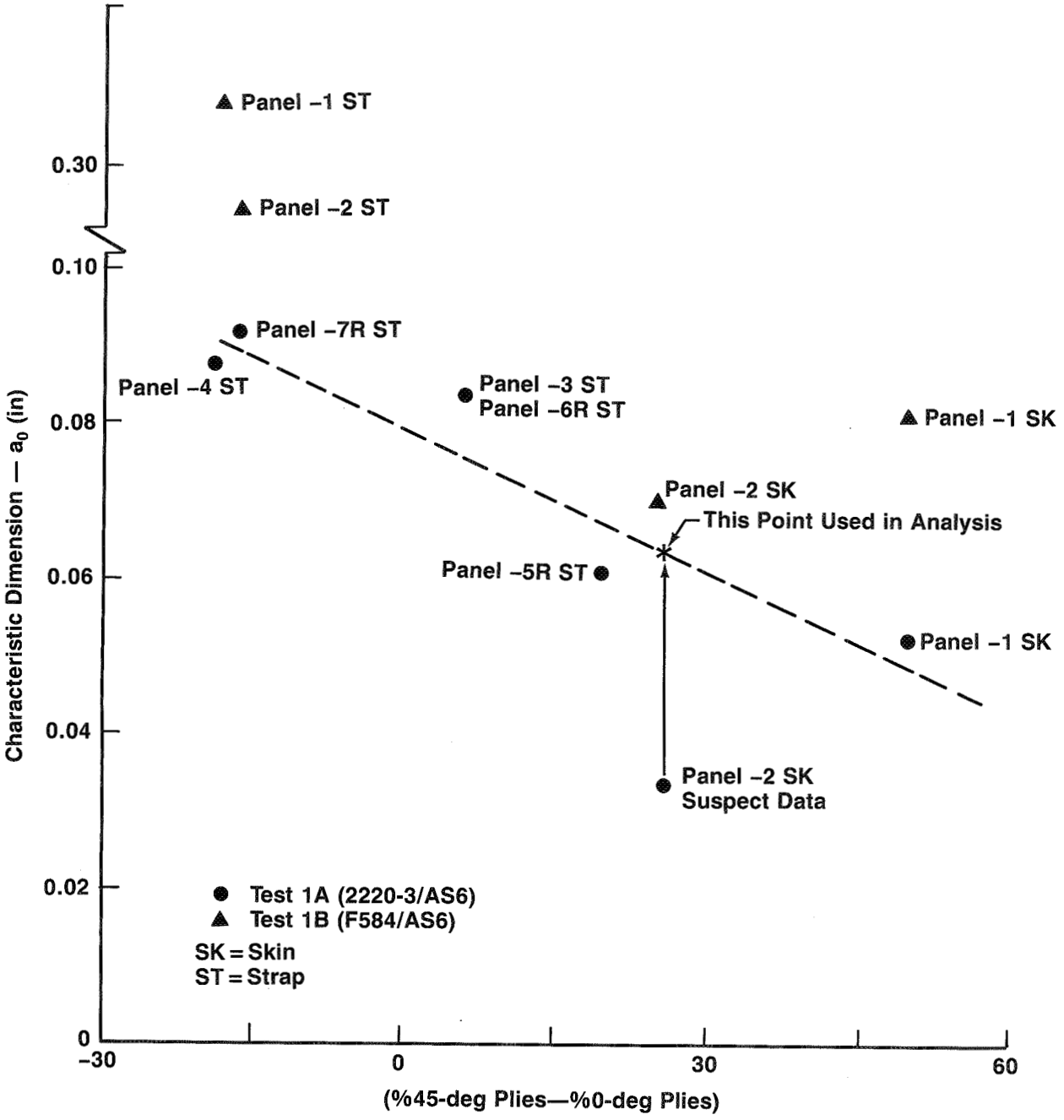

Figure 95. Calculated Characteristic Dimensions for Test 1A and 1B Materials

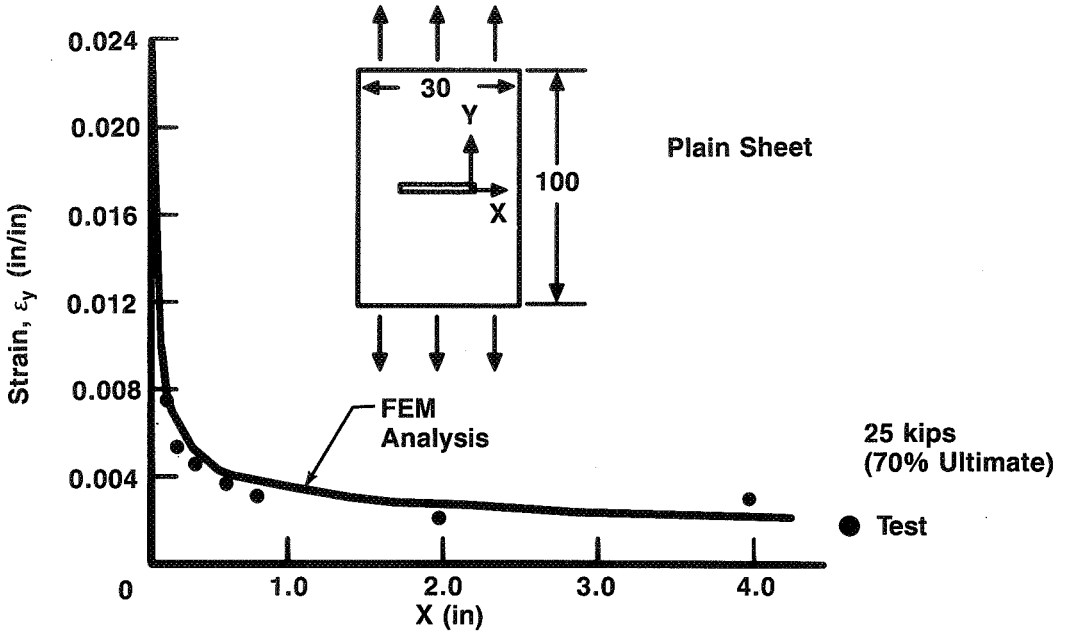

Figure 96. Predicted and Test-Derived Strains Near Damage Tip in an Unstiffened Fracture Panel (Test 1A-1)

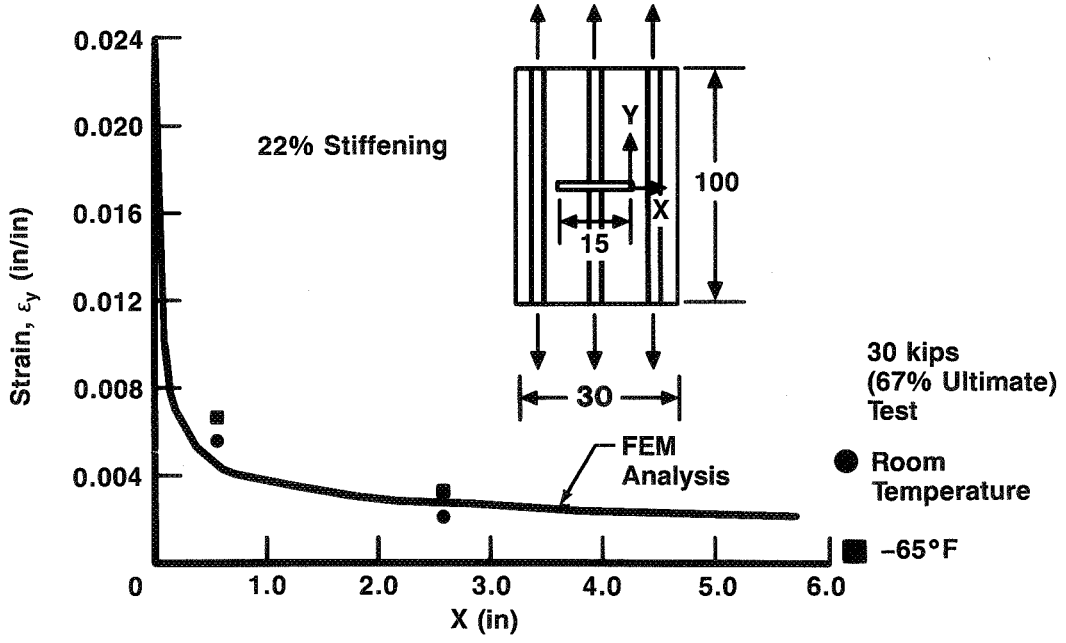

Figure 97. Predicted and Test-Derived Strains Near Damage in a Stiffened Fracture Panel (Test 1A-5)

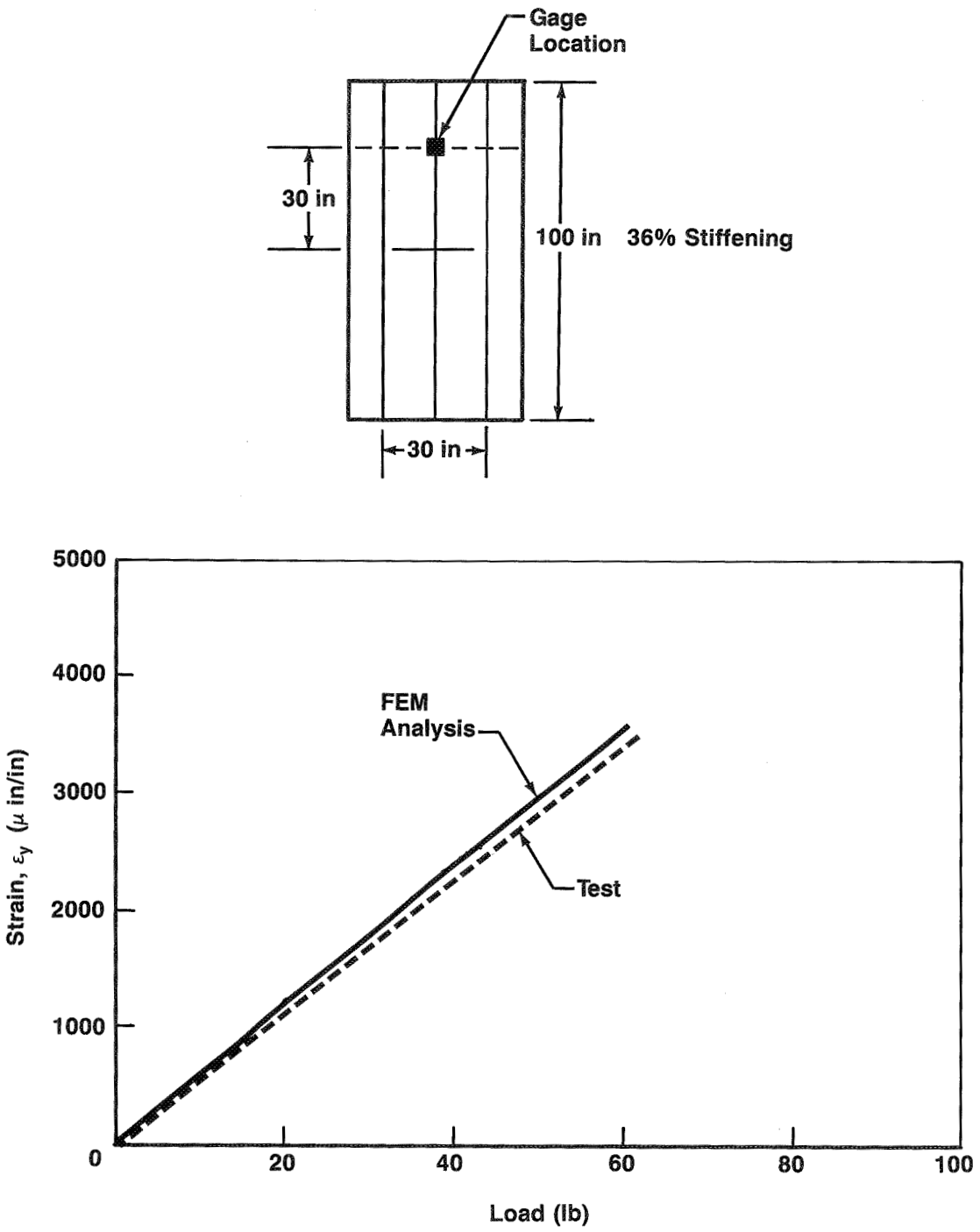

Figure 98. Analysis Verification (Test 1A), Plot of Strain Versus Load for a Far-Field Gage (Panel –6)

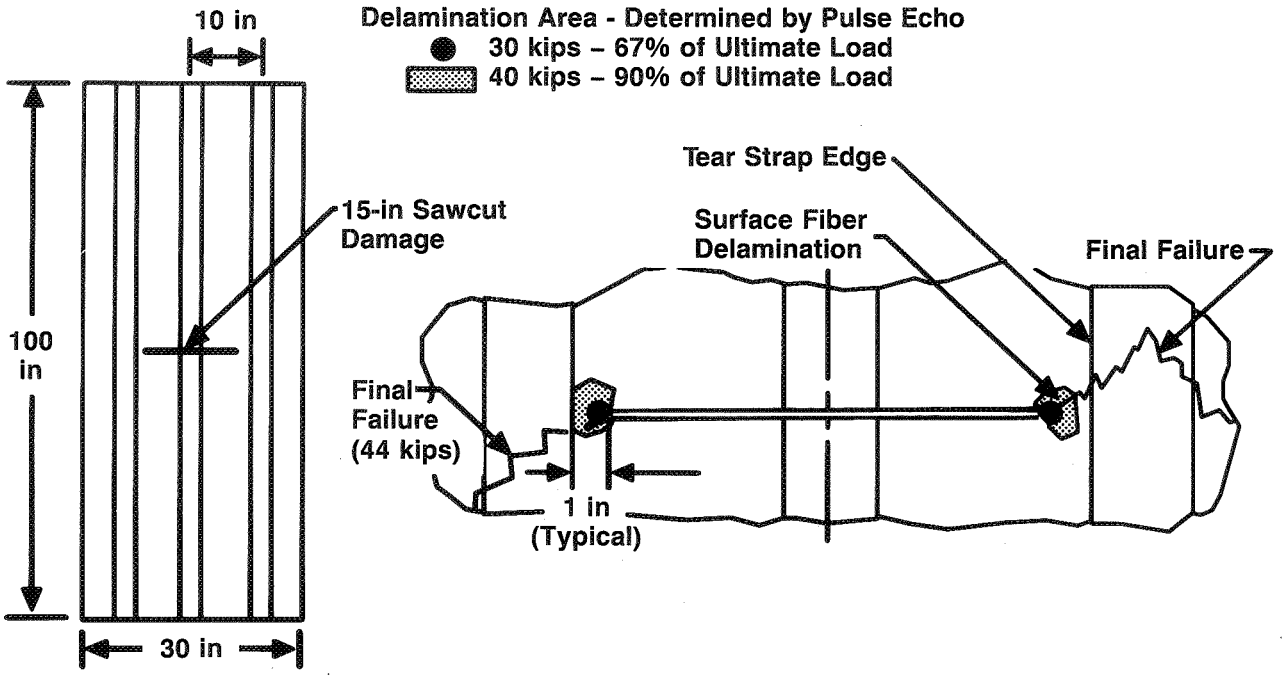

Figure 99. Typical Delamination Growth in a Stiffened Fracture Panel (Test 1A-5)

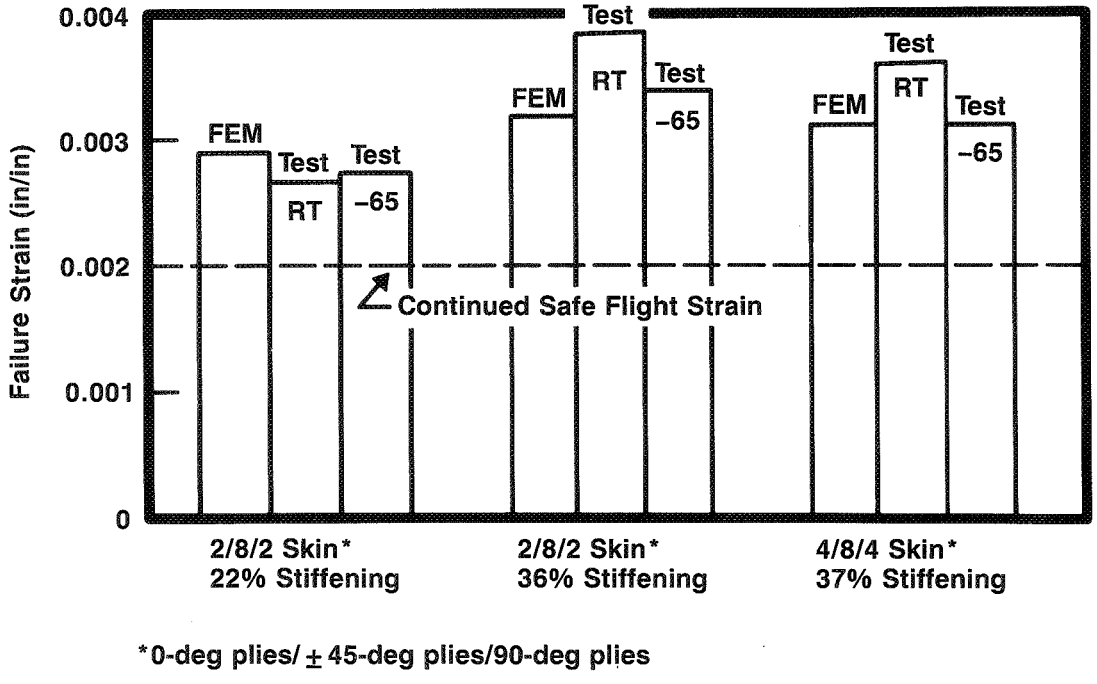

Figure 100. Environmental Flat Fracture Panel Tests

6.1.1.2 Flat Honeycomb Fracture Panel Tests—The configurations of the two honeycomb panels for test 1B, analysis failure load predictions, and test results are included with the flat laminate tests in Figure 89. The honeycomb panels carried higher load than the laminate panels with equivalent tear strap spacing and stiffening. Since the inverse of load is plotted on the ordinate of the tear strap design curve (fig. 90), the plotted values for the honeycomb structure fall below the laminate data.

Similar FEM analysis models were used to analyze the honeycomb panels as were used for the stiffened laminate panels. Application of the test load to the panels was in bearing at the test fixture grip bolts. For this reason, the load was introduced into each panel face sheet at the same deflection rate. Therefore, it was decided to analyze the honeycomb sandwich panels as two separate face sheets retained inplane by the honeycomb core.

The material characterization testing performed on the Hexcel F584/AS6 material system used for the honeycomb panels indicated that failure strains greater than 0.015 in/in could be used in these analyses. A 0.0175-in/in strain and the characteristic dimension analysis method discussed earlier were used to predict panel failure loads.

Results from the coupon testing performed were incorporated into the FEM analysis, and new calculated characteristic dimensions were used to produce the predicted failure loads shown. Laminate properties for the F584/AS6 material obtained from the coupons for each panel follow.

Panel -1		Panel -2	
Basic Skin	Tear Strap	Basic Skin	Tear Strap
E_1 = 5.32E6	E_1 = 11.99E6	E_1 = 7.16E6	E_1 = 10.58E6
E_2 = 5.32E6	E_2 = 4.35E6	E_2 = 7.16E6	E_2 = 5.26E6
G = 3.74E6	G = 2.5E6	G = 3.18E6	G = 2.34E6
ν_{12} = 0.4405	ν_{12} = 0.459	ν_{12} = 0.323	ν_{12} = 0.321

The basic skin coupons for panels -1 and -2 demonstrated characteristic dimensions of 0.08 and 0.068, respectively. These are shown with the calculated characteristic dimension data for the 2220/AS6 material of test 1A (fig. 95). Calculated characteristic dimensions from tear strap regions of panels -1 and -2 were 0.253 and 0.372, respectively. These results for this material system, stacking sequence, and coupons tested show that the tear strap is much less sensitive to the damage tip than the F584/AS6 basic skin for test 1B and all the 2220/AS6 configurations tested for test 1A.

The laminate properties and characteristic dimensions were then incorporated into the FEMs for each face sheet. The results were then summed as discussed to estimate the new predicted failure loads. These represent a -2% to +9% difference from actual failure loads, compared to the original -10% to -8% difference.

During testing of the honeycomb panels, pulse echo inspection showed that damage propagated from the sawcut tips as delaminations, in similar fashion to the laminate panels. Figure 101 shows the extent of delamination damage observed at 64% of the ultimate load. These delaminations tended to propagate from the sawcut tips on both face sheets at almost the same rate. At intermediate loads, the pulse echo inspection seemed to suggest that the tear straps slowed damage propagation on both face sheets.

During continuous loading of the 1B-2 honeycomb panel, a loud noise and the instrumentation indicated that failure had occurred at 190 kips. However, the load cell showed that the panel was still carrying 130 kips. Upon inspection of the panel, it was found that one face sheet had fractured but the tear strap reinforced face sheet was heavily delaminated but not fractured (fig. 102). The fiberglass honeycomb core provided shear capability to allow for load transfer from one face sheet to the other.

A three-dimensional FEM of the test 1B honeycomb panels was undertaken. Each panel face sheet was modeled similarly to the laminate panels. The individual face sheet models were then connected by shear plate elements having thickness and properties consistent with those of the fiberglass honeycomb core used in panel fabrication. This 3-D model predicted failure loads nearly identical to those obtained by modeling the honeycomb face sheets as two separate panels and summing their predicted failure loads.

6.1.2 Curved Laminate Fracture Panels

Tests and analyses were performed to evaluate the effects of pressure, biaxial loading, curvature, damage under load, and temperature on fracture response. Pressure tests were performed on six curved constant thickness laminate panels. The laminates used for the fracture panels were representative of circumferential and longitudinal tear strap construction.

The test plan is summarized in Figure 103, and the test setup is diagramed in Figure 104. Five tests were performed at room temperature, and one test at -65°F. Four of the panels were damaged with a 12-in sawcut and loaded to failure with combinations of pressure and axial loading. The remaining two panels were loaded undamaged to continued safe flight loads and then damaged under load with a guillotine blade. These two panels both survived the guillotine impact. They were submitted to NDI to determine the extent of the damage inflicted by the guillotine impacts, resealed, and loaded to failure with combinations of pressure and axial loads.

A photograph of a typical pressure test setup is shown in Figure 105. The panel shown (panel 2-1) was loaded by pressure, with the resultant hoop load reacted through an evener system lined up tangent to the panel edges. Panels 2-2 through 2-6 were loaded in axial tension and internal pressure. Prior to the test of each panel, pressure was applied to check the operation of the strain gages.

The panels with pretest sawcuts were sealed with a rubber bladder to prevent pressure loss during the tests. The laminate of panels 2-1 through 2-4 is representative of a circumferential tear strap that arrests a longitudinally oriented damage. The laminate panels 2-5 and 2-6 are representative of a longitudinal tear strap that arrests a circumferentially oriented damage.

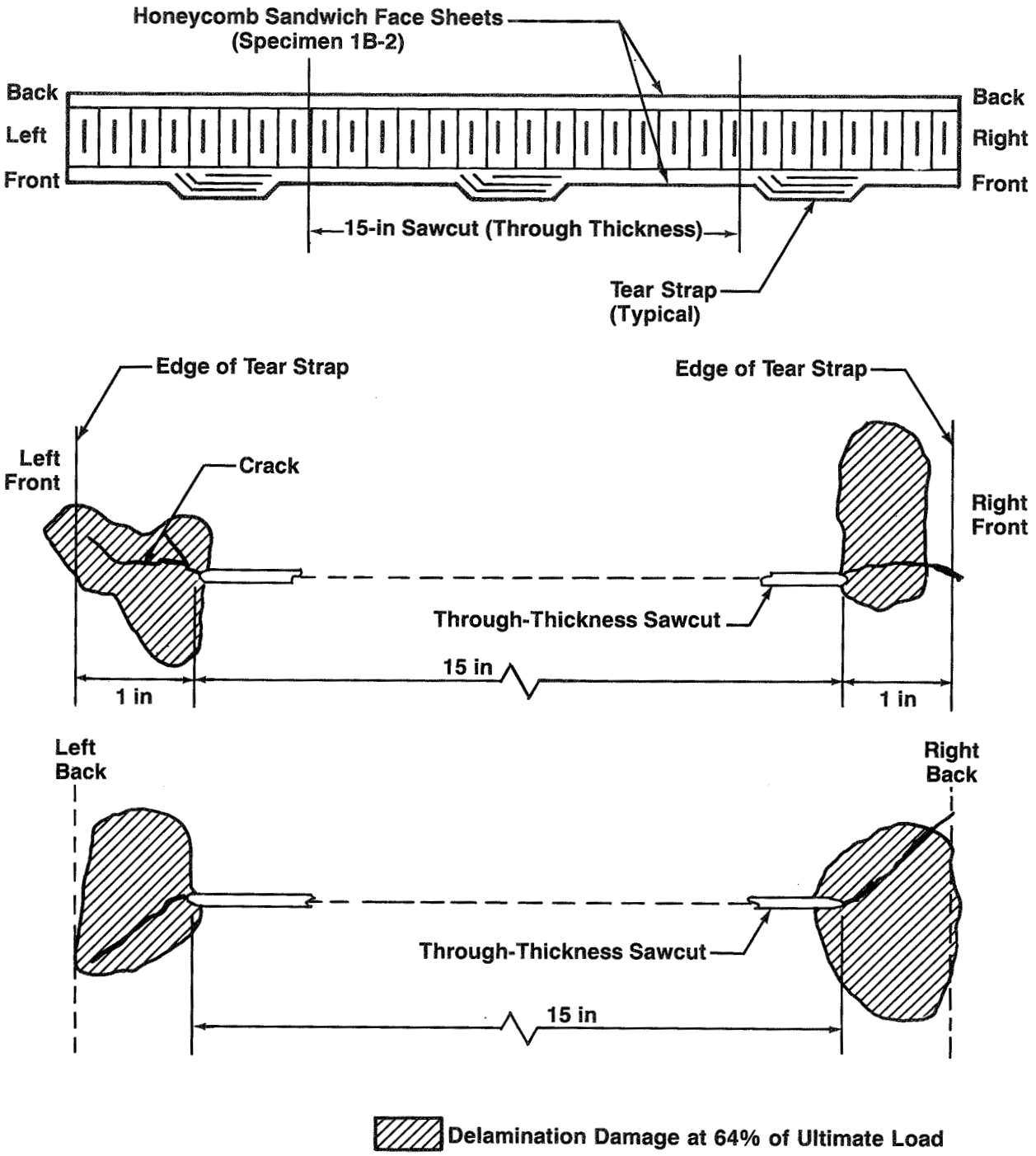

Figure 101. Typical Delamination Growth in a Stiffened Honeycomb Panel

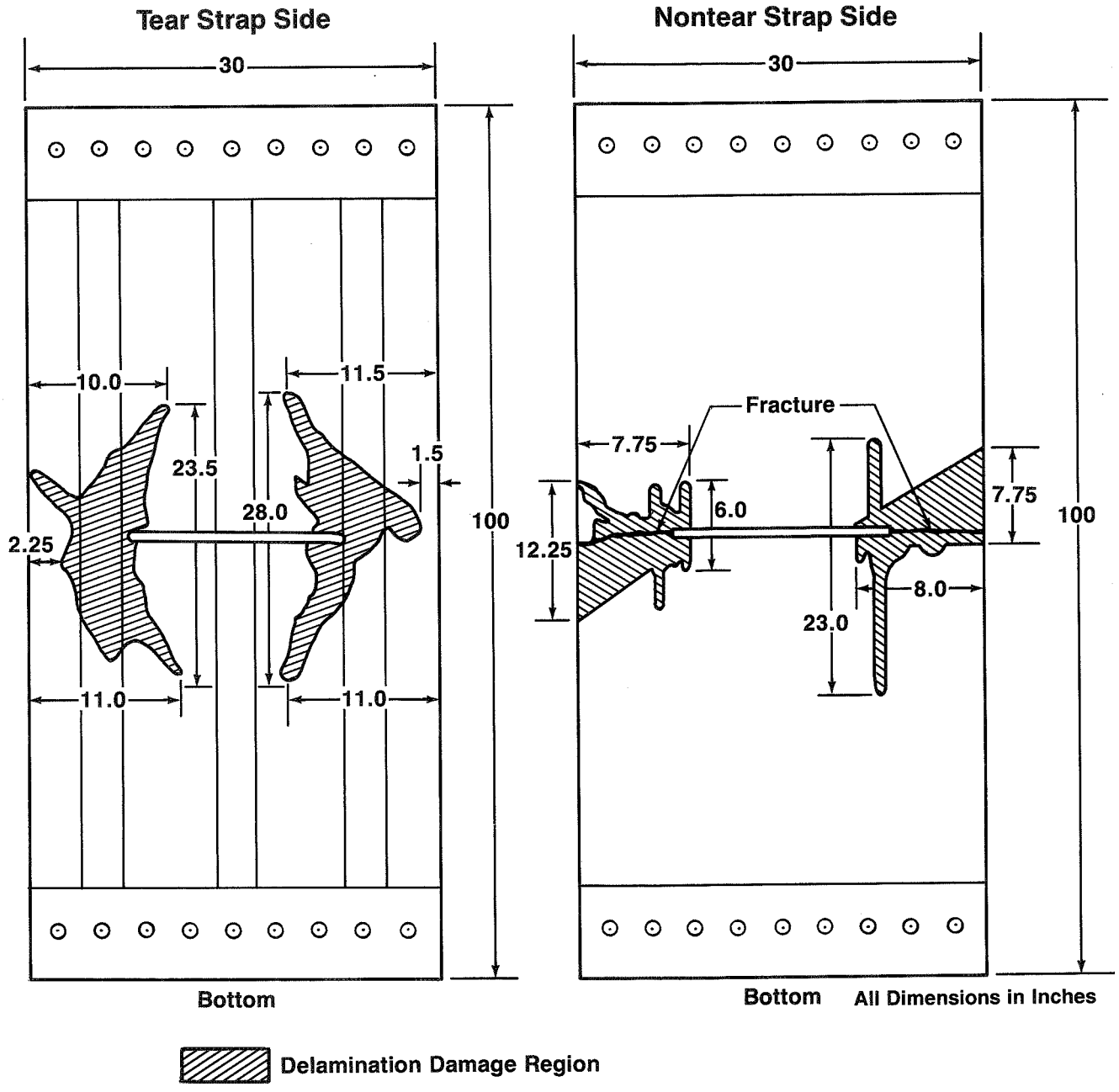

Figure 102. Postfailure Pulse Echo Inspection of the -2 Panel (Test 1B)

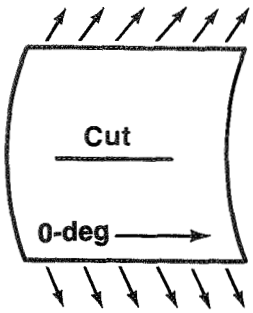

Panel 2-1.
Pressure Loading
Only Precut

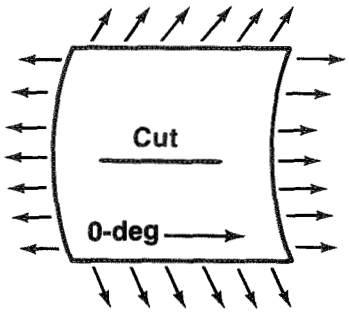

Panels 2-2 and 2-3.
Pressure + Axial
Loading Precut

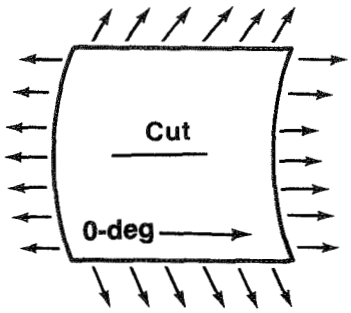

Panel 2-4.
Pressure + Axial Loading
Guillotine Under Load

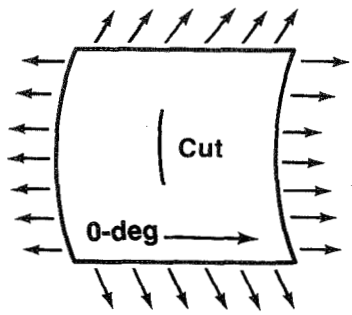

Panel 2-5.
Pressure + Axial
Loading Precut

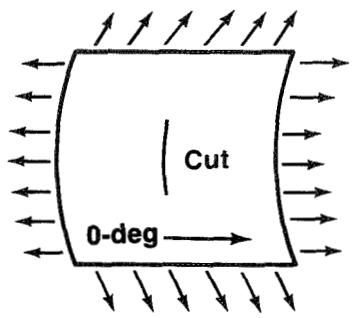

Panel 2-6.
Pressure + Axial Loading
Guillotine Under Loading

Panel Number	Layup*	Loading	Type of Cut	Cut Orientation	Test Temperature
2-1	2/8/7	Pressure	Sawcut	0-deg	Room Temp.
2-2	2/8/7	Pressure + Axial	Sawcut	0-deg	Room Temp.
2-3	2/8/7	Pressure + Axial	Sawcut	0-deg	-65°F
2-4	2/8/7	Pressure + Axial	Guillotine Under Load	0-deg	Room Temp.
2-5	7/8/2	Pressure + Axial	Sawcut	90-deg	Room Temp.
2-6	7/8/2	Pressure + Axial	Guillotine Under Load	90-deg	Room Temp.

*Constant gage panels

Note: Panels 2-1 through 2-4: longitudinal damage in circumferential tear strap laminates
Panels 2-5 and 2-6: circumferential damage in longitudinal tear strap laminates

Figure 103. Curved Fracture Panels (Test 2)

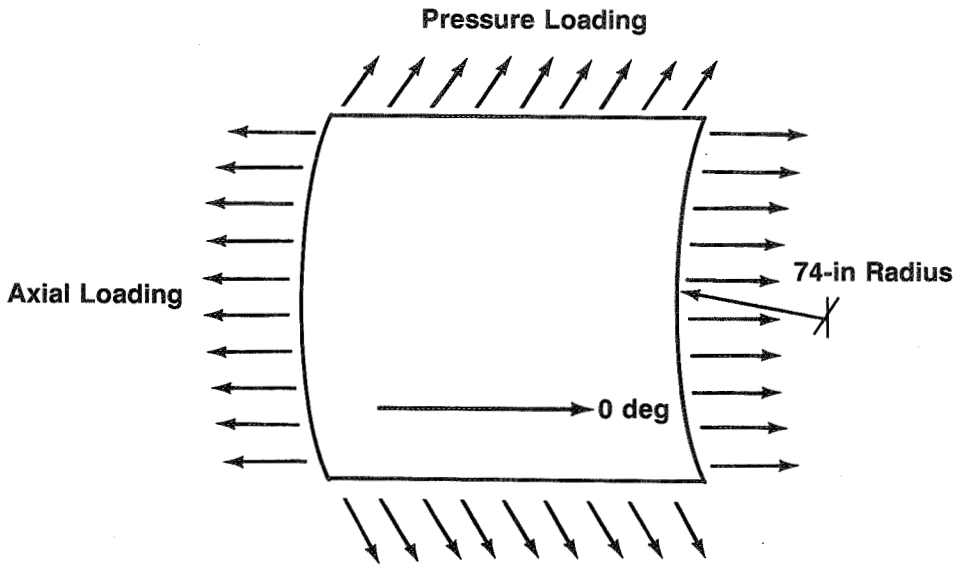

- Panel Size = 40 in x 40 in
- Laminates $(+45/0_2/-45/90/45/-45/\bar{0}_3)_s$
  $(-45/90_2/45/0/-45/45/\bar{9}0_3)_s$
- Constant Gage Panels With Tear Strap Representative Layups

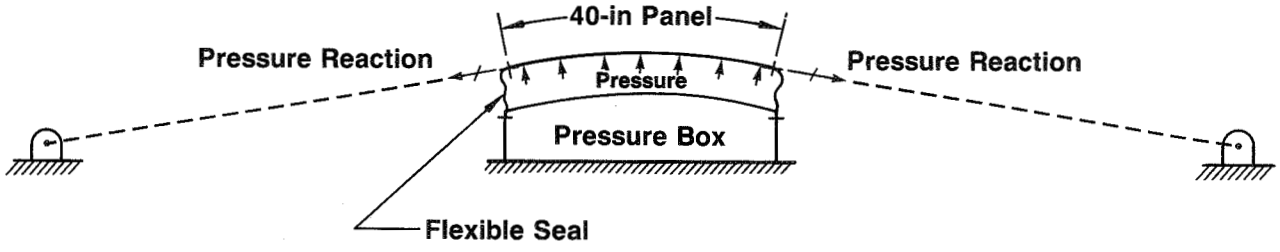

Figure 104. Curved Fracture Panel Test Setup

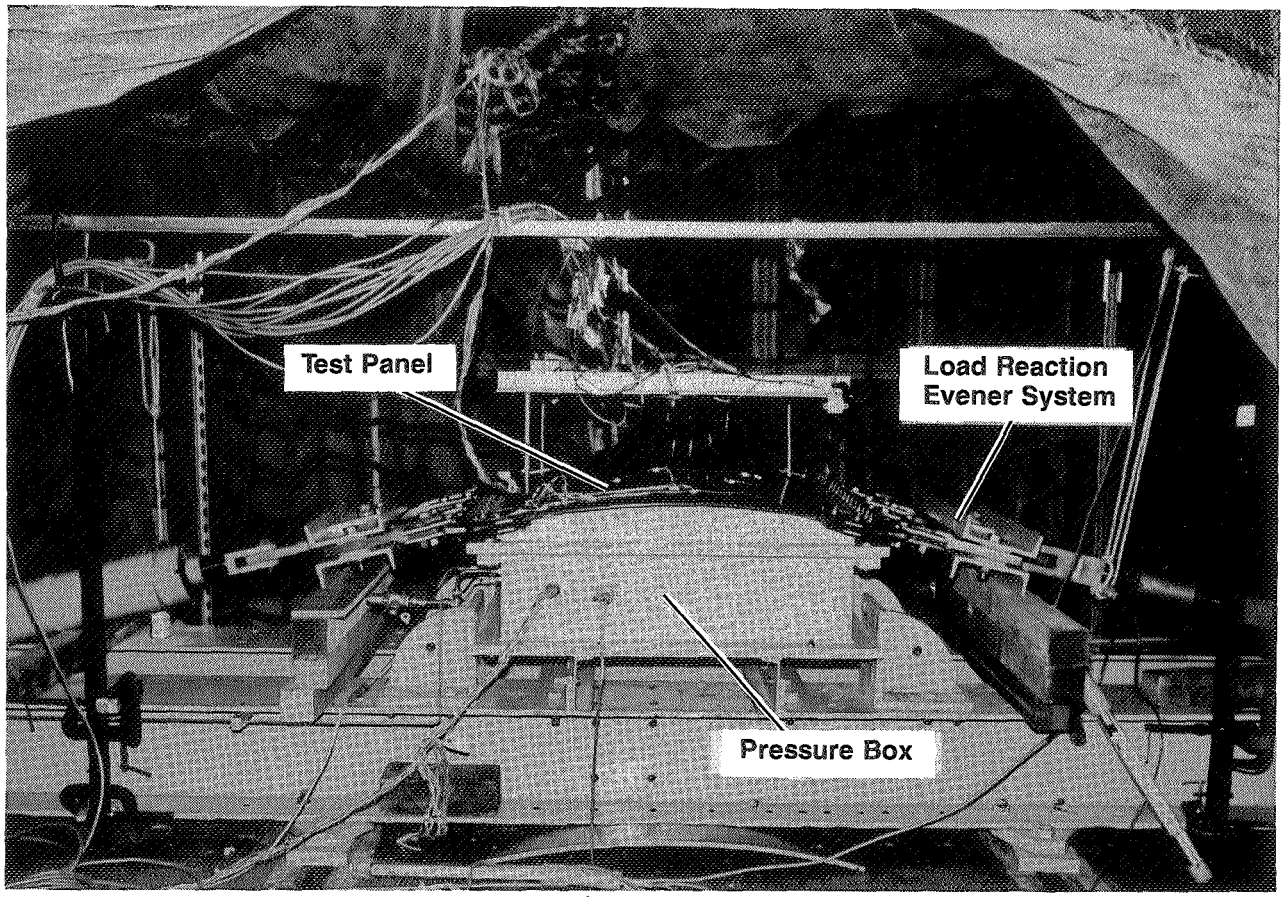

Figure 105. Curved Fracture Panel Pressure Test Setup

The two-dimensional finite element analysis applied to the flat fracture panels of tests 1A and 1B was considered inadequate to predict the structural response of curved fracture panels with inplane loads and normal pressure applied. The out-of-plane effects of the internal pressure loading had to be considered. When the cut is longitudinal (perpendicular to hoop direction), the internal pressure causes the edge of the cut to open and displace in the radial direction. This causes a high biaxial strain field at the ends of the damage due to the out-of-plane bending strain in addition to the inplane bypass strain.

The panels of test 2 were analyzed using quarter-cylinder FEMs. These models were based on results obtained from a Boeing IR&D-developed analysis. A schematic diagram of a typical model is shown in Figure 106. The analysis included out-of-plane effects due to the pressure loading and curvature. Failure predictions for this analysis were based on the same 0.10-in characteristic dimension and 0.015-in/in critical fiber strain used in the flat fracture analyses. The analysis results are compared with test data in Figures 107 and 108.

The panels that were tested with longitudinally oriented damage are discussed in Section 6.1.2.1. The circumferential damage panels are discussed in Section 6.1.2.2. After the testing was complete, additional analyses were performed to evaluate the effects of discrete stiffening and various curvatures on fracture response.

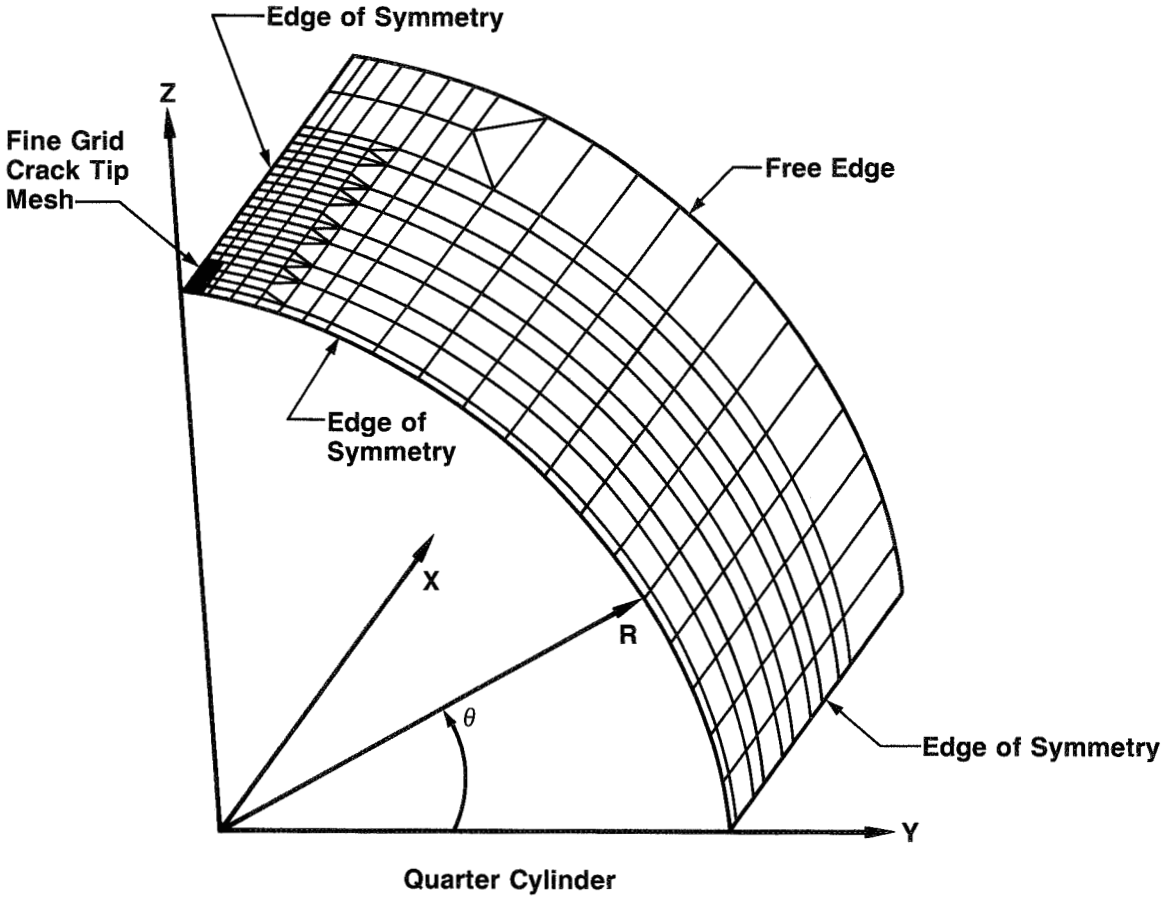

Figure 106. Typical Finite Element Model for Curved Fracture Panel Analysis

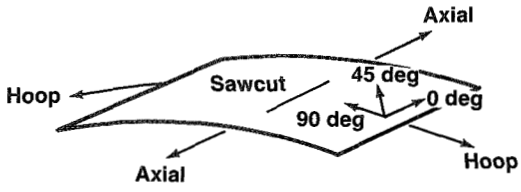

Two 0-deg Plies/Eight 45-deg Plies/Seven 90-deg Plies
Panels -1, -2, -3, -4

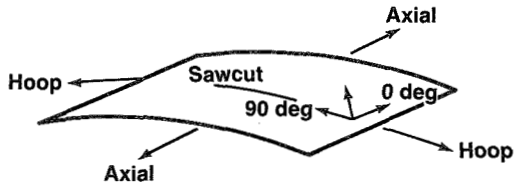

Seven 0-deg Plies/Eight 45-deg Plies/Two 90-deg Plies
Panels -5, -6

FEM Failure Prediction [1]

Panel	Test Temperature (Dry Environment)	Damage Type (12-in size)	Boeing Curved Panel Analysis [2]		Test Failure	
			Axial (lb/in)	Hoop (lb/ft^2)	Axial (lb/in)	Hoop (lb/ft^2)
2-1	Room Temp.	Sawcut 0-deg Orientation	—	14.3	—	16.25
2-2	Room Temp.	Sawcut 0-deg Orientation	790	18.2	790	18.5
2-3	–65°F	Sawcut 0-deg Orientation	790	18.2	840	19.9
2-4	Room Temp.	Guillotine Blade 0-deg Orientation	790 [3]	8.6	818	17.9
2-5	Room Temp.	Sawcut 90-deg Orientation	2360	8.6	2200	9.7
2-6	Room Temp.	Guillotine Blade 90-deg Orientation	1740 [3]	8.6 [3]	2550	8.6

[1] Failure predictions based on 12-in damage using NASTRAN finite element models. Critical fiber strain = 0.015 in/in at a_o = 0.10 in

[2] Boeing curved panel analysis includes curvature, out-of-plane, and pressure effects

[3] 12-in damage inflicted with guillotine blade. Load conditions applied prior to damage

Figure 107. Curved Laminate Fracture Panel Test Summary

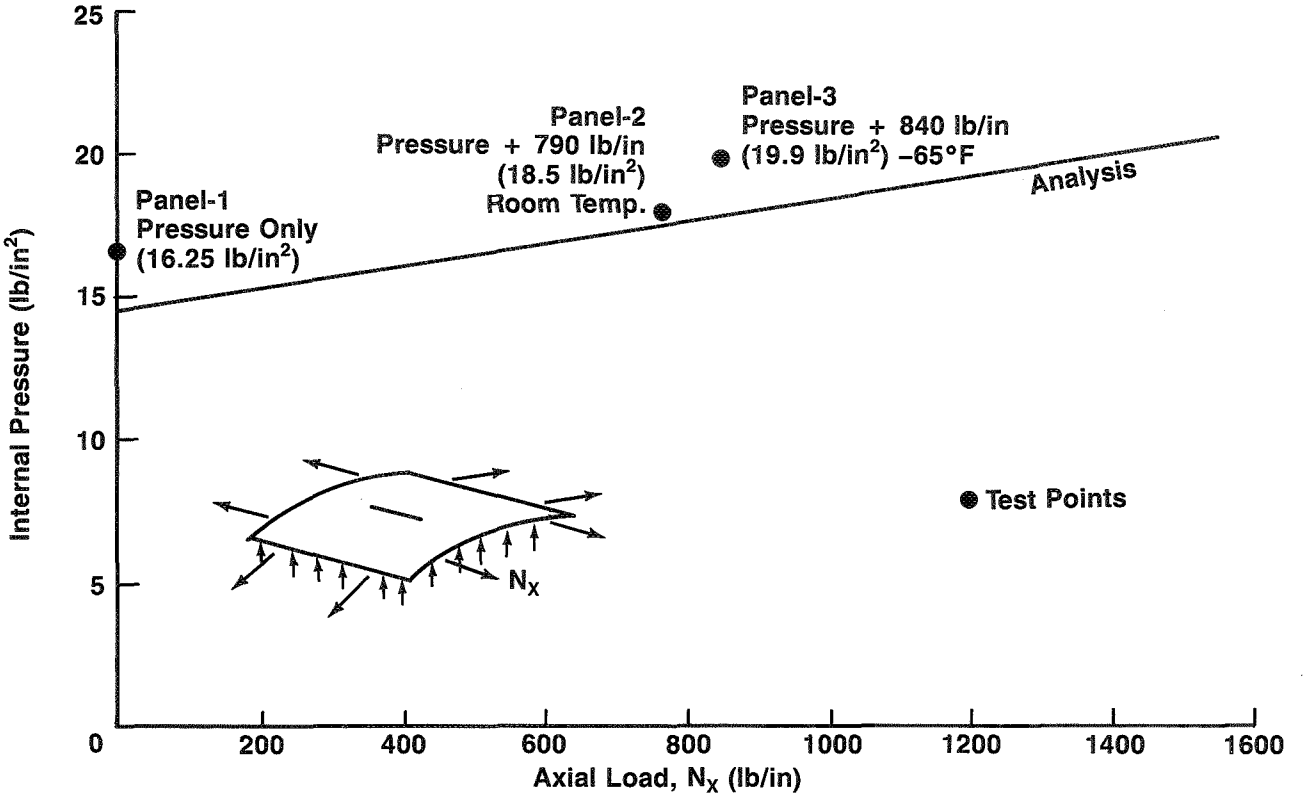

Figure 108. Comparison of Test and Predicted Failure Pressures

6.1.2.1 Longitudinal Damage Tests—Four panels were tested to evaluate the effects of pressure load on shell structure with longitudinal damage. Panels 2-1 and 2-2 were tested with an existing 12-in sawcut at room temperature. Panel 2-1 was pressure tested without axial loading. Prior to pressurization, panels 2-2 through 2-4 were loaded with an axial load of 790 lb/in. This load is representative of continued safe flight conditions. During the subsequent incremental application of pressure, the axial load was held constant within ± 6% of the continued safe flight load of 790 lb/in. Panel 2-3 was tested in the same manner as the 2-2 panel, but at -65°F. Panel 2-4 was loaded undamaged with pressure and axial loads to safe flight conditions and then damaged by a guillotine blade.

Figure 109 shows a typical failure pattern for these pressure loaded panels. Failure occurred perpendicular (circumferential) to the sawcut and appeared to occur at nearly the same time from both tips of the damage. This mode of failure is more acceptable than one that progresses fore and aft along the fuselage. The damage is self-relieving from the local effects of internal pressure, and pressure leakage will allow easier and earlier discovery of the damage.

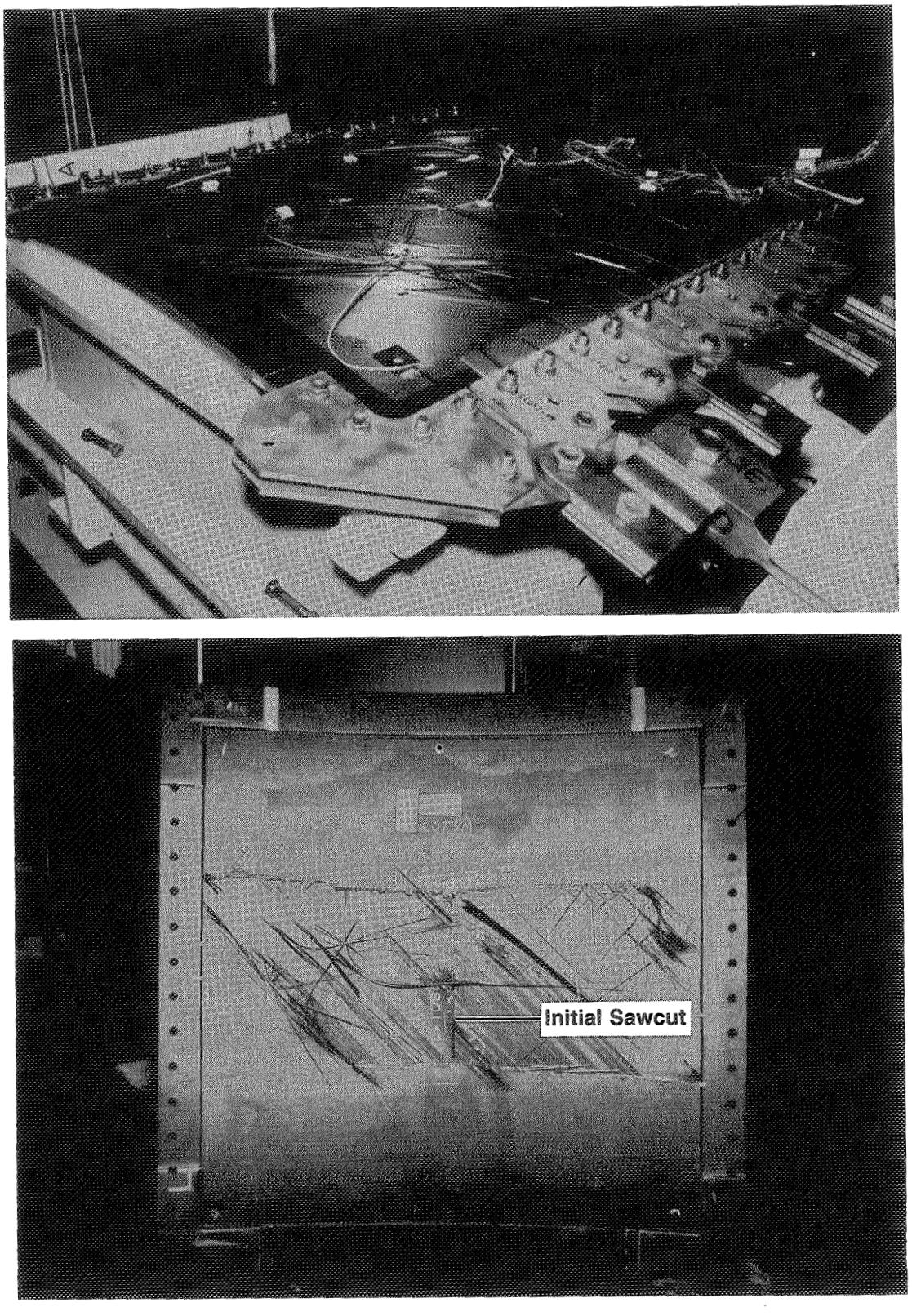

Figure 109. Curved Fracture Panel Failure

Predicted and test-derived displacements and strains are shown in Figures 110 and 111. In the pressure only panel (panel 2-1), the hoop tension load caused the crack to open and produced compressive stresses parallel to the sawcut due to Poisson's effects. This condition caused bulging in the vicinity of the crack, as evidenced by the large radial displacements, shown in Figure 110. For panel 2-2, the axial preload offset the compressive stresses and reduced the radial displacements near the sawcut. With less radial displacement, the bending strains near the end of the saw tip were reduced in the panels with combined loading, therefore leading to a higher failure load (fig. 111).

Panel 2-4 was loaded to 31.6-kips (790-lb/in) axial tension and then pressurized to 8.6 lb/in^2. This combined loading was derived from continued safe flight loads of one factor cabin pressure and 0.002-in/in axial strain in the skin. With the panel under load, a 12-in-wide, 3-lb guillotine blade was fired through the center of the panel. The blade, which produced a longitudinally oriented cut in the panel, was propelled at 202 ft/s, resulting in 1950-ft-lb impact energy. Figure 112 shows the test setup prior to firing the blade. With the exception of some fiber breakout on the interior side of the panel, the blade created a relatively clean cut in the panel. An onsite TTU inspection revealed a 1-in-radius zone of delaminations around the periphery of the cut. The panel was subsequently resealed and tested to failure in the same manner as panel 2-2. Failure occurred at 818-lb/in axial tension load and 17.9 lb/in^2 in the same manner as the panels with sawcut damage.

6.1.2.2 Circumferential Damage Tests—Two panels were tested to evaluate the effect of axial loading on pressurized shell structure with circumferential damage. The first panel (panel 2-5) was tested with a sawcut oriented in the hoop direction. This panel was loaded with constant pressure (8.6 $\pm$ 1.2 lb/in^2), and then axially loaded until failure. The failure loads for this panel were 9.7-lb/in^2 internal pressure and 2200-lb/in axial tension load. Panel 2-6 was loaded to 69.6-kips (1740-lb/in) axial tension, pressurized to 8.6 lb/in^2, and then impacted with a guillotine blade. The test setup was the same as that described for panel 2-4, with the exception that the continued safe flight loads were derived from one factor cabin pressure combined with 0.002-in/in axial strain in longitudinal tear straps. With the panel at load, the 12-in-wide, 3-lb guillotine blade was fired through the center of the panel. This time the blade, which produced a circumferentially oriented arc, was propelled at 240 ft/s, resulting in impact energy of 2700 ft-lb. The blade penetration again produced a relatively clean cut with a 1-in zone of delaminations around the periphery of the cut. The panel was subsequently sealed and tested to failure in the same manner as the sawcut panel 2-5, discussed previously. The panel failed at 2550-lb/in axial tension load and 8.5-lb/in^2 internal pressure. This compares well to the sawcut damaged panel.

6.1.2.3 Analysis of Curvature and Stiffening Effects—In addition to analyzing the test 2 results, panels with various radii of curvature and percent stiffening were evaluated.

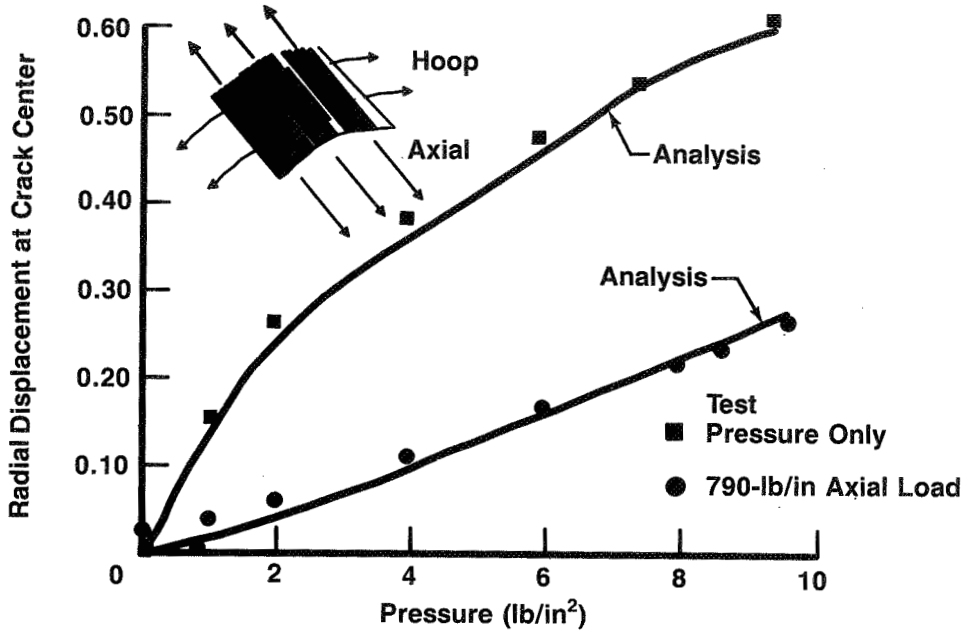

Figure 110. Predicted and Test-Derived Deflections in Curved Fracture Panel Test

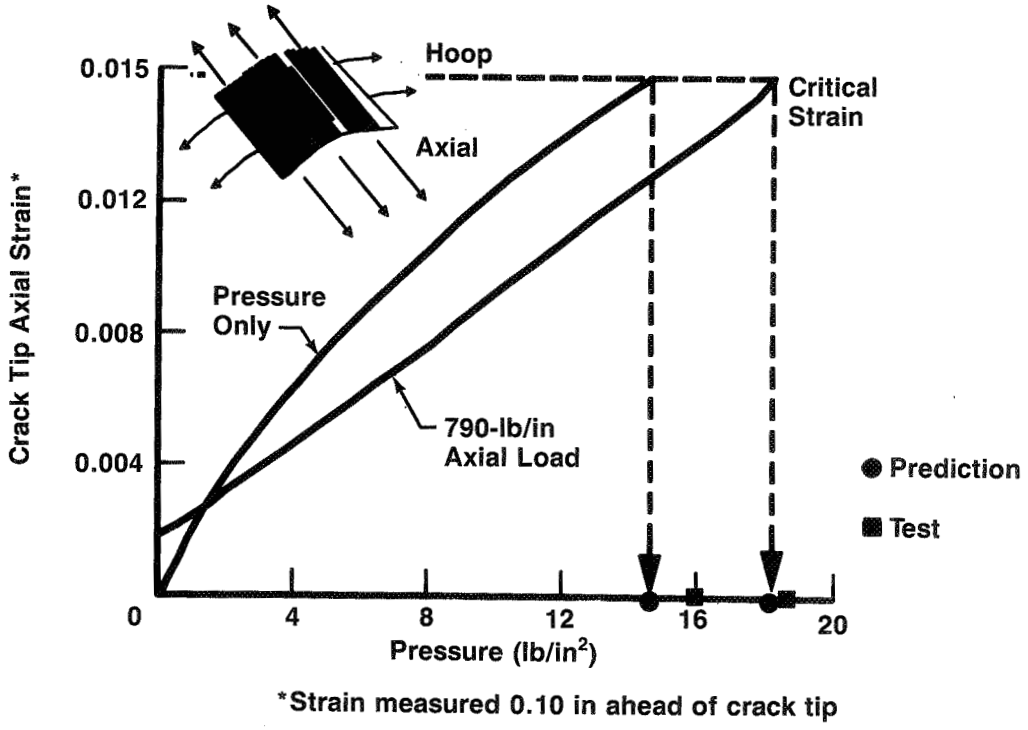

Figure 111. Curved Fracture Panel Failure Analysis

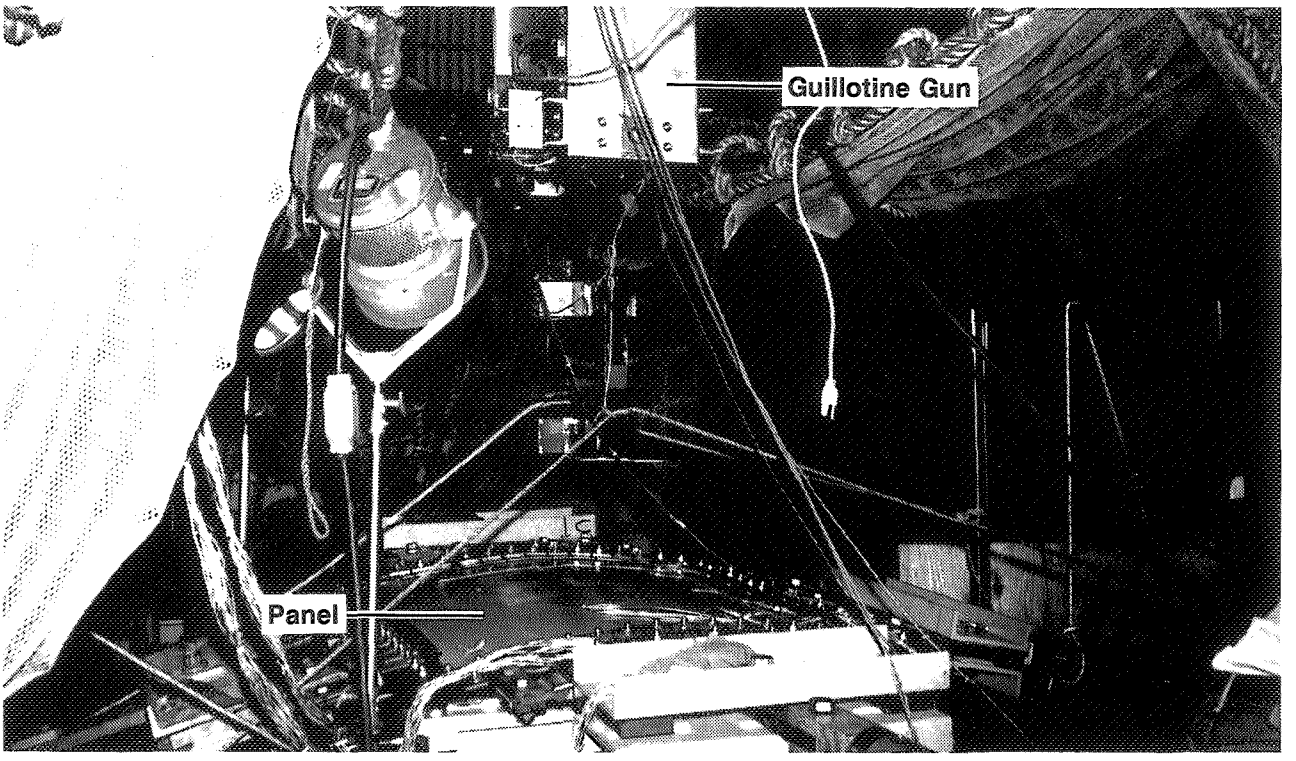

Figure 112. Test Setup for Guillotine Tests (Test 2, Panels -4 and -6)

The results of the study of the influence of radius of curvature on the residual strength of a curved pressurized panel with a 12-in longitudinal cut are presented in Figure 113. The loading was limited to normal pressure only (no end load), and failure was assumed to occur when the material at 0.10 in ahead of the sawcut tip reached 0.015-in/in strain. Due to the orthotropy of the shell, the total (midplane + bending) longitudinal strain is higher than the total hoop strain. The shape of the curves suggests that the effect of a change in radius on residual strength is most pronounced for smaller radii. At some point beyond a radius of 126 in, the asymptotic nature of the curves indicates insensitivity of residual strength to increased radius.

The results of the study of the effects of hoop tear strap stiffening on the residual strength of a curved pressurized panel with a 17-in longitudinal cut are presented in Figures 114 and 115. Specimens with 3.0-in-wide tear straps with spacings of 10.0 in and 20.0 in were studied. The loading was limited to normal internal pressure with no end loading. Results for 5.76-lb/in^2 internal pressure are presented for the unstiffened shell and shells with stiffening ratios of 22% and 36%. For the study purposes, the thickness of the 10-in spaced tear straps was 50% of the thickness of the 20-in spaced tear straps.

The results plotted in Figure 115 are for total hoop and longitudinal strains at 0.1 in ahead of (and in line with) the cut and for hoop strain at 0.1 in from the cut along the edge of the tear strap (perpendicular to the line of the cut). Separate curves are provided for 10- and 20-in spacing.

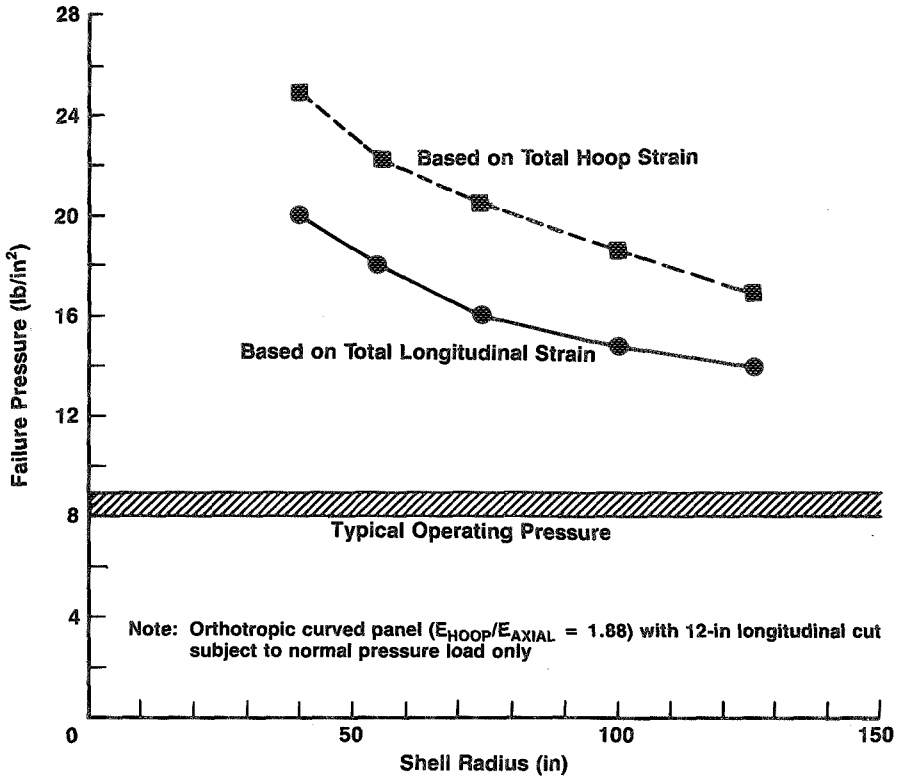

Figure 113. Effect of Radius on Residual Strength of Curved Panel

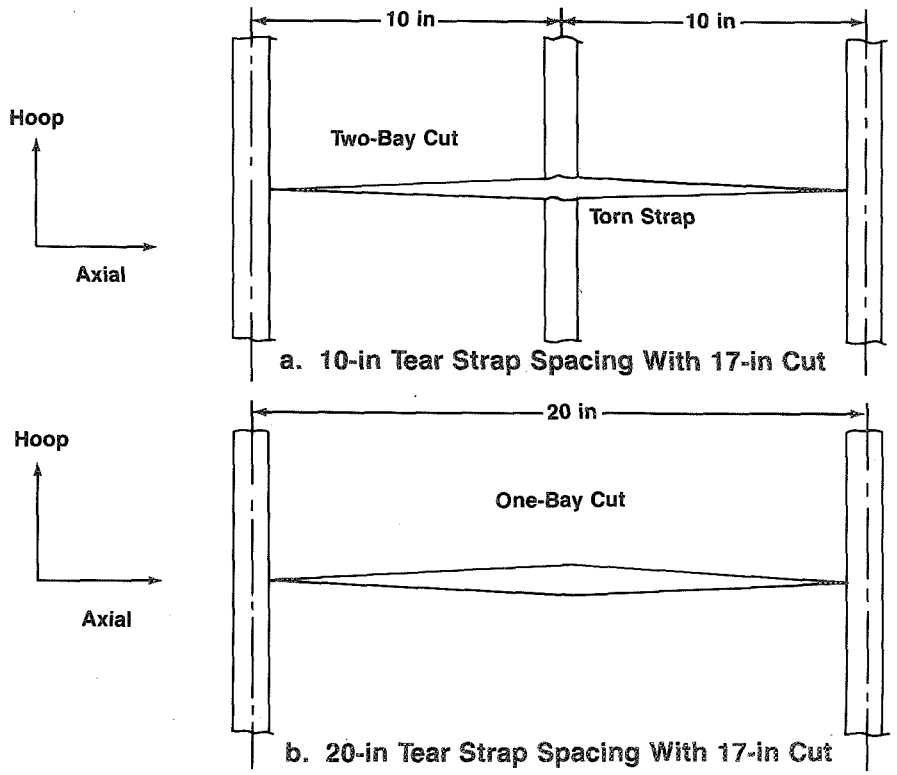

Figure 114. Tear Strap Spacing Effect on Stiffening Study

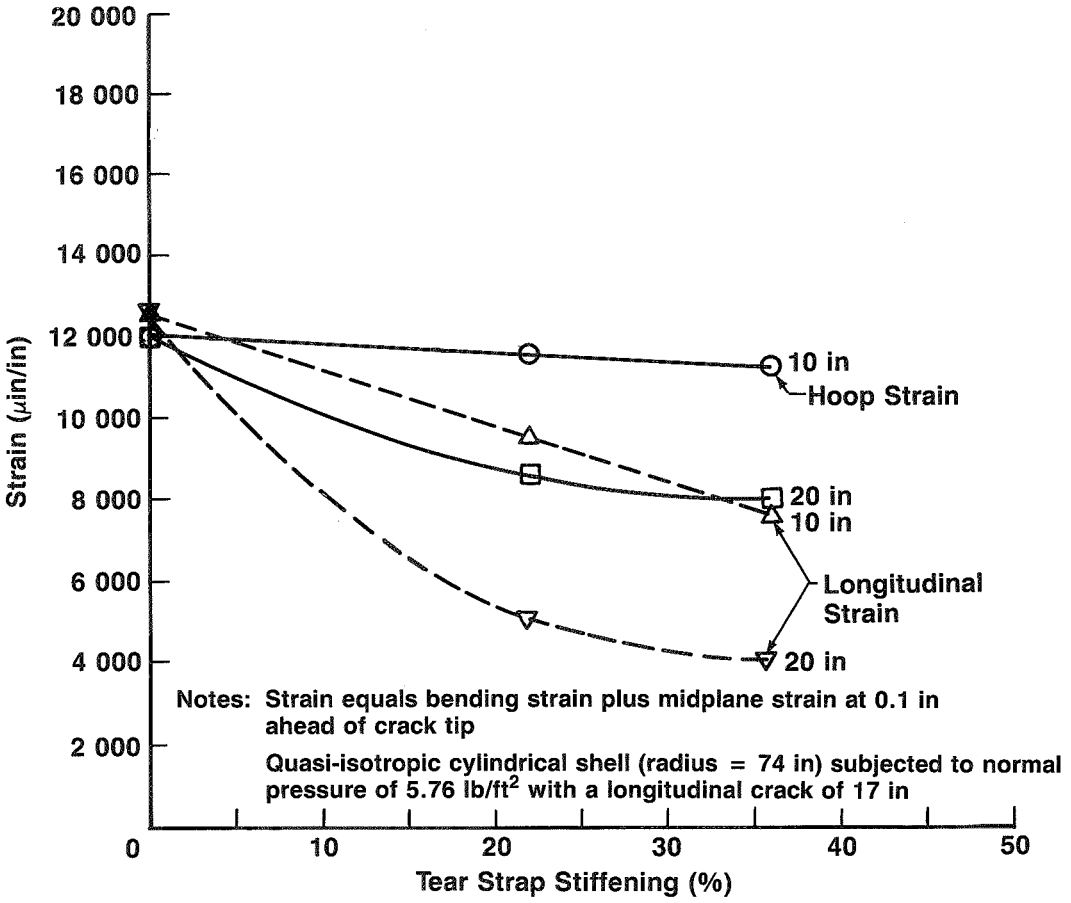

Figure 115. Effect of Tear Strap Stiffening on Strain Near Crack Tip

Results show that residual strength is moderately sensitive to stiffening with the 10-in strap spacings and strongly sensitive to a 20-in strap spacing. With a two-bay cut of the 10-in tear strap spacing, the benefit due to the tear strap stiffening is offset by the redistribution of load from the torn central tear strap into the skin. For a one-bay crack of the 20-in tear strap spacing, an increase in stiffening fully benefits the reduction of near field stress.

The curves for 20-in spacing flatten considerably between 22% and 36% stiffening, suggesting decreasing benefit due to increased stiffening. The longitudinal strain is much more sensitive to stiffening for both tear strap spacings.

6.2 Buckling and Postbuckling

The compression capability of typical crown and keel sections was evaluated by testing five single-stiffener crippling elements (test 3) and four curved skin-stringer panels (test 4). The shear capability of a panel representative of the side of the fuselage located between the crown and the window belt was evaluated by testing two flat skin-stringer panels (test 5). The detailed design of the configurations used for these tests is discussed in Section 3.1.1. The crippling element and compression panel tests are discussed in Section 6.2.1 and the shear tests in Section 6.2.2.

Finite element analyses were used to model the initial buckling and postbuckling of the compression panels of test 4 and the shear panels of test 5. The results of the tests and analyses are discussed in following sections.

6.2.1 Skin-Stringer Compression Tests

The crippling element and compression panel test articles were based on the crown and keel fuselage sections discussed in Section 3.1.1. Design details are shown in Figures 27 and 28. The single-stringer specimens (test 3) evaluated the local buckling and crippling characteristics of the stringers. The skin-stringer panels (test 4) were used to evaluate skin buckling and postbuckling characteristics.

The keel panels were designed to represent station 1200 (fig. 8) and to support a compressive DUL of 5000 lb/in (fig. 116). At that DUL, the compression strain is 0.0047 in/in. The skin was designed to buckle at 26% DUL. Localized stringer buckling or crippling and Euler column buckling were designed above 100% DUL. The loading capability of the crown panel, summarized in Figure 116, was designed to represent station 1460 (fig. 8). The selected design results in a strain of 0.0057 in/in for a tension load of 3000 lb/in. In the reverse load direction, the crown section is at a strain of 0.0025 in/in for a compression load of 1000 lb/in. Since the tension extensional stiffness requirements in the crown exceed compressive requirements, the crown panel is at relatively low strain levels in compression. The skin was designed to buckle at 50% DUL. The stringer was designed for local buckling and Euler column buckling to occur well above 150% DUL.

6.2.1.1 Single-Stringer Crippling—Five one-stringer elements, three representing the fuselage crown skin-stringer configuration and two representing the keel configuration, were tested in compression to failure. These tests were conducted to determine the local stability and crippling capability of the stiffener elements. The stringer elements were designed to be stable to above 100% of DUL. The predicted stringer web and cap buckling values for the crown and keel specimens are shown in Figure 117. Figures 118 and 119 summarize the test results of the crippling elements.

	Keel 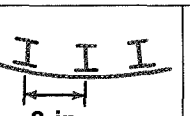 8 in	Crown 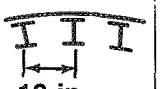 10 in
Body Station	1200	1460
Compression Loading		
Design Ultimate Load (DUL)	5000 lb/in	1000 lb/in
Design Strain (ε_c) [1]	0.0047 in/in	0.0025 in/in
Skin Buckling Load	26% DUL	50% DUL
Local Stringer Flange Buckling Load	125% DUL	160% DUL
Euler Column Buckling Load	160% DUL	230% DUL
Tension Loading		
Design Ultimate Load (DUL)	[2]	3000 lb/in
Design Strain (ε_T)	[2]	0.0057 in/in

[1] Compression strain allowable: 0.005 in/in
Tension strain allowable: 0.006 in/in

[2] Tension loading in keel does not influence design

Figure 116. Skin-Stringer Design for Compression Tests

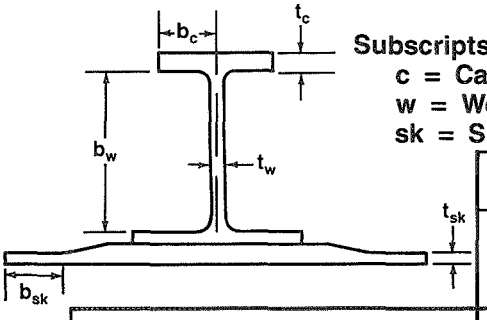

Subscripts:
c = Cap Flange
w = Web
sk = Skin

	Crown			Keel		
	Cap Flange	Web	Skin [5]	Cap Flange	Web	Skin [5]
Element Thickness t (in)	0.062	0.067	0.056	0.112	0.112	0.067
Element Width b (in)	0.5	1.2	0.3	0.6	1.2	0.3
b/t	8.1	17.9	5.4	5.6	10.7	4.5
E (msi) [1]	8.9	6.2	3.8	11.6	10.9	6.2
F_{CR} (ksi) [2]	36.1	50.7	70.0	67.8	123.4	90.0
ε_{CR}(in/in) [3]	0.004	0.0082	0.018	0.0059	0.011	0.015
M.S. - Margin of Safety [4]	0.60	2.28	6.20	0.25	1.34	2.19

[1] E: extensional modulus
[2] F_{CR}: critical buckling stress
[3] ε_{CR}: critical buckling strain
[4] M.S.: MS = $\varepsilon_{CR}/\varepsilon_{DUL}$ - 1 where ε_{DUL} is section strain at 100% DUL
ε_{DUL} values: crown - 0.0025 in/in, keel - 0.0047 in/in
[5] Skin element represents the edge of the test 3 and 4 panels

Figure 117. Local Buckling Analysis for Skin-Stringer (Tests 3 and 4)

Test Specimen [1]	Actual Cap Width (in)	Actual Skin Width (in)	Initial Buckling Load (kips)	Initial Buckling Stress (ksi)	Initial Buckling Strain, P/AE (in/in)	Failure Load (kips)	Failure Stress (ksi)	Failure Strain, P/AE (in/in) [2]
Crown								
3C-1	1.00	3.55	19.2	35.8	0.0049	25.15	46.8	0.0065
3C-2	0.98	3.55	19.3	35.9	0.0049	23.70	44.1	0.0061
3C-3	0.98	3.52	19.3	35.9	0.0049	25.10	46.9	0.0066
Average			19.3	35.9	0.0049	24.65	45.9	0.0064
Keel								
3K-1	1.25	3.96	32.7	39.6	0.0039	40.7	49.3	0.0048
3K-2	1.20	3.92	53.1 [3]	64.5	0.0063	55.5	67.4	0.0066

[1] Material: AS6/2220-3, grade 145

[2] Strains at design ultimate load: crown - 0.0025 in/in; keel - 0.0047 in/in

[3] Skin edge supports used to stabilize skin

Figure 118. Single Stiffener Element Crippling Test Results (Test 3)

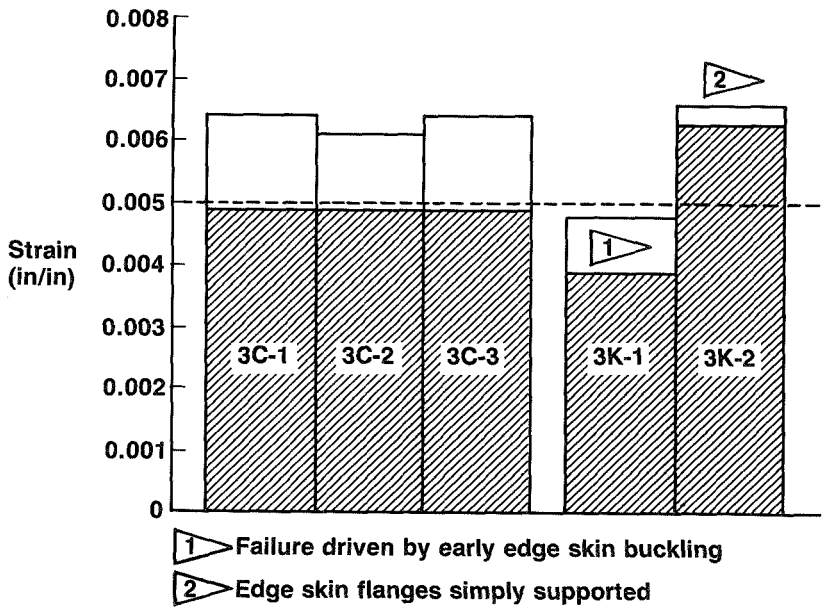

Figure 119. Single Stringer Element Local Buckling and Failure Strains (Test 3)

TTU inspection prior to testing indicated that all three crown elements contained areas of low compaction at the skin-stringer interface. The amount of low compaction area per specimen, shown in Figure 120, varied from low (specimen 3C-1), to medium (specimen 3C-2), to high (specimen 3C-3). These crown elements, designed primarily for tension loads, were required to be capable of compression strains of 0.0025 in/in. All three elements failed above 0.006 in/in (0.0064 in/in average) and failed within 1 kip of each other (fig. 118). The free edge of the skin proved to be the critical area. The stringer section remained stable until the free edge of the skin buckled, precipitating the instability of the stringer skin flange. The free edge of the skin buckled at 0.0049 in/in, which was 23% higher than the predicted value of 0.004 in/in (fig. 119). Figure 121 shows the buckling mode and failure of one of the crown elements.

The first of the keel elements started to buckle at the skin edge (as occurred in the crown elements). The edge of the skin initiated the instability of the stringer element at a lower strain than expected (0.0039 versus 0.0059 in/in), so the full capability of the stringer was not obtained. It failed at 0.0048 in/in, which was lower than the compression design ultimate strain of 0.005 in/in.

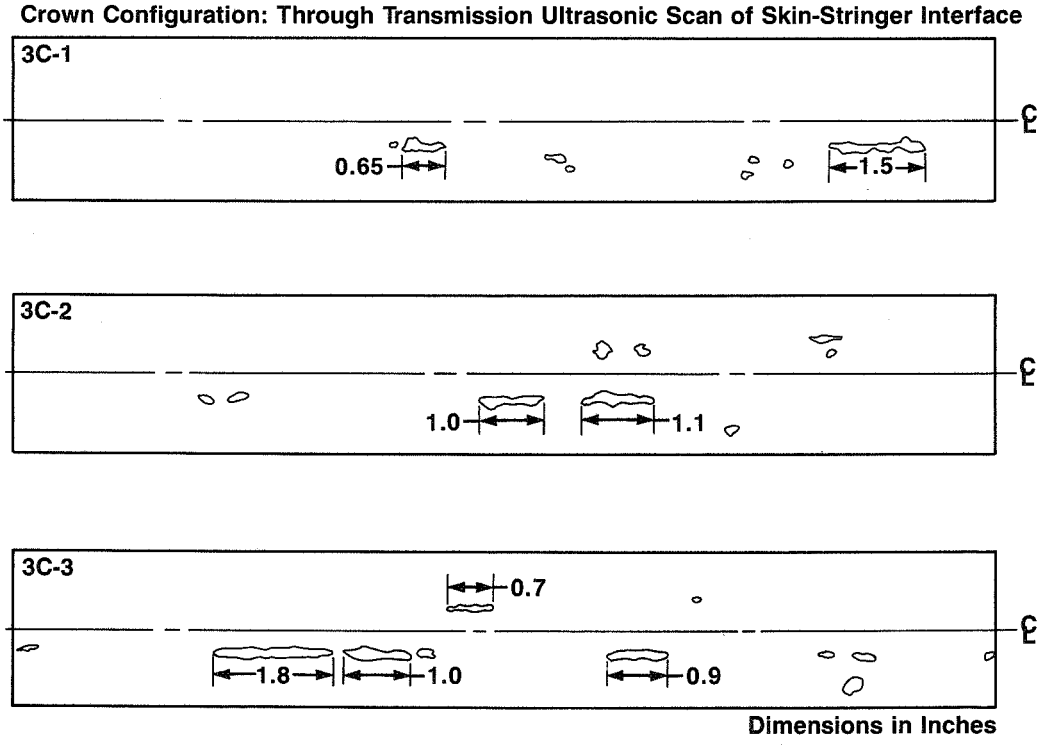

Figure 120. Areas of Low Compaction in Skin-Stringer Crippling Elements

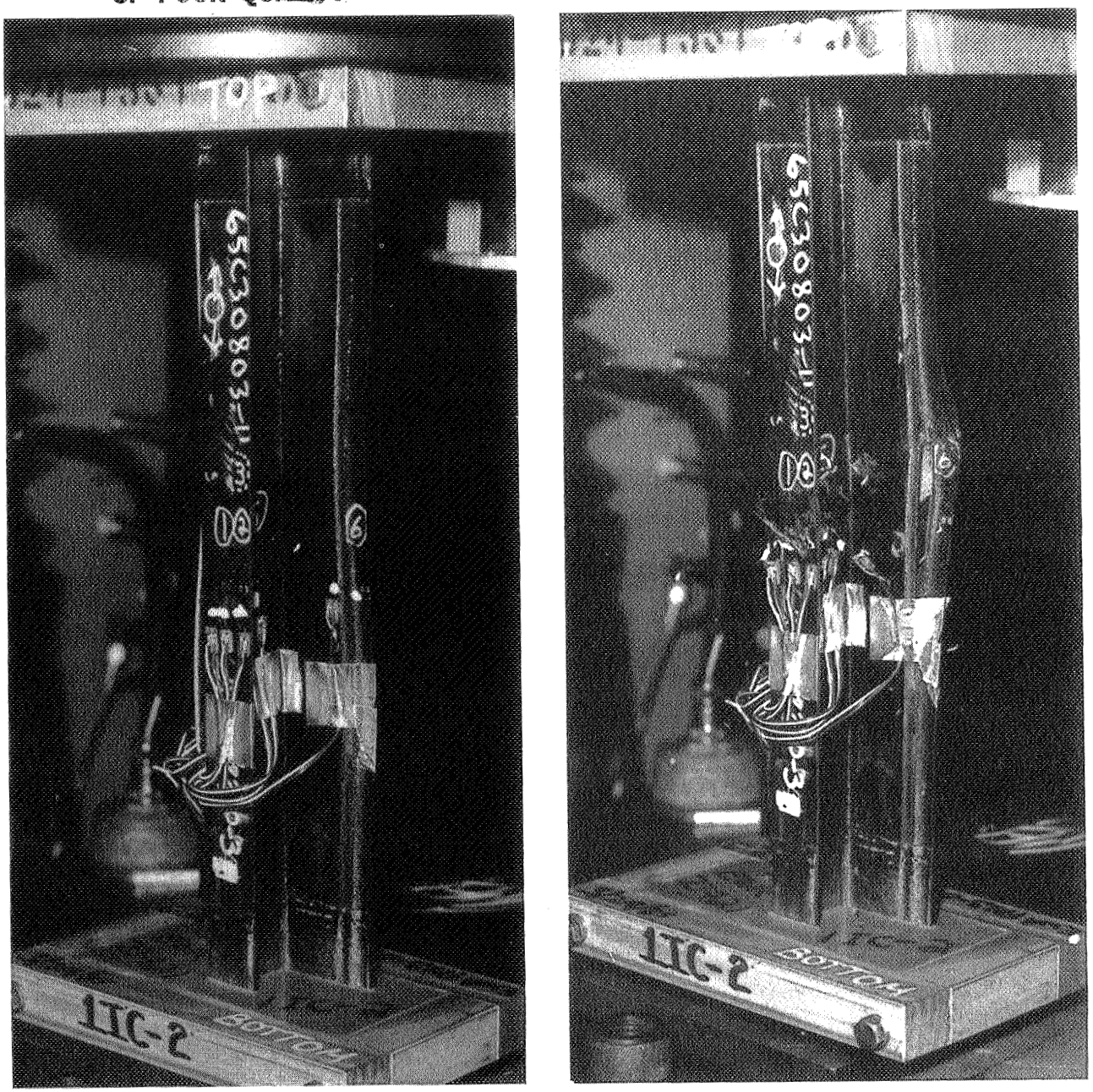

P = 23 kips

Failed Crown Element
P_{Fail} = 23.7 kips

Figure 121. Local Buckling Mode and Failure Pattern of a Single Stringer Crown Crippling Element

The second keel element was tested using aluminum tubular supports at the skin edges. These supports were used to stabilize the edges of the skin so that the strength of the element could be determined. The buckling strain for this specimen was 0.0063 in/in, and the failure strain was 0.0066 in/in (figs. 118 and 119). This test result demonstrated that the web and the cap of the stringer are capable of being stable at strains above the compression design ultimate strain of 0.005 in/in.

6.2.1.2 Skin-Stringer Compression Panels—Four curved compression panels were tested undamaged to evaluate the postbuckling behavior of the two skin-stringer fuselage configurations. The testing was conducted in a room temperature, dry environment. The results of the tests and analyses are summarized in Figure 122.

The crown panels sustained loads to an average of 280% of the compressive DUL, and the keel panels sustained loads to an average of 112% of the DUL requirement.

Aluminum tubular supports were used to stabilize the skin edges, as shown in Figure 122. The panels were instrumented with strain gages and moire spectrometry to provide data for analysis correlation. The strain gages were located on the skin and stringers (fig. 123). During test, the strains were used to ensure that the panels were loaded evenly prior to buckling and to monitor the load distribution after the initiation of buckling. Moire fringe photographs that show the progression of buckling in the keel and crown panels are in Figures 124 and 125.

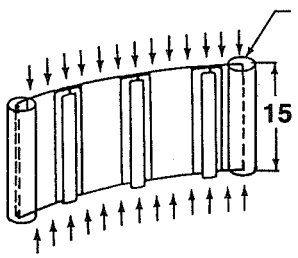

Test Panel [1]	Unbuckled Extensional Stiffness, EA (msi-in^2)	Buckled Extensional Stiffness, EA (msi-in^2) [2]	Initial Buckling: Load (kips) STAGSC	Initial Buckling: Load (kips) Test [3]	Initial Buckling: Strain (in/in) STAGSC	Initial Buckling: Strain (in/in) Test [3]	Ultimate: Design Ultimate Load (kips)	Ultimate: Test Failure Load (kips)	Ultimate: Design Ultimate Strain (in/in)	Ultimate: Test Failure Strain (in/in)
Crown										
4C-1	14.4	12.0	14.9	16.0	0.0010	0.0011	30.1	82.25	0.0025	0.0068
4C-2	14.4	12.0	14.9	20.0	0.0010	0.0014	30.1	90.00	0.0025	0.0075
Keel										
4K-1	28.5	25.7	34.1	36.0	0.0012	0.0013	120.9	138.25	0.0047	0.0054
4K-2	28.5	25.7	34.1	38.0	0.0012	0.0013	120.9	134.50	0.0047	0.0052

[1] Material: AS6/2220-3, grade 145 tape
[2] Buckled skin effective width based on $1.7t\sqrt{1/\varepsilon}$ for ε = 0.005 in/in
[3] Initial buckling determined from moire fringe photos and strain gage data

Figure 122. Curved Compressed Panel Test Results (Test 4)

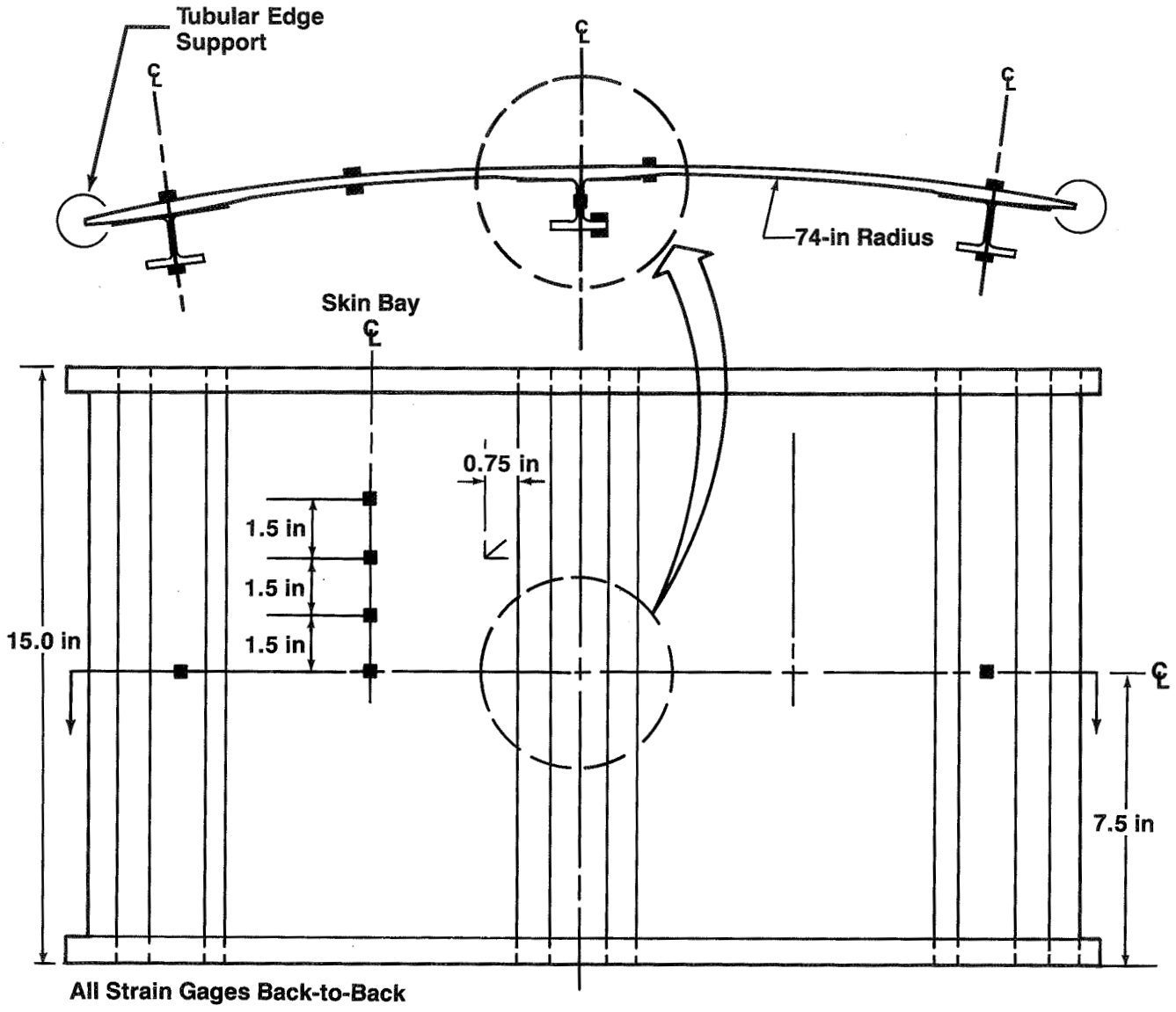

Figure 123. Test Panel Configuration and Strain Gage Locations for Curved Compression Panels (Test 4)

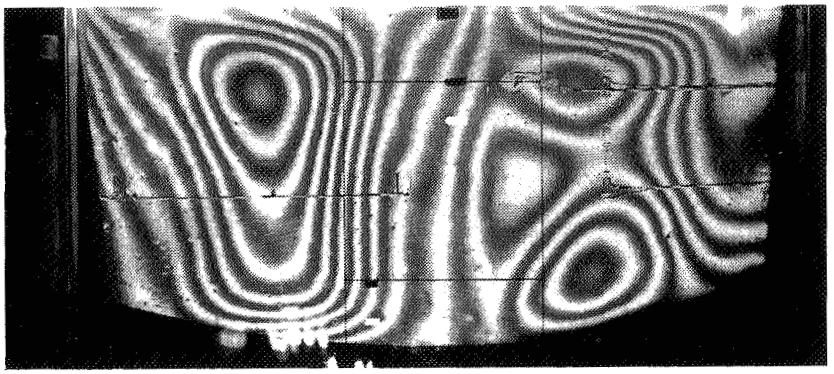

Load = 20 kips

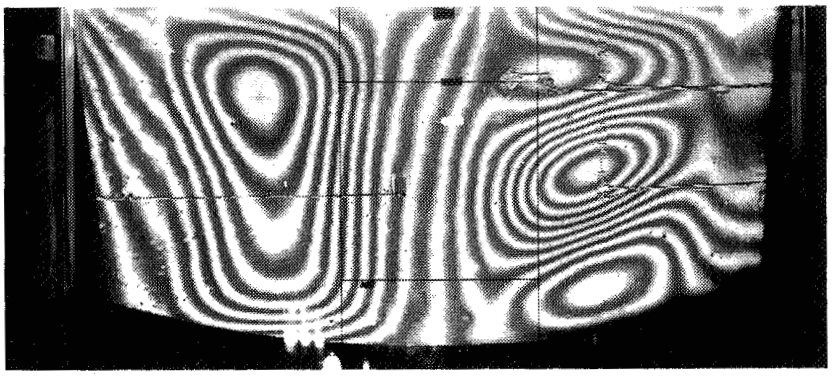

Load = 21 kips

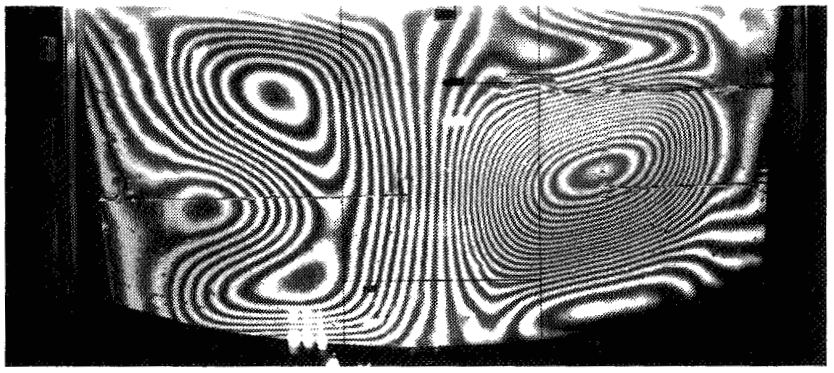

Load = 39 kips

Buckling Mode at Panel Centerline (Exaggerated)

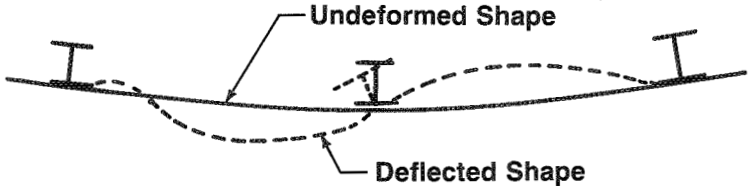

Note: One fringe = 0.0173 in

Figure 124. Moire Fringe Patterns of a Crown Skin-Stringer Compression Panel

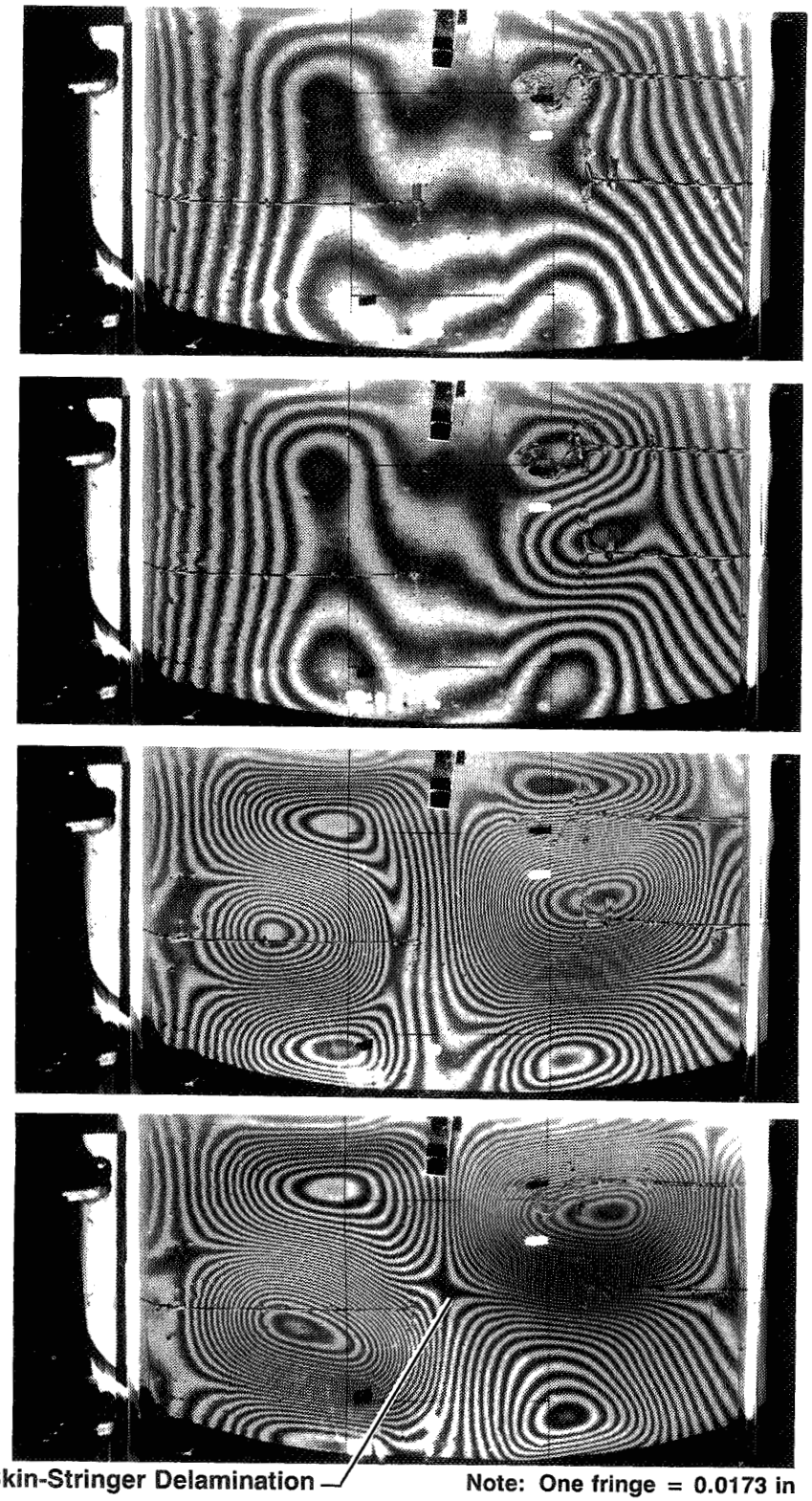

Figure 125. Moire Fringe Patterns of a Keel Skin-Stringer Compression Panel

All of the panels failed after the highly buckled skin separated from the central stringer. This is shown in the last moire fringe photograph of a keel panel in Figure 125. The buckling pattern changes after the center stringer has separated from the skin.

The stability and postbuckling characteristics of the skin-stringer panels were analyzed using the STAGSC finite element code (ref. 16). Single curved shell STAGSC models were created for the skin elements of the keel and crown compression panels. The skin panels were modeled to the edge of the stringer padup ramps with simple support boundaries at the padups. The STAGSC buckling mode shapes and buckling load values are shown in Figure 126. These values are consistent with the buckling values predicted by the Boeing analysis code LEOTHA.

Two STAGSC models, shown in Figure 127, were developed for the crown and keel skin-stringer compression test panels. Each model consists of 19 shell members. Each shell member is a constant thickness plate used for building the model. Each shell is further divided into finite elements. The shell members are rigidly connected at common boundaries to ensure continuity of lateral and angular displacements. The load is introduced to the panel by uniformly displacing one end and reacting the load at the other end. The loaded ends are modeled with fixed ends (no rotation), whereas the unloaded skin edges are free. These models have been used to calculate initial buckling loads for the test panels. The crown and keel panel buckling mode shapes that result from the first STAGSC eigenvalue solution are shown in Figure 128. In each case, the skin buckled without distorting the stringers. The buckling strain predictions based on the 19-shell model are very close to the Boeing LEOTHA analysis values, which were used to design the test panels.

The STAGSC finite element models have been used to perform the postbuckling analysis of the crown and keel compression panels. The assumed shape of the unloaded structure influences the response of postbuckling models. Three assumptions were considered for the imperfected shape of the panels. The assumed shapes were based on (1) the lowest buckling mode shape with the maximum amplitude set equal to 1% of the skin gage; (2) the lowest buckling mode with an 0.05-in amplitude; and (3) the measured imperfected shape, represented by Fourier series equations. The amplitude of the imperfection in the first assumption (1% of skin gage) was used in Reference 17 and represents an idealistic panel containing no manufacturing imperfections. A more realistic, larger imperfection of 0.05 in was selected for the second assumption, based on potential warpage that can occur during fabrication.

The imperfect shapes of the crown and keel compression panels were measured prior to testing. The assumed shape of the structure influences the response of the STAGSC postbuckling models. The measured imperfect shapes of the panels were incorporated into the model using a user-written subroutine. To perform this, Fourier series mathematical expressions were developed for describing the imperfected shape of one crown panel and one keel panel. Contour plots of the measured and imperfected shapes of the crown and keel panels are shown in Figure 129. These plots indicate that the Fourier series relationships accurately represent the measured panel imperfections.

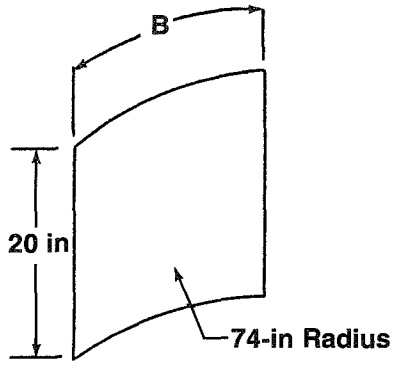

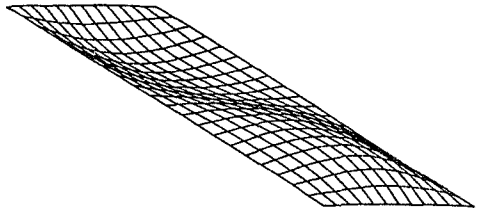

STAGSC Mode Shape—Crown

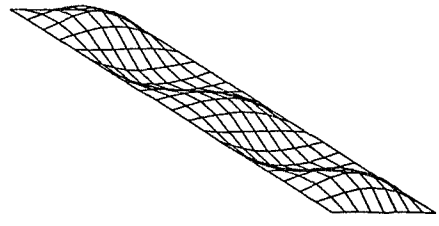

STAGSC Mode Shape—Keel

	Crown b_{Skin} = 6.8 in [1] Laminate: $(\pm 45/90/\pm 45)_s$		Keel b_{Skin} = 4.6 in [1] Laminate: $(\pm 45/90/\pm 45/0)_s$	
	Buckling Load N(lb/in)	Buckling Strain (in/in)	Buckling Load N(lb/in)	Buckling Strain (in/in)
Boeing Analysis				
LEOTHA [2]	200	0.00094	475	0.00115
STAGSC [2]	196	0.00092	456	0.00110

[1] B: panel width based on skin width measured between the bottoms of the padup ramps

[2] Simple support boundary conditions—all edges

Figure 126. Skin Buckling Analysis for Skin-Stringer Crown and Keel Panels (Test 4)

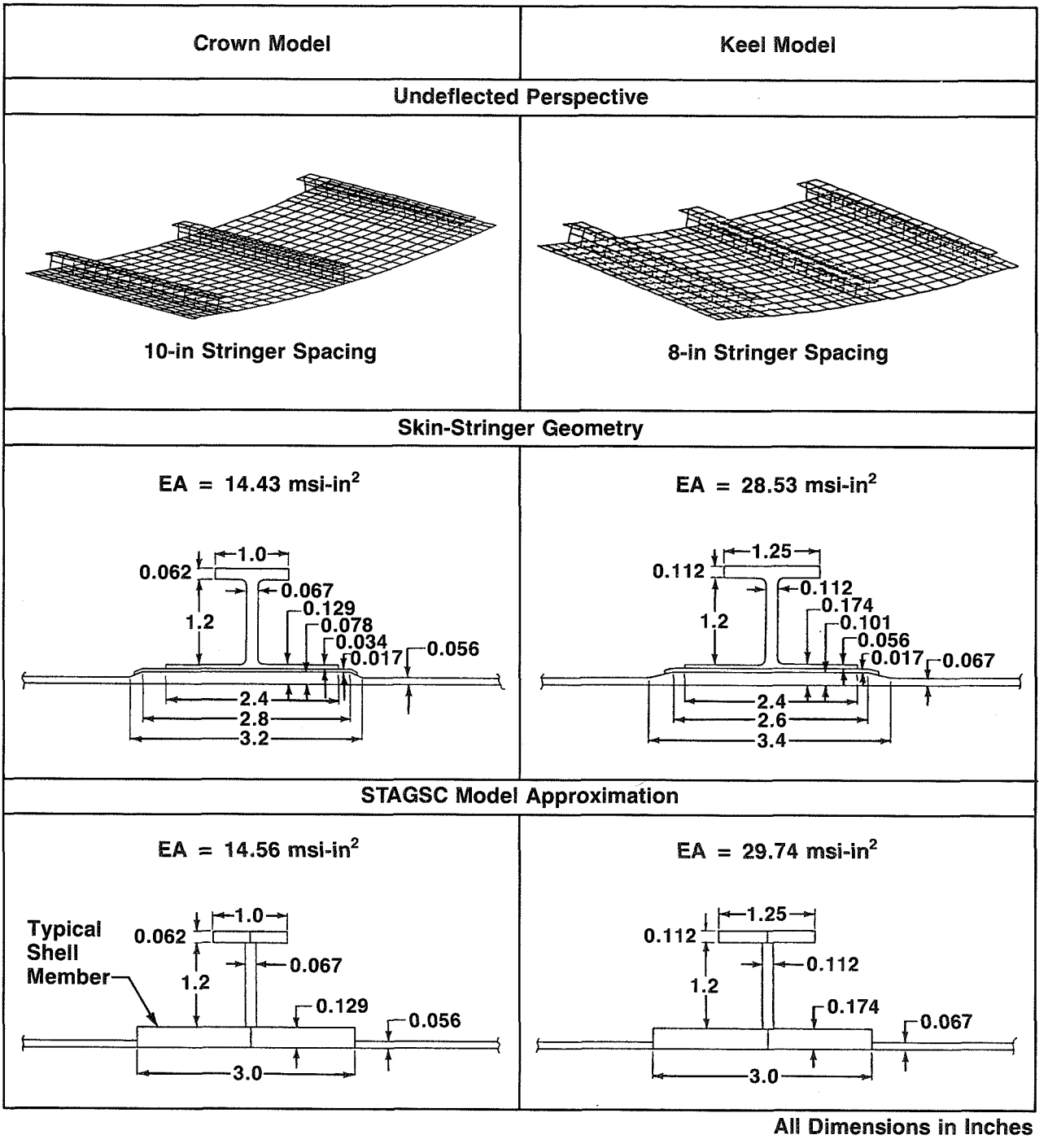

Figure 127. Nineteen-Shell STAGSC Postbuckling Model of Three-Stringer Compression Panels (Test 4)

	Crown		Keel	
	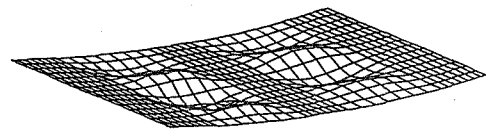 Perspective View of Mode I Buckled Shape (Stringers Not Shown for Clarity) 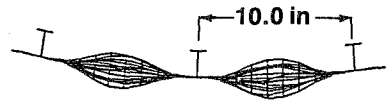 End View of Mode I Buckled Shape		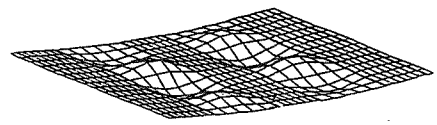 Perspective View of Mode I Buckled Shape (Stringers Not Shown for Clarity) 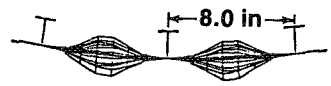 End View of Mode I Buckled Shape	
	Load P(kip)	Strain (in/in)	Load P(kip)	Strain (in/in)
Design Values:				
Buckling	13.6	0.0009	32.8	0.0012
Design Ultimate Load (DUL)	30.1	0.0025	120.9	0.0047
STAGSC—19-Shell Model Buckling	14.9	0.0010	34.1	0.0012

Figure 128. Nineteen-Shell STAGSC Buckling Analysis of Skin-Stringer Crown and Keel (Test 4)

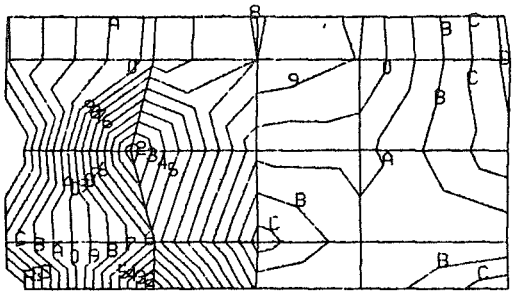

Measured Initial Imperfections of Keel Panel 4K-2

Contour Line	Imperfection Height (in)
1	-0.20
2	-0.18
4	-0.14
6	-0.10
8	-0.06
0	-0.02
A	0
B	0.02
D	0.06
F	0.10
H	0.14

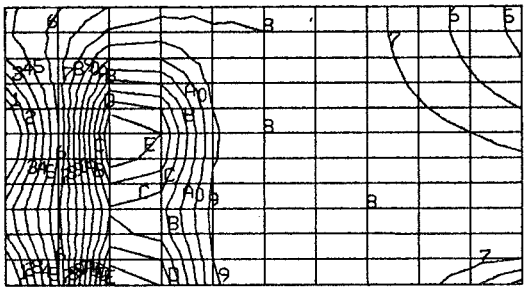

Fourier Series Representation of Panel 4K-2 To Be Used in STAGSC Analysis

Contour Line	Imperfection Height (in)
1	-0.14
2	-0.12
4	-0.08
6	-0.04
8	0
0	0.04
A	0.06
B	0.08
C	0.10
D	0.12
E	0.14

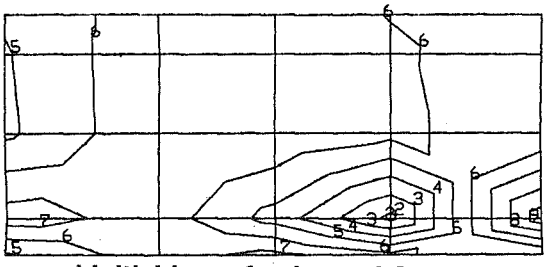

Measured Initial Imperfections of Crown Panel 4C-1

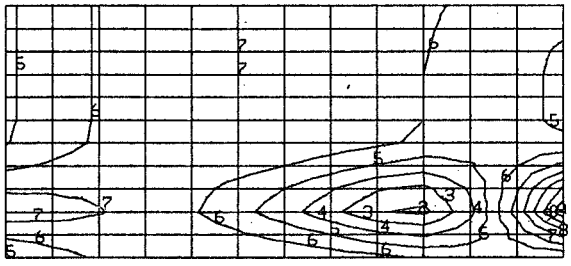

Fourier Series Representation of Panel 4C-1 To Be Used in STAGSC Analysis

Contour Line	Imperfection Height (in)
1	-0.10
2	-0.08
3	-0.06
4	-0.04
5	-0.02
6	0
7	0.02
8	0.04
9	0.06
0	0.08
A	0.10

Figure 129. Measured and Fourier Series Contour Representations of Skin Imperfections in Curved Skin-Stringer Compression Models

Strains predicted by the STAGSC analyses are compared with test strains in Figures 130 through 135.

The strains at the centerline of the base and cap of the edge stringer of a keel panel, shown in Figure 130, increase evenly at the same rate. Corresponding data for crown panel 4C-1 are shown in Figure 133. These data indicate that the panel did not exhibit any column mode bending or buckling, which agrees with prediction. As shown in the figure, the STAGSC predicted strains correlate very well with the test data.

Comparison of predicted and measured strains at the base of the stringer, next to the skin edge and in the middle of the skin, is shown in Figure 131. The STAGSC model, based on an assumed imperfection of 1% of the skin gage, and the measured imperfections, correlate very well with the test data prior to and after initial buckling. The model, based on an assumed imperfection of 0.05-in magnitude (not shown), predicted significant bending in the skin prior to buckling and, accordingly, did not model the strain values in the center of the skin as accurately. All of the models, independent of the assumed imperfections, predicted very well the strain distribution at the edge of the padup ramp.

The strain values on the center web of the keep panel increased at a fairly even rate until failure and correlated well with the STAGSC predicted strains, as shown in Figure 132. Similar results were obtained in the crown panel, shown in Figure 135.

The strain values on the cap edge of the center stringer, shown in Figure 132, diverge from the STAGSC prediction after the initiation of skin buckling. The change in slope of the cap strains (figs. 132 and 135) would indicate that, after skin buckling has developed, the stringer may exhibit some torsional-flexure-mode buckling. Since the slope of the strain curves taken from the web did not diverge in a like manner, it is concluded that the stringer flexure occurred due to deflections imposed on the stringer base due to skin buckling, and not due to local buckling or crippling of the stringer web. To verify this, the results of the single-stringer crippling tests (test 3) and the moire fringe data for both the keel and crown three-stringer panels were reviewed. The single-stringer crippling tests showed that in the absence of deflections induced from skin buckling, the stringer sections can remain stable to strains more than twice that at which the cap strains diverged in the buckled skin-stringer panels. The moire fringe data for the keel and crown panels (figs. 124 and 125, respectively) show that in a given test, the skin buckles develop asymmetrically between the two skin bays. For example, the moire photograph of the crown panel shown in Figure 124 indicates that at 21 kips, there are three fully developed buckles in one skin and only one in the apposing skin. The skin deflections associated with the asymmetric buckles in the apposing skins cause the center stringer to rotate in a flexural twisting mode, as shown in Figure 124.

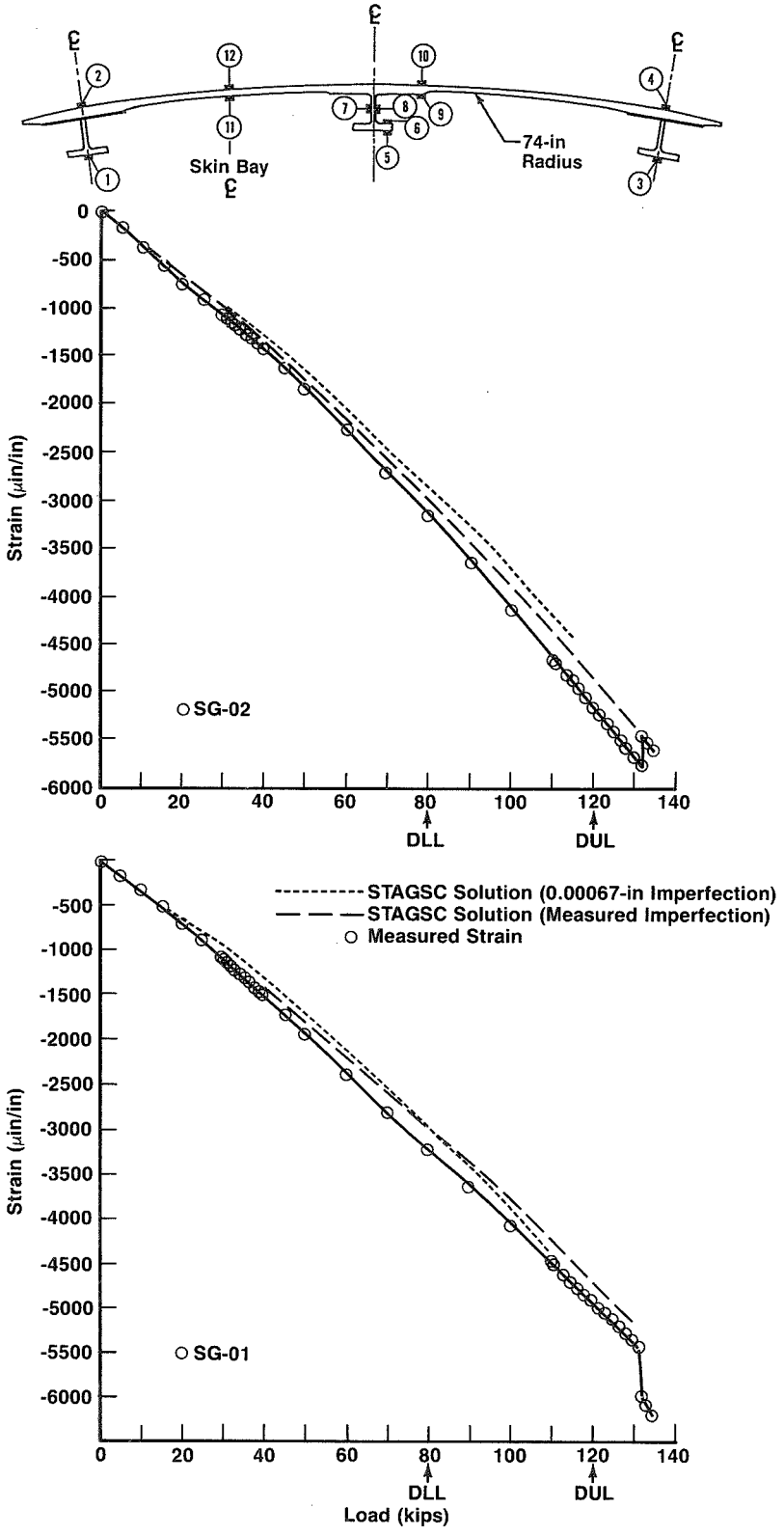

Figure 130. Measured and Predicted Strains in Outside Stringer Cap and Skin Side of Keel Compression Panel 4K-2

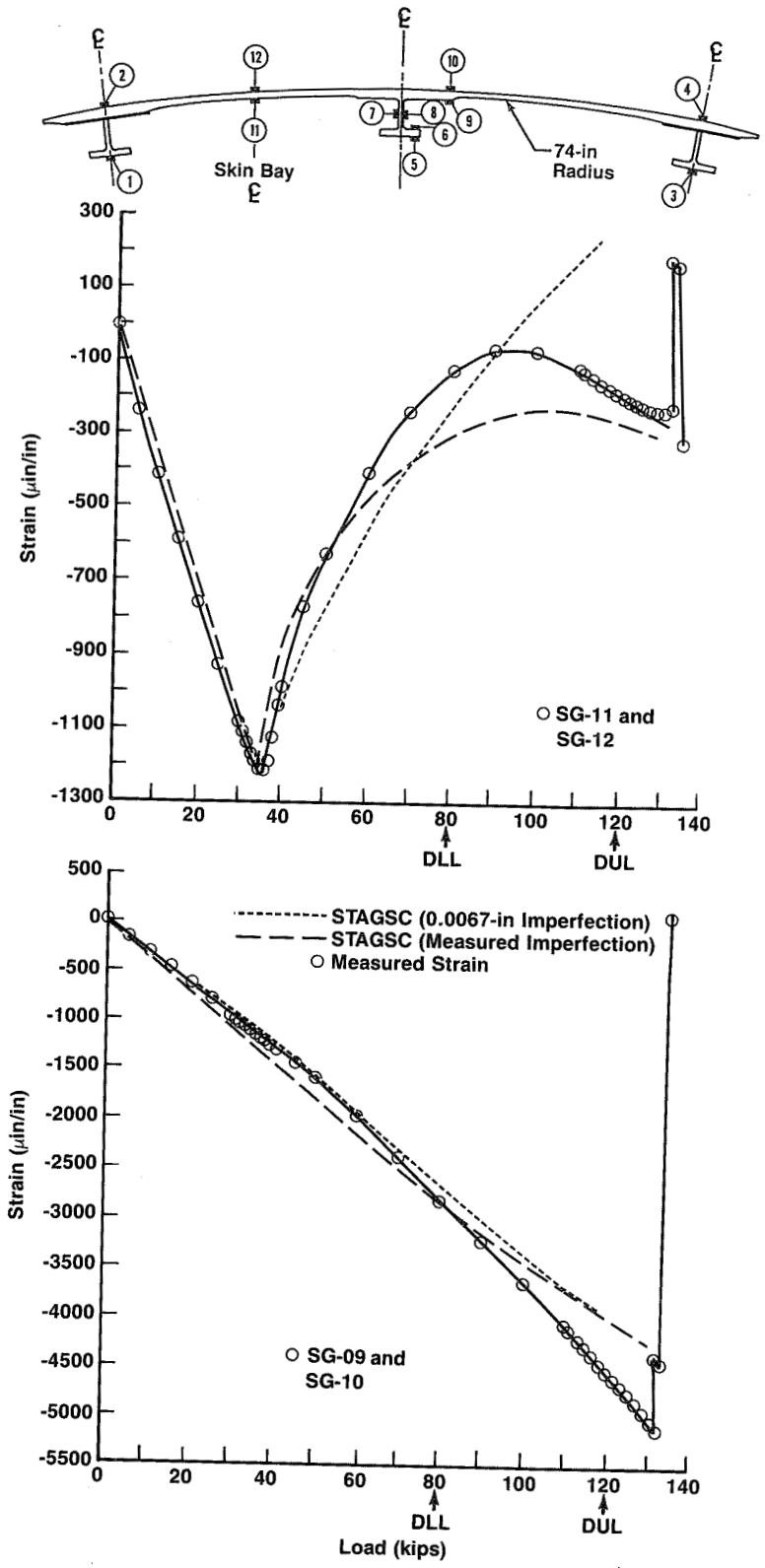

Figure 131. Measured and Predicted Strains in Stringer Fixed Flange and Skin of Keel Compression Panel 4K-2

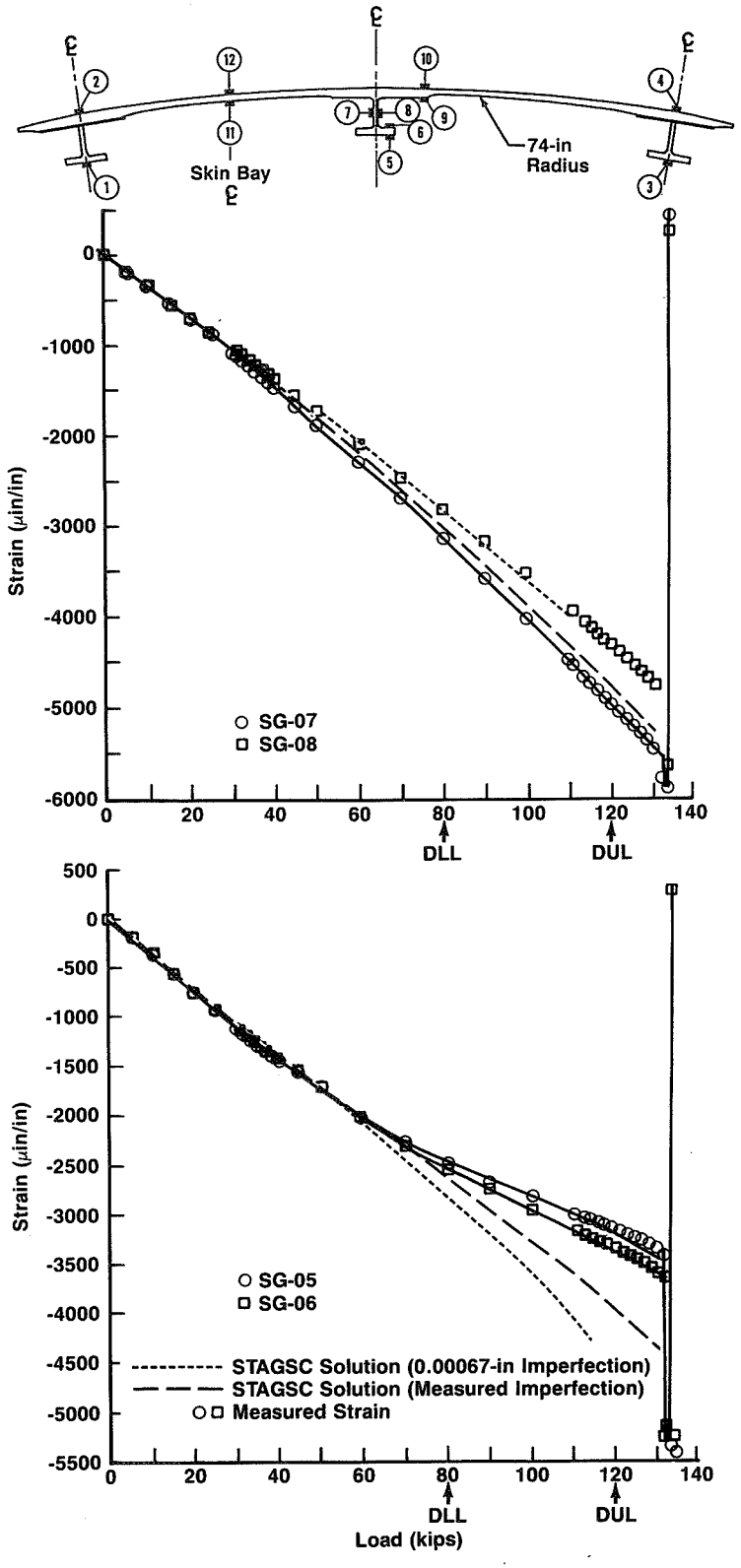

Figure 132. Measured and Predicted Strains in Center Stringer Web and Cap of Keel Compression Panel 4K-2

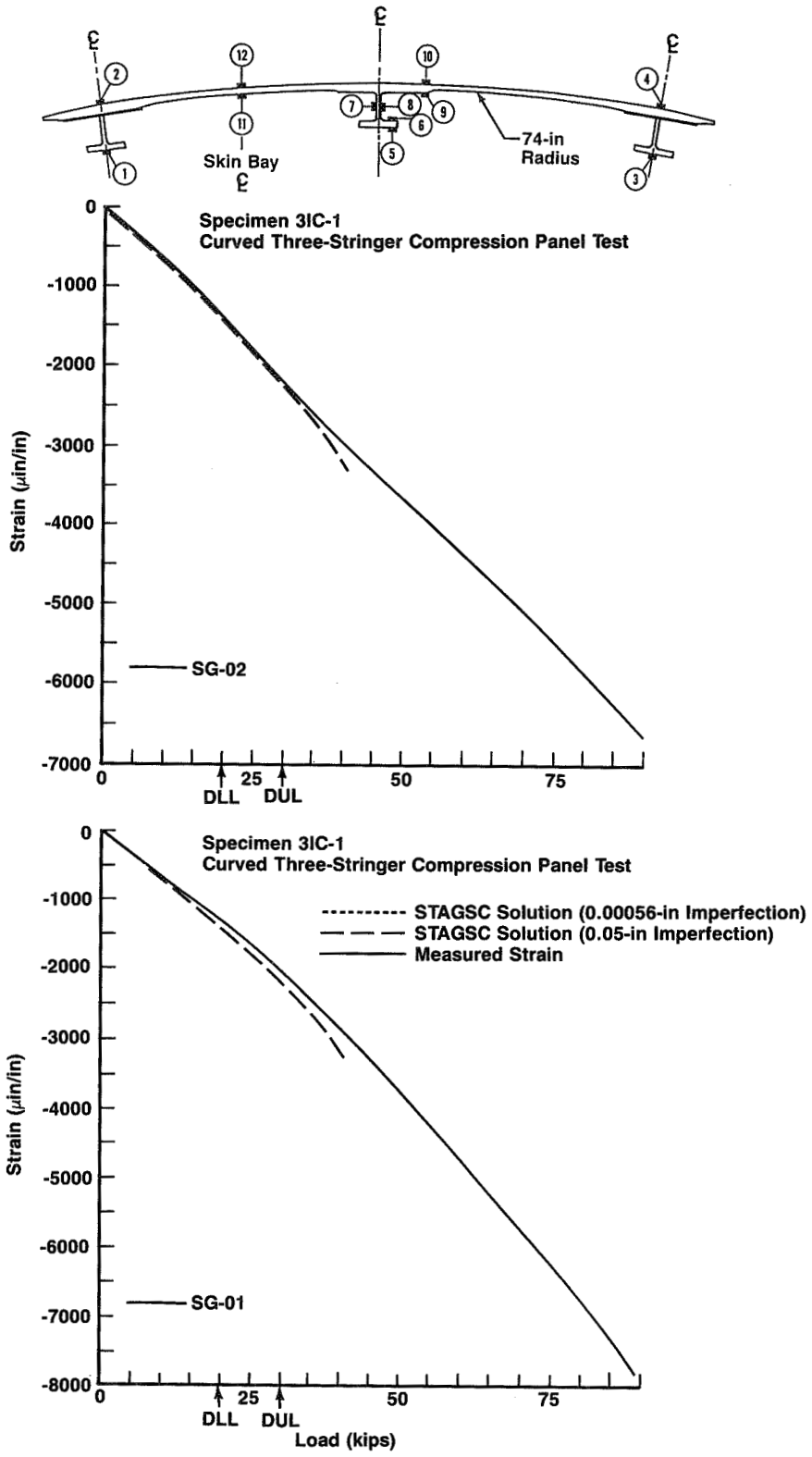

Figure 133. Measured and Predicted Strains in Outside Stringer Cap and Skin Side of Crown Compression Panel 4C-1

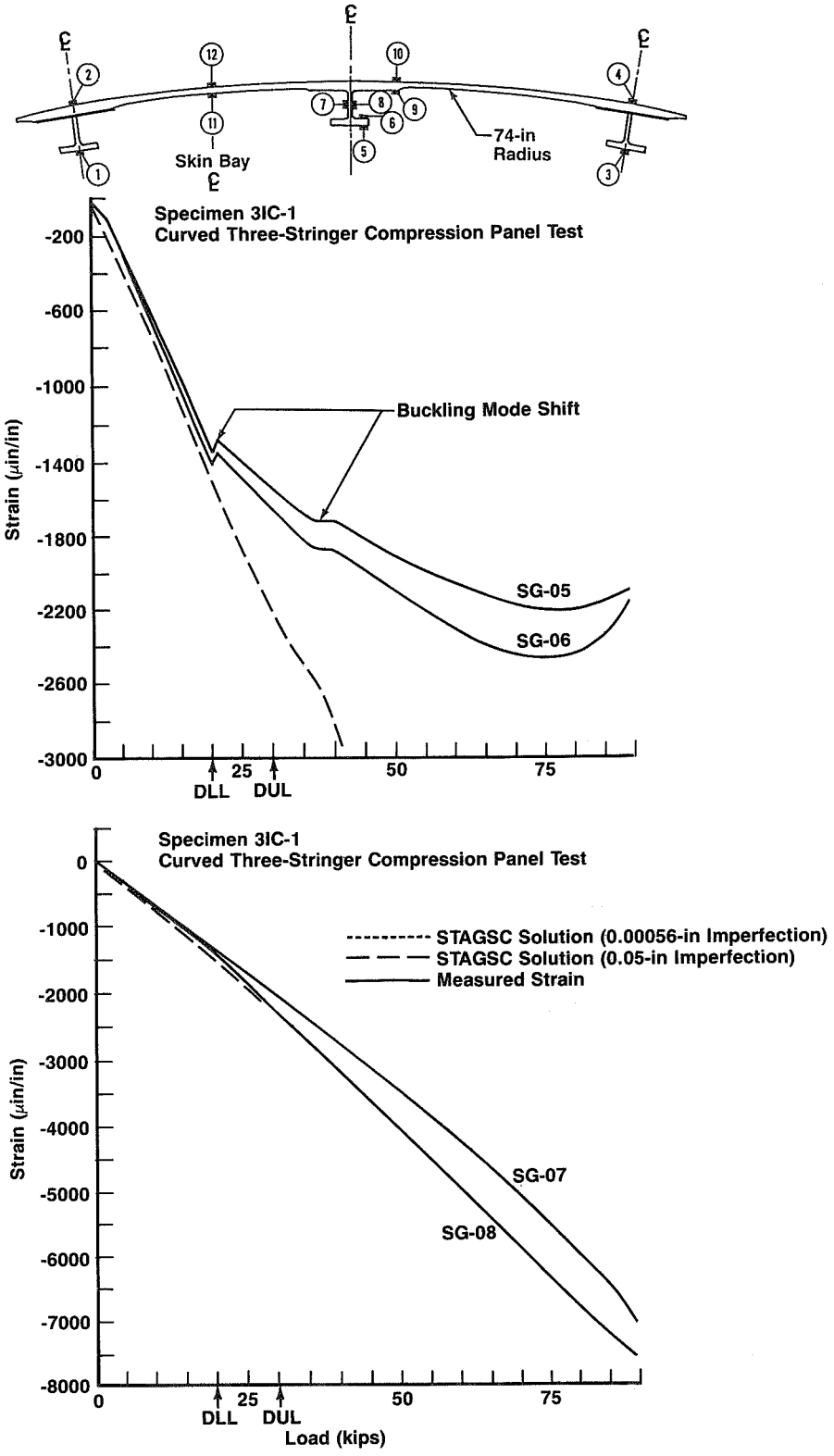

Figure 134. Measured and Predicted Strains in Center Stringer Web and Cap of Crown Compression Panel 4C-1

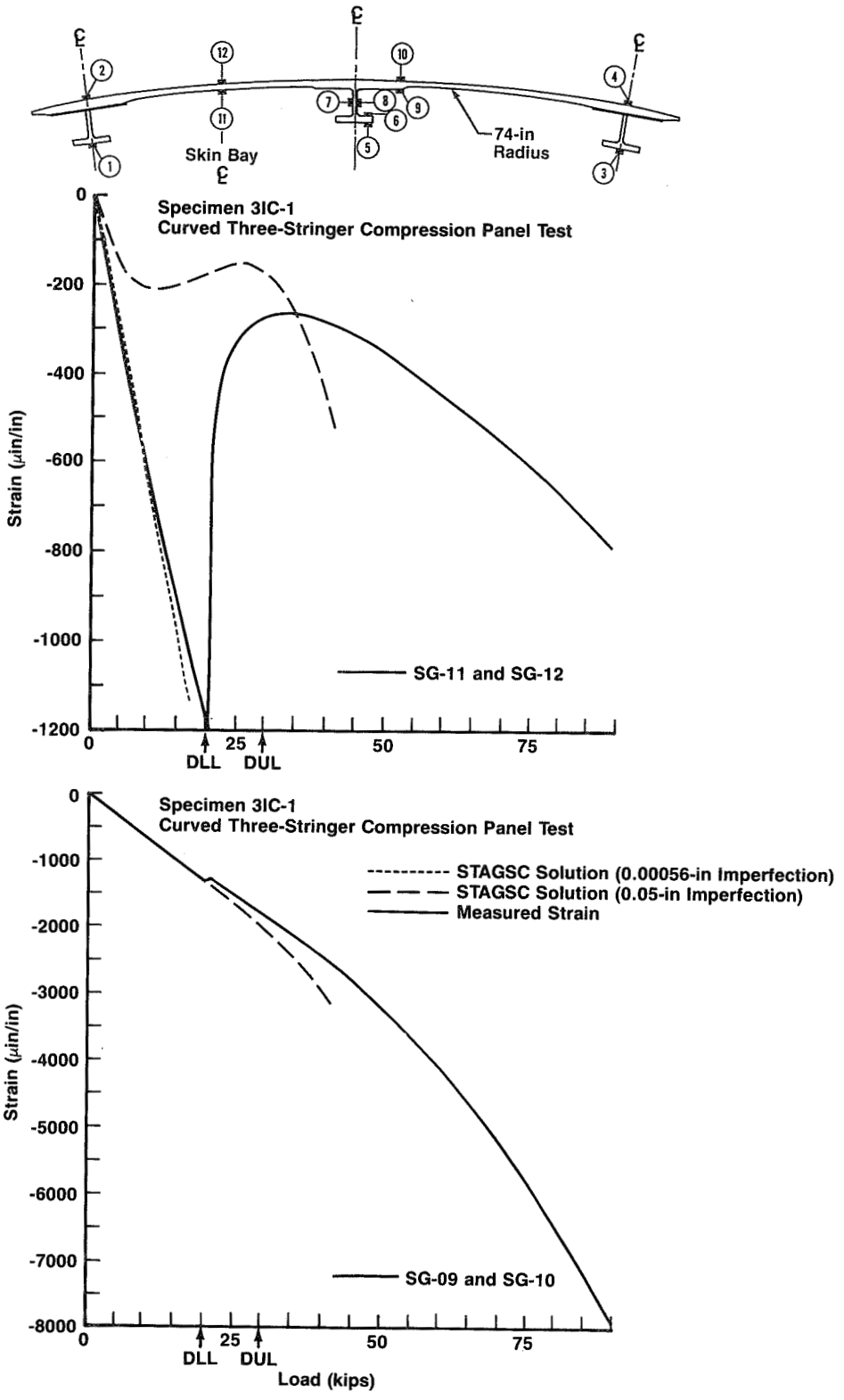

Figure 135. Measured and Predicted Strains in Stringer Fixed Flange and Skin of Crown Compression Panel 4C-1

6.2.2 Skin-Stringer Shear Panels

The shear panels were designed to represent station 1460 and have the skin and stringer layups, shown in Figure 28. The design ultimate shear load is 733 lb/in. The corresponding shear strain in the skin is 0.0033 in/in. The results of the tests and analyses are summarized in Figure 136. The shear panels tested above the DULs by 50%.

The basic configuration of the I-stringer stiffened shear panel (test 5) is shown in Figure 137. The skin has a predominately ±45-deg layup with tear straps located under the stringers and frames. The stringer layup and longitudinal tear straps are the same as for the crown stringer configuration shown in Figure 28. The four 90-deg plies of the circumferential tear straps, shown in Figure 29, are located at the body frame stations. The stringer spacing for this panel was 9 in. This is representative of the shear designed region on the side of the fuselage between the crown, where stringers are spaced at 10 in, and the keel, where stringers are spaced at 8 in. Doublers were applied along the edge of the panel to prevent localized bearing failures. The panel configuration was sized to use an existing 36.6-in by 36.6-in picture frame test fixture. The picture frame test fixture is shown in Figure 138. The shear load is transferred from the rigid frames to the test panel via steel channels. The flexibility of the steel channel sections allows the test panel edge to distort, thereby minimizing pinching problems in the corner regions of the panel. This picture frame fixture was used successfully to test stiffened panels in the NASA-ACEE studies for the Advanced Composites Stabilizer for the Boeing 737 Aircraft, contract NAS1-15025, (ref. 18).

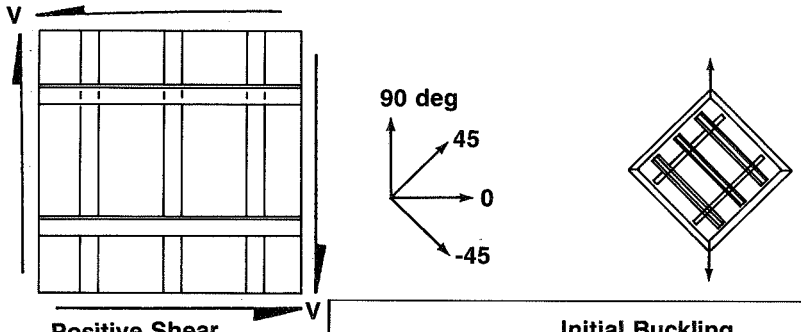

	Initial Buckling				Ultimate	
	Shear Load (lb/in)		Shear Strain			
	STAGSC	Test (1, 2)	STAGSC	Test (1, 3)	Design Ultimate Shear Load (lb/in)	Test Failure Shear Load (lb/in) (2)
Panel 5-1						
Positive Shear	240	380	0.0011	0.0017	—	—
Negative Shear	175	350	0.0008	0.0016	733	1096
Panel 5-2						
Negative Shear	175	260	0.0008	0.0012	—	—
Positive Shear	240	330	0.0011	0.0015	733	1114

1 Initial buckling derived by watching moire fringe and strain gage data
2 Based on total panel applied load
3 Measured shear strain at center of skin bays

Figure 136. Skin-Stringer Shear Panel Test Summary (Test 5)

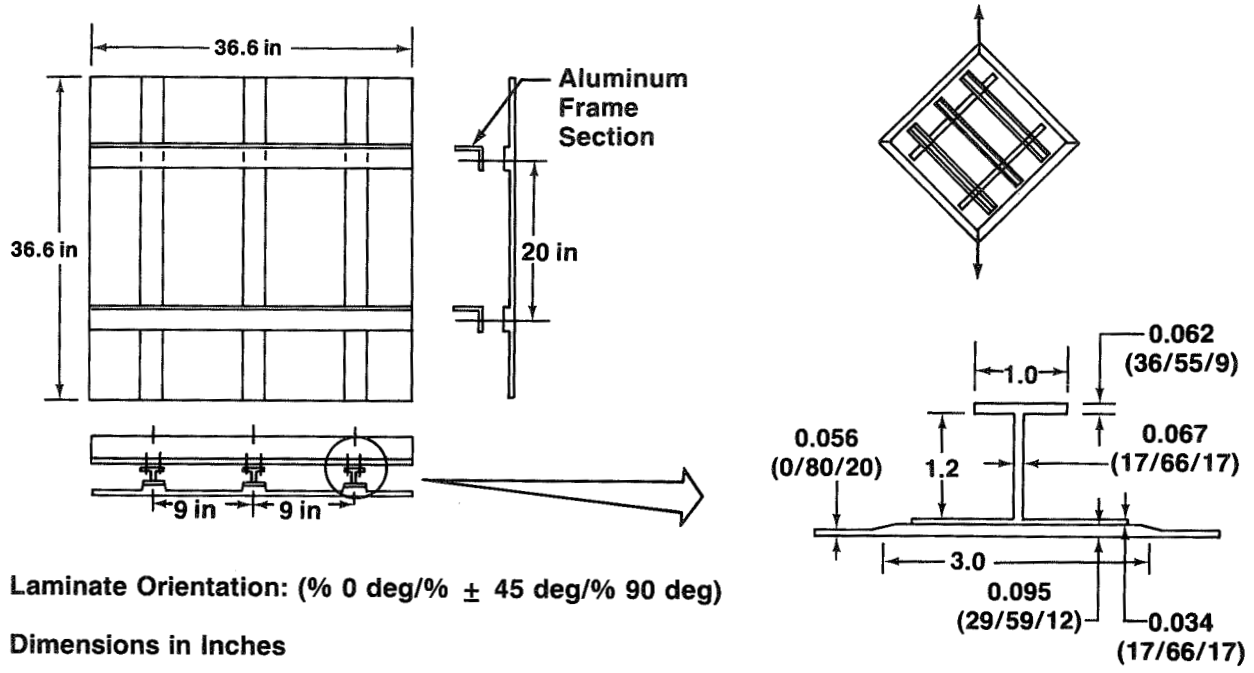

Figure 137. Skin-Stringer Shear Panel Configuration (Test 5)

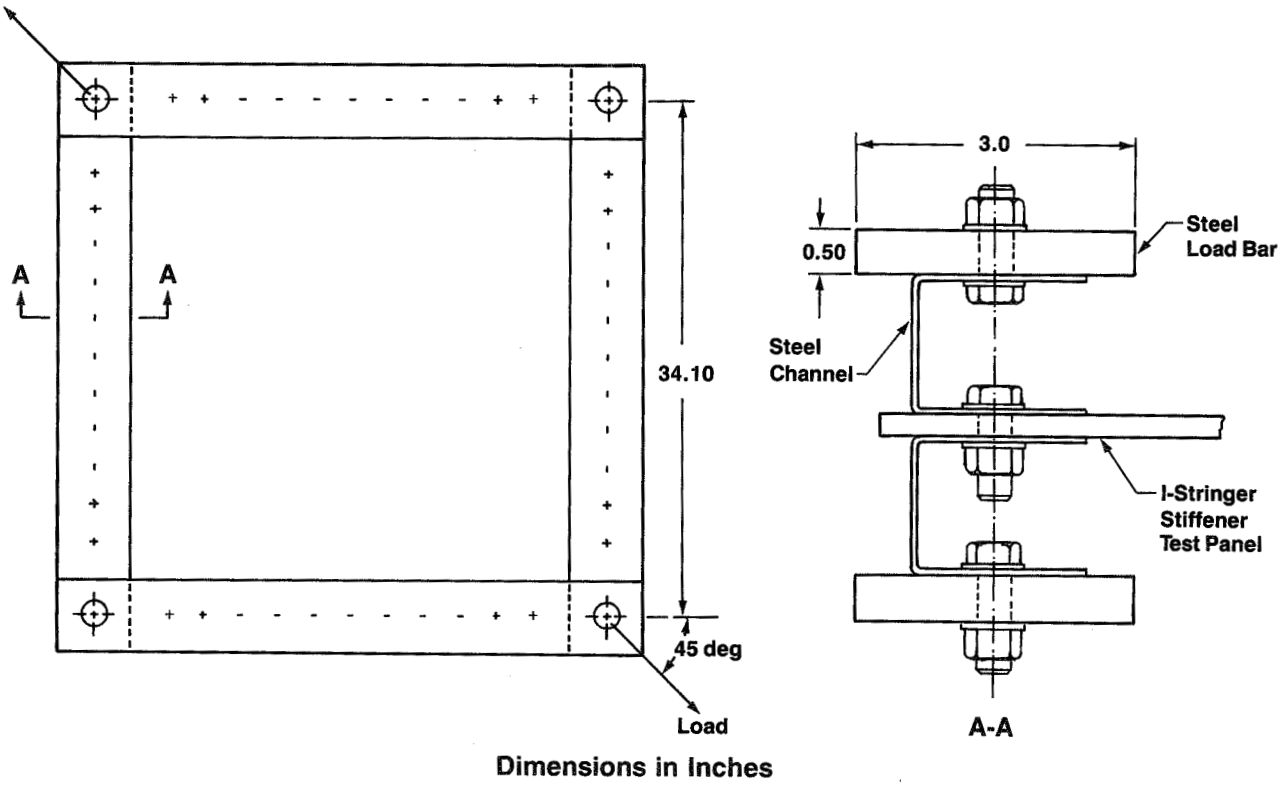

Figure 138. Picture Frame Test Fixture for Shear Panel (Test 5)

The test 5 shear panels were tested at room temperature. The panels were instrumented with strain gages and moire fringe for monitoring the initial buckling and the postbuckling response.

One of the panels, panel 5-1, was considerably warped after fabrication. Prior to installing the panel in the test fixture, the strain gages were connected to the data acquisition system. The strains were then monitored during the assembly of the panel into the test fixture. The maximum strain resulting from flattening the edges of the panel was 0.00016 in the edge of the panel.

The strain gages along the edges of the panels were used to verify that the load was introduced into the panel evenly. An example plot of the strains along the edges of panel 5-1 is shown in Figure 139. During the initial loading, the strains in the corners of the panel were not significantly greater than the strains along the middle of the edges of the panels. This demonstrates that the test fixture introduced the load into the panel evenly without pinching the corners of the panel.

An analysis was performed to determine the buckling load of the skin element of the flat test panel. The analysis was performed using LEOTHA, a Boeing analysis code for plate buckling, and verified with a finite element STAGSC model. Both analyses indicated that the skin laminate panel has a preferred direction of shear buckling (fig. 140). The least resistant buckling direction is negative shear and has a buckling load that is approximately 75% of the load for the reversed direction (positive shear).

The preference for a shear buckling load direction exists since the laminate bending stiffness is different for the +45-deg and -45-deg directions. The phenomenon is discussed by Ashton, (ref. 19). When the shear load on the panel is positive, the first buckling mode is predicted to develop at 235 lb/in. When the shear load direction is negative, buckling is predicted to occur at -170 lb/in.

A more accurate study was made of the buckling characteristics of the shear panel with a 19-shell member FEM that includes skin and stringer structure. The primary objectives of this analysis were (1) to determine the load at which instability is initiated, and (2) to predict postbuckled panel deflections and mode shapes. The initial buckling load predicted by this analysis is 174 lb/in. This is very close to the value predicted by approximating the skin as a simply supported plate.

The simplified calculation was based on a simply supported 5.8-in-wide skin panel, representing the width of the skin that extends to the edge of the padup ramp. In the current 19-shell model, the skin shell is 6.0 in wide, extending to the middle of the padup ramp, and is attached rigidly to the padup shell. The buckling mode shape of the 19-shell model is shown in Figure 141. The relative deflections predicted by the model indicated that in the buckled state, the stringer sections would remain virtually undeformed.

The 19-shell member model in the padup region was stiffer than the actual test configuration. A more detailed model was developed that better approximated the padup region. This model

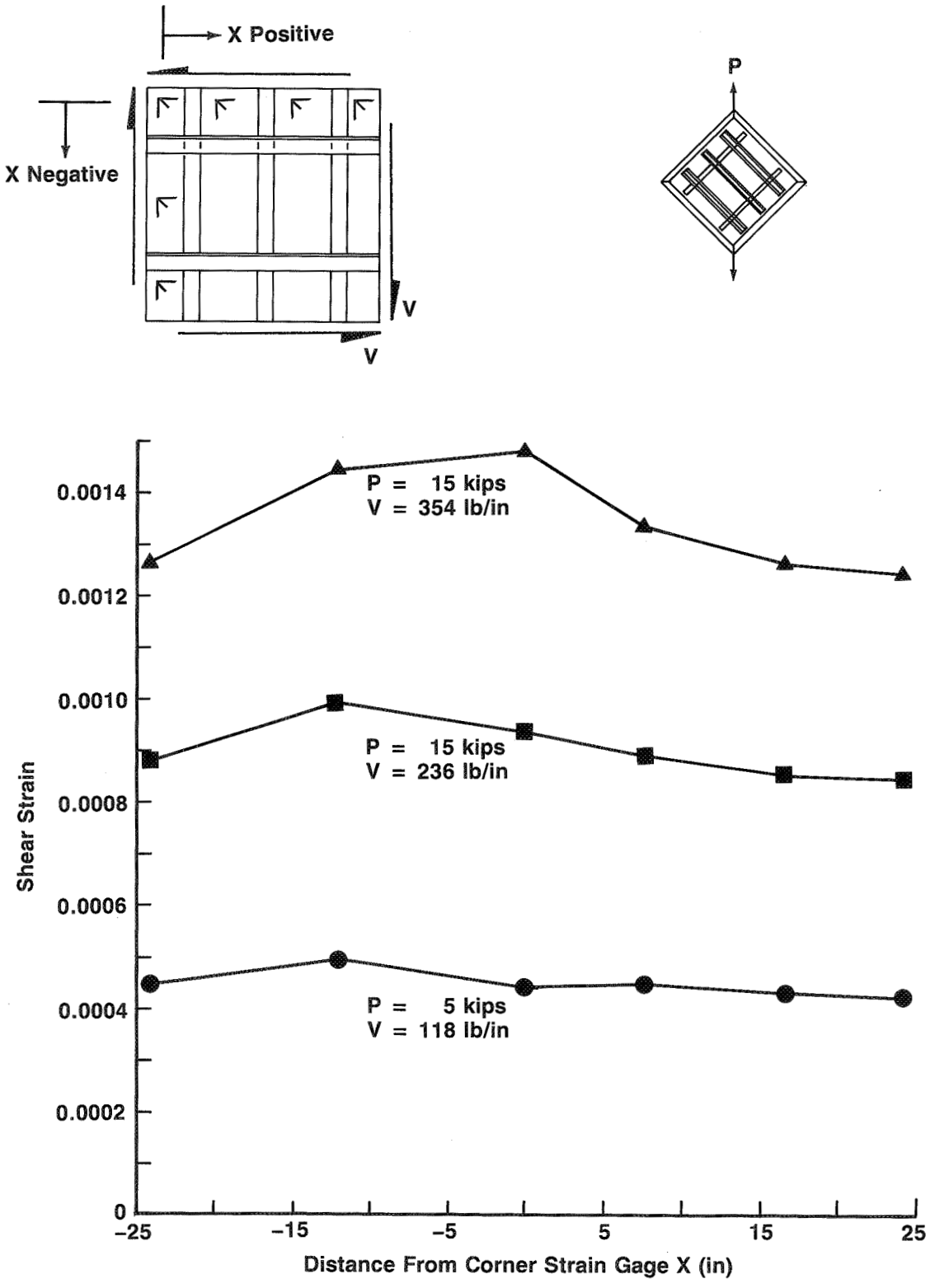

Figure 139. Shear Strains Along Edge of Skin-Stringer Shear Panel (Panel 5-1)

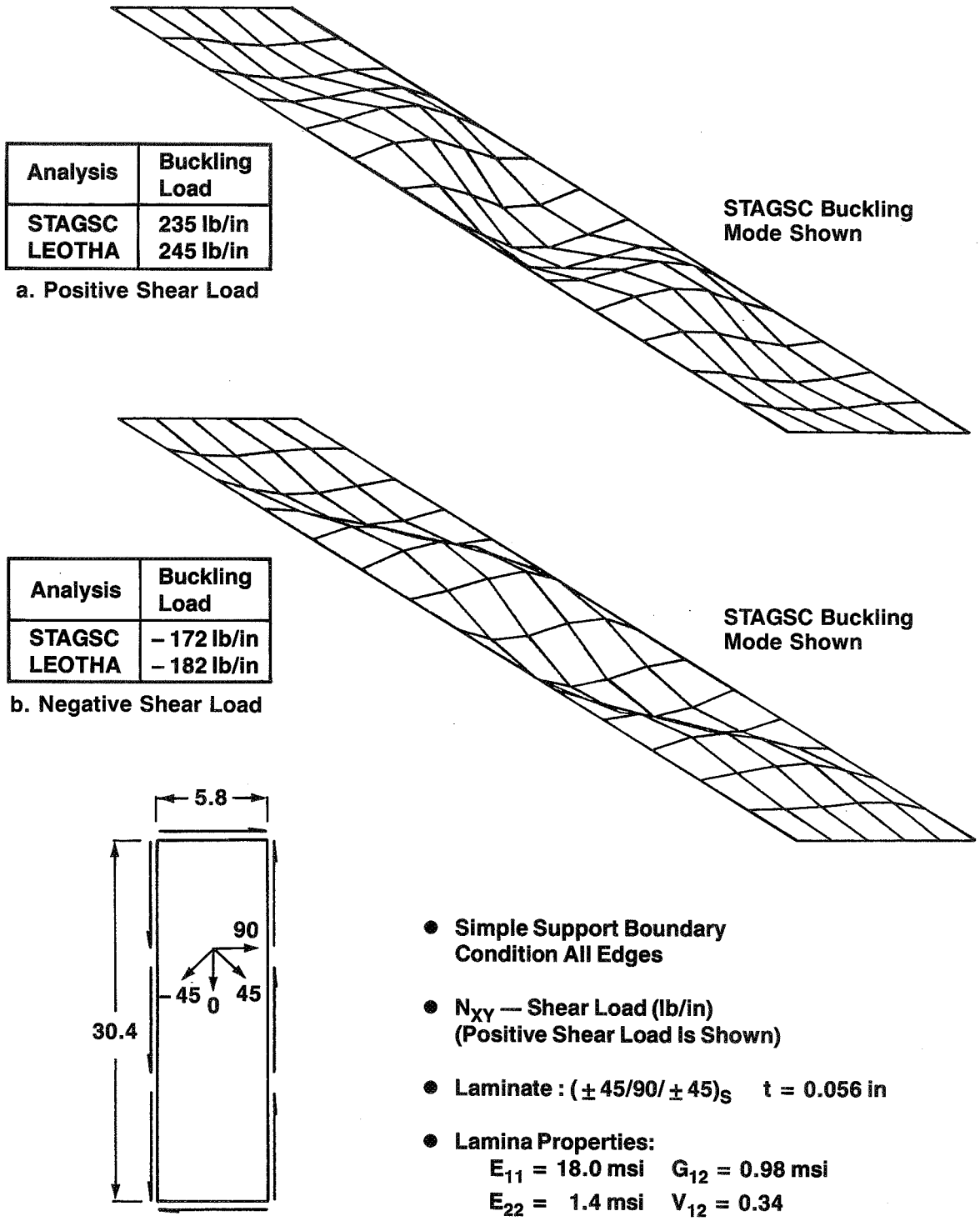

Figure 140. Skin Buckling Analysis for Skin-Stringer Shear Panel (Test 5)

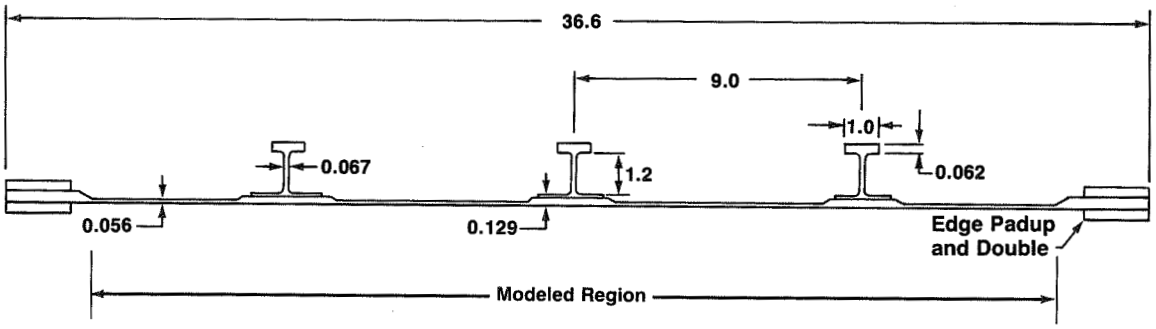

STAGSC Model Geometry	Buckled Shape [1] and Critical Buckling Shear Load
19-Shell Model 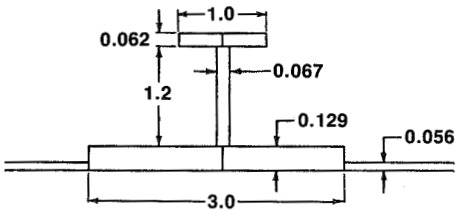	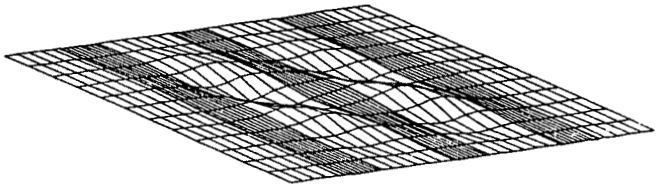 N_{xy} = 174 lb/in
25-Shell Model 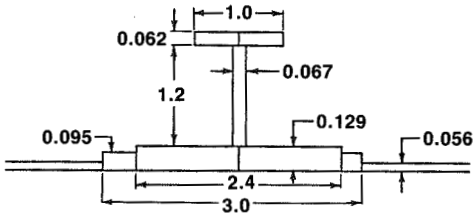	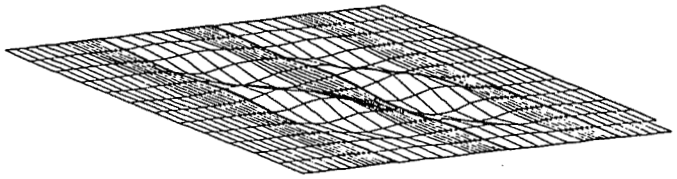 N_{xy} = 167 lb/in

[1] Stringer not shown for clarity

Dimensions in Inches

Figure 141. Skin-Stringer Shear Panel Models

had 25 shell members. The geometric approximations for this model and the predicted buckling load and mode shape for the first eigenvalue are shown in Figure 141. The buckling load predicted by the 25-shell model is 167.4-lb/in shear, which is 4% below the buckling load predicted by the coarser 19-shell model. Since the geometric enhancement of the padup region in the 25-shell member model did not significantly affect the buckling load, the less costly 19-shell model was selected for correlation with test.

The STAGSC postbuckling model was then updated to include a Fourier series representation of the imperfected skin shape. The procedure was the same as that used with the test 4 curved compression panels, discussed in Section 6.2.1.2. Contour plots of the measured and Fourier series representations of the imperfected skin shape of panel 5-1 are shown in Figure 142. The imperfected shape of panel 5-1 was included in the STAGSC model.

To evaluate whether the skin-stringer panels had a load direction preference for buckling, each of the two panels was loaded twice. In the first loading, the panel was loaded until initial buckling was established. This was performed by monitoring the back-to-back strain gages on the skin and the moire fringe buckling patterns. After demonstrating initial buckling, each panel was unloaded, removed from the test machine, and reinstalled for loading in the reverse direction. The panels were then loaded to demonstrate initial buckling and subsequently to failure. Specimen 5-1 was loaded to failure in negative shear, and specimen 5-2 was loaded to failure in positive shear.

Photographs of the unloaded panels are shown in Figure 143. These photographs give an indication of the amount of initial warpage in each panel. During loading, the moire fringe patterns were monitored and compared to the strain gage data for identifying the initiation of skin buckling. The back-to-back strain gages are more sensitive to the behavior of the panel and identify initial buckling at slightly lower loads than observed using moire fringe.

Typical moire fringe photographs of panel 5-1 under load are shown in Figure 144. The first photograph, marked A, was taken just after the initiation of buckling. Three buckles are shown in each skin bay. The second photograph, marked B, was taken at 98% of the failure load. In addition to the initial three skin buckles, the outer region of skin between the angle body frames and the loading fixture, and between the outside stringers and the loading fixture, was also buckled.

During test, panel 5-1 buckled at approximately 380 lb/in when loaded in positive shear and at 350 lb/in when loaded in negative shear. The second panel buckled at 330 lb/in when loaded in positive shear and at 260 lb/in when loaded in negative shear (fig. 136). In both cases, the panel remained stable to a higher shear load when the load was positive with respect to the inset diagram in Figure 136. The difference between the positive and negative shear buckling loads is not as great as the difference predicted by the single-shell analysis.

The test-derived buckling loads, reported in Figure 136, are calculated based on the total load applied to the panel and test fixture. The results of shear panel tests, reported in Reference 18, indicated that the edge doublers and test fixture carry as high as 10% of the total applied load. Therefore, the shear load applied to the test region of the panel is lower than reported in Figure 136. The test-derived shear strains were recorded at initial buckling and can be compared to the shear strains in the STAGSC model. The test-derived shear strains exceeded the

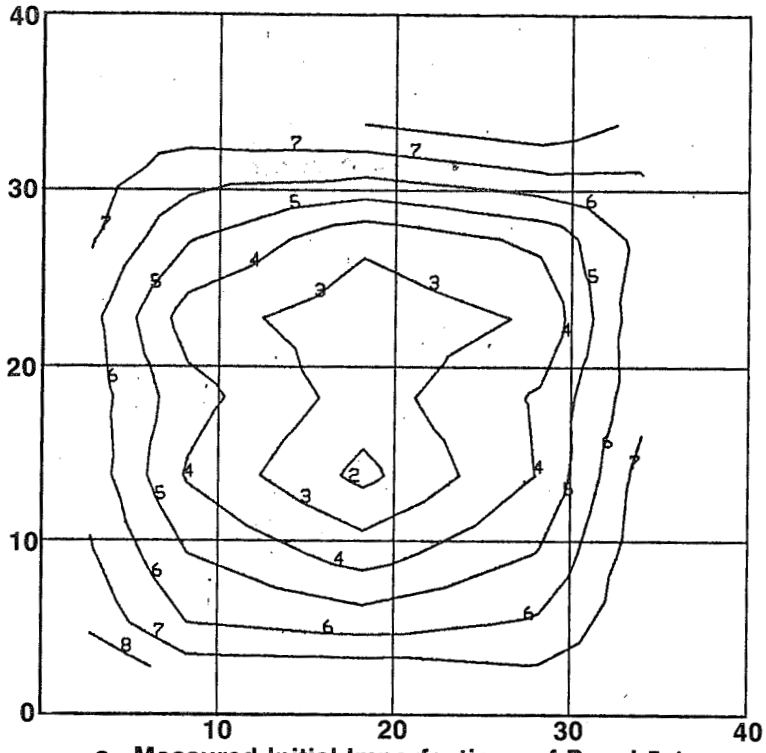

a. Measured Initial Imperfections of Panel 5-1

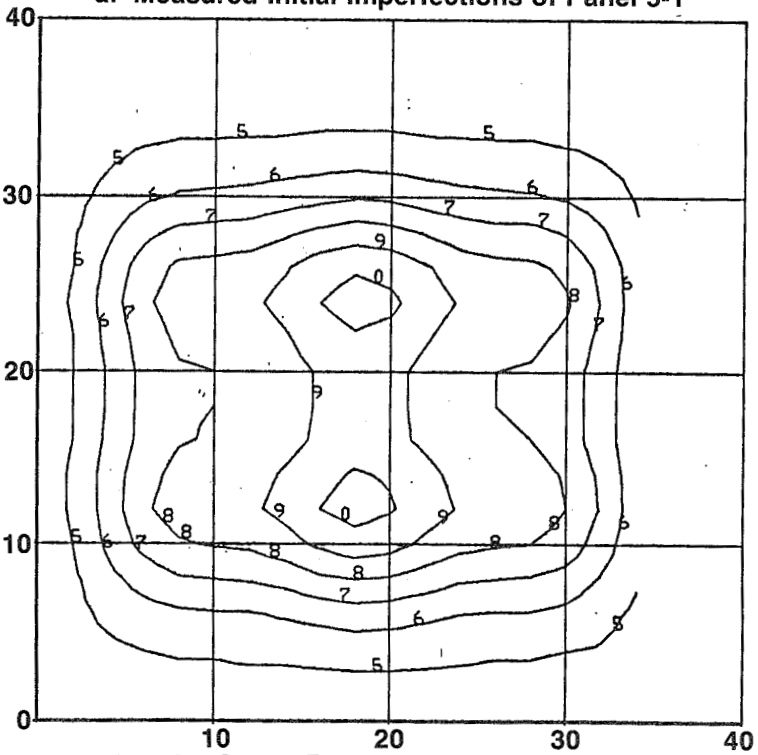

b. Fourier Series Representation of Panel 5-1
To Be Used in STAGSC Postbuckling Analysis

Gradient Number	Height (in)
1	-0.05
2	-0.04
3	-0.03
4	-0.02
5	-0.01
6	0
7	0.01
8	0.02
9	0.03
0	0.04
A	0.05

Figure 142. Measured and Fourier Series Contour Representations of Skin Imperfections in Skin-Stringer Shear Panel 5-1

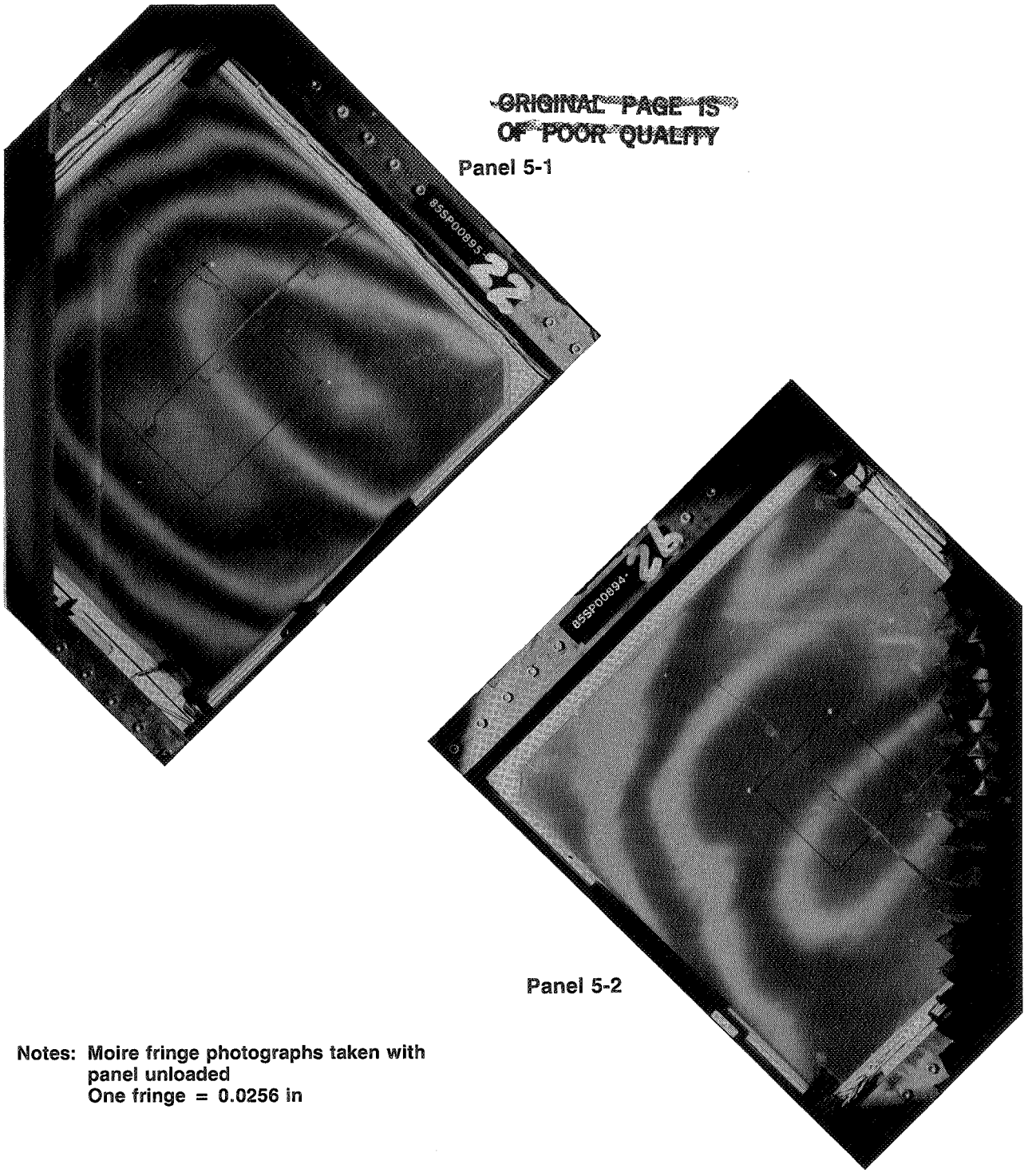

Notes: Moire fringe photographs taken with panel unloaded
One fringe = 0.0256 in

Figure 143. Indication of Initial Warpage in Skin-Stringer Shear Panels From Moire Fringe

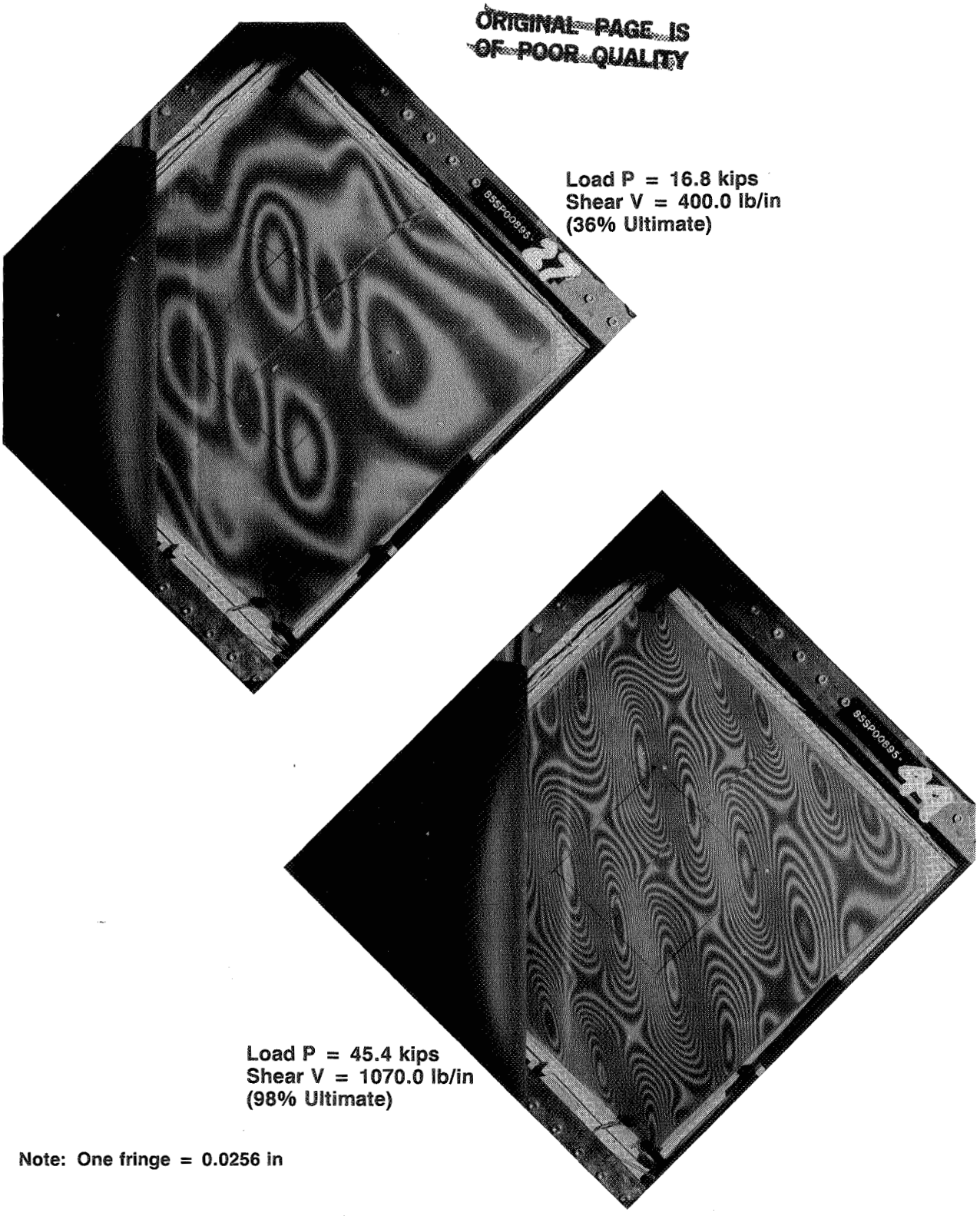

Figure 144. Moire Fringe Buckling Patterns of a Skin-Stringer Shear Panel (Panel 5-1)

predicted shear strains. The predicted strain at buckling in positive shear was 0.0011 and 0.0008 in negative shear. The predicted strains at buckling in the warped panel 5-1 were 21% and 42% lower than the test strains. In panel 5-2, which was unwarped prior to testing, the predicted strains at buckling were 20% and 8% lower than in test.

Plots of the predicted and test strains of the skin of panel 5-1 are shown in Figure 145. The STAGSC-predicted shear strains, including both measured and hypothetical initial imperfections in the center of the skin bay, correlate well with test strains.

After failure, the panels were surveyed to identify areas of fracture. In each case, a region of the center stringer and skin had disbonded, indicating that peeling forces developed in the skin had caused the skin to separate from the stringer flange.

6.3 Compression Damage Tolerance Panels

Tests have been performed to evaluate damage containment of fuselage structure subjected to compression loads. The test plan for the skin-stringer (test 6A) and honeycomb (test 6B) compression damage tolerance tests is summarized in Figure 146. The damage types evaluated were (1) impact damage that would not be easily visible or detectable during a routine in-service inspection; (2) impact damage that would be easily visible during inspection; and (3) large-area damage that severs a stringer, or tear strap, or both. The panels were impact damaged by dropping spherical weights onto the skin side of the panel. The energy level and location of the impact required to achieve the various levels of damage were determined from Boeing IR&D impact studies.

Each of the skin-stringer and honeycomb panels was designed to loads for the keel near station 1200. The load requirements for each configuration are summarized in Figure 147. The details of the panel configurations, impacting, and testing are discussed in the following sections.

6.3.1 Skin-Stringer Compression Fracture

The design of the test 6A skin-stringer compression panels was based on the same keel configuration as test 4. The panel was designed to meet the load requirements shown in Figure 147. The geometry of the test article is shown in Figure 148. The panels had a DUL requirement of 5 kips/in. The skin was designed to buckle at 28% DUL. The stringers were designed to remain stable locally and at an Euler column to above 100% DUL.

Three panels were required to evaluate the three damage levels numerated in Section 6.3. The panels were impacted by dropping 20-lb, 1-in-diameter spherical steel weights onto the skin side of the panel.

The Boeing studies showed that when the skin region of the panel is impacted with more than 400 in-lb of energy, the resulting damage would be easily visible. When the impact is located at the edge of the stringer, the resulting damage does not become easily visible until impacted with 800 in-lb of energy. When the trial panel was impacted with up to 1000 in-lb on the skin directly over the stringer web, the resulting damage remained nonvisible. Nondestructive ultrasonic inspection indicated that the internal damage resulting from an impact over the

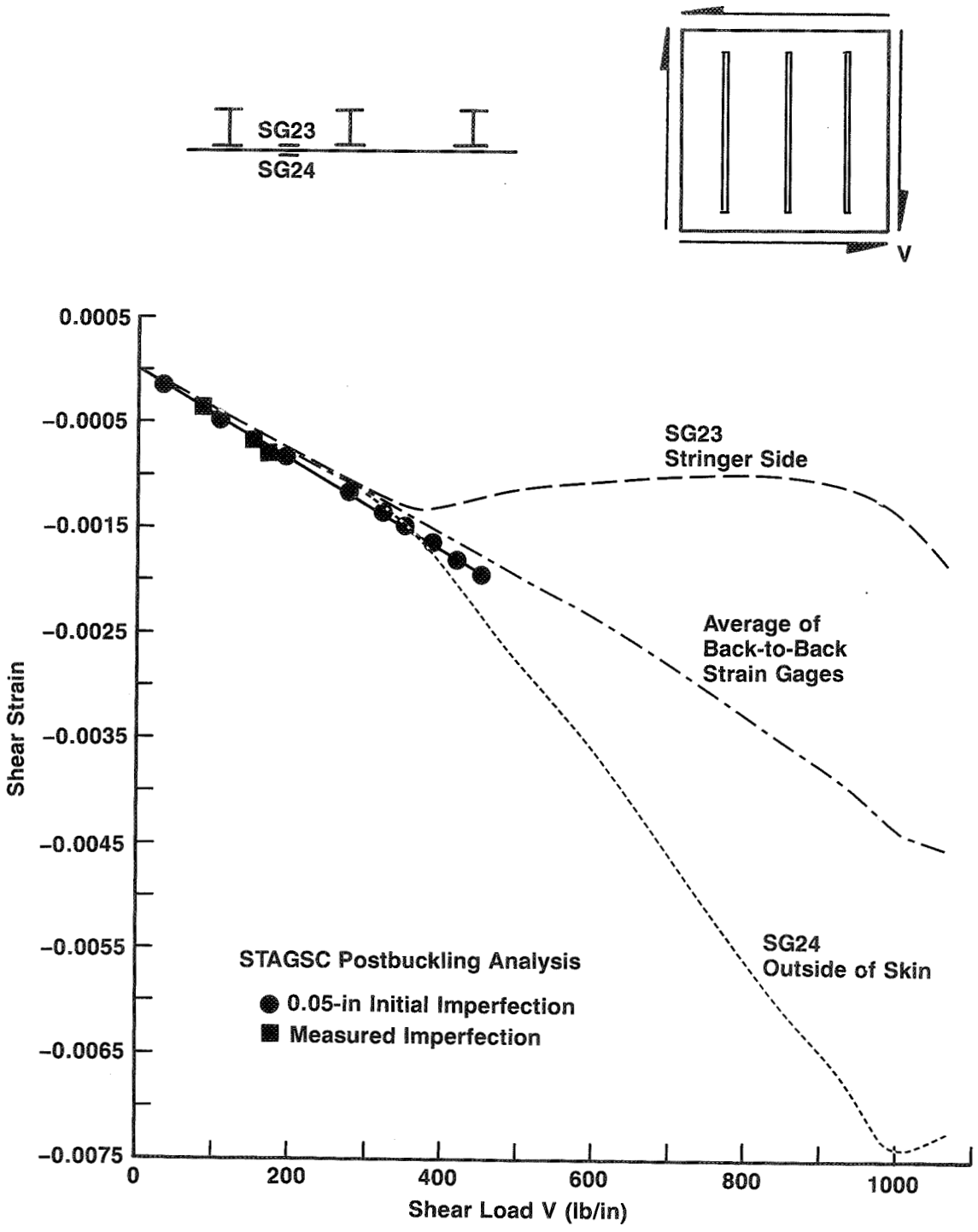

Figure 145. Measured Versus Predicted Shear Strains in Center of Skin Bay of Shear Panel

Panel	Damage	Test Procedure
6A-1 6B-1	Nonvisible Damage Impact Skin Side of Panel With 1-in-Diameter Sphere	Load Panel to Failure
6A-2 6B-2	Visible Damage Impact Skin Side of Panel With 1-in-Diameter Sphere	Load Panel to Limit Load Perform Data Survey Unload Panel
	Large Area Damage Skin-Stringer Panel: Sever Center Stringer and Pad-Up Skin Honeycomb Panel: Sever Center Longitudinal Tear Strap, Core, and Opposite Face Sheet	Load Panel to Safe Flight Load Condition (33% DUL) Perform Data Survey Load Panel to Failure

Figure 146. Test Plan for the Compression Damage Tolerance Panels (Tests 6A and 6B)

			Design Condition			Test		
	Damage Type	Load Condition	Design Load (kip/in)	Panel Load (kip)	P/AE Strain (in/in)	End Load (kip/in)	Panel Load (kip)	P/AE Strain (in/in)
Test 6A Skin-Stringer Configuration (Station 1240)	Nonvisible Impact	Ultimate	5.0	120.9	0.0047	3.80	92.0	0.0035
	Visible Impact [1]	Limit	3.3	80.6	0.0031	3.32	81.0	0.0031
	Large Area [1]	Continued Safe Flight	1.7	40.3	0.0016	3.30	78.2	0.0030
Test 6B Honeycomb Configuration (Station 1240)	Nonvisible Impact	Ultimate	5.0	150.0	0.0047	1.7	50.0	0.0016
	Visible Impact [2]	Limit	3.3	100.0	0.0031	[4]	[4]	[4]
	Large Area [3]	Continued Safe Flight	1.7	50.0	0.0016	1.4	43.0	0.0013

[1] 800-in-lb impact with 1-in-diameter impactor
[2] 1000-in-lb impact with 1-in-diameter impactor
[3] 1000-in-lb impact with 1/2-in-diameter impactor
[4] Limit load case not evaluated in test 6B

Figure 147. Load Conditions and Test Data for Compression Damage Tolerance (Tests 6A and 6B)

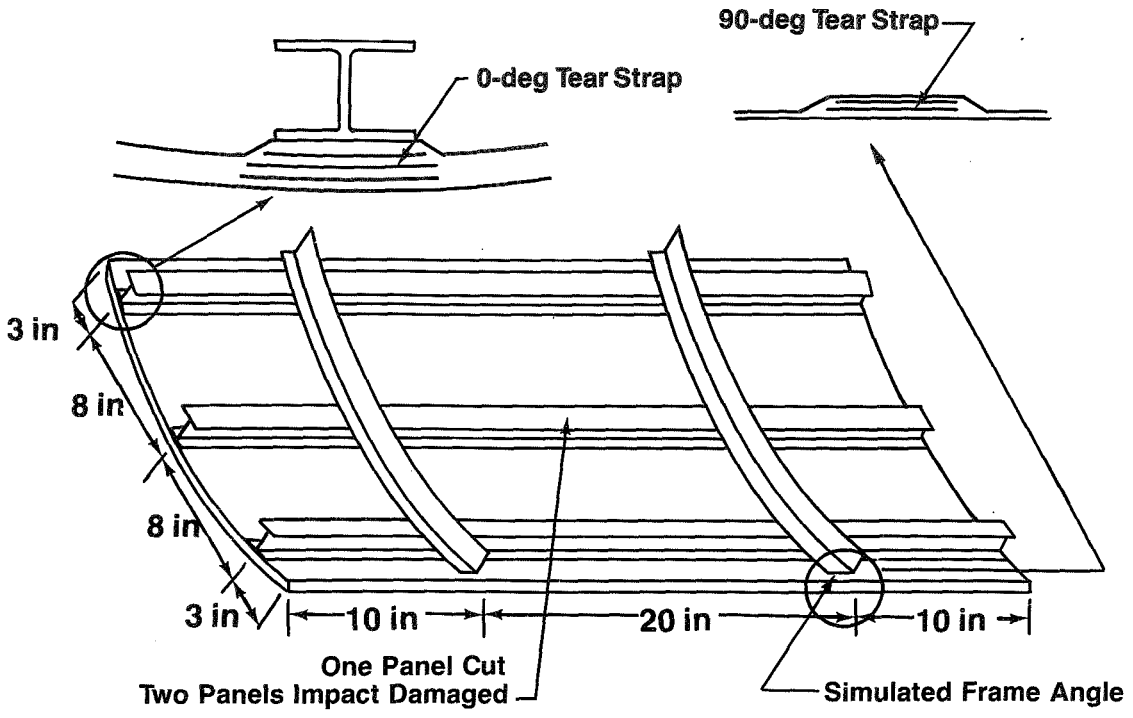

Figure 148. Configuration of Skin-Stringer Compression Damage Containment Panel (Test 6A)

edge of the stringer and padup ramp with up to 800 in-lb of energy was more extensive than damage caused by an impact closer to the stringer web. Based on these results, the panels were impacted at the edge of the padup ramp with 800 in-lb of energy with the 1-in-diameter steel impactor.

Each of the panels was subjected to NDI to determine the extent of internal damage due to impacting. The pulse echo scans of the panels used for the limit load and ultimate load tests are shown in Figure 149. As shown, the internal damage under the stringers in each of the panels is approximately the same. The skin of the panel selected for ultimate load test remained undamaged. The damage in the skin of the limit load test panel was extensive. The panel used for continued safe flight testing was impact damaged with the same amount of damage as the limit load panel (fig. 149), and then incrementally sawcut.

Restraints were applied to the edges of the panel to restrict the skin edge flanges from buckling locally. The edge supports are constructed from 1.5-in-diameter aluminum slotted tubes. This edge support system was successfully used for the single-element crippling of test 3 (sec. 6.2.1.1).

The limit load panel (specimen 6A-1) was instrumented with strain gages, moire fringe, and acoustic emission transducers. The strain gages were used to ensure that the load was introduced into the panel evenly. As the load was increased, the back-to-back strain gages on the skin and the moire fringe patterns were monitored to identify the onset of buckling. At 81.0 kips (100% of the limit load requirement), the center stringer disbonded from the skin and the

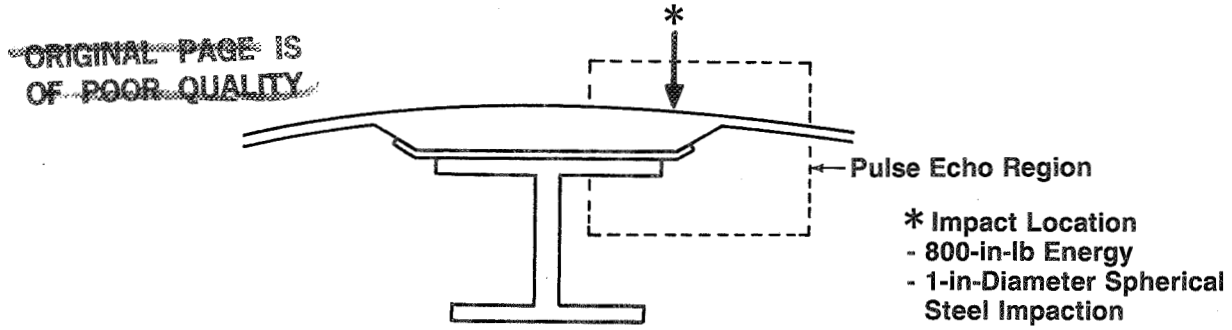

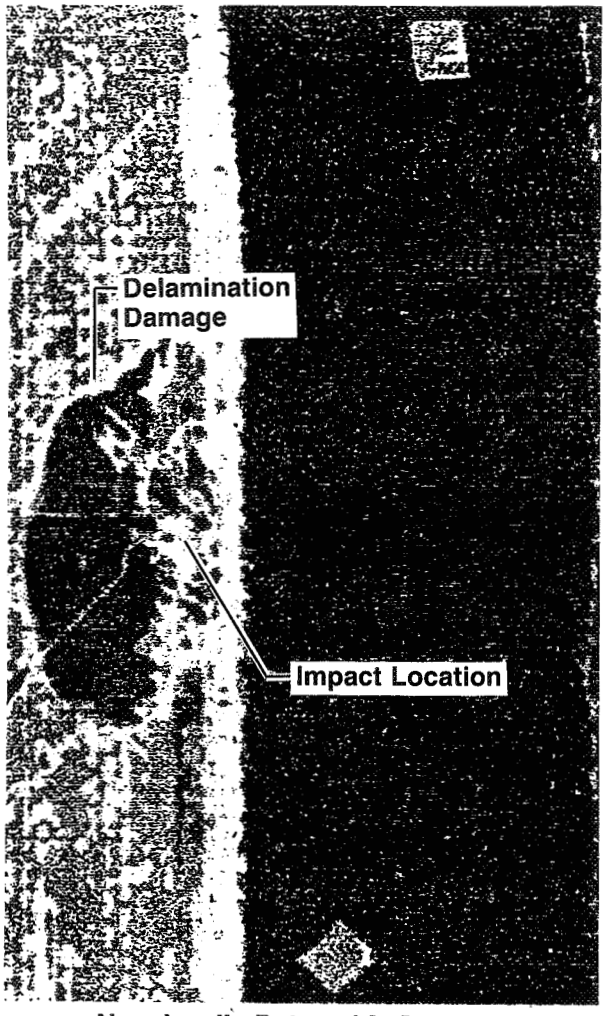

Nonvisually Detectable Damage
Ultimate Load Panel

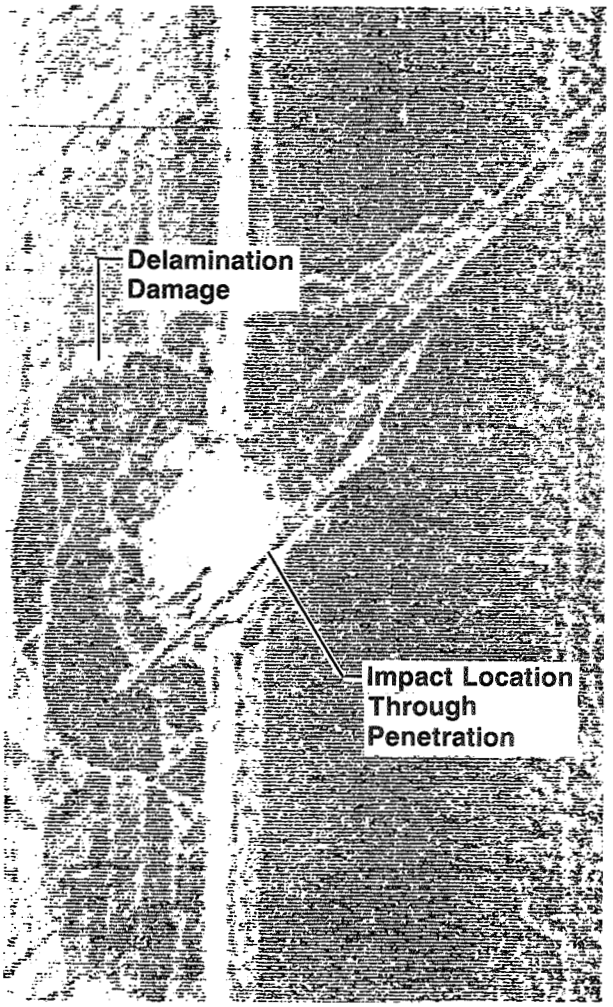

Easily Visible Damage
Limit Load Panel

Figure 149. Pulse Echo Inspection of Skin-Stringer Compression Fracture Panels After Impacting

panel load dropped to 66 kips. Since the center stringer and the outer skin-stringer regions were still intact, the load on the panel was again increased. The panel finally failed at 78 kips due to stringer crippling.

The safe flight panel was tested to the required load (40.3 kips) seven times, each time with a larger sawcut in the middle of the panel. The panel was instrumented with strain gages and acoustic emission transducers. The sawcut progression, shown in Figure 150, started in the skin padup region of the center stringer. The panel continued to carry the continued safe flight load until the sawcut had been extended 3 in into each of the two skin bays (6-in total cut width), and the stringer had been completely severed. Since the panel could still carry the safe flight load with this extreme damage, the sawcut was extended half way into each skin bay (8-in total cut width). The sawcut gap was widened to approximately 0.20 in to ensure that the stringer sections would not come into contact under load. The panel was then loaded to failure at 78.2 kips. This load is 260% of the safe flight load and is 97% of the limit load. The panel failure extended from the edges of sawcut, across the remaining skin and stringers. A photograph of the failed 6A-2 panel is shown in Figure 151.

The surface strain distribution in the impacted panel (specimen 6A-1) and the sawcut panel (specimen 6A-2) are shown in Figures 152 and 153, respectively. The strains are shown at the continued safe flight load and prior to failure. At continued safe flight, the strains in the stringers are relatively low. Prior to failure, the strains at the base of the stringer were above 0.005 in/in in the impacted panel, specimen 6A-1, and above 0.006 in/in in the sawcut panel, 6A-2. The corresponding strain in the undamaged keel panels from test 4 were in the same range (just below 0.006 in/in).

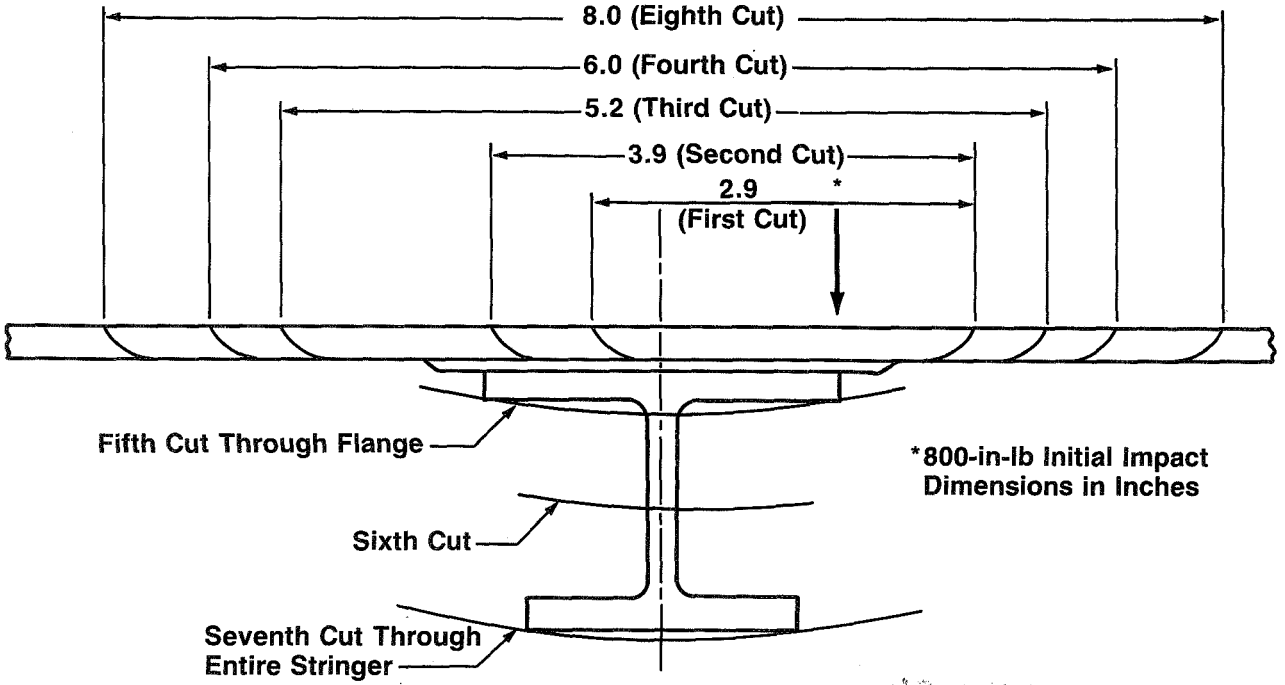

Figure 150. Sawcut Increments for Continued Safe Flight (Panel 6A-2)

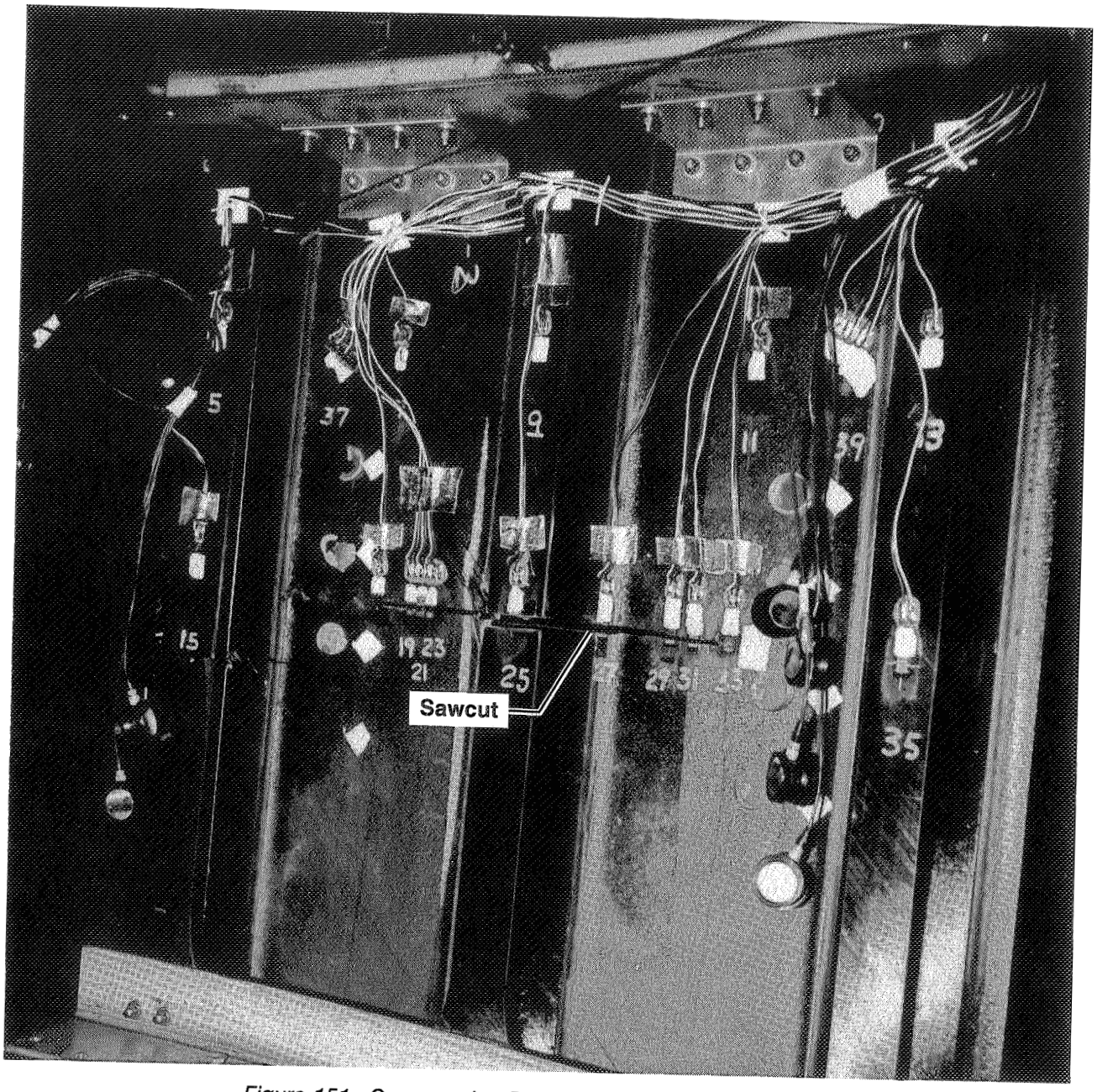

Figure 151. Compression Damage Tolerance (Panel 6A-2)

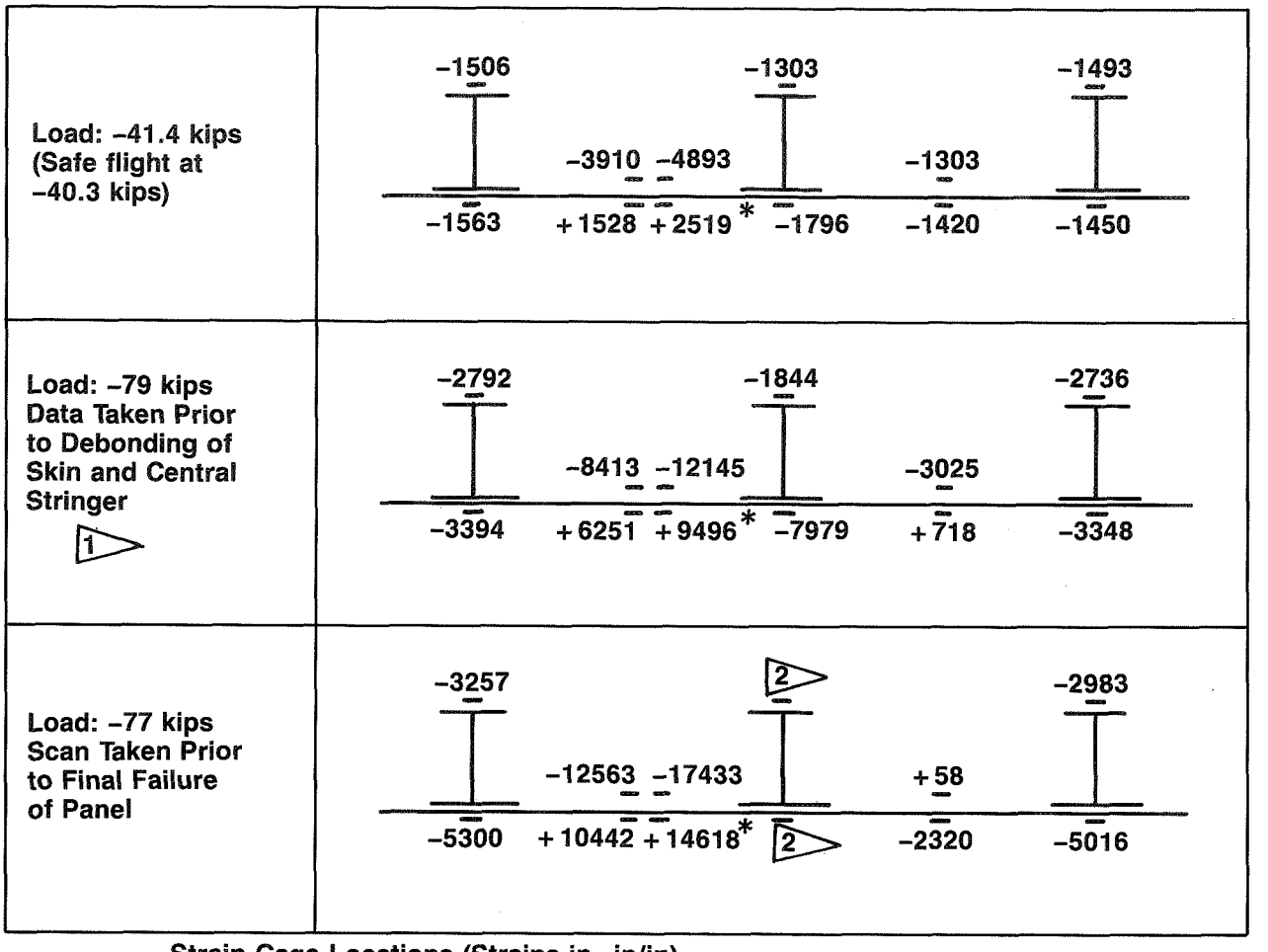

— Strain Gage Locations (Strains in μin/in)
* Through-Penetration Impact Location (800 in-lb With 1-in-Diameter Steel Impactor)

1 Panel load subsequently dropped to 66.2 kips and the panel was reloaded to failure at 78.2 kips
2 Strain level out of strain gage range

Figure 152. Strain Distribution in Curved Skin-Stringer Compression Damage Tolerance Panel With Through-Penetration Impact (Panel 6A-1)

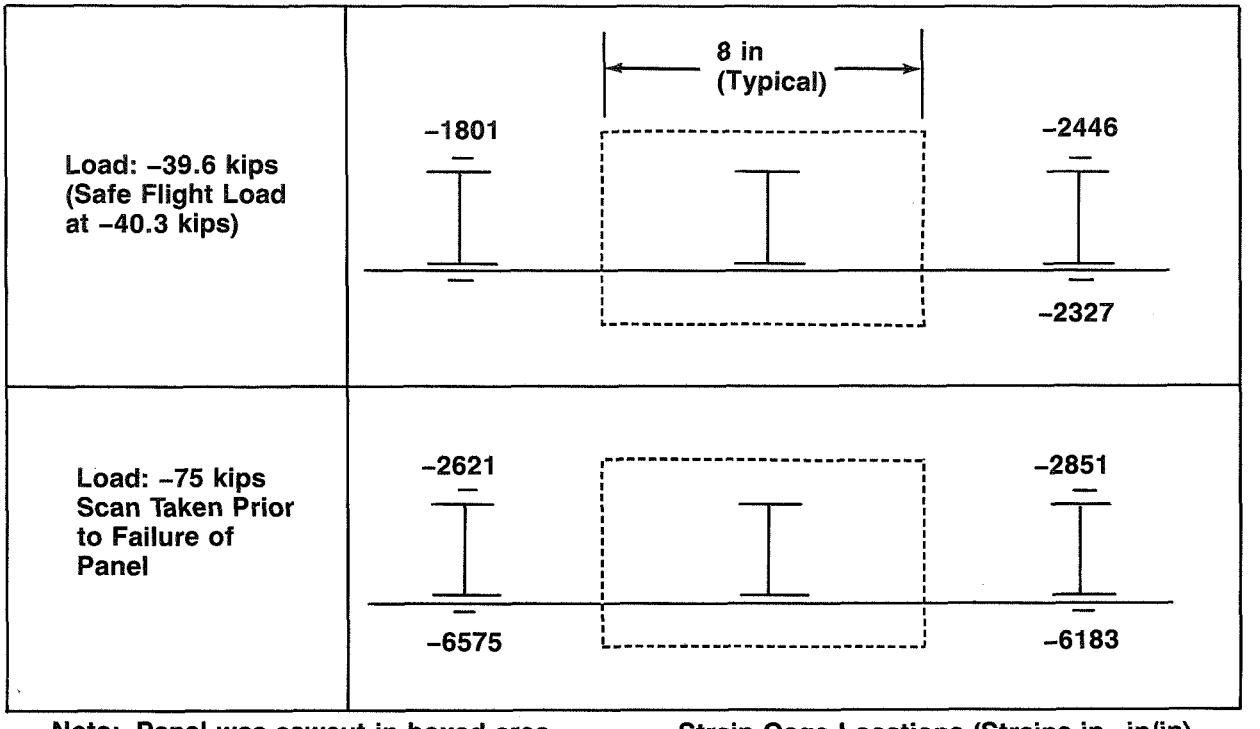

Figure 153. Strain Distribution in Curved Skin-Stringer Compression Damage Tolerance Panel With Center Sawcut (Panel 6A-2)

The failure of the ultimate load panel initiated in the skin-to-stringer interface at the location of the impact damage. The stringer separated and buckled away from the central stringer between 80 and 85 kips load. This is shown in a moire fringe photograph in Figure 154. The panel subsequently failed at 92 kips (2800 lb/in). This failure load represents 76% of the DUL.

A plot of the strains at the centerline of the panel at four load levels is shown in Figure 155. Large bending strains were present in the skin adjacent to the centerline of the central stiffener at 85 kips load.

The test results of the skin-stringer panels verified the damage tolerance of the design for the easily visible impact and large-area damage load conditions. The ultimate load condition with nonvisible impact damage was not verified. To improve the impact damage tolerance of the design, various refinements have been considered. Early buckling of the skin affects the skin-stiffener interface strength. This effect can be reduced by delaying skin buckling by one or more of the following design modifications: increased skin gage, increased number of padup planks, and increased width of padup. If one or both of the latter two modifications were employed in the affected keel area, the increase in weight of the total fuselage study section would be less than 1.0%.

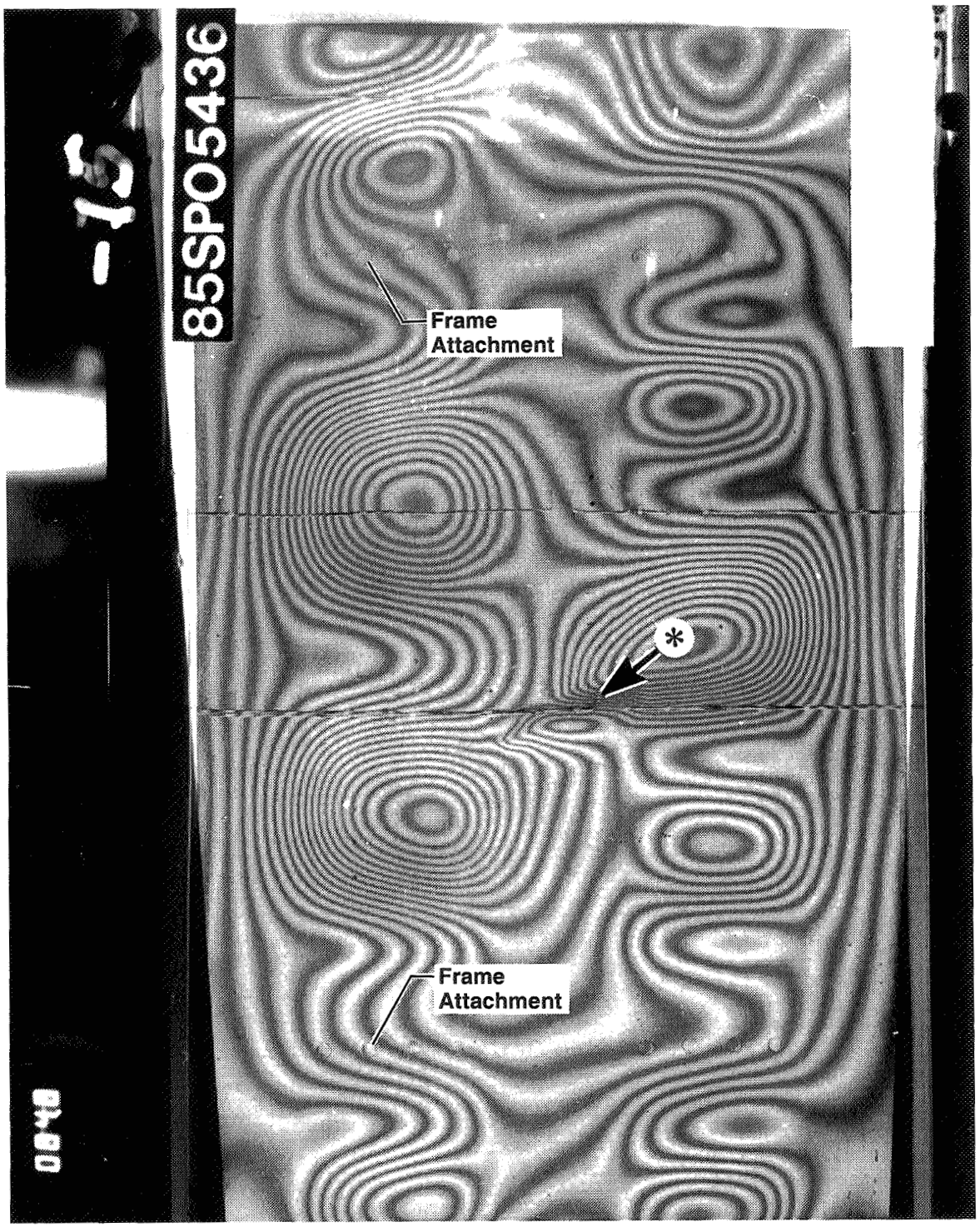

***Area of localized buckling indicating separation of skin from stringer flange in impact damage region. Panel load equals 85 kips**

Note: One fringe = 0.0622 in

Figure 154. Moire Fringe Photograph of Skin-Stringer Compression Damage Tolerance Panel With Nonvisible Impact (Panel 6A-3)

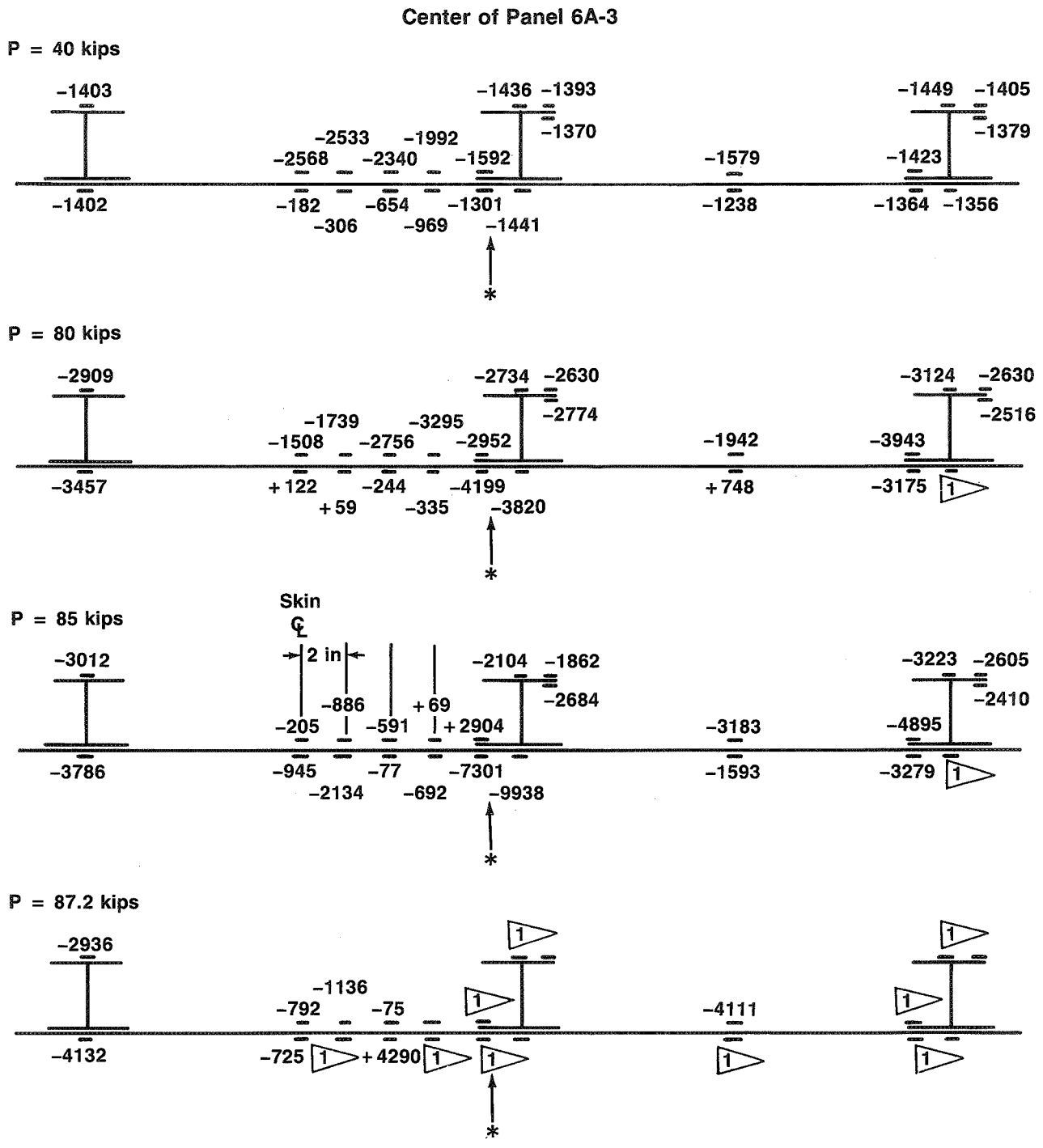

Figure 155. Strain Scans of Compression Damage Tolerance Panel With Nonvisible Impact (Panel 6A-3)

6.3.2 Honeycomb Compression Fracture

The configuration of the test 6B honeycomb fracture panels is shown in Figure 156.

The compression DUL requirement for the honeycomb test panels is 150.0 kips. At this load, the compression strain is 0.0047 in/in (fig. 147). The skin buckling load predicted for these panels (159 kips) is 6% higher than the DUL requirement. The buckling load was calculated using the Boeing analysis code LEOTHA. This analysis assumes simple support boundary conditions on all sides.

The predicted Euler column buckling load for the panels was only 5% above the DUL. To eliminate the occurrence of Euler column buckling, edge supports were attached to the sides of the panels for test. The edge supports were constructed from 4-in-diameter aluminum slotted tubes. The edge supports provided simple support boundary conditions consistent with the boundary assumptions used in the LEOTHA buckling analysis. The honeycomb panels were instrumented with strain gages. In addition, damage initiation and growth were monitored with acoustic emission. The test setup is shown in Figure 157.

Both honeycomb panels were impacted on the outside face sheet at the center of the panels over the middle longitudinal tear strap. During impacting, the panels were supported at the frames. A 20-lb impactor with a hemispherical steel tip was dropped from a height of 50 in to achieve 1000 in-lb of energy. Panel 6B-1 was impacted using a 1-in-diameter impactor that caused barely visible damage on the surface of the skin. Panel 6B-2 was impacted using a 0.5-in-diameter impactor that caused through-penetration damage (penetrating both face sheets

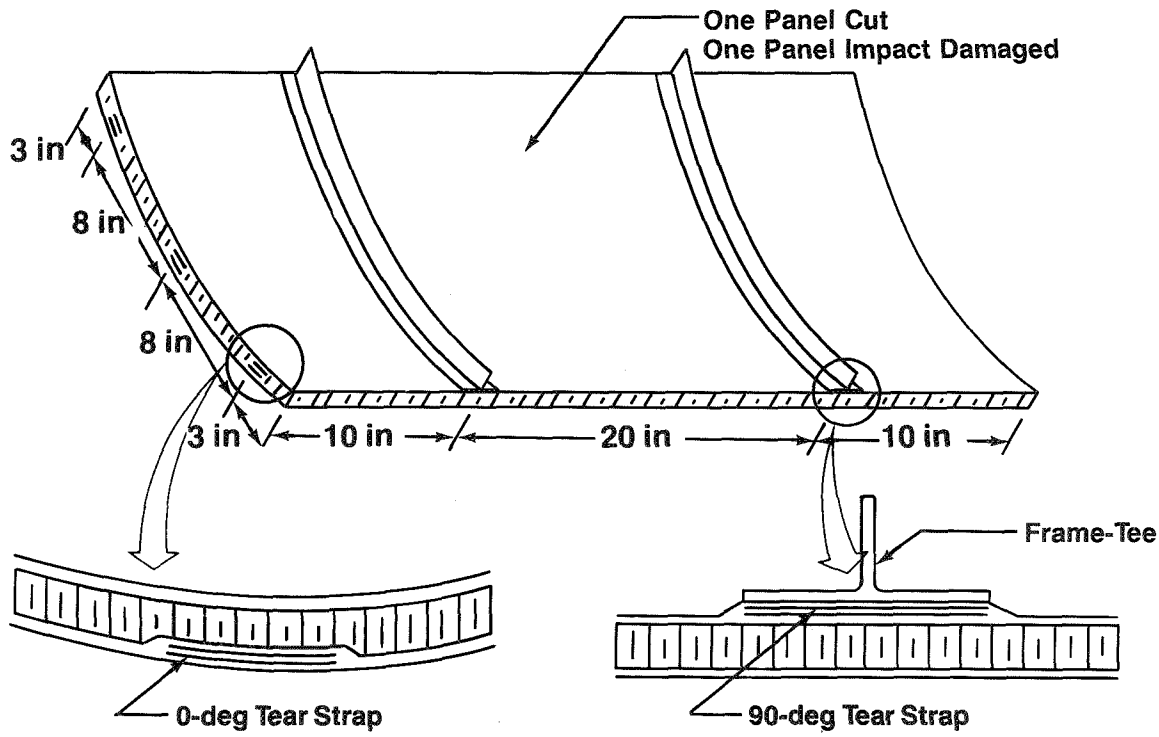

Figure 156. Honeycomb Compression Damage Containment (Test 6B)

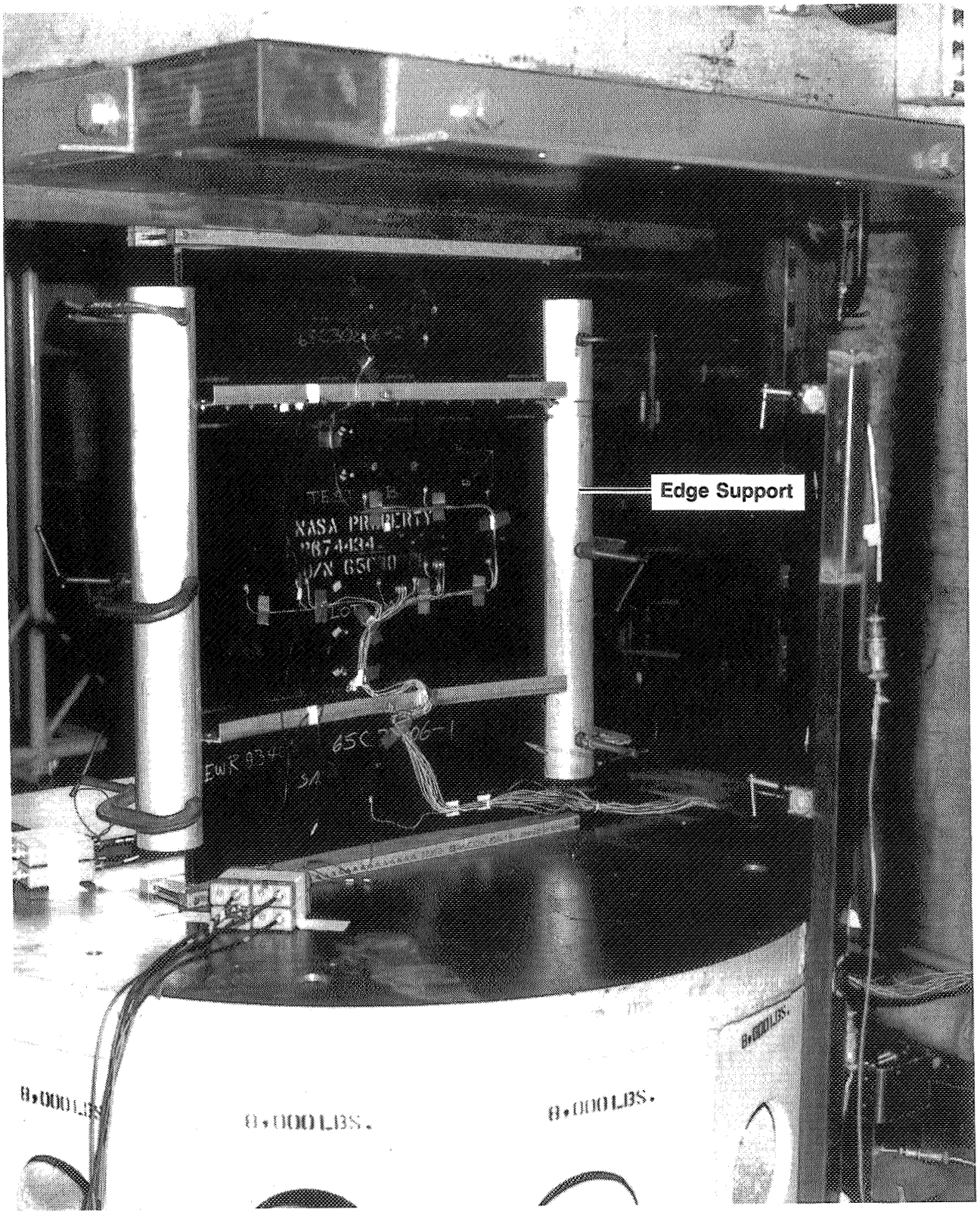

Figure 157. Honeycomb Compression Panel Test Setup (Test 6B)

and the core). Both panels were subjected to NDI, using TTU, and pulse echo to determine the extent of the impact damage. The face sheets was inspected using pulse echo, and the honeycomb core was inspected using TTU.

Figures 158 and 159 show the NDI C-scans of the impacted areas for the panels. The pulse echo scan of the panel 6B-1 face sheet revealed a delamination of approximately 1.75 in by 2.15 in within the outer face sheet. The TTU scan of the core revealed damage within the core extending in a circular area with approximately 8-in diameter centered by the impact (fig. 158). No skin-core disbond was detected. A cross sectional analysis performed after the test revealed that there were two types of core damage. The damage in the region directly below the impact site was characterized as core crush, evidenced by compressed cells. This core crush region was approximately 1.5 in in diameter. Outside of this region, the core damage was marked by cracks in the core cell oriented at 45 deg, indicating a shear failure (fig. 160).

Panel 6B-1 was to be subjected to DUL (150 kips) with a barely visible damage. During test, noise associated with core failure propagation started at approximately 20 kips and continued to panel failure. The outside face sheet started to buckle near 35 kips due to core failure propagation. This local skin buckling propagated laterally in a diamond shape to the edge of the tear straps, at which point the panel held 50 kips maximum and then dropped to 46 kips. After this, the panel was unloaded and the test was terminated.

Visual inspection of the tested panel, shown in Figure 161, revealed that there were no surface skin failures. Externally, it was difficult to see any panel damage after the test load was removed from the panel. NDI, TTU, and pulse echo scans revealed that the impact damage in the skin did not grow, but the core damage propagated to the shape and size of the buckled skin witnessed during the test. Figure 162 shows both skin pulse echo and core TTU scans. Panel 6B-1 failure was 50 kips, one-third of the required DUL. The failure mode was face sheet buckling due to progressive core failure.

A plot of the back-to-back strain data located 2.5 in from the panel center is shown in Figure 163. The figure indicates face sheet buckling occurred at a strain of 0.0012 in/in. A simple analysis was performed to evaluate the local skin buckling.

Assuming that the face sheets did not have any lateral support in the damaged core region, the local stability of the face sheets was analyzed by approximating each of the local face sheet areas by a curved rectangular element loaded in compression. The inside face sheet was modeled as a 5-in square inscribed on the inside of the core damaged area. Fixed boundary conditions were assumed around the edges since the adjoining core was still intact and would restrain the face sheet. The buckling strain for the inside face sheet, predicted by the code LEOTHA, was 0.00086 in/in.

The outside face sheet, where the tear strap is located, was modeled as a rectangular strip with the same width and layup as the tear strap. For this analysis, simple support boundary conditions were assumed around the edges of the tear strap analysis element. The skin adjoining the tear strap inside the core crush region could deform, allowing the edge of the tear strap to rotate. This is approximated better by simple support boundary conditions than by fixed. With these assumptions in effect, the buckling load predicted for the outside tear strap was 0.0009 in/in, or 25% below the buckling load observed in test.

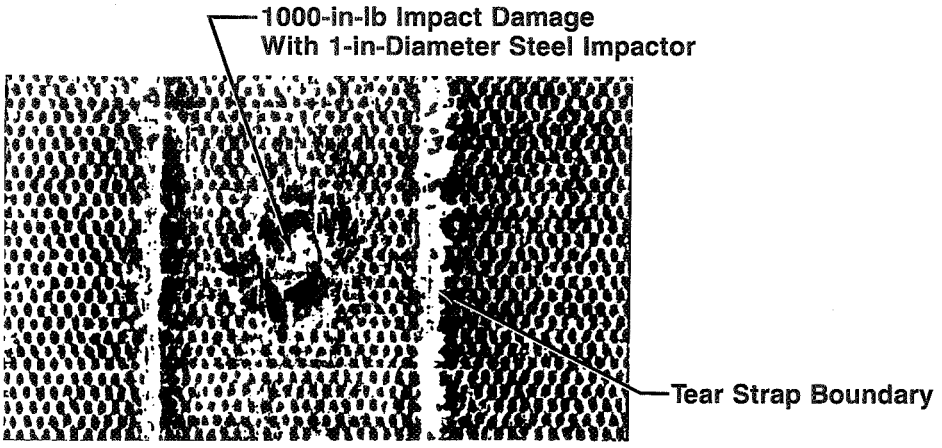

a. Pulse Echo Scan of Outside Face Sheet

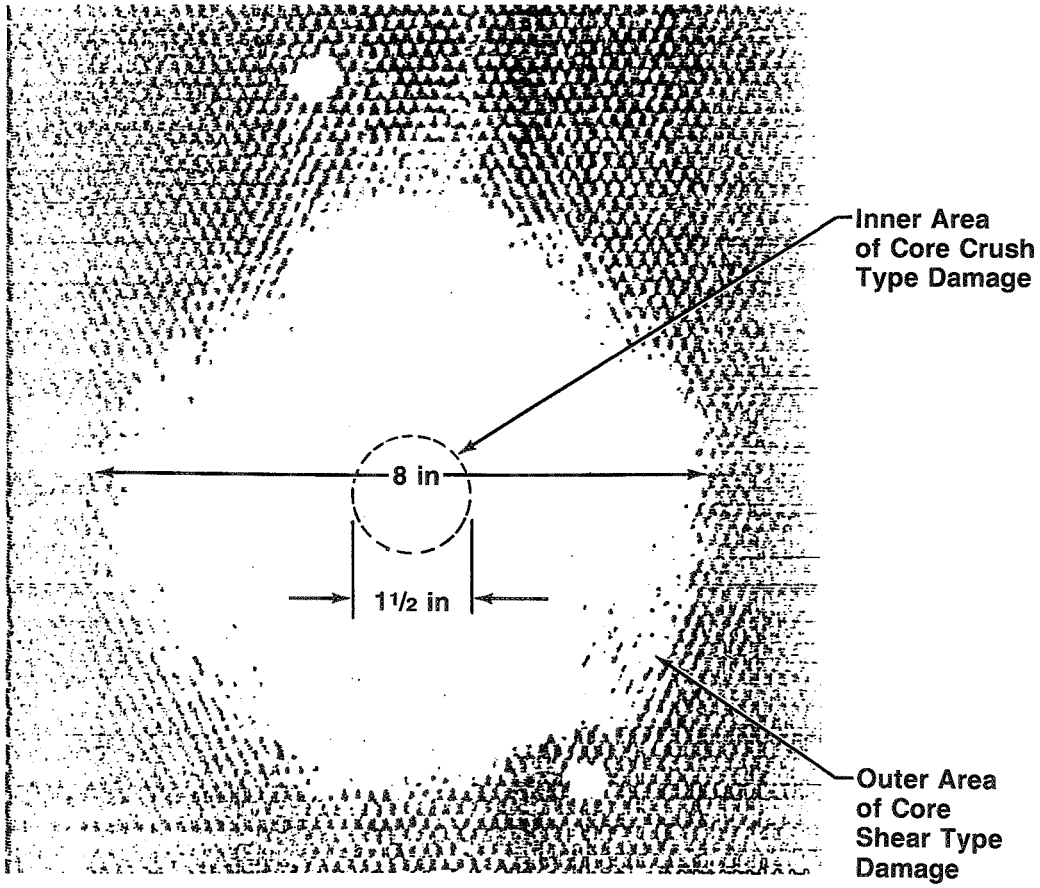

b. TTU Scan of Honeycomb Core

Figure 158. Nondestructive Inspection Scans of Impacted Area (Panel 6B-1)

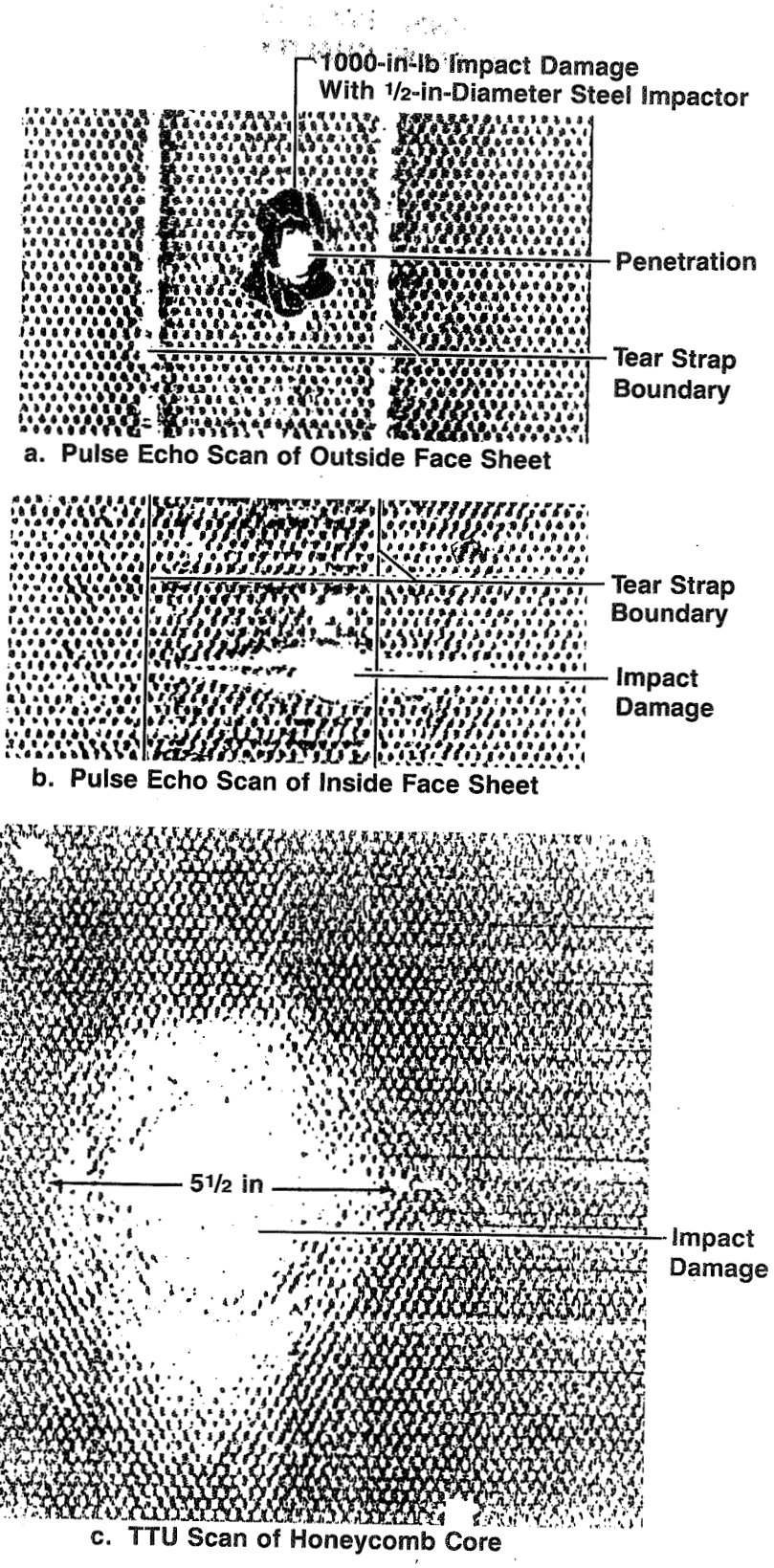

Figure 159. Nondestructive Inspection Scans of Impacted Area (Panel 6B-2)

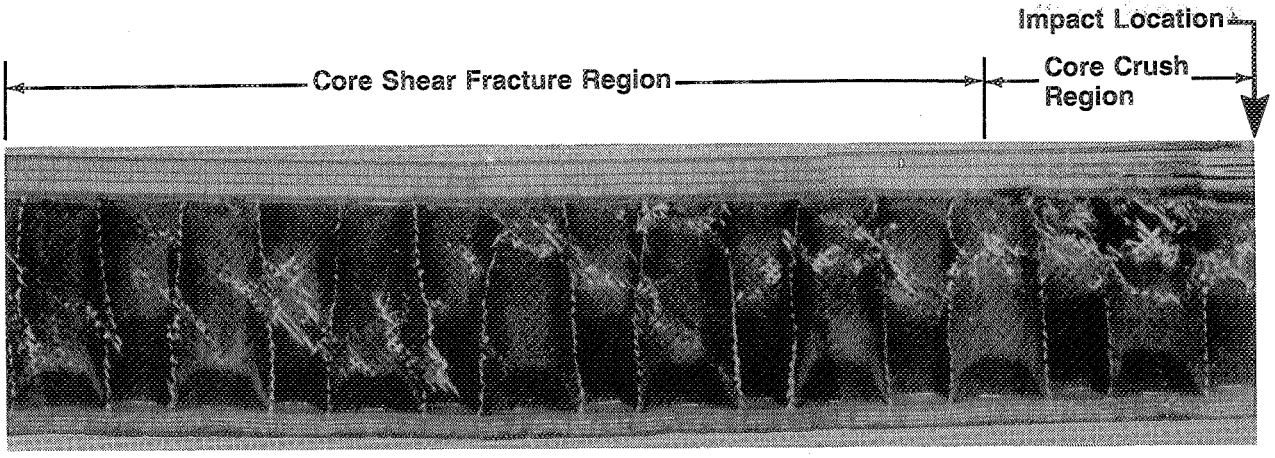

Figure 160. Micrograph of Honeycomb Showing Core Fracture Modes (Panel 6B-1)

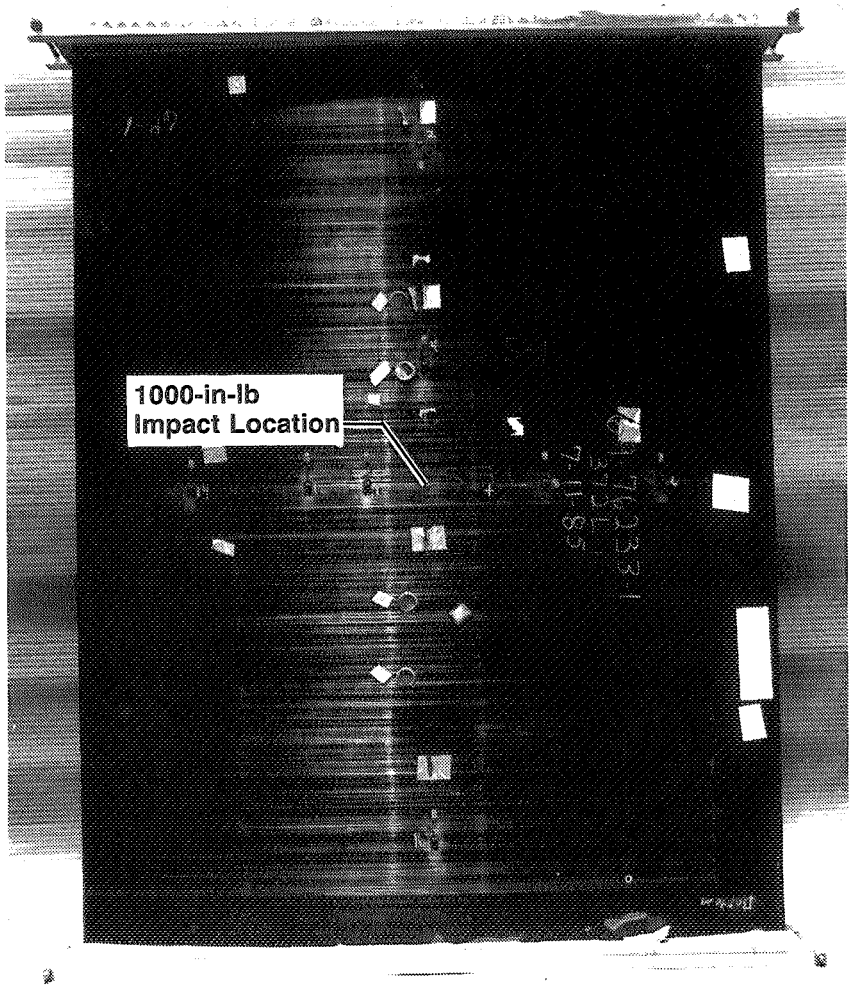

Figure 161. Honeycomb Panel After Compression Test (Panel 6B-1)

a. Pulse Echo Scan of Outside Face Sheet

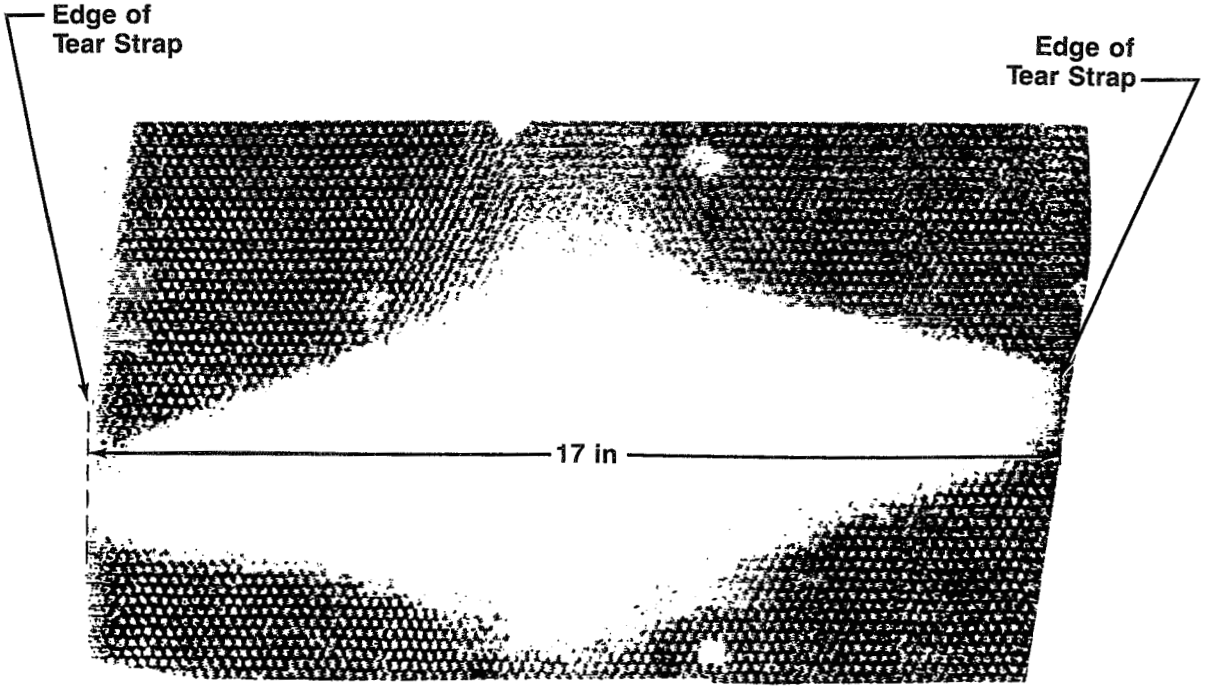

b. TTU Scan of Honeycomb Core After Failure

Figure 162. Nondestructive Inspection Scans of Impacted Area After Compression Test (Panel 6B-1)

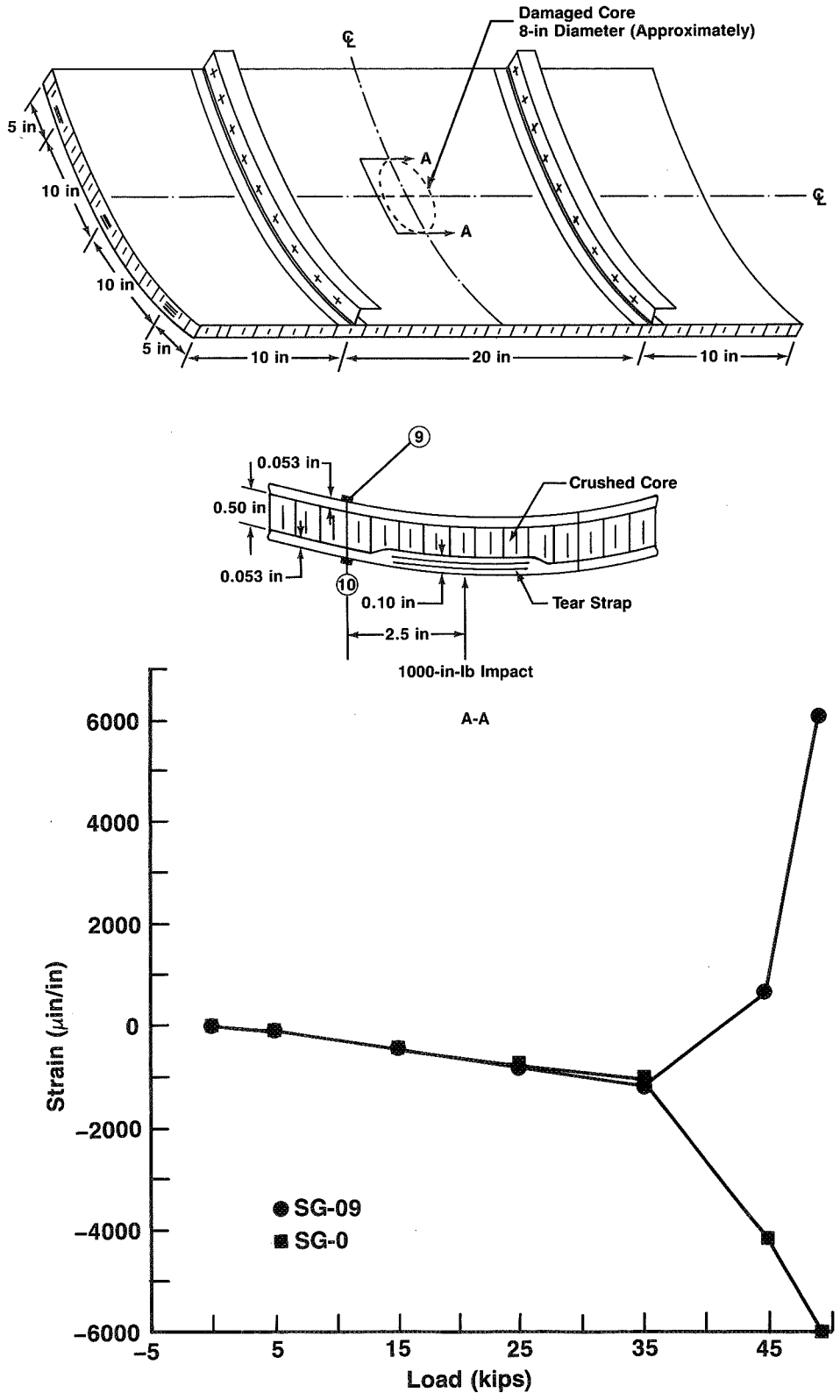

Figure 163. Honeycomb Compression Strain Gage Data (Test 6B, Panel 6B-1)

Panel 6B-2 was tested in compression with an 8-in-long sawcut in the center of the panel (fig. 164). The sawcut severed both face sheets, the center tear strap, and core. The test plan for this panel was to load it in compression up to continued safe flight load (50 kips). Panel 6B-2 failed at 43 kips (0.0014 in/in). The face sheets failed due to local instability caused by progressive core failure emanating from the ends of the sawcut.

To improve the capability of the honeycomb configuration, a tougher core material is needed that would minimize the extent of damage due to an impact and limit core damage propagation during test. A simple buckling analysis indicates that the maximum allowable diameter of unsupported skin (resulting from damaged core) is 2 to 3 in for a design strain of 0.005 in/in.

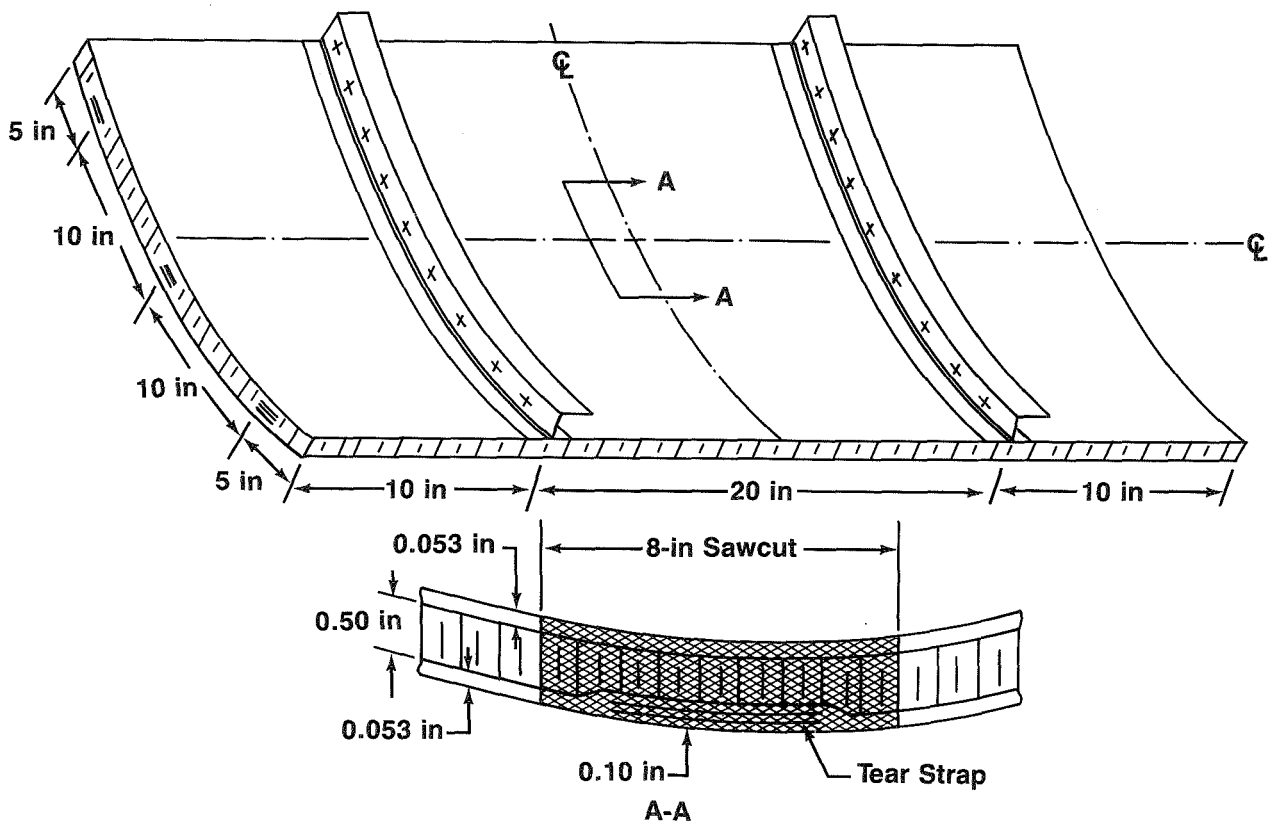

Figure 164. Honeycomb Compression (Panel 6B-2)

6.4 Pressure Pillowing

Tests were performed to determine the pulloff load capability of the frame and stringer from the fuselage skin. The test panel configurations for the skin-stringer and honeycomb concepts are shown in Figures 165 and 166. These tests were designed to model panel behavior under pressure and measure frame-stringer and stringer-skin pulloff loads. The test panel configurations are representative of the fuselage crown region where the frame-stiffener attachment loads are the highest, based on a Boeing 757 fuselage FEM. The FAA requires that fuselage structure be strong enough to withstand the pressure differential loads corresponding to the maximum relief valve setting multiplied by a factor of 2, omitting other loads (ref. 20). This pressure load factor includes a 1.5 factor of safety. The resulting pulloff load for this case, taken from a FEM of the 757, is 575 lb.

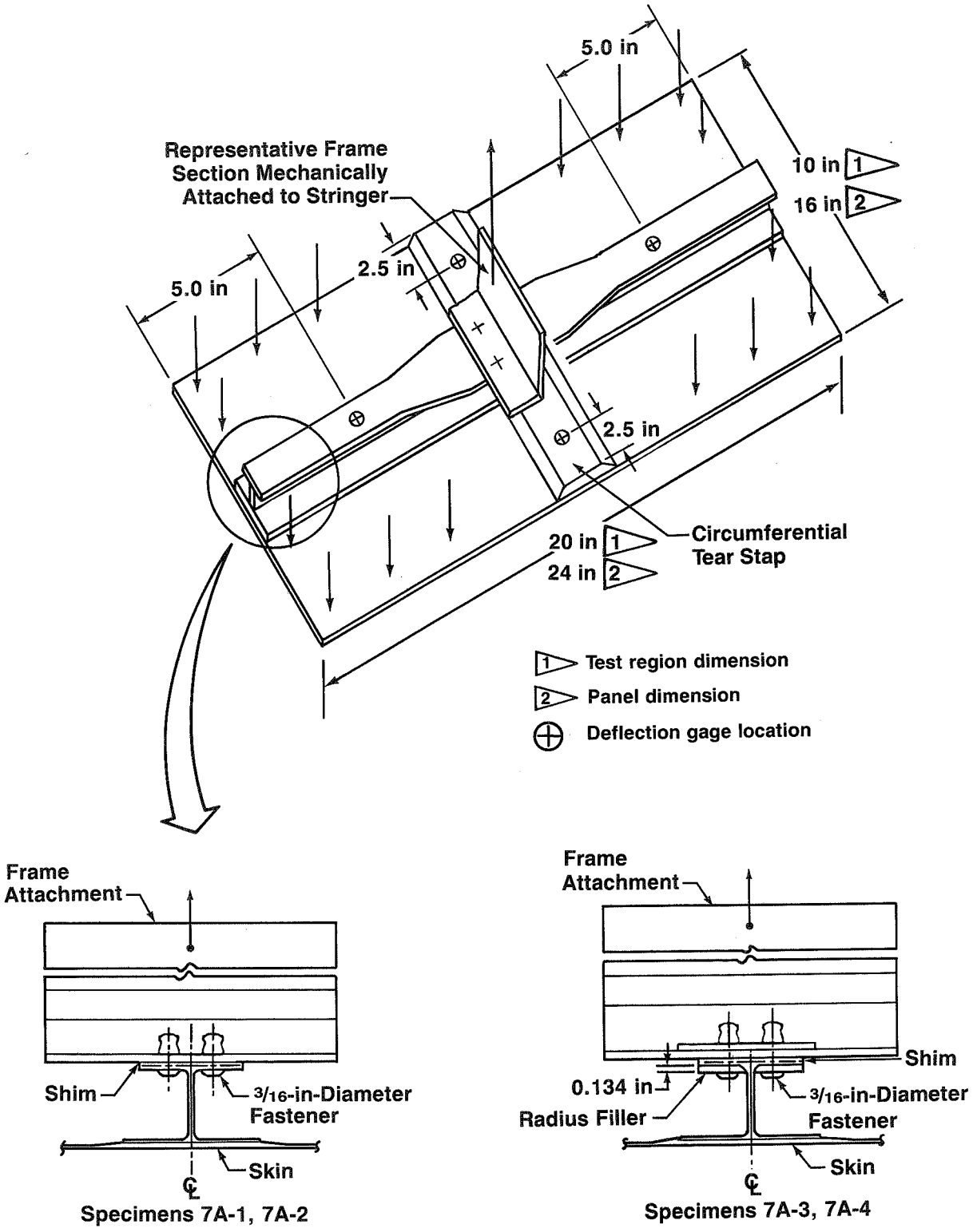

Figure 165. Skin-Stringer Pressure Pillowing Pulloff (Test 7A)

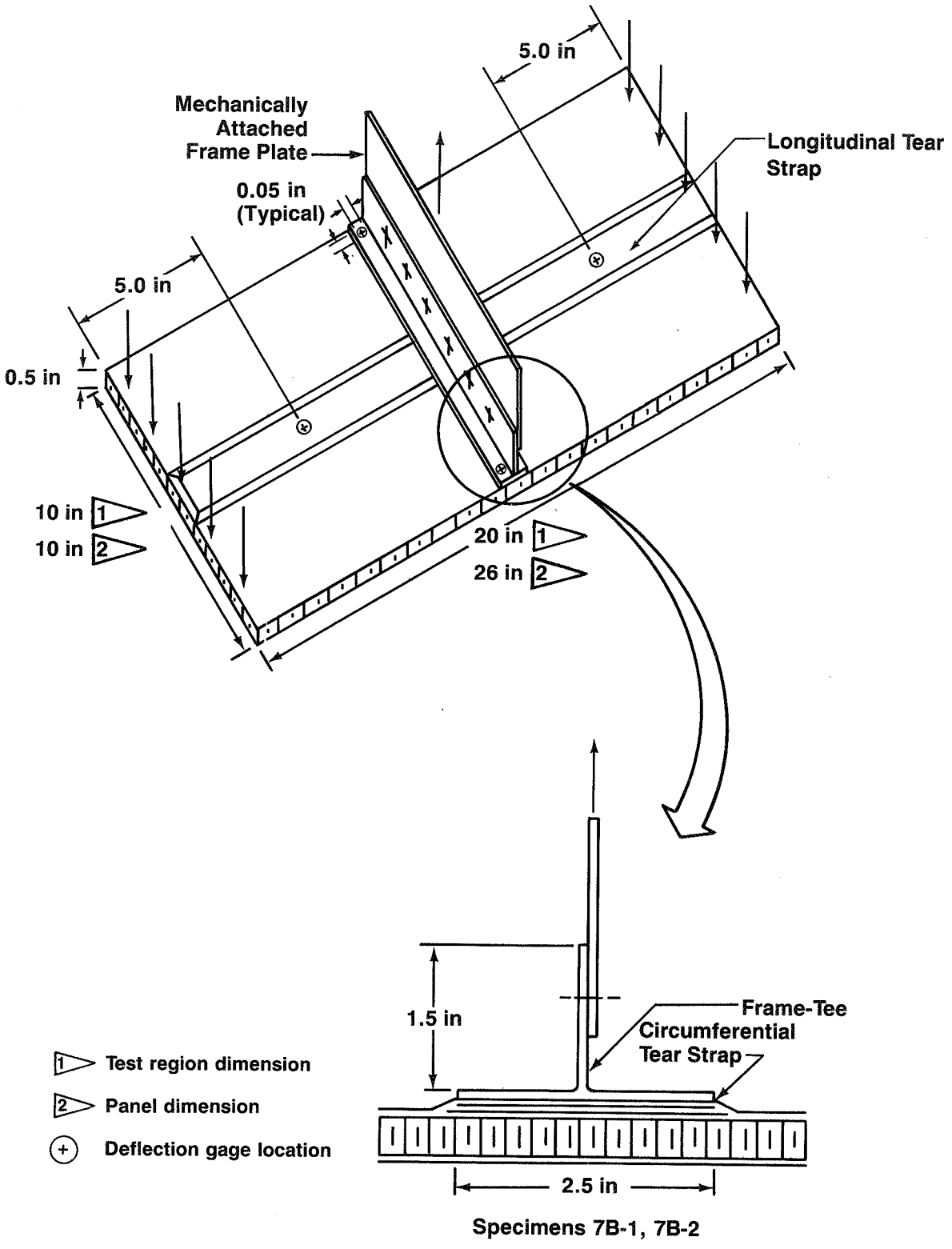

Figure 166. Honeycomb Pressure Pillowing Pulloff (Test 7B)

The configuration of the skin-stringer panels includes longitudinal and circumferential tear straps. The test plan included tests to determine the effect of radius fillers nested in stringer and frame flanges on the frame-to-stringer pulloff load. The panels were clamped along each of the four edges. This approximates the fixity of a panel section representative of one fuselage bay. A special test fixture used for clamping the edges of the test specimens is shown in Figure 167.

The results of the tests are summarized in Figure 168. The specimens without radius fillers failed at 722 lb average. Easily audible noise associated with local delaminations started to occur at 400 to 500 lb and continued until failure. Figure 169 shows the type of failure for these specimens, where the fasteners pulled through the stringer cap. The specimens with radius fillers failed at 2120 lb average, well above the required design load. The graphite-epoxy frame attachment deformed considerably before specimen failure. The failure occurred at the boundary between the stringer web and cap flanges. The cap flanges were sheared off the web by the radius fillers, as shown in Figure 170.

The configuration of the honeycomb panels includes both longitudinal and circumferential tear straps. The two 10-in-wide ends were clamped to simulate actual fuselage conditions. This configuration is typical of one fuselage bay bounded by the frames and longitudinal tear straps. The honeycomb shell concept, when loaded by pressure only, is restrained circumferentially at the frames and is unrestrained longitudinally. To model this, the honeycomb specimens were designed to fit the fixture with the ends fixed and the sides unrestrained (fig. 167). Figure 171 shows the test setup for the honeycomb sandwich specimens.

The two factors' internal relief valve pressure produces a running load on the frame-to-skin interface of 164 lb/in (or 1640-lb test specimen load). Figure 172 presents a summary of the first honeycomb specimen (7B lot 2M) test results. It includes specimen configuration, damage location, TTU C-scan showing size of core damage, load requirement, failure load, and failure mode. The specimen was loaded to 2365 lb, at which time a core shear failure occurred. After this failure, the specimen continued to support 1000 lb and the test was terminated. The design load requirement was exceeded considerably. The core failure occurred because the core shear capability was exceeded (236 lb/in^2 versus 200 lb/in^2 allowable). A NDI of the failed specimen revealed the core damage and showed that there was no frame tee-skin disbond or skin-core disbond beneath the frame.

The second honeycomb specimen (7B lot 1M) was impacted on the outside face sheet, as shown in Figure 173. It was inflicted with 500 in-lb of impact energy using a 2.5-in-diameter lead ball (2.0 lb) and supported as shown in Figure 173. In this test, the objective was to evaluate the design load capability of the frame tee-skin interface after being subjected to a barely visible impact damage. A NDI revealed skin delamination (1.4 in wide by 2.3 in long), core damage at the impact location (3.0 in approximately), and core damage at a location where the specimen was supported during the impact event. Figure 173 shows the location and size of the different damages detected using TTU and pulse echo.

The specimen was loaded to 1440 lb at which time the damaged core failed 5 in from the frame. The core damage started to propagate at 425 lb and finally failed at 1440 lb. TTU and pulse echo scans of the skins and core were taken to determine the extent of the damage. This inspection revealed and confirmed that the core damage away from the impact was the critical location. The damages at the impact site did not grow. The interface between the frame-tee and skin did not delaminate during test.

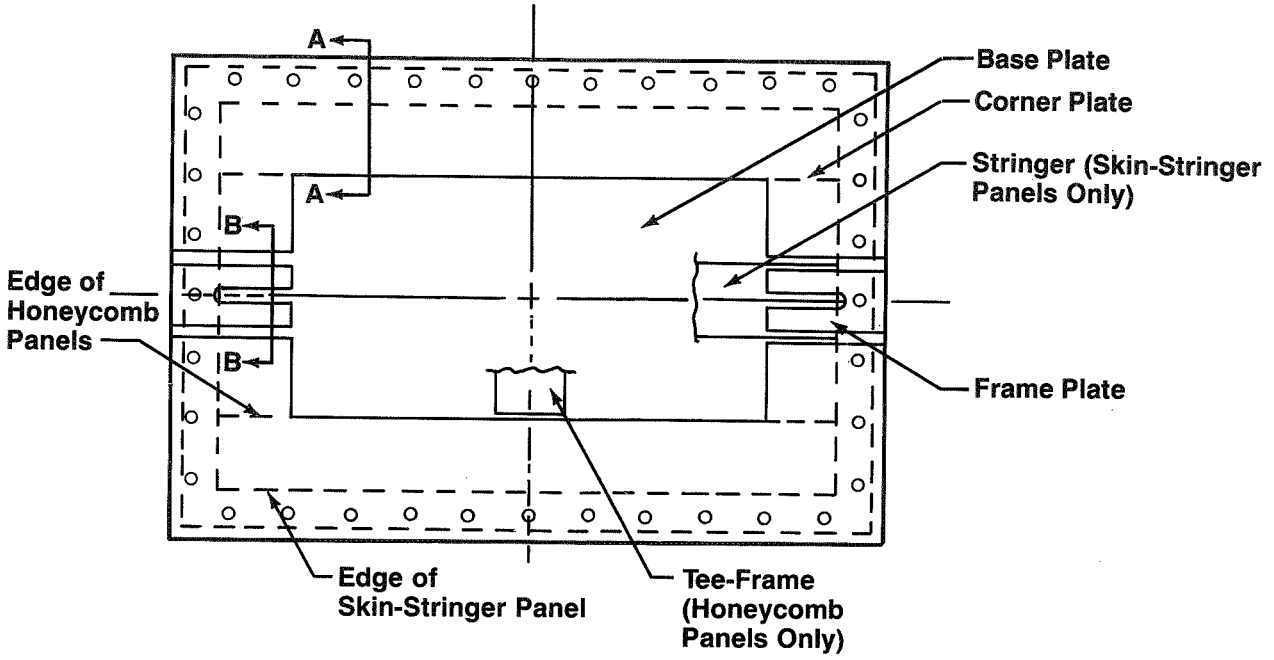

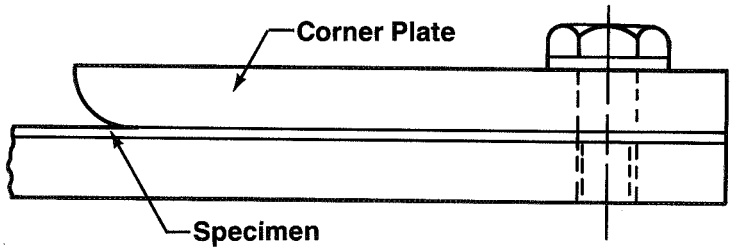

Section A-A

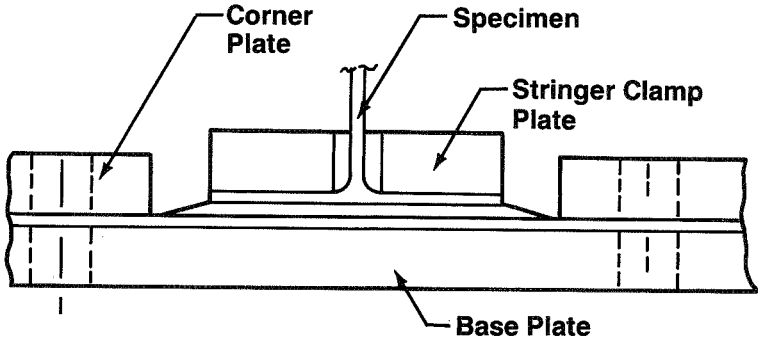

Section B-B

Figure 167. Fixture for Pressure Pillowing Panel Tests (Test 7)

Specimen Number	Specimen Type	Radius Filler Usage	Design Load (lb)	Failure Load (lb)	Impact Energy (in-lb)	Failure Mode
7A-1	Skin-Stringer	No	575	700	None	Fasteners Pulled Through Stringer Cap
7A-2	Skin-Stringer	No	575	745	None	
7A-3	Skin-Stringer	Yes	575	2050	None	Radius Fillers Sheared Off Stringer Cap
7A-4	Skin-Stringer	Yes	575	2190	None	
7B-1	Honeycomb	No	1380	2365	None	Core Shear Failure
7B-2	Honeycomb	No	1380	1440	500	Damaged Core Failed in Shear

Figure 168. Pressure Pillowing Test Results

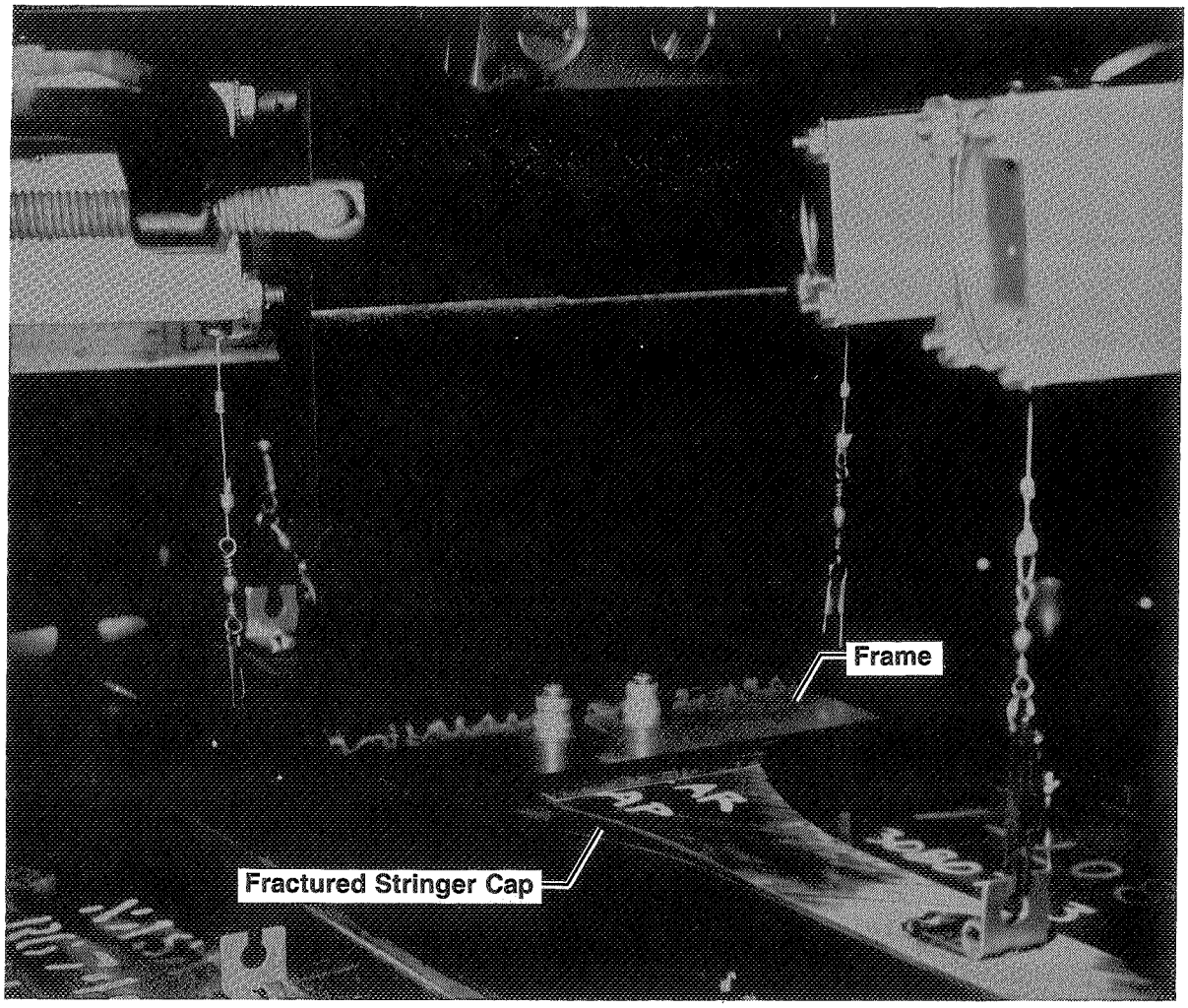

Figure 169. Skin-Stringer Failed Specimen, No Radius Fillers (Test 7A)

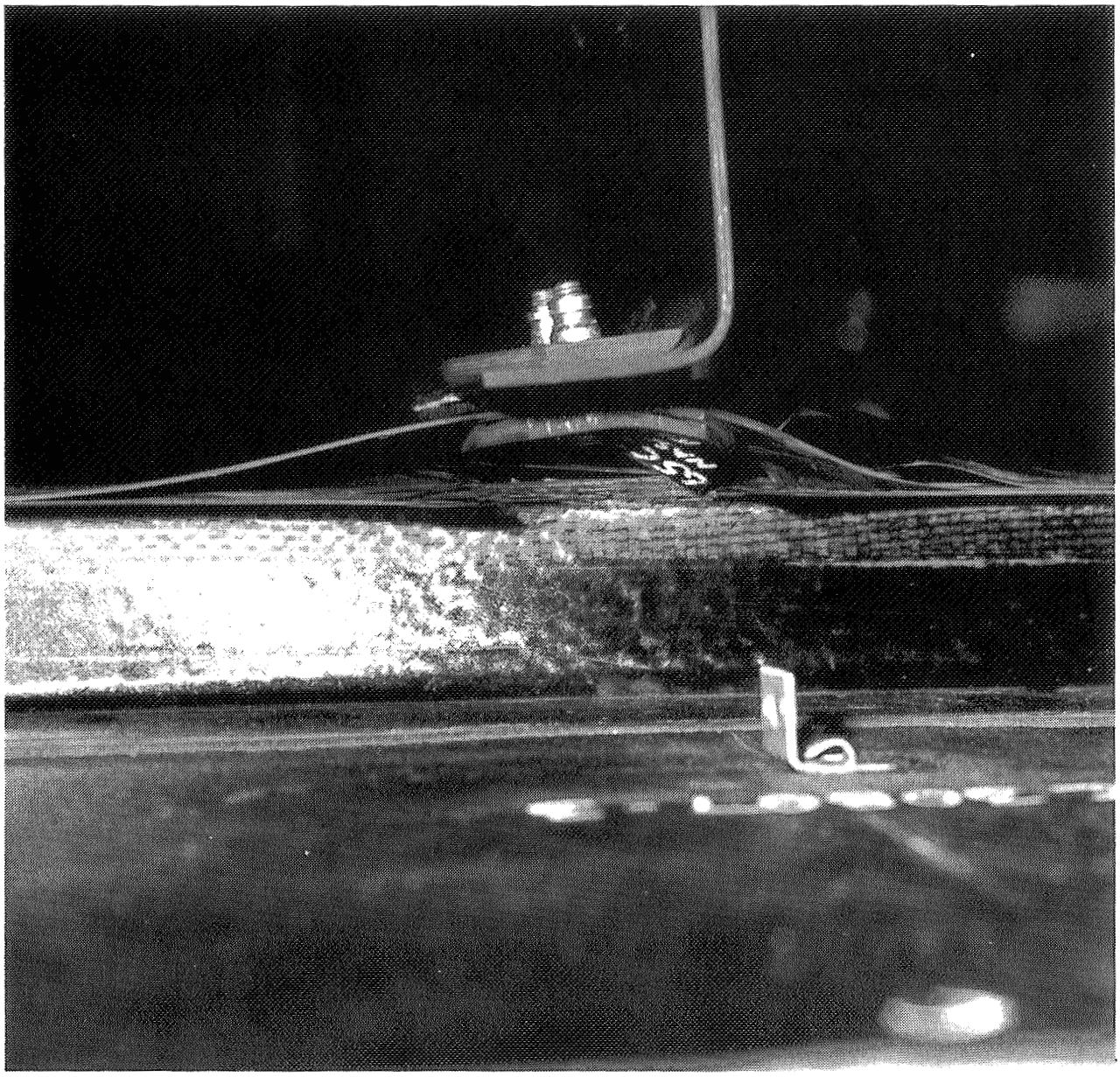

Figure 170. Pressure Pillowing Skin-Stringer Specimen With Radius Fillers, Failed Specimen

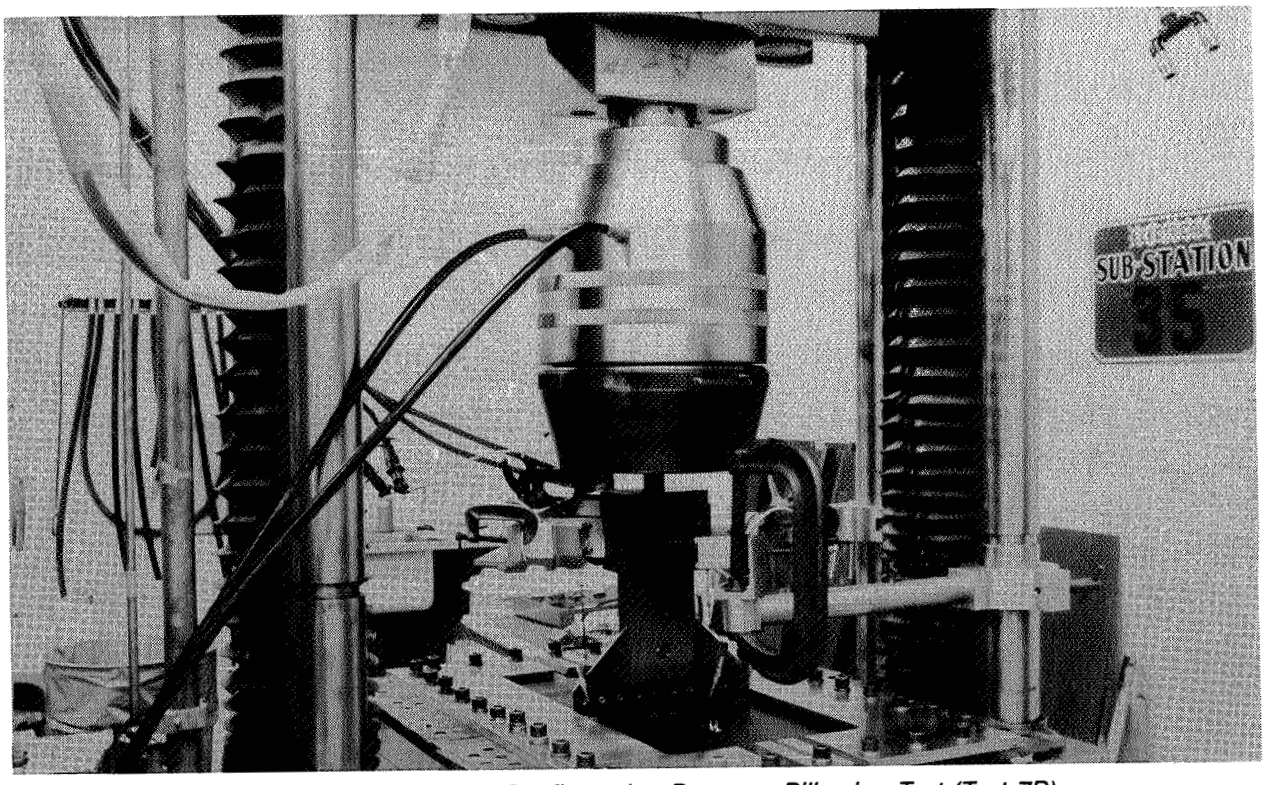

Figure 171. Honeycomb Configuration Pressure Pillowing Test (Test 7B)

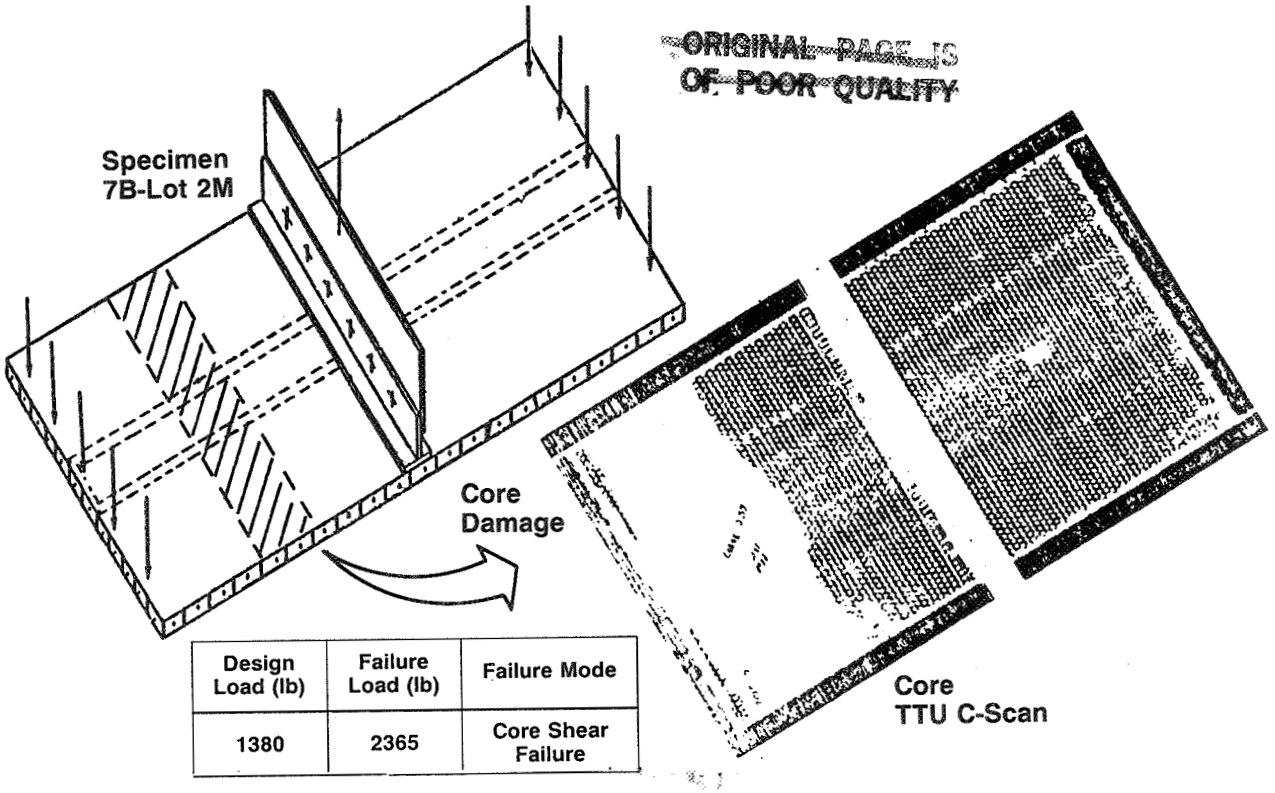

Design Load (lb)	Failure Load (lb)	Failure Mode
1380	2365	Core Shear Failure

Figure 172. Honeycomb Specimen 7B-2 Test Results (Test 7B)

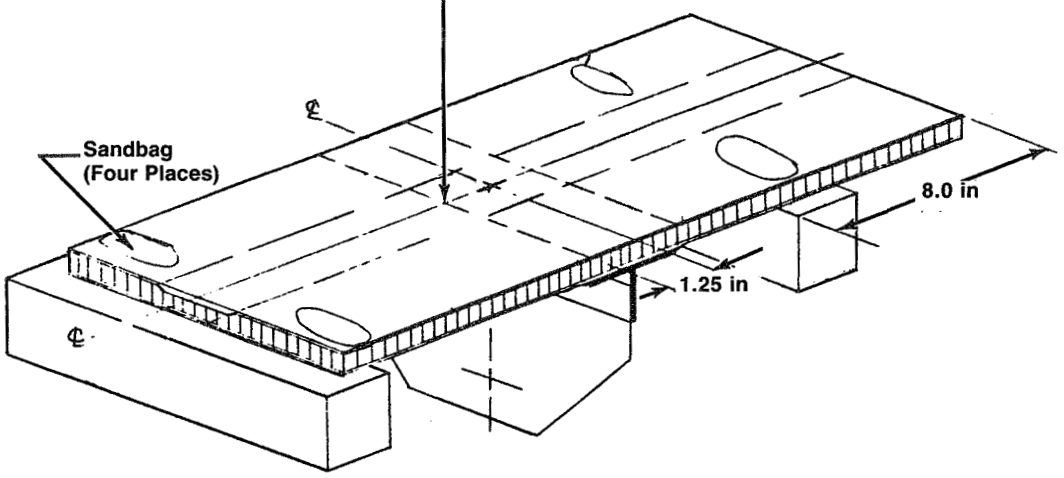

Core TTU C-Scan After Impact

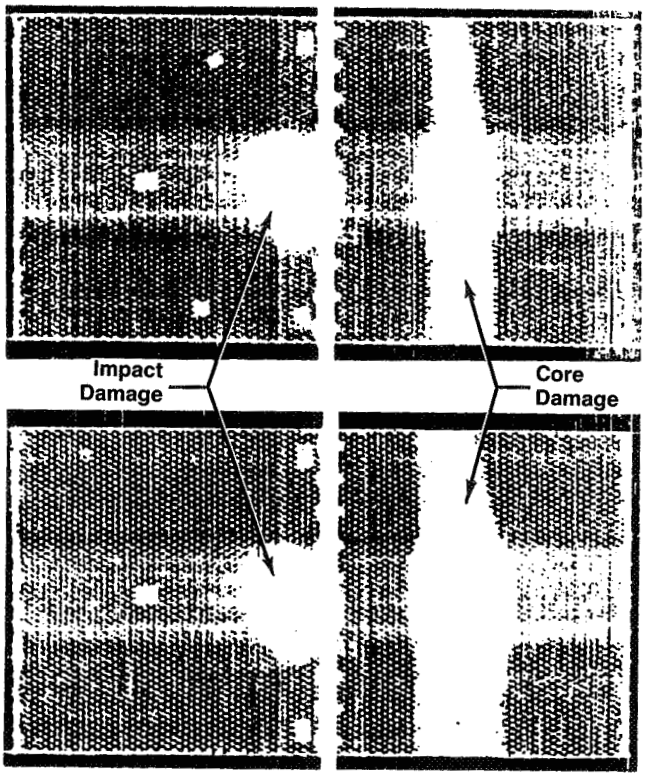

Core TTU C-Scan After Test

Design Load (lb)	Failure Load (lb)	Failure Mode
1380	1440	Damaged Core Failed in Shear

Figure 173. Honeycomb Specimen 7B-Lot 1M Test Results (Test 7B)

7.0 CONCLUSIONS

The principal issues of damage tolerance and pressure containment for a transport aircraft fuselage were addressed in this program. Skin-stringer and honeycomb sandwich composite fuselage shell designs were evaluated for these issues. Analyses were developed to model the structural response of these shell designs, and a development test program evaluated the selected design configurations to appropriate load conditions.

A basic damage tolerance criterion selected for the evaluation was that the fuselage shell must survive a significant damage to the structure during flight. In addition, the structure must be designed for a type of impact damage that may be barely visible. Panels were tested with damages that ranged from barely visible impact damage to that which severed a whole skin-stringer bay.

The tests of the skin-stringer shell designs showed adequate damage tolerance and pressure containment characteristics for the more serious impact and discrete damage cases. The keel skin-stringer design did not meet the ultimate compression load requirements for the barely visible impact condition. Design changes to meet load requirements of the skin-stringer shell design would cause less than 1.0% increase in weight of the participating fuselage structure. The tests indicated the criticality of the skin-stringer interface and design modifications must reduce the effect of skin buckling on this area. The effects of skin buckling can be reduced by one or more of the following design modifications: increased skin gage, increased number of padup planks, and increased width of padup. The lesson learned in these tests is that initial compression skin buckling should not occur below 40% of design ultimate panel loading to prevent skin-stringer separation at a damage location.

The honeycomb sandwich crown design showed good damage tolerance in tension and pressure pillowing pulloff strength for the impact damaged shell-frame interface. The honeycomb keel design did not meet the residual compression strength requirements after either impact damage or large area damage. The 4.0-lb/ft^3, 3/16-in glass core proved to be too brittle, fracturing under impact, and failing in shear emanating from the damage area. Metal core, such as aluminum, would be tougher and may provide sufficient stability in compression after damage. The metal core would deform more locally during impact events and therefore would be more visible. Further tests would be needed to determin wheather 4.0-lb/ft^3 metal core would be adequate or whether a higher density core would be necessary. A smaller cell size may also prove more damage tolerant.

The analyses of the test panels produced failure load and skin buckling predictions taht, in general, correlated well with the test results. The NASTRAN analyses used for the flat and curved tension fracture panels produced failure predictions that were within 15% of the test failure values. The STAGSC-1 analyses used for compression panels yielded initial skin buckling predictions that were within 26% of the test valures. The STAGSC-1 initial buckling strains for the shear test were from 8% to 20% lower than those determined from the test strain and moire results of the nonwarped panel, depending on shear load direction. Descrepancies of 21% to 42% occured on a test panel that was warped during the edge doubler cure. The shear panel initial buckling responses seemed to be sensitive to (1) prestrain from the assembly of the panels to the test frame, (2) the boundary conditions exerted on the panel by

the test frame and edge padups, and (3) the panel loading direction. The contribution of the edge padups to panel load capability has been found to be as high as 10% in past experience.

The AS6/2220-3 material used for the skin-stringer shell design proved to have good processibility and produced good void-free laminates. The material proved to have high strain capability that provided good damage tolerance in tension. The compression damage tolerance may have been improved if the material had greater toughness, although the critical failure mode seems to have been skin-stringer separation at the damage location promoted by skin buckling.

The AS6/F584 material used for the honeycomb sandwich shell design exhibited good damage tolerance in tension. Due to the core failures, the compression damage tolerance of the face sheet material was not evaluated. The process of single-cure honeycomb sandwich fabrication produced acceptable test panels and is considerably less labor and time extensive than the two-stage cure cycle initially considered for this effort.

A weight reduction anlaysis was performed, based on the stiffened laminate shell design, and compared to the original aluminum baseline design. The comparison was made on that aluminum structure considered participating for a composite shell design only. The weight of participating graphite-epoxy fuselage compared with aluminum was reduced by 22.7%. Modifications to the keel section to meet the ultimate compression damaged tolerance requirements would reduce the total fuselage weight saving to 21.7%.

The wing and fuselage equally share a majority of the total aircraft structural weight. The potential weight reduction and cost savings associated with applying composites to these structures are significant. This program, along with the manufacturing technology program (Air Force contract F33615-82-C-3213), has shown that composite fuselage structure is weight and cost competitive. Further development is needed, such as large curved panel validation and full-scale section testing, to provide a data base to proceed with a full-scale composite fuselage development program.

8.0 REFERENCES

1. Johnson, R. W., Thomson, L. W., Wilson, R. D., "Study on Utilization of Advanced Composites in Fuselage Structures of Large Transports," NASA CR-172406, February 1985.

2. Porter, T. R., and Pierre, W. F., "Tear Strap Design in Graphite Epoxy Structure," Volume II, NASA TM-84116, Volume II, January 1981.

3. Starnes, J. H., and Williams, J. G., "Failure Characteristics of Graphite-Epoxy Structural Components Loaded in Compression," NASA Technical Memorandum 84552, September 1982.

4. Agarwal, B. L., "A Model To Simulate Failure Due to Stiffener-Web Separation of Composite Tension Field Panels," Northrop Corporation, Hawthorne, California, 1982.

5. McCarty, J. E., and Roeseler, W. G., "Durability and Damage Tolerance of Large Composite Primary Aircraft Structure (LCPAS)," Sixth DOD/NASA Conference on Fibrous Composites in Structural Design, New Orleans, January 1983.

6. Davenport, O. B., "Buckling of Orthotropic, Curved, Sandwich Panels Subjected to Edge Shear and Axial Compression," a thesis submitted to the graduate faculty at the University of Oklahoma, 1972.

7. Davenport, O. B., and Bert, C. W., "Buckling of Orthotropic, Curved, Sandwich Panels Subjected to Edge Shear Loads," *Journal of Aircraft*, July 1971, revised March 1972.

8. Dickson, J. N., and Brolliar, R. M., "The General Instability of Ring-Stiffened Corrugated Cylinders under Axial Compression," NASA TN D-3089, 1965.

9. McCarty, J. E., and Ratwani, M. M., "Damage Tolerance of Composites," Air Force Contract F33615-82-C-3213, Interim Report No. 6, September 1985.

10. Boeing Commercial Airplane Company, "Manufacturing Technology for Large Aircraft Composite Primary Structure - Fuselage," Air Force Contract F33615-83-C-5024, Interim Reports 1 (March 1984) through 9 (March 1986).

11. McCormick, Caleb W. (ed.), MSC/NASTRAN User's Manual: MSC/NASTRAN Version 62, The MacNeal-Schwendler Corporation, February 1981.

12. Whitney, J. M., and Nuismer, R. J., "Stress Fracture Criteria for Laminated Composites Containing Stress Concentrations," *Journal of Composite Materials*, Vol. 8, July 1974.

13. Garbo, S. P., and Ogonowski, J. M., "Effect of Variance and Manufacturing Tolerances on the Design Strength and Life of Mechanically Fastened Composite Joints," AFWAL-TR-81-3041, April 1981.

14. Johnson, R. W., McCarty, J. E., and Wilson, D. R., "Damage Tolerance Testing for the Boeing 737 Graphite/Epoxy Horizontal Stabilizer," Proceedings of the Fifth DOD/NASA Conference on Fibrous Composites in Structural Design, NADC81096-60, Vol. II, January 1981.

15. Fuchs, H. O., and Stephens, R. J., "Metal Fatigue in Engineering," Wiley-Interscience Publication, Wiley and Sons, 1980.

16. User's Manual for STAGSC, Structural Mechanics Laboratory, Lockheed Palo Alto Research Laboratory, March 1978.

17. Knight, N. F., and Starnes, J. H., "Postbuckling Behavior of Selected Curved Stiffened Graphite-Epoxy Panels Loaded in Axial Compression," Proceedings of the AIAA/ASEM/ASCE/AHS 26th Structures, Structural Dynamics and Materials Conference, AIAA Paper No. 85-0768-CP, Orlando, Florida, April 1985.

18. Aniversario, S. T., et al, "Design, Ancillary Testing, Analysis, and Fabrication for the Advanced Composite Stabilizer for the 737 Aircraft," Vol. II-Final Report, NASA CR-166011, December 1982.

19. Ashton, J. E., and Whitney, J. M., "Theory of Laminated Plates," Technomic Publications, 1970, pp. 91-95.

20. Code of Federal Regulations for Aeronautics and Space, Part 25, Sections 25.303 and 25.365, January 1, 1983.

Standard Bibliographic Page

1. Report No.	2. Government Accession No.	3. Recipient's Catalog No.
NASA CR-3996		

4. Title and Subtitle	5. Report Date
Development of Pressure Containment and Damage Tolerance Technology for Composite Fuselage Structures in Large Transport Aircraft	August 1986
	6. Performing Organization Code

7. Author(s)	8. Performing Organization Report No.
P. J. Smith L. W. Thomson R. D. Wilson	

9. Performing Organization Name and Address	10. Work Unit No.
Boeing Commercial Airplane Company P. O. Box 3707 Seattle, WA 98124	
	11. Contract or Grant No. NAS1-17740

12. Sponsoring Agency Name and Address	13. Type of Report and Period Covered
National Aeronautics and Space Administration Washington, DC 20546-0001	Contractor Report
	14. Sponsoring Agency Code 534-06-23-10

15. Supplementary Notes

Langley Technical Monitor: Jon S. Pyle

16. Abstract NASA sponsored composites research and development programs were set in place to develop the critical engineering technologies in large transport aircraft structures. This NASA-Boeing program focused on the critical issues of damage tolerance and pressure containment generic to the fuselage structure of large pressurized aircraft. Skin-stringer and honeycomb sandwich composite fuselage shell designs were evaluated to resolve these issues. Analyses were developed to model the structural response of the fuselage shell designs, and a development test program evaluated the selected design configurations to appropriate load conditions.

17. Key Words (Suggested by Authors(s))	18. Distribution Statement
Composite structures, Transport Aircraft, Composite Fuselages, Pressure Containment, Damage Tolerance, Composite Materials, Analytical Methods, Composite Testing.	[redacted] Subject Category 24

19. Security Classif.(of this report)	20. Security Classif.(of this page)	21. No of Pages	22. Price
Unclassified	Unclassified	190	

[redacted]

NASA-Langley, 1986